

Targeted Functional Proteomics to Study Protein Post-Translational Modification and Protein-Protein Interactions

by

Zhe Zhang

M.S. China Pharmaceutical University, 2001

B. S. China Pharmaceutical University, 1998

Submitted to the Graduate Faculty of
School of Pharmacy in partial fulfillment
of the requirements for the degree of
Doctor of Philosophy

University of Pittsburgh

2007

UNIVERSITY OF PITTSBURGH
SCHOOL OF PHARMACY

This thesis was presented

by

Zhe Zhang

It was defended on

June 5, 2007

and approved by

Billy W. Day, Ph.D., Professor, Department of Pharmaceutical Sciences, School of Pharmacy;
Department of Chemistry, School of Arts and Sciences

Jorge L. Sepulveda, M.D., Ph.D., Assistant Professor, Department of Pathology, School of
Medicine

Robert B. Gibbs, Ph.D., Professor, Department of Pharmaceutical Sciences, School of
Pharmacy

Yu Jiang, Ph.D., Assistant Professor, Department of Pharmacology, School of Medicine

Michael A. Zemaitis, Ph.D., Professor, Department of Pharmaceutical Sciences, School of
Pharmacy

Copyright © by Zhe Zhang

2007

TARGETED FUNCTIONAL PROTEOMICS TO STUDY PROTEIN POST- TRANSLATIONAL MODIFICATION AND PROTEIN-PROTEIN INTERACTIONS

Zhe Zhang, M.S.

University of Pittsburgh, 2007

The rapid development of proteomic techniques in the post-genomics era has allowed much attention to be paid to the understanding of molecular mechanisms of functional regulatory proteins. This amazingly fast transformation from “know-how” to “know-why” has allowed the determination of if functional regulation is based on up- or down-regulation, or based on any particular chemical modification on the amino acid residues of protein targets.

Here, different biologically important regulatory proteomes or protein targets were investigated using comprehensive combinations of proteomics techniques. A large emphasis was placed on expression techniques suitable for protein and protein binding partner affinity purification for targeted analysis of phospho-proteins. The main protein of interest in these particular studies was an important transcriptional factor in cardiac development, serum response factor-1. Several proteomics methods were examined and, along with the difficulties encountered, the results are presented. Small molecule-protein interaction was examined with the cell cycle regulatory protein Cdc25B incubated with an inhibitor. Post-translational modification-related functional proteomics were also studied, first in a rodent early hemorrhage model wherein *S*-nitrosylation of plasma proteins were determined, then the phosphorylation of serum response factor-1. Finally, top-down functional proteome mapping was represented by a detailed and very successful analysis of the proteins found enriched in brain tumor cell pseudopodia.

This dissertation illustrates the vast range of potential of proteomics technologies in studying function-related biological systems. Meanwhile, some pioneering work using targeted functional proteomics strategies was achieved, and the results will help in part to advance the field of “targeted functional proteomics”, the combination of cell and molecular biological techniques with chemical, affinity and mass spectrometric approaches to study regulation of biological systems.

TABLE OF CONTENTS

PREFACE	XIII
1.0 INTRODUCTION	1
1.1 PHOSPHORYLATION	4
1.1.1 The difficulties in studying protein phosphorylation	5
1.1.1.1 The matter of math (i.e., stoichiometry)	5
1.1.1.2 The matter of location (e.g., subcellular locale)	6
1.1.1.3 The matter of pattern (combination of phosphorylation sites)	7
1.1.1.4 The matter of the model system; (low copy protein in mammalian system) 8	
1.1.2 Proteomic methods of studying phosphorylation	9
1.1.2.1 Enrichment of phosphorylated protein/peptides	9
1.1.2.2 Multi-dimensional separation methods	11
1.1.2.3 Mass spectrometry based methods	12
1.1.2.4 Bioinformatic algorithm for prediction of phosphorylation	13
1.2 PROTEOMICS METHODOLOGIES	14
1.2.1 Sample preparation in proteomics	14
1.2.1.1 Multi-dimensional protein separation	15
1.2.1.2 Protein enrichment/elimination	18

1.2.1.3	Isotope labeling in sample preparation.....	19
1.2.2	Advanced mass spectrometry technologies	22
2.0	CDC25B – LIGAND BINDING STUDY.....	24
2.1	THE BIOLOGIC IMPORTANCE OF CDC25B	24
2.2	SMALL MOLECULE INHIBITORS OF CDC25B	25
2.3	CDC25B – NSC93957 INTERACTION	27
2.3.1	Materials and methods.....	27
2.3.2	Results.....	29
2.3.3	Discussion	36
3.0	S-NITROSYLATION IN EARLY HEMORRHAGIC SHOCK	42
3.1	BIOLOGICAL IMPORTANCE OF S-NITROSYLATION.....	42
3.2	S-NITROSYLATION OF PLASMA PROTEINS IN EARLY HEMORRHAGE 44	
3.3	DETECTION OF S-NITROSYLATION	45
3.4	EARLY HEMORRHAGE MODEL AND NO DONOR TREATMENT.....	45
3.5	IDENTIFICATION OF S-NITROSYLATION AND ALTERATION OF RAT PLASMA PROTEOME IN HEMORRHAGE.....	47
3.5.1	Materials and methods.....	47
3.5.2	Results.....	55
3.5.3	Discussion	72
4.0	SERUM RESPONSE FACTOR	85
4.1	THE FUNCTION OF SERUM RESPONSE FACTOR IN CARDIAC HYPERTROPHY	85

4.2	THE PHOSPHORYLATION OF SRF.....	86
4.3	SELECTIVE PHOSPHOPEPTIDE LABELING	88
4.4	NEW PHOSPHORYLATION SITES ON SRF	90
4.4.1	Materials and methods.....	90
4.4.2	Results.....	100
4.4.3	Discussion	106
4.5	TANDEM AFFINITY-TAGGED PURIFICATION.....	108
4.6	STABLE TRANSFECTION OF SRF.....	111
4.6.1	Materials and methods.....	111
4.6.2	Results.....	114
4.6.3	Discussion	121
5.0	IDENTIFICATION OF PSEUDOPODIA PROTEOMES	124
5.1	PSEUDOPODIA PROTEOME PREPARATION	124
5.2	IDENTIFICATION OF PSEUDOPOD PROTEOMES	125
5.2.1	Materials and methods.....	125
5.2.2	Results.....	130
5.2.3	Discussion	136
APPENDIX A.....		140
ABBREVIATION		157
BIBLIOGRAPHY		160

LIST OF TABLES

Table 1. Summary of protein post-translational modifications.	2
Table 2. Summary of physicochemical properties of α -amino acids found in proteins.	35
Table 3. Peptide fragments from LC-MS/MS for “TRFE_HUMAN serotransferrin precursor (transferrin)”	64
Table 4. MALDI-MS matching results for NO donor-treated human transferrin <i>in vitro</i>	65
Table 5 MASCOT searching result for rat plasma treated with NOC7	69
Table 6 Protein identification and relative ratios of protein levels (compared to control) for rat plasma proteome with NOC-7 treatment.	71
Table 7 Calculation table for PhIAT reaction adducts.	101
Table 8 Peptide identification chart for PhIAT labeled SRF-pA digest after avidin column elution.	102
Table 9 The peptides identified by MALDI-TOF-MS and –MS/MS for GST-SRF.	105
Table 10 Stoichiometry of SRF for study of its direct binding partners and phosphorylation.	107
Table 11. The differentiation delay and protein expression levels of SRF-pA versus SRF.	118
Table 12. Ratio of differences in protein levels between pseudopodia and whole cell lysates from U87 cells.	132
Table 13. MS-MS peptide summary for the 68 kDa band in lysate of Ps formed by cultured astrocytoma cells.	134

LIST OF FIGURES

Figure 1 Molecular structure of NSC95397	25
Figure 2 Trypsin digestion map of Cdc25B after interaction with NSC95397	29
Figure 3 Trypsin digestion map of Cdc25B adduct after interaction with NSC95397.....	30
Figure 4 3-D crystal structure adapted from protein data bank (PDB entry ID No: 1QB0).	31
Figure 5 Possible reaction mechanisms between Cdc25B catalytic domain and NSC95397 (Adducts 1, 2 and 5).....	32
Figure 6 Possible reaction mechanisms between Cdc25B catalytic domain and NSC95397 (Adducts 3)	32
Figure 7 Possible reaction mechanisms between Cdc25B catalytic domain and NSC95397 (Adducts 4)	33
Figure 8 Possible reaction mechanisms between Cdc25B catalytic domain and NSC95397 (Adduct 6).....	33
Figure 9 The biological functions that <i>O</i> -phosphorylation and <i>S</i> -nitrosylation share.....	43
Figure 10 Quality control during the biotin switch assay with albumin depletion for rat plasma samples	57
Figure 11 Fluorescence analysis of deposition of <i>S</i> -nitrosothiols in red blood cells and traditional 2-D gel stained by SYPRO-Ruby fluorescence dye.	58

Figure 12 Schematic diagram of the biotin switch <i>S</i> -nitrosylation assay.	60
Figure 13 The decomposition of SIN-1 and generation of ONOO ⁻	62
Figure 14 Schematic of the formation of nitrite from peroxynitride.	62
Figure 15 Base peak of full scan mode for human transferrin tryptic digest after treatment with ONOO ⁻	64
Figure 16 Sequence homology between human and rat ceruloplasmin.	68
Figure 17 1-D SDS-PAGE gel (Coomassie blue staining) for <i>in vitro</i> ONOO ⁻ -treated rat plasma samples.	68
Figure 18 Representative DiGE results after DeCyder software analysis of albumin depleted rat plasma.	70
Figure 19 The reactions in the phosphopeptide isotope affinity tag (PhIAT) method	89
Figure 20 Avidin column OD ₂₈₀ readings for elutions and washings of PhIAT-labeled peptides.	100
Figure 21 SYPRO-Ruby stained gel images for GST-SRF quantification and phospho-SRF identification.	103
Figure 22 The optimization of G418 concentration for stable transfection of SRF-pA	115
Figure 23 Retained function and cellular localization of SRF-pA, and retained differentiability of SRF-pA stably transfected C2C12 cells.	116
Figure 24 Level of SRF expression in different transfection systems.	118
Figure 25 Optimization of temperature and time of TEV cleavage conditions.	119
Figure 26 IgG column coupled TEV cleavage optimization for DTT concentration, incubation temperature and time.	120
Figure 27 Representative DiGE images of paired whole cell and pseudopodia lysates	131

Figure 28 The topographically rendered densitometry results for BSA isoforms in the DIGE gel shown in Figure 27.....	132
Figure 29 Identification of pseudopodia proteins compared to proteins in the unmigrated cell.	133
Figure 30. MALDI-TOF-TOF-MS spectra for precursor ion m/z 1479.77.....	134
Figure 31. Adherence of F-BSA to newly-formed Ps of LN229 cells.....	135

PREFACE

I would like to thank Profs. Billy W. Day and Jorge L. Sepulveda for giving me the great opportunity to work on very exciting projects in their laboratories, and allowing me to learn such a wide range of methods. Without their constant support and guidance, both morally and technically, the fulfillment of these projects would not have been possible.

I would also like to thank many collaborators, Profs. Marie Beckner, John Lazo, Peter Wipf and Kaikobad Irani, and Col. James Atkins and Dr. Nikolai Gorbunov for providing to me great chemical and biological systems, technical assistance and a supportive environment for me to perform a wide range of work.

Special thanks go to Nancy Huang for all her practical and theoretical advice as well as for her daily and spontaneous help in many occasions.

I want to thank also the current and previous members of the Proteomics Core Lab whose practical suggestions helped me grasp many proteomics techniques: Drs. Emanuel Schreiber, Manimalha Balasubramani, Tamanna Sultana and Ashraf Elamin, and Xuan Chen, and Jiyan An. They provided an excellent working environment and technical support.

I am also grateful for assistance from and creative discussions with Yuan Yao and Wen Yan (Sepulveda lab), Dr. Raghavan Balachandran, Miranda Sarachine, Brianne Raccor, Guangyu Zhu and Yun Fan (Day lab), and my fellow graduate students at the School of Pharmacy.

Last but not least, I would like to thank my best friend Beilei Zhang for her loving support and my parents for giving me the freedom to study whatever I wanted and for always supporting me as best as they possibly could.

This work was supported in part by the School of Pharmacy, the Nick Eric Wichman Foundation, The Beez Foundation, NINDS K08 NS41340, and DoD/TATRC USAMRMC grant 04145001.

1.0 INTRODUCTION

After their translation from mRNA, proteins are often chemically altered by biological machinery. This post-translational modification (PTM) extends the range of function of target proteins. PTMs come in many forms. Often, they are the result of enzyme-mediated covalent attachment of a variety of biochemical functional groups to the protein, including most commonly acetate, phosphate, carbohydrates and lipids. In addition, non-enzymatic modifications may occur often on particular reactive amino acids, such as cysteine (e.g., disulfide bond formation, *S*-nitrosylation) and methionine (e.g., sulfoxidation). Furthermore, restricted proteolysis (e.g., enzymatic conversion of preproalbumin to proalbumin, which is followed by enzymatic proteolysis to form albumin) or chemical group removal (deamidation of a glutamine) are also commonly encountered protein modifications. It should be noted that even very minor structural modifications could inactivate, or activate, a particular function of a protein. Structural alterations as a result of PTM can be very subtle, but critical for the functionality that gained or lost during the process of modifications. Table 1 summarizes all the presently known potential PTMs for amino acid residues.

PTMs including addition of functional groups	
Acetylation	N-terminus
Alkylation	Methylation at lysine or arginine
Biotinylation	Acylation of conserved lysine
Glutamylation	Covalent linkage of glutamic acid to tubulin and some other proteins
Glycylation	Covalent linkage of one to more than 40 glycine residues to the tubulin C-terminal tail
Glycosylation	Addition of a glycosyl group to either asparagine, hydroxylysine, serine, or threonine,
Isoprenylation	Addition of isoprenoid group, e.g. farnesol and geranylgeraniol
Phosphopantetheinylation	Addition of a 4'-phosphopantetheinyl moiety from coenzyme A, as in fatty acid, polyketide, non-ribosomal peptide and leucine biosynthesis
Phosphorylation	Addition of a phosphate group to serine, threonine, tyrosine and histidine;
S-nitrosylation	Addition of a nitroso group to cysteine
Sulfation	Addition of a sulfate group to tyrosine
PTMs including addition of other proteins or peptides	
Isgylation	The covalent linkage to the ISG15 protein (Interferon-Stimulated Gene 15)
SUMOylation	The covalent linkage to the SUMO protein (Small Ubiquitin-related MOdifier)
Ubiquitination	The covalent linkage to the protein ubiquitin
PTMs changing the chemical nature of proteins	
Citrullination/Deimination	The conversion of arginine to citrulline
Deamidation	The conversion of glutamine to glutamic acid or asparagine to aspartic acid
PTMs involving structural changes	
Disulfide bridge	Covalent linkage of two cysteine amino acids

Table 1. Summary of protein post-translational modifications.

Proteomics, a term coined to draw an analogy to genomics, is the large-scale study of proteins, with particular emphasis on identifying all, many or the altered proteins in a biological system. Proteomics also includes the study of protein structure and function. Most importantly, while the genome is a rather constant entity, the proteome differs from cell to cell and is constantly changing due to its biochemical interactions with the genome and the environment. A multicellular organism invariably has radically different protein expression levels and identities in its different parts, in the different stages of its life cycle, and in different environmental conditions. The proteome refers to all the proteins produced by an organism, much like the

genome is organism's entire set of genes. Even though there are only 25,000-30,000 human genes, it is estimated that the human body may contain more than 1,000,000 different proteins, each having different functions.[1, 2] Thus, proteomics is the study of the composition (and when possible, also structure and function) and the interactions of the proteins directing the activities of each living cell.

As the main components of the physiological pathways of the cells, proteins serve vital functions in the body. Functional proteomics is the study of proteins in a dynamic system, in which PTMs and protein-protein interaction analyses presently play a prominent role. In contrast with high-throughput proteome screening for biomarker detection, where large-scale identity-based screening is done in searching of potential network components and interaction partners[3-7], functional proteomics emerged to ask more specific questions regarding the relationship between the chemical modification(s) of a particular proteome and functionality of the biological system.[5, 8, 9] Whereas high-throughput screening and functional proteomics are both hypothesis-generating approaches, targeted functional proteomics is a hypothesis-driven approach. It is possible to question and study a post-translational modification of one protein only when the regulatory network enclosing this protein has been well studied. In targeted functional proteomics, the focus is on understanding the characteristics as well as kinetic relationships between a particular regulatory protein and a known biological system using mass spectrometry-based techniques. In this dissertation, pioneering work in targeted functional proteomics, with special focus on the role and PTM status of one protein (i.e., serum response factor-1) during malfunction-related biological process (i.e., myoblast cell differentiation), is presented. At the same time, broader functional proteomics work regarding the relationship between plasma proteome regulation and early hemorrhage was studied.

1.1 PHOSPHORYLATION

Phosphorylation of hydroxyl groups on side chains in proteins (i.e., serine, threonine and tyrosine hydroxyls) is estimated to affect nearly 30% of the eukaryotic proteome, and is a major regulatory process for many basic cellular events. [10, 11] Thanks to recent and fast development of high throughput proteomics technologies, the understanding of phosphorylation on a global scale is increasing. [10-12] However, much work is still needed in order to decipher the biological relevance of these phosphorylations.

The four basic criteria whereby the physiological significance of phosphorylation-dephosphorylations as they pertain to enzyme function consist of the:

1. Demonstration *in vitro* that the enzyme can be phosphorylated stoichiometrically at a significant rate in a reaction(s) catalyzed by an appropriate protein kinase(s) and dephosphorylated by a phosphoprotein phosphatase(s);
2. Demonstration that functional properties of the enzyme undergo meaningful changes that correlate with the degree of phosphorylation;
3. Demonstration that the enzyme can be phosphorylated and dephosphorylated *in vivo* or in an intact cell system with accompanying functional changes;
4. Correlation of cellular levels of protein kinases and/or phosphoproteins phosphatase effectors and the extent of phosphorylation of the enzyme.

1.1.1 The difficulties in studying protein phosphorylation

1.1.1.1 The matter of math (i.e., stoichiometry)

It is widely known that human genome has about 35,000 genes. An active cell has about 40,000 mRNA molecules at any given time. Each medium sized mammalian cell has approximately one billion (total) protein molecules.[13, 14] Excluding the 100 most abundant proteins, which account for about 90% of the dry protein mass, the range of the copy number of the remaining 10% less-abundant proteins is easily 6 orders of magnitude, from matrix proteins (e.g., actin), to putative regulatory protein, which are present at only only 50 or fewer copies per cell. Therefore, in order to study low copy number regulatory protein (e.g., a transcription factor, whose typical copy number per cell is about 100-500) and knowing that the yield from a 10-cm culture dish (assuming cells are grown to 2×10^6 cells/dish) would maximally yield 1.5×10^{-15} moles (i.e., 1.5 fmol), considerable cell culture efforts must be expended. The situation is in fact even more challenging if phosphorylation/dephosphorylation is an important part of the protein's function. In any activation/de-activation event, the amount of the phosphorylated form of that protein would typically be no more than 10% of its total population. Therefore, from 2 million cells, there is, at most, 0.15×10^{-15} mole (i.e., 150 amol) of that protein in its activated form. Because of the low stoichiometry of the phospho-proteome, it is no surprise that anyone choosing a direct study of phosphorylated proteins faces a tremendous challenge in terms of separation/enrichment methods, as well as the feasibility of detection/reading systems used. Another complicating matter is that alkyl phosphate esters (i.e., phosphorylated serine and phosphorylated threonine) are chemically labile. Finally, the determination of a single time point “snapshot” of the phosphoproteome is almost invariably inadequate, as biological phosphorylation is highly dynamic.

Unlike traditional reading systems such as the Western blot, which can amplify the signals up to 1×10^6 -fold based on the high affinities of antibodies, mass spectrometry-based proteomics provides limited, if any, signal amplification. However, modern mass spectrometry can reveal the identity of proteins, including sometimes the even very detailed information regarding PTMs. The capacities and limitation as well as the advantages and disadvantages of mass spectrometry-based proteomics technology in phosphorylation studies will be discussed more in detail in section 1.1.2.

1.1.1.2 The matter of location (e.g., subcellular locale)

In eukaryotic cells, the cytoplasm occupies nearly half of the cell volume, and contains the most abundant structural and metabolic proteins, such as actin, GAPDH, etc., and comprises almost 80% of the cellular mass. In the nucleus, because about 90% of the mass is chromatin (when extracted using isotonic (~150 mM KCl) buffers), the amount of non-chromatin protein in the nucleus therefore accounts for about 2% of the total cellular protein. Overall, in a mammalian cell lysate, the extraction ratio between cytosolic and nuclear proteins often ranges from 10:1 to 20:1 under isoelectric conditions.[15] Therefore, serious attention must be paid to the cellular location of the protein in question when employing proteomics approaches, in that mass spectrometry has the requirement for a higher amount of protein than does traditional antibody-based methods.

In addition to the stoichiometry problem, other subcellular compartment-related issues exist. For example, phosphate-containing contaminants can vary dramatically depending upon the subcellular locale, and they should be carefully removed, or avoided. Phospholipids can be extracted from protein preparations using chloroform/methanol or ether/ethanol mixtures to them when studying cytosolic targets.[16] Phosphate-associated contamination from nucleotides and

nucleic acids can be eliminated by incubation of protein preparation with DNAase or RNAase when studying nuclear proteins, such as transcription factors.[17] However, if changes in enzyme activities in extracts are to be used as indirect reading indices to assess protein phosphorylation, partial or complete purification of the protein from phosphate-containing contaminants is not always a necessity.

1.1.1.3 The matter of pattern (combination of phosphorylation sites)

The tendency of a protein to be a target for phosphorylation is basically determined by its amino acid sequence. Conformational change due to phosphorylation is the key triggering event during functional regulation processes. This structural consequence of phosphorylation usually requires not a single, but several phosphorylatable sites to act simultaneously. The amino acids flanking a phosphorylatable site help in kinase recognition, and the entire region is called a “motif”. [18-21] Quite often, function-related process involves the participation of more than one motif from a key regulatory protein, or several cooperating protein partners with different sets of motifs. The conservative nature of these motifs has assured their evolutionary importance, so that the knowledge of these motifs is of great interest for the understanding of the molecular mechanisms behind many diseases. Over a time course, the dynamic on/off of phosphates and the multi-site nature of phosphorylation give this complex event many snapshots, which we call a “pattern” of phosphorylation.[22-24] One or maybe several combinations of phosphorylation pattern(s) can determine the level, extent and status of phosphorylation. For example, out of 10 molar target proteins phosphorylated in a cellular event, only three moles of the protein may have phosphorylated serine-A, but 10 moles may have phosphorylated serine-B and threonine-C; whereas in another event, 10 out of 10 moles of the protein may be phosphorylated at serines A,

B and C. This would make serine-A the critical regulatory site in functional switching between the two cellular events based on the two different patterns of the protein's phosphorylation.

In other words, simply knowing whether or not the protein is phosphorylated is not satisfactory, because the pattern of phosphorylation, which demonstrates the combination of the sites and the extent of the event, contains more valuable and physiologically relevant information. Microanalysis of phosphorylation can better describe the matter in the modern study of phosphorylation. Such microanalysis, by definition, is the chemical identification and quantitative analysis of very small amounts of matter.

1.1.1.4 The matter of the model system; (low copy protein in mammalian system)

Mammalian systems have the most intensive known phosphorylation potency. About 30% of the mammalian proteome is phosphorylated, whereas about 7% of yeast proteins are phosphorylated. Across bacteria and other lower level kingdoms, on average, it is predicted that from 18% (*Caenorhabditis elegans*) to 32% (*Drosophila melanogaster*) of all serine residues in eukaryotic proteome are phosphorylated (at any given point in time), whereas this number ranges from only 2% in bacteria to 7% in viruses. Similarly, the percentage of predicted phosphorylated threonines in eukaryotic proteomes (5~9%) exceed those in bacteria (2%) and archaea (2%). The percentage of tyrosine phosphorylation is similar across all species, from 4 to 5% in prokaryotes, viruses and archaea, and from 6 to 8% in eukaryotes. [19] Therefore, it is, in some sense, advantageous to study mammalian phosphorylation because of its larger pool of the overall phosphorylated proteome. However, as stated above, the stoichiometry of mammalian phosphorylation makes for a challenge to in-depth targeted phosphorylation research, in that comparing to other model systems, not only the scale of controllable protein expression is

smaller in mammalian system, but the greater complexity of mammalian functional network brings in extreme challenge.

There have been several large scale phosphoproteomic studies to date, including yeast[10], mouse[25], human[11, 26-31], and plants[32]. Among these studies, the trend of focusing on a particular organism or cellular compartment and/or toward looking at a certain disease or malfunction-related pathway proteome is very obvious. Although these high-throughput screening approaches did give us vast amount of information not only of the overall picture of the phosphorylation networks, they also facilitated a hypothesis-generating process. The result is that the regulatory relationship between the network components still requires further in-depth exploration.

1.1.2 Proteomic methods of studying phosphorylation

Phosphorylation or de-phosphorylation is one of the most important regulative chemical behaviors that are vital to almost all cell signaling processes. Nearly 30% of the proteome is phosphoproteins, whose function is regulated by the interplay of two counteracting classes of enzymes, protein kinases and phosphatases. There has been a revolutionary change as to the methodologies of phosphorylation, indicated by the trend from mainstream characterization and semi-quantitation methods towards pattern recognition and kinetics-motivated, new approaches.

1.1.2.1 Enrichment of phosphorylated protein/peptides

Due to the low stoichiometry, heterogeneity and low abundance, enrichment of phosphorylated protein/peptides is crucial for phosphoproteomics research. In addition to the traditional strategy of multi-peptide separation, which is based on different hydrophilic nature of

the complex mixture, more selective approaches for phosphopeptides have been developed over the last decade.

The first is antibody-based affinity chromatography. Immunoprecipitation using anti-phosphoserine, -phosphothreonine, or -phosphotyrosine antibodies have become more and more specific and also commercially available. To date, antibodies specific to pTyr residues have been the most common for use because of the availability of a variety of high affinity, high specificity antibodies; this is also true but to a lesser extent for are antibodies to pSer and pThr. Although the ratio of pSer-pThr-pTyr sites naturally found in proteins is about 90:10:1 and it has been shown that in many cases the determination of pTyr sites was greater than one would suspect according to their prevalence.[33] This may be due to the presumption of greater importance of pTyr sites in signaling pathways and thus a greater effort to discern these sites on signaling proteins. In light of the fact that more of the endogenous phosphorylable sites are serines than tyrosines, it will be only the matter of time that we see more commercially available specific antibodies specific to pSer, as well as more researchers point more attention and focus onto its study.

The second is ion exchange chromatography (IEC). IEC represents a fast growing, “re-discovered” research method. In the phosphoproteomics world, a more often used IEC method is immobilized metal affinity chromatography (IMAC). IMAC uses immobilized (by chelation) multiple positively charged heavy metal ions to bind to negatively charged regions of the peptides, among which phosphate groups are the major targets for the affinity (actually, ion-pairing) binding. However, due to the nature of the positive/negative charge-based pairing mechanism, not only are phosphopeptides bound, but also acidic peptides and peptides containing histidine. Despite a recent work-around method developed by Ficarro et al., who

converted carboxylic acid groups to methyl esters, this pitfall of the IMAC approach still remains as a great concern, in e.g., analysis of DNA-bound transcription factors, where hidden interfering side groups might escape from the chemical modifications in response to extracellular stimulations or biological function. [11]

The third method is β -elimination. The phosphoric acid groups from in phosphoserines/phosphothreonines can be induced to undergo an β -elimination reaction. β -Elimination of phosphoserine/phosphothreonine leads to loss of one equivalent of phosphoric acid. The net result is that the β -elimination reaction leaves a marker, the equivalent of water loss on the amino acid residues that are phosphorylated, which facilitates the determination of the site(s) of phosphorylation by tandem mass spectrometry.[34, 35] For phosphoserines, the difference in m/z values of adjacent y ions is 69 with the presence of the β -elimination product; that is, dehydroalanine (69 Da) is detected, rather than an unmodified serine (87 Da). Since phosphorylated serine and threonine residues, but not phosphotyrosine, can undergo β -elimination very efficiently, this method can only be used for the study of phosphorylation by serine/threonine kinases or dual specificity phosphatases. [36, 37]

1.1.2.2 Multi-dimensional separation methods

Two dimensional tryptic peptide mapping coupled with $[\gamma\text{-}^{32}\text{P}]\text{-ATP}$ labeling and autoradiography can be a useful in vitro probing tool for the study of phosphorylation.[38] However, this method does not work as well for multisite phosphorylated peptides as it does for single phosphorylated peptides, and the accessibility of radioactive label and trypsin cleavage is a detriment to the quantification potential of this method. The reader should be reminded that phosphorylation is one of only many posttranslational modifications that occur in the proteome; other modifications, such as deamidation,[39] uridylylation,[40] adenylylation,[41]

methylation[42], acetylation[43] and amino acid substitution (i.e., isoforms) may occur intracellularly, while proteolysis and oxidation may occur during purification. In addition, carbamylation (the reaction of cyanate, formed from e.g., urea, with amino and sulphydryl groups) may occur during electrophoresis in urea. All of these factors will impair the direct link between net charge difference and molecular weight-based two-dimensional separation of phosphorylated components. In other words, the mobility shift noted for a protein in a gel might be caused by any variety of intracellular modifications other than solely by phosphorylation.

In addition, when a sodium dodecylsulfate (SDS)-based 2D gel system is used, phosphorylation can disturb effective SDS-protein binding by altering the accessibility of binding sites. Consequently, the increased negative charges brought about by phosphorylation might not affect the pronounced net negative charge imparted by the SDS-protein binding, which in turn determines the electrophoretic mobility of the target protein.

2D Gel electrophoresis no longer requires the use of SDS; other ion-carrier systems can be used to provide less interference and better resolution. Although the 2D gel techniques (see section 1.2.1.1 for more detail) used today has already passed its infancy and became a widely used technique for phosphorylation researchers, it is important to note that only a further mass spectrometric fingerprinting can tell if the separated spots represent series of phosphorylation stages, because the separation itself cannot guarantee the recognition of the type of PTM (again see Table 1).

1.1.2.3 Mass spectrometry based methods

Isotopic labeling approaches have emerged since the early 1990's to facilitate to some extent separation but more importantly ratio-based quantification. [44-46] Two basic methods, either substitution or tagging of the phosphopeptide with an isotopically coded derivatizing agent

in a single process, or by coding and selecting phospho-peptides in separate operations, are used in phosphoproteomics. In some reports, absolute quantification has been claimed to be achieved by using internal standards, in which an isotopically labeled isoform of a standard synthesized peptide is added to a mixture at a known concentration.[47, 48] One of the surprises is that isotope coding can be a valuable aid in the examination of intermolecular association of proteins through stimulus-response studies. MS is able to deliver information about the location of phosphorylation sites, but phosphospecific properties with respect to ionization present obstacles. Therefore, multidimensional approaches involving several analytical methods are often necessary to conquer phosphorylation site identification. More detailed information about stable isotope labeling is included in the Section 1.2.1.3.

1.1.2.4 Bioinformatic algorithm for prediction of phosphorylation

In addition to the fact that about one-third of all the eukaryotic proteins are phosphorylated, about half of the kinase genome (a.k.a. kinome) has been found by chromosomal mapping to be disease- or cancer-related.[49] Therefore, recent development of prediction of phosphorylatable substrates has been in great demand for rational drug design and mechanistic studies. There are several open-source website or search engines for phosphorylation site prediction. NetPhos 2.0 is a web server that gives an *in silico* prediction of phosphorylation sites based on “artificial neural network (ANN)”. [20, 21] Scansite 2.0 was created to search for short peptide motifs within proteins that are likely to be phosphorylated by specific protein kinases or bind to other proteins via SH2, 14-3-3 or PDZ domains, etc.[18] Another similar method, PredPhospho [50] is a search engine based on support vector machines limited to phosphorylation sites catalyzed by four protein kinase families and four protein kinase groups, with accuracy of the predictions ranging from 83% to 95% at the kinase family level, and 76% to

91% at the kinase group level. A newer computational method, GPS [51], has greater precision and computer power over Scansite and PredPhospho, and was built on a group-based phosphorylation site prediction algorithm. The disorder-enhanced phosphorylation sites predictor (DISPHOS v1.3) [19] computationally predicts serine, threonine and tyrosine phosphorylation sites in proteins from a training set of over 2000 non-redundant experimentally confirmed protein phosphorylation sites (1,079 serine, 666 threonine and 375 tyrosine sites). Aside from the differences in their fundamental algorithms, all of the above follow at least a widely adopted rule that a protein kinase's substrates can be phosphorylated at the specific sites with consensus sequences/motifs/functional patterns.[52]

The ability to predict potential phosphorylation sites, especially for novel proteins, gives a helping hand to discovery of new phosphorylation-related biological processes. There still remains the need, however, for careful experiment design, including traditional biology techniques and many others, to understand phosphorylation in a profound way regarding the context of living organisms.

1.2 PROTEOMICS METHODOLOGIES

1.2.1 Sample preparation in proteomics

Compared with the traditional protein extraction methods (that precipitate, or phase-separate proteins from complex mixtures), proper protein sample handling in a proteomics study requires additional cautions in that the compatibility with the mass spectrometry interface is a key factor that determines the unique requirements and fundamental controls used in proteomic

approaches. Along with the increasing capacity of handling sub-femtomole (i.e., 1×10^{-15} mole), in some cases even attomole (i.e., 1×10^{-18} mole), levels of protein sample due to advanced mass spectrometry, it becomes more challenging to prepare samples that will fully utilize the highly sensitive instruments' capacity without losing important, biologically-relevant information. In other words, successful protein handling prior to mass spectrometric analysis is pivotal in order to amplify the signals in physiological conditions to an extent that is readable by the current techniques.

1.2.1.1 Multi-dimensional protein separation

Two-dimensional gel electrophoresis, commonly abbreviated as 2-DE or 2-D electrophoresis, is a form of gel electrophoresis commonly used to analyze a complex mixture of proteins. Opposed to 1-D electrophoresis, which separates denatured proteins (or other analytes) by the rate at which they traverse an acrylamide-based matrix under the influence of an electric field (i.e., according to their apparent molecular radii) in one dimension, 2-D electrophoresis begins with isoelectric focusing followed by acrylamide-based electrophoresis in a direction 90 degrees from the first. The result is that the analytes are spread out across a 2-D surface rather than along a line. Because the chance is smaller of two analytes having both the same isoelectric point (pI) and molecular radius (Mr), analytes are more effectively separated in 2-D electrophoresis than in 1-D electrophoresis.

To separate the proteins by pI , a gradient of pH is applied to a gel and an electric potential is applied across the gel, making one end more positive than the other. At pHs other than their isoelectric point, proteins will be charged. If they are positively charged, they will be pulled towards the more negative end of the gel, and if they are negatively charged they will be

pulled to the more positive end of the gel. The proteins applied in the first dimension will move along the gel and will accumulate at their isoelectric point. That is, the point at which the overall charge on the protein is 0 (i.e., a net neutral charge). In practice, the process is aided by imbedding ampholytes, low molecular weight molecules of zwitterionic character that comprise a multitude of varying pI -values, into agarose or polyacrylamide gels so that a linear pH gradient will be built up when an electric field is applied. The ampholyte molecules carry a net charge and thus migrate in the electric field between the electrodes as long as they will reach the position of their corresponding pI . They will stop moving then and form small plateaus (stationary stacks).

Before separating the proteins, they are treated with denaturing agent, which unfolds them into long, straight molecules. This is a way to equalize effects on structurally dissimilar proteins so that length (when unfolded) is roughly proportional to its mass. In addition, proteins will not migrate in an electric field when they have no charge (a result of the isoelectric focusing step); therefore the negative charge of the hydrophobic detergent (e.g., SDS) used in the second dimension allows migration, and the number of negative charges associated with the protein is a function of its length/molecular weight. In the second dimension, an electric potential is again applied, but perpendicular from the first field. The proteins will be attracted to the more positive side of the gel proportionally to their mass-to-charge ratio. The gel therefore acts like a molecular sieve when the current is applied, separating the proteins on the basis of their molecular weight with larger proteins being more retained in the gel and smaller proteins being able to pass through the sieve and reach lower regions of the gel, with proteins spread out on its surface.

Proteins segregated in such ways can then be detected by a variety of means, but the most commonly used stains are silver ion-based and Coomassie blue staining. In former case, a silver

colloid is applied to the gel. The silver ions binds to sulfur-containing groups (cysteine and methionine) within the protein, and and then oxidized (darkened) by exposure to ultraviolet light. The darkness/density of the resulting silver oxide can be related to the amount of silver ions trapped by the protein, and therefore the amount of protein at a given location on the gel. This measurement can only give approximate amounts, but is adequate for most purposes. Recently developed high sensitivity fluorescent stains, e.g., the SYPRO[®] series (SYPRO-ruby, red, orange, green) label lysines and arginines in proteins with different chemical fluorophores for visualization of different types of proteins on 2D gels, and they have comparable sensitivity with silver staining, but with a simpler procedure.

2-D gel electrophoresis makes possible the separation and estimation of as many as 5000 different proteins in a single experiment. This capability can be critical when studying expression patterns among some subset of the proteome or, alternatively, when studying concentration changes in one or more individual proteins of interest. 2-D gel electrophoresis also has the capacity to resolve various PTMs, changes that cannot be discerned from the corresponding expression patterns in DNA arrays. While this technique provides good single pass coverage for proteins falling in a window bracketed by *pI*s ranging from 3.5 to 10 and *M_r*s ranging from 7000 to 250,000, it does exclude proteins that are very large ($M_r > 250\text{KDa}$) or very small ($M_r < 7\text{KDa}$) and highly acidic ($pI < 3.0$) or highly basic ($pI > 10$) unless the gel format is varied. Sample loading limitations can also cause 2-D gel electrophoresis to fall short in the detection of proteins present at low concentrations. Also, the gel separation system, such as the difference in protein absorption to IPG strips, and the solubility of proteins in rehydration buffer, and so on, can introduce artifacts.

1.2.1.2 Protein enrichment/elimination

As mentioned previously, the cellular abundance of proteins can range across six orders of magnitude. To obtain sufficient quantities of lower copy regulatory proteins for analysis, selective enrichment of target proteins or elimination of over-abundant protein counterparts becomes inevitable, especially for samples that have >90% common proteins as interferences, e.g., albumin in serum samples, and actin or GAPDH in cell lysate samples.

The majority of these current elimination (a.k.a. depletion) methods use antibody-based affinity approaches to extract the proteins from the samples. There are a variety of IgG-based depletion kits that are commercially available. Although the capacities and specificities vary, they share an important common property, which is, unfortunately, an incomplete elimination of albumin. The reason for this is that mammalian serum or plasma is an extraordinarily complex mixture of proteins so that many molecules, including other proteins, bind to albumin, masking it from the IgG. On the flip side, if the entire albumin is removed, many other more valuable proteins or potential biomarkers would also be removed. Therefore, it is preferred that < 85% of the total albumin be removed, which allows for analysis of the albumin-associated proteins.

Often times, the elimination approach is accompanied with the outcome of enriched signals for a subfraction of low abundance proteins. Several methods have been developed based on differential characteristics of target proteins or proteomes. For the study of membrane-associated proteins, i.e., lipoproteins and glycoproteins, they can be enriched and selectively separated from elimination or fractionation of cellular compartments. Another characteristic of these proteins, large molecular weight, e.g., G-protein coupled receptors, can be used to advantage in separating them from smaller and more hydrophilic contaminating proteins by size

exclusion chromatography. Eliminating basic fractions of the sample using isoelectric focusing or pH-dependent precipitation can enrich acidic proteins.

1.2.1.3 Isotope labeling in sample preparation

There are several sample preparation approaches that involve isotope labeling. No matter which isotope or labeling site used, they share a fundamental similarity in that they are all ratio-based (i.e., relative) quantification methods. For most biological questions, which require the ability to perform some type of differential comparison of protein levels with reference to a control state, ratio-based analysis will contribute to an understanding of disease function/processes, as well as of drug treatment and therapeutics.

A number of advances involving stable isotope technology for quantitative profiling via mass spectrometry have been established. The most widely known is the ICAT (isotope coded affinity tags) approach developed by Reudi Aebersold et al. in 1999. [53, 54] In ICAT, two samples are labelled with chemically identical tags that differ only in isotopic composition (heavy and light pairs) and contain a maleimide group (which covalently links to cysteine residues) and a biotin moiety. The samples are individually labeled, combined, enzymatically digested, and the labeled peptides are selectively enriched via biotin-avidin affinity chromatography. Since the difference in mass of the ICAT-labeled peptide fragments is a constant, they can be separated and quantified via mass spectrometry. The advantage of ICAT, which is also its disadvantage, comes from the specific labeling of only cysteine residues in any given protein sample. On one hand, complex samples are simplified, thus allowing the analysis of an increased dynamic range of peptides; on the other hand, because of this cysteine-specificity, many important cysteine-free proteins, including those with post-translational modifications, are overlooked by this technique.

Another similar approach for comparative profiling of proteins in cells is stable isotope labelling by amino acids in cell culture (SILAC), developed by Matthias Mann et al. in 2002.[55, 56] This method incorporates isotopic labels into proteins via metabolic labelling in the cell culture itself, rather than using a covalently linked tag. Thus, cell samples to be compared are grown separately in media containing either a heavy or light form of an essential amino acid (e.g., one that cannot be synthesized by the cell). The advantages of SILAC are that it has higher fidelity than ICAT (incorporating nearly 100% efficiency) and does not require multiple chemical reactions and purification steps, thus ensuring similar conditions for the samples to be compared throughout the experiment. This approach, however, requires viable, actively proliferating cell lines to allow for the complete incorporation of the respective heavy/light amino acids into the protein samples. Complete isotope incorporation is critical, but sometimes not feasible, for all experimental samples.

The iTRAQ (isobaric tags for relative and absolute quantitation) reagents, a new class of isobaric reagents, was developed by Darryl Pappin et al. in 2004, [57] can be used for multiplexed protein profiling of up to four different samples. This unique approach labels samples with four independent reagents of the same mass that, upon fragmentation in MS/MS, give rise to four unique reporter ions ($m/z = 114\sim 117$) that are subsequently used to quantify the four different samples, respectively. The reagents were designed as isobaric tags consisting of (1) a charged reporter group that is unique to each of the four reagents, (2) a peptide reactive group, and (3) a neutral balance portion to maintain an overall mass of 145 Da. The reporter ions are used to quantify their respective sample in MS/MS fragmentation. In addition to giving strong reporter ion signals, tagged peptides also yield strong signature y and b fragment ions without

changing the charge state of the peptide, allowing for more confident protein identification simultaneously with the quantification. The peptide reactive group was designed to react with all primary amines, including the N-terminus and the ϵ -amino group of the lysine side chain. Therefore, all peptides in a tryptic digest are labeled, and the label enhances peptide coverage for any given protein, while allowing for retention of other important structural information such as PTMs. The region in the mass spectrum chosen for the reporter ion was selected for two primary reasons: (1) to keep the additive mass to the fragments as small as possible to minimize any effect in either the MS or MS/MS modes, and (2) to eliminate any interference with other immonium or fragment ions to allow for the highest degree of confidence in interpretation.[48, 58] The disadvantage of this method is that it requires the low mass resolving power for the reporter ions, which should only represent one peptide from the mass spectrometry. This requirement of single peptide separation makes analysis of complex mixtures adventurous, because multiple peptides can give an accumulated reporter ion signal, which impairs the semi-quantitative feature of iTRAQ.

Overall, each of these methods has its specific applicability and disadvantages for biological samples, but there is still no single best procedure for all questions. Despite of its current stage of early development, there are two essential cautions to be noted: (1) isotope ratio analysis of protein concentration between samples does not necessarily relate directly to protein expression and rate of PTM, and (2) that multiple new methods must be developed and applied simultaneously to make existing stable isotope quantification methods more meaningful. Although stable isotope coding methods are powerful new techniques, multiple analytical issues must be solved for such techniques to reach their full potential as a tool to study biological

systems.

1.2.2 Advanced mass spectrometry technologies

Looking back on the history of mass spectrometry, from the ion cyclotron that has been coupled with the Fourier transform (FT) to build the FT-ICR-MS instrument, to the invention of matrix-assisted laser desorption/ionization time of flight (MALDI-TOF-MS), which has been widely adapted in proteomics research, the development as well as the application of mass spectrometry is a strong trend in basic life sciences research. In addition to MALDI, another soft ionization method -- electrospray ionization (ESI) -- broadens the sample handling capacity of mass spectrometry from nanomolar to the sub-femtomolar range. Currently, there are many commercially available tandem MS platforms useful in proteomics, such as nanospray LC-ESI-MS, LC-ESI-3D- and -linear ion trap-MS, MALDI-TOF-TOF-MS, LC-ESI-qTrap-MS, MALDI-TOF-TOF-MS, FT-ICR-MS, LC-MALDI-TOF-TOF-MS, etc. Different platforms have their advantages and disadvantages in terms of sampling capacity, detection, quantification potential, data analysis, and so on.

Electrospray ionization MS/MS has been proven to generate diagnostic and PTM-specific ions or fragments using precursor ion scans or neutral loss scans. However, liquid-based sample preparation, excellence and/or good luck in the chromatographic separations, as well as specific mass spectrometric hardware and software is required to make these scanning methods applicable to the analysis of the highly complex peptide mixtures.

The main advantage of MALDI-TOF-MS is its ease of use, as well as robustness and high sensitivity. There is an increasing interest in combining MALDI-TOF-MS/MS with peptide

separation techniques. [59] In addition, capillary chromatography and electrophoresis have been interfaced to MALDI-TOF-MS/MS in various ways.[60]

Fourier transform ion cyclotron resonance (FT-ICR) MS inherently provides very high mass accuracy and resolving power. Electron capture dissociation (ECD) FT-ICR-MS is a novel technique suited for sequencing of post-translationally modified peptides as it cleaves only the peptide backbone while leaving the modified amino acid side-chains intact.[61] Thus, ECD enables efficient sequencing of phosphopeptides, glycopeptides and other types of modified peptides as well as of intact, modified proteins up to 45 kDa.[62, 63]

2.0 CDC25B – LIGAND BINDING STUDY

2.1 THE BIOLOGIC IMPORTANCE OF CDC25B

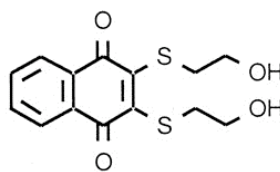
Cdc25B is a dual-specificity phosphatase (DSPase) frequently amplified in common cancers, especially in breast cancer, with >30% overexpression. Overexpression of Cdc25B in transgenic mice results in mammary gland hyperplasia and increased steroid hormone responsiveness that is independent of its C-terminal phosphatase activity. Cdc25B regulates mitosis by the removal of inhibitory phosphates from threonine-14 and tyrosine-15 residues in Cdc2.[64-66] It is known as an initiator of the G2/M transition.[67] Its mRNA is expressed throughout the cell cycle, but is elevated in G2.[68] Overexpression of dominant-negative Cdc25B mutant blocks all evidence of mitosis and results in G2 arrest.[69] Although both Cdc25B and Cdc25C are involved in the control of G2/M transition,[70-72] Cdc25B induces mitosis more efficiently than does Cdc25C.[73]

As a dual-specificity phosphatase, the function of Cdc25B has long been known to be performed through the C-terminus catalytic motif “HCXXXXXR”.[74, 75] where H is a highly conserved histidine residue, C is the catalytic cysteine, the five X residues form a loop in which all of the amide nitrogens hydrogen-bond to the phosphate of the substrate, and R is a highly conserved arginine that hydrogen bonds to the phosphorylated amino acid of the substrate. While the DSPases retain the conserved HCX₅R motif, they are unique in their ability to hydrolyze both

phosphoserine/threonine and phosphotyrosine residues on the same protein substrate.

2.2 SMALL MOLECULE INHIBITORS OF CDC25B

Serine, threonine, or tyrosine phosphorylation can affect catalytic activity or promote protein-protein interactions that influence subcellular location and functionality of kinases and phosphatases.[76] Small molecule inhibitors have provided important tools to decode the roles of kinases and phosphatases participating in specific cellular signaling pathways, because they are generally reversible and readily enter cells. Natural product inhibitors of serine/threonine protein phosphatases, such as okadaic acid and calyculin A, have been extremely valuable reagents to probe serine/threonine phosphatase function. Although the crystal structure has been published for the Cdc25B catalytic domain,[74] (PDB identification code: 1QB0) the nature of interactions with small molecule inhibitors as well as some key conformational changes of protein substrate were not demonstrated.



NSC 95397

Figure 1 Molecular structure of NSC95397

NSC 95397 is a potent *in vitro* Cdc25 inhibitor that was identified using a high throughput screen of 10,070 compounds in a publicly available chemical repository of the National Cancer Institute for *in vitro* inhibitory activity against oncogenic, full-length, recombinant human Cdc25B. NSC 95397 was more potent than any inhibitors of dual specificity

phosphatases described previously and 125- to 180-fold more selective for Cdc25A than VH1-related dual-specificity phosphatase or protein tyrosine phosphatase 1b, respectively.[77] NSC 95397 is a *para*-quinone that showed significant growth inhibition against human and murine carcinoma cells and blocked G2/M phase transition with an IC_{50} of $3.6 \pm 0.6 \mu\text{M}$ for Cdc25B.[78]. A potential Cdc25 site of interaction was postulated in previous study based on molecular modeling with these quinines, where interactions were built between the diones of the inhibitor and the guanidinium side chains of R544, R482 and the phenolic OH of Y428.[77] In this study, the hypothesis was that NSC95397 binds to the catalytic motif of human Cdc25B₂. There were two working hypotheses: (1) NSC95397 binds to Cdc25B via covalent bond(s); and (2) the conformation of Cdc25B changes after interaction with NSC95397. The trypsin protection method and MALDI-TOF-TOF-MS were used to reveal a new interaction site as well as several reaction mechanisms in addition to those found in a previous study. From the information, adduct formation and absence/presence of trypsin-digestible amino acid residues, a new binding pocket for NSC95397 during *in vitro* protein-ligand binding was proposed.

In this study, a trypsin protection assay[79-81], whose basis is that the structural hindrance caused by the binding of an inhibitor will alter the interaction of the enzyme with the protein bound by the inhibitor, was used to map out the potential interaction site(s) between the small molecule inhibitor, specifically NSC95397, and recombinant His₆-tagged Cdc25B₂ catalytic domain (hereafter called Cdc25B). Meanwhile, the possibility of several reaction mechanisms and conformational changes due to ligand binding was also suggested based on the information obtained. This study was designed to give an alternative protein-ligand binding study tool taking advantage of mass spectrometry, which, in this case, was MALDI-TOF-TOF-MS.

2.3 CDC25B – NSC93957 INTERACTION

2.3.1 Materials and methods

In vitro inhibitor binding. Recombinant human Cdc25B catalytic domain was constructed with the QE-30-H25B plasmid (originally obtained from Baylor college, Houston, TX) which expresses His₆-Cdc25B₂. 211 AA), Epitope-tagged His₆-Cdc25B₂, was expressed in *Escherichia coli* and purified by nickel-nitrilotriacetic acid affinity chromatography (obtained from MR. John Skoko in Prof. John Lazo's lab, Department of Pharmacology, University of Pittsburgh, Pittsburgh, PA). Cdc25B was dissolved in buffer containing 10 mM tris-(2-carboxyethyl)phosphine, (TCEP) 150 mM imidazole, and 10% glycerol. Crystalline NSC95397 (obtained from, after its synthesis in, Prof. Peter Wipf's lab, Department of Chemistry, University of Pittsburgh, Pittsburgh, PA) was dissolved in DMSO All other chemicals were purchased from Sigma-Aldrich (St. Louis, MO). The NSC95397 solution was added into Cdc25B-containing buffer solution at molar ratio of NSC95397-Cdc25B of 1:1 and 30:1. The mixed solutions were incubated at room temperature for 1 h, with gentle shaking every 10 minutes.

Trypsin digestion. Porcine trypsin (Gold® version, Promega, Madison, WI) was dissolved at 5 μM in 50 mM ammonium bicarbonate, pH=8.0. Dithiothreitol (DTT) was added, immediately before the digestion, into the trypsin solution to a final concentration 5 mM. The protein was added and the mixture (trypsin–protein ratio of 1:100 (w/w)) was incubated at 37 °C for 2 hours. An additional equal aliquot of trypsin was added and the digestion was continued at 37 °C overnight.

Desalting of the digestion solution. The digested sample solution was desalted using a C₁₈ ZipTip (Millipore, Billerica, MA) following the manufacturer's instructions. Briefly, 1:1 (v/v) of 0.2% TFA-H₂O was added into the sample solution, vortex mixed and centrifuged to pellet any

solids. The ZipTip was pre-wet using 10 μ l of 50% acetonitrile-H₂O, then pre-equilibrated with 10 μ l of 0.5% trifluoroacetic acid (TFA). Digested peptides were bound to the ZipTip by pipetting the digestion solution through it at least 10 times, and salt contaminants were washed off the peptides by pipetting 0.5% TFA-H₂O through the sample five times. After discarding the wash, peptide was collected by gradient pipetting of 25%-100% aqueous acetonitrile. Eluents were pooled and lyophilized to complete dryness.

Mass spectrometry and data analysis. The dried sample was re-dissolved into 5 μ l of matrix solution (50% acetonitrile-H₂O with 0.1% TFA). A matrix solution (saturated matrix solution of α -cyano-4-hydroxycinnamic acid (CHCA) at 10 mg/ml) was mixed 1:1 (v/v) with the sample solution. An aliquot (0.5 μ l) of the mixture was applied onto the ABI 4700 192AB chip and allowed to air dry. Samples were then analyzed by MALDI-TOF-MS on a 4700 Proteomics Analyzer with TOF/TOF optics (Applied Biosystems, Foster City, CA). Internal calibration was achieved using the monoisotopic masses of trypsin autoproteolysis peaks at m/z 842.5094 and 2211.1046. Peptide mass fingerprint searches with the Mascot (<http://www.matrixscience.com>) program, and the MS-Fit, MS-digest, and MS-product programs (<http://prospector.ucsf.edu>) were used for protein identification utilizing the NCBI and SwissProt databases. Search parameters included *Homo sapiens*, all pI 's, monoisotopic peptide masses, tolerance of 20 ppm m/z measurement error, and up to one and four missed trypsin cleavage site per peptide for intact Cdc25B or inhibited Cdc25B, respectively. Other parameters included potential modification of cysteines by acrylamide, oxygenation of methionine and changes at the amino termini, such as conversion of glutamine to pyro-glutamate and acetylation. Trypsin autolysis and keratin-derived peptides were listed as possible contaminants. Protein identifications were accepted when the

observed and predicted molecular range and designation were consistent and scores indicated nonrandom identifications at a significance level of $p < 0.05$.

2.3.2 Results

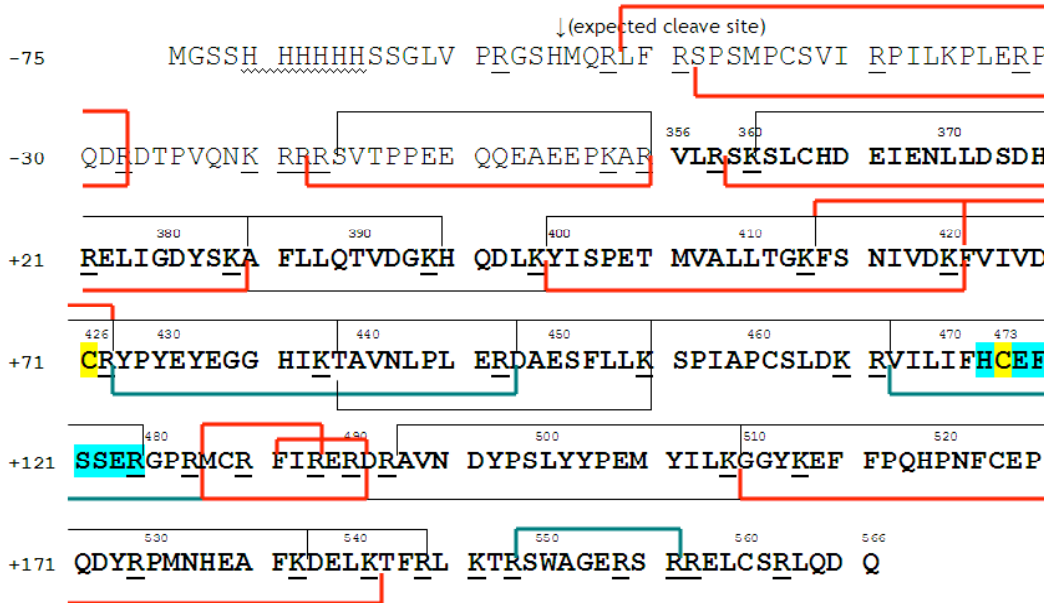


Figure 2 Trypsin digestion map of Cdc25B after interaction with NSC95397

The His₆-Cdc25B₂ catalytic domain sequence is shown. The black letters are amino acid sequence of Cdc25B₂ catalytic domain; the gray letters are amino acid sequences that encode the His tag, and linker peptide at the N-terminus of Cdc25B. The downward arrow shows the His-tag cleavage site. Black lines above/below the sequence encodes the tryptic peptide fragments of the native Cdc25B. Red and blue lines indicate the new and absent tryptic peptide fragments after binding, respectively. The catalytic motif HCY₃R is highlighted in bright blue. The catalytic cysteines are highlighted in bright yellow.

By comparing the theoretical digestion of intact Cdc25B catalytic domain with the experimental mass spectrum, the trypsin digestion map with/without adduct after the interaction with NSC95397 was drawn, shown as Figures 3 and 4.

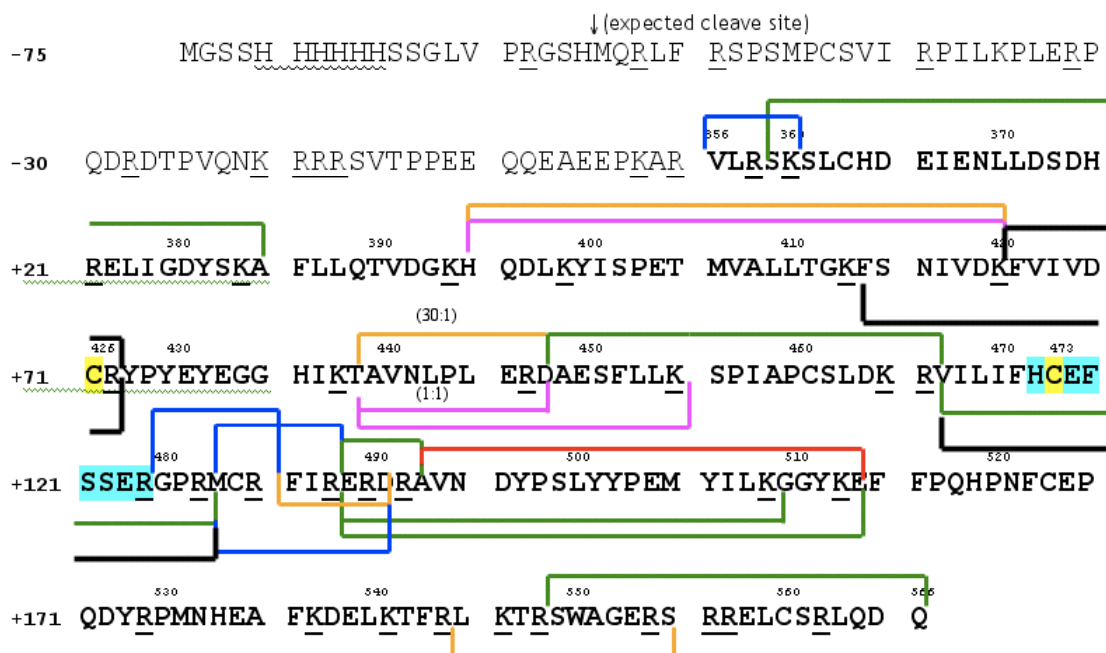


Figure 3 Trypsin digestion map of Cdc25B adduct after interaction with NSC95397

Green lines represent adduct: Cdc25B+NSC95397 (adducts 1); purple lines represent adduct: Cdc25B+NSC95397-2H (adducts 2); orange lines represent adduct: Cdc25B+NSC95397-H₂O (adducts 3); red lines represent adduct: Cdc25B+2NSC95397-2H₂O (adducts 4, this adduct only appeared in samples that have 30:1 ratio of NSC95397: Cdc25B); blue lines represent adduct: Cdc25B+NSC95397+Na (adducts 5). black lines represent adduct: Cdc25B+NSC95397-SCH₂CH₂OH+2H (adducts 6). Molar ratio of 1:1 incubation and 1:30 incubation was noted above the lines. Other letters and highlights are as same as Fig 3. The calibration error was less than 20 ppm for reflector mode MS spectrum, and 100 ppm for MS/MS spectra, both acceptable values.

There were three sites protected from tryptic digestion after incubation with NSC95397, (Fig 4) including ⁴²⁸YPY⁴²⁶EYEGGHIKTAVNLPLERDR⁴⁴⁷, ⁴⁶⁷VILIFHCE⁴⁶⁷FSSERGPR⁴⁸², which enclose the catalytic domain of Cdc25B, and a C-terminal peptide, ⁵⁴⁹SWAGERSR⁵⁵⁶. From these results, it was apparent that previously accessible arginines, namely R447, R482 and R556, were protected from trypsin after the interaction of NSC95397 with Cdc25B. After excluding the N-terminal tail, which does not encode the Cdc25B catalytic domain, there were nine new tryptic fragments after ligand binding. From the new peptide fragments, it can be conclude that K384,

413, 420 and 541, and R427, 488 and 490 became more exposed to trypsin after the protein interacted with NSC95397. (See Fig 5.)

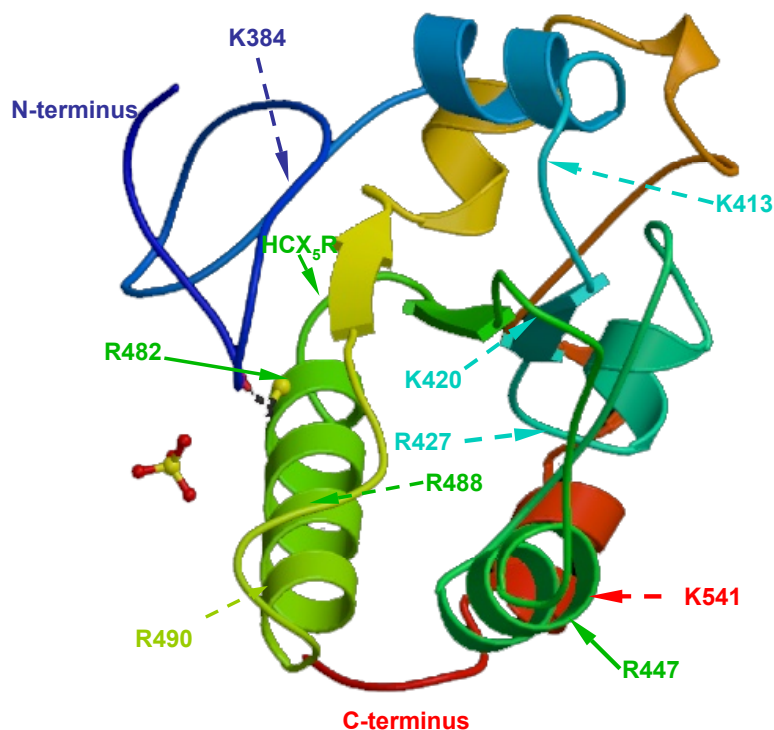
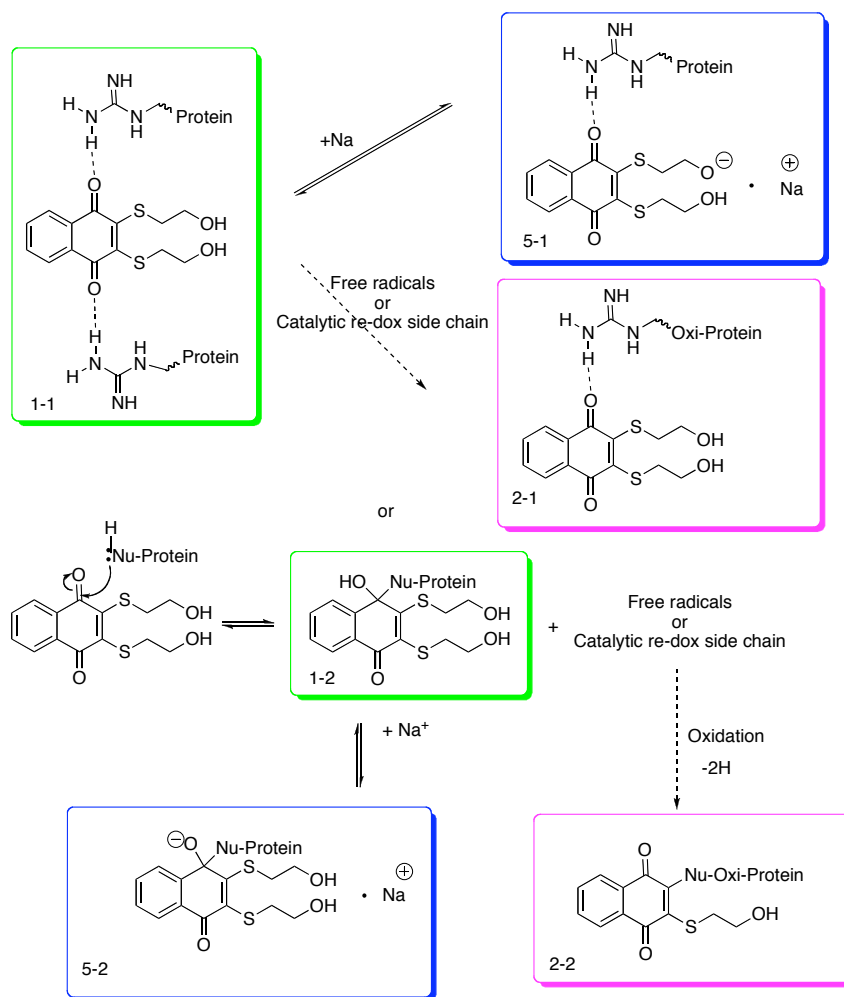


Figure 4 3-D crystal structure adapted from protein data bank (PDB entry ID No: 1QB0).

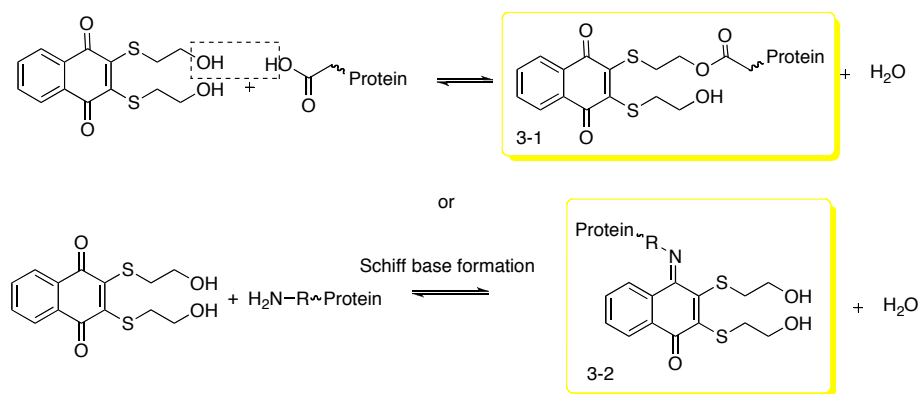
The Cdc25B₂ catalytic domain is shown with secondary and tertiary structure. The covered amino acid sequence is from Asp374~Trp550. The colors of the lines correspond to the locations of the secondary structures; the dashed and the straight lines point to new and eliminated, respectively, tryptic cleavage sites after protein-ligand interaction.

Based on the MS and MS/MS spectra, the analysis of each of the adducts was as below:
(For information about amino acids and their structures that will be discussed, please see Table 2 and Figures 6-9)



Adduct 1: Cdc25B+NSC95397 (Delta m/z= +310.03)
 Adduct 2: Cdc25B+NSC95397-2H (Delta m/z= +308.03)
 Adduct 5: Cdc25B+NSC95397+Na (Delta m/z= +333.02)

Figure 5 Possible reaction mechanisms between Cdc25B catalytic domain and NSC95397 (Adducts 1, 2 and 5).



Adduct 3: Cdc25B+NSC95397-H₂O (Delta m/z=+292.01)

Figure 6 Possible reaction mechanisms between Cdc25B catalytic domain and NSC95397 (Adducts 3)

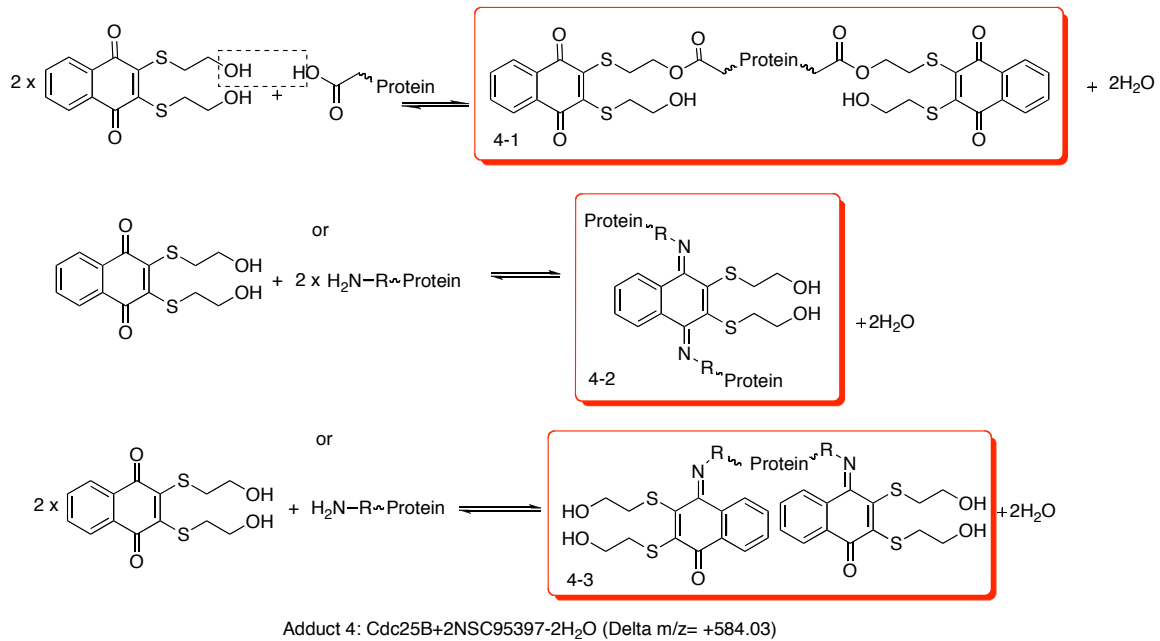


Figure 7 Possible reaction mechanisms between Cdc25B catalytic domain and NSC95397 (Adducts 4)

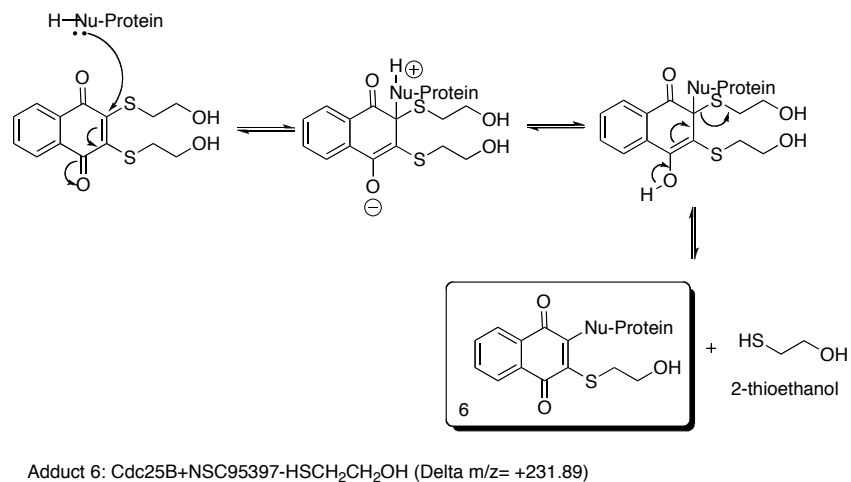


Figure 8 Possible reaction mechanisms between Cdc25B catalytic domain and NSC95397 (Adduct 6)

The adduct Cdc25B+NSC95397 represents zero neutral loss after the binding of Cdc25B and the ligand; i.e., the difference in m/z between the peptide fragments of intact Cdc25B and adduct 1 is equal to the m/z of the ligand, which is 301.03. The adduct Cdc25B+NSC95397-2H

represents the loss of two protons after the binding; i.e., the difference in m/z between the peptide fragments of intact Cdc25B and adduct 2 is 308.03. The adduct Cdc25B+NSC95397-H₂O represents a loss equal to a water molecule after the binding; i.e, the difference in m/z between the peptide fragments of intact Cdc25B and the adduct 3 is 292.01. The adduct Cdc25B+2NSC95397-2H₂O represents the mass loss equal to two water molecules after the binding; i.e., the difference between the peptide fragments of intact Cdc25B and the adduct 4 is m/z 584.03. The adduct Cdc25B+NSC95397+Na represents the addition of a sodium ion during aqueous incubation, which then consequently ionized with zero neutral loss, because the difference in m/z between the intact Cdc25B peptide fragments and the adduct 5 is 333.02. The adduct Cdc25B+NSC95397-HSCH₂CH₂OH represents that it has mass loss equal to one molecule of 2-thioethanol; i.e. the difference in m/z between the intact Cdc25B peptide fragments and the adduct 6 is 231.89.

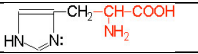
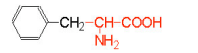
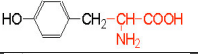
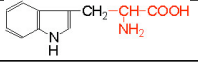
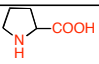
Amino Acid	Symbol	Structure	pK ₁	pK ₂	pK R Group	Hydropathy Index
			(COOH)	(NH ₂)		
Amino Acids with Aliphatic R-Groups						
Glycine	Gly - G	$\text{H}-\text{CH}-\text{COOH}$ NH_2	2.4	9.8		-0.4
Alanine	Ala - A	$\text{CH}_3-\text{CH}-\text{COOH}$ NH_2	2.4	9.9		1.8
Valine	Val - V	$\text{H}_3\text{C}-\text{CH}-\text{COOH}$ $\text{H}_3\text{C}-\text{NH}_2$	2.2	9.7		4.2
Leucine	Leu - L	$\text{H}_3\text{C}-\text{CH}-\text{CH}_2-\text{CH}-\text{COOH}$ $\text{H}_3\text{C}-\text{NH}_2$	2.3	9.7		3.8
Isoleucine	Ile - I	$\text{H}_3\text{C}-\text{CH}_2-\text{CH}-\text{CH}-\text{COOH}$ $\text{H}_3\text{C}-\text{NH}_2$	2.3	9.8		4.5
Non-Aromatic Amino Acids with Hydroxyl R-Groups						
Serine	Ser - S	$\text{HO}-\text{CH}_2-\text{CH}-\text{COOH}$ NH_2	2.2	9.2	~13	-0.8
Threonine	Thr - T	$\text{H}_3\text{C}-\text{CH}-\text{CH}-\text{COOH}$ $\text{HO}-\text{NH}_2$	2.1	9.1	~13	-0.7
Amino Acids with Sulfur-Containing R-Groups						
Cysteine	Cys - C	$\text{HS}-\text{CH}_2-\text{CH}-\text{COOH}$ NH_2	1.9	10.8	8.3	2.5
Methionine	Met-M	$\text{H}_3\text{C}-\text{S}-(\text{CH}_2)_2-\text{CH}-\text{COOH}$ NH_2	2.1	9.3		1.9
Acidic Amino Acids and their Amides						
Aspartic Acid	Asp - D	$\text{HOOC}-\text{CH}_2-\text{CH}-\text{COOH}$ NH_2	2	9.9	3.9	-3.5
Asparagine	Asn - N	$\text{H}_2\text{N}-\text{C}-\text{CH}_2-\text{CH}-\text{COOH}$ $\text{O} \quad \text{NH}_2$	2.1	8.8		-3.5
Glutamic Acid	Glu - E	$\text{HOOC}-\text{CH}_2-\text{CH}_2-\text{CH}-\text{COOH}$ NH_2	2.1	9.5	4.1	-3.5
Glutamine	Gln - Q	$\text{H}_2\text{N}-\text{C}-\text{CH}_2-\text{CH}_2-\text{CH}-\text{COOH}$ $\text{O} \quad \text{NH}_2$	2.2	9.1		-3.5
Basic Amino Acids						
Arginine	Arg - R	$\text{HN}-\text{CH}_2-\text{CH}_2-\text{CH}_2-\text{CH}-\text{COOH}$ $\text{C}=\text{NH} \quad \text{NH}_2$	1.8	9	12.5	-4.5
Lysine	Lys - K	$\text{H}_2\text{N}-(\text{CH}_2)_4-\text{CH}-\text{COOH}$ NH_2	2.2	9.2	10.8	-3.9
Histidine	His - H		1.8	9.2	6	-3.2
Amino Acids with Aromatic Rings						
Phenylalanine	Phe - F		2.2	9.2		2.8
Tyrosine	Tyr - Y		2.2	9.1	10.1	-1.3
Tryptophan	Trp-W		2.4	9.4		-0.9
Imino Acids						
Proline	Pro - P		2	10.6		

Table 2. Summary of physicochemical properties of α -amino acids found in proteins.

In molecular structures, red letters represent the amino acids' backbone, whereas the black letters are side chains. Hydropathy index of a protein is a number representing its hydrophilic or hydrophobic properties. The larger

the number is, the more hydrophobic is the amino acid. The most hydrophobic amino acids are isoleucine (4.5) and valine (4.2). The most hydrophilic ones are arginine (-4.5) and lysine (-3.9).

2.3.3 Discussion

Compared with the other α -amino acids, arginine (R) can be considered to be a basic amino acid as the part of the side chain nearest to the backbone is long, carbon containing and hydrophobic, whereas the end of the side chain is a complex guanidinium group. With a pKa of 12.48 (See Table 2), the guanidinium group is positively charged in neutral, acidic and even most basic environments. Because of the conjugation between the double bond and the nitrogen lone pairs, the positive charge is delocalized. This group is able to form multiple H-bonds. In addition, its geometry, charge distribution and ability to form multiple H-bonds make arginine ideal for binding negatively charged groups. For this reason arginine prefers to be on the outside of the proteins where it can interact with the polar environment.

All the above-mentioned properties of arginine give the interaction of Cdc25B and NSC95397 reasonable explanations. In a previous study, the *para*-quinone Cdc25 inhibitors were believed to exploit the large anionic electrostatic potentials on their carbonyl groups to form interactions with the guanidinium side chains of R482 and R544, which are $<2.9 \text{ \AA}$ from the ligand carbonyls.[77] Compiling the trypsin protection assay with the mass spectral analysis, a conformational change caused by the ligand binding can be pictured, in which the α -helix between residues R479 and A493 rotates counter-clockwise, causing the following secondary structure change, and making the previously protected arginines and lysines rotate to the outside of the protein and available to the active site of trypsin. The rotation of the helix may be caused directly by the binding of NSC95397 on the catalytic domain of Cdc25B, where the secondary

structure of the catalytic domain formed an alcove instead of a straight line that pulled the helix sequence toward the catalytic motif. This initial change causes a series of conformational alterations up- and down-stream of the interaction site, as the seven newly emerged trypsin digestible arginine and lysine residues shown in Figure 5.

According to the adduct map (Fig. 4), there are several reaction mechanisms postulated to fit the observed differences before and after ligand binding.

The adduct that had the zero neutral loss could be a simple hydrogen bond formation between the lysine or arginine's primary amine hydrogen and the carbonyl oxygen of the NSC95397. (Figure 6, Adduct 1-1) This hydrogen bond-linked bridge represents the closeness between the inhibitor and the target protein, in which the spatial ~ 6 Å distance between two arginines (R485~R548 and R482~R544) is approximately the surface distance between one NSC95397 and two arginine side chains. In another word, the arginine bridge serves as an intermediate form, bringing inhibitor molecule closer to the target binding sites. This weak hydrogen-bond association then in turn facilitates further covalent binding between the two. More likely, it could be the product from a classic *ipso*-reaction that formed a covalent bond with one of the symmetrical carbonyl groups on the quinone ring. (Figure 6, Adduct 1-2). Based on the adduct map in Figure 5, the adducted side chain of Cdc25B could be any of the nucleophilic amino acids that were within the peptide sequence, cysteines, arginines or histidines. The adduct 2 formed possibly through redox mechanisms facilitated by the catalytic site cysteine. (Figure 6, Adduct 2-1 and 2-2) [82-84]

The dehydration adducts 3 could represent a mixed population of different products bearing the same m/z value in the mass spectrum. One possibility illustrated is an acid-base reaction through an acidic side chain on Cdc25B and the thioethoxy group on NSC95397 (Figure

7, Adduct 3-1); the second possibility is a Schiff base formed between the reactive amine on an Cdc25B side chain and the carbonyl on the quinone ring of NSC95397 (Figure 7, Adduct 3-2); the third and more likely mechanism is MALDI matrix (a cinnamic acid)-based dehydration of a serine or a threonine before or during the ionization process. In the latter case, covalent linkage between the ligand and Cdc25B might follow the mechanism described for adduct 1. In other words, adduct 3 might be the side product of adduct 1, which mimic the b-H₂O ions often seen in typical trypsin-digested peptide components. The formation of adducts 4 under excess ligand condition (30:1 ligand-protein), whose *m/z* loss equals to two water molecules, however, supports the acid-base or the Schiff base reaction mechanisms. (Figure 8, Adducts 4-1 and 4-2) Due to the poor quantitative properties of MALDI-TOF-MS, the reaction kinetics could not be further analyzed in order to clarify through the path through which the reaction took place. Adduct 6, ⁴⁹³AVNDYPSLYYPEMYILKGGYK⁵¹³, contains two acidic residues, D496 and E504, both in the β-sheet portion of the crystal structure, which might be able to form a 2:1 ligand-protein complex. However, again, because of the mainly qualitative nature of the mass spectrometry, the kinetics behind this reaction mechanism could not be elaborated based solely on the tryptic digestion information.

The metal ion product, adducts 5, may be another side product of the adduct 1, (Figure 6, Adducts 5-1 and 5-2), especially given the spatial geometry of Cdc25B and the general accessibility of small sodium ions in aqueous solution. Being the most common component in both physiological and experimental conditions, sodium quasi-molecular ions of peptide fragments are often observed during mass spectrometric analyses.[85]

The most complicated adduct, adduct 6, (Figure 9, Adduct 6) had a delta *m/z* equal to an elimination of 2-thioethanol after covalent bond formation between NSC95397 and Cdc25B.

Regardless of which intermediate led to adduct 6 formation, the end product represents the replacement of the 2-thioethanol group with a nucleophilic side chain of Cdc25B. Here, the soft nucleophiles that facilitated the displacement could be the two catalytic cysteines at the three fragments ⁴¹⁴FSNIVDKFVIVDCR⁴²⁷, ⁴²¹FVIVDCR⁴²⁷ and ⁴⁶⁷VILIFHCEFSSERGPR⁴⁸².

There were several new findings from this study. (1) From the proposed chemical reactions and six different Cdc25B adducts, several possibilities of covalent bond formation were found, including *ipso* reaction, Schiff-base reaction, oxidation, dehydration, and nucleophile attack and displacement. (2) With the high molar ratio of inhibitor to target protein (30:1), the possible binding site is also inferred to be the pocket ⁴⁸⁰GPRMCRFIRERD⁴⁹¹. This is the first time that a new binding pocket for NSC95397-Cdc25B interaction was found. (3) A new interaction model, an Arg-NSC-Arg bridge, was proposed based on adduct information and the 3D crystal structure of Cdc25B's catalytic domain. This model has never been proposed before. In contrast to the intra-protein salt-bridge previously proposed, this arginine bridge utilized both active >N=NH groups and the carbonyl group on the inhibitor molecule. This Arg-NSC-Arg bridge, or "arginine bridge", specified the reactivity that was governed by both spatial constraints and reactive chemical groups. This provides a new way to explain the ligand-inhibitor binding mechanism, and could be useful in future design of small molecule inhibitors. (4) The conformational change after inhibitor binding was also inferred based on the results from the trypsin protection assay, in which the α -helix preceding the catalytic loop HCXXXXXR rotated counter-clockwise (Figure 4) so that previously trypsin-accessible arginines became hidden, whereas several other previously hidden sites became exposed to trypsin. This is the first time that a conformational change model, which used the point-editing method (i.e., digestion site on/off from trypsin protection assay), has been proposed. This method, the trypsin protection

assay coupled with MALDI-TOF/TOF-MS/MS analysis, will definitely serve as a promising alternative for 3-D simulation before and after inhibitor binding and thus, in part, assist in rational drug design.

As all proteins bind to other molecules to realize their biological function,[1] different chemical reactivity of a protein's amino acid side chains with its ligand can bring some evidence to light, such as a protein's conformational preference and specificity upon ligand-protein binding. Computational modeling based on biophysical characteristics of protein and its ligand includes functional site localization, similarity matching and ligand docking as three major steps. [86] All these steps require known information as the knowledge database or learning set for simulating and computing, whereas site-directed mutagenesis of amino acid residues serves as test-of-hypothesis tool to verify the *in silico* predictions.[87-90] As a liberation from the vast data handling and professional computation skill necessary for the computational/mutation approach, this study showed the potential of MALDI-TOF-TOF-MS for the study of protein-ligand binding at a detailed molecular level based on chemical reactivity of amino acid residues and ligand groups. The time-efficient experiments in this study as compared to crystal structure determination, in combination with traditional 3-D molecular modeling, yielded interpretable results. As the maturity of mass spectrometry increases, the quantification potential of MS could be well applied to help protein-ligand binding and QSAR studies. It is still necessary, however, to verify the *in vitro* findings from an MS approach through traditional function assays both *in vitro* and *in vivo*. To do so, the therapeutic concentration of the inhibitor should be used, instead of the excess used here, to demonstrate the physiologically-relevant binding behaviors between target protein and the small molecule inhibitor. Furthermore, owing to the high resolving power

of MS and fast interface for low femtomole level sampling, high-throughput screening for small molecule libraries and target protein binding could also be explored in a whole new way.

3.0 S-NITROSYLATION IN EARLY HEMORRHAGIC SHOCK

3.1 BIOLOGICAL IMPORTANCE OF S-NITROSYLATION

Since the discovery of nitric oxide (NO) as a physiological mediator in the early 1980s, research devoted to the biological role of this molecule has evolved rapidly, both in intensity and extent. The crucial processes within the cell that NO can regulate include those such as the response to redox perturbations, protein function, and gene expression through non-enzymatic modifications. [91-96] *S*-Nitrosylation of proteins is one potential mechanism underlying these events that has attracted increasing interest in recent years.

S-Nitrosylated proteins form when a free thiol of a protein reacts with the free radical nitric oxide (NO) in the presence of an electron acceptor to form a nitrosothiol (*S*-NO) bond. Physiologically, the electron acceptors can be oxygen, NAD^+ or reactive iron species.[97, 98] Although there is no precedent for a reaction of NO itself with thiol groups under physiological conditions, the formation of NO quickly yields an NO^+ equivalent upon interaction with electron acceptors, and ONOO^- (peroxynitrite) upon interaction with superoxide anion O_2^- . *S*-Nitrosylated proteins (RSNO) form when the NO^+ equivalent transfers on a free thiol group of a protein. *S*-Nitrosylation and NO transfer reactions (trans-nitrosation reactions) are involved in almost all classes of cell signaling, ranging from the regulation of ion channels and G-protein coupled reactions to receptor stimulation and activation of nuclear regulatory proteins. [99]

Furthermore, it is now apparent that the synthesis, transport, activation, and catabolism of SNOs are regulated.

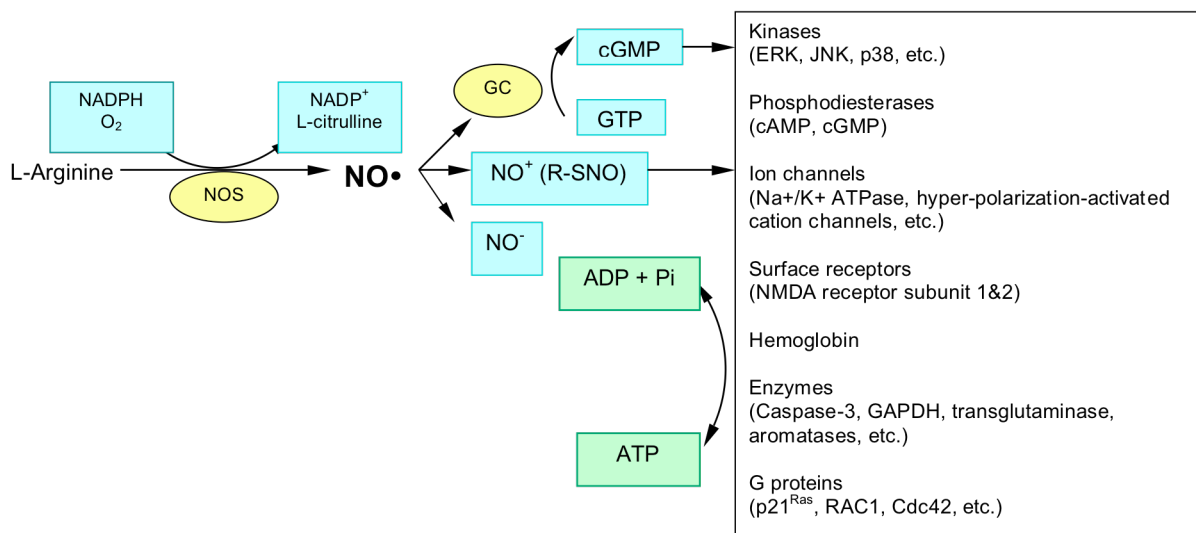


Figure 9 The biological functions that *O*-phosphorylation and *S*-nitrosylation share.

Reversible protein *O*-phosphorylation regulates all facets of cellular life. Although the list of protein targets are far from completion, for each of the depicted functional classes of target proteins known to be regulated by *O*-phosphorylation, at least one example of a target protein has been revealed to be regulated by *S*-nitrosylation. The brown text box includes biological functions that have been found involved *S*-nitrosylation and *O*-phosphorylation. (Reformatted and edited from references [99-101].)

Protein-mediated or protein-catalyzed formation of *S*-NO, in addition to less important inorganic chemical reactions involving N_2O_3 and other intermediates, can involve several initiating factors. These include activation of NO synthase (NOS), reactivity of and *S*-NO-derived $NO^-/NO/NO^+$ equivalent with a target protein consensus motif, and metalloprotein-catalyzed reactions.

Both *O*-phosphorylation and *S*-nitrosylation involve covalent attachment of a small molecule, phosphate and NO, respectively, to an amino acid side chain. Despite their overlaps in regulatory functional pathways (shown in Figure 1), one major difference between *O*-phosphorylation and *S*-nitrosylation is that *O*-phosphorylation is enzyme-driven, whereas *S*-

nitrosylation is achieved through the non-catalyzed chemical modification of a protein residue, almost invariably cysteine. Compared to the relatively more studied phosphorylation, however, the spectrum of *S*-nitrosylation, which may represent a ubiquitous and fundamental mechanism for post-translational control of protein activity, is substantially less well understood.

3.2 S-NITROSYLATION OF PLASMA PROTEINS IN EARLY HEMORRHAGE

Since the short half-life of the NO radical restricts not only its activity but also its spatial spread, in a cell. NOS produces an NO radical that may, through an as yet incompletely understood set of reactions, produces more stable RSNOs. Low molecular weight RSNOs are believed to play an integral role in a variety of different NO-dependent physiological processes, particularly in the vasculature. The physiological relevance of RSNOs has been confirmed by the demonstration that the predominant redox form of NO in mammalian plasma is *S*-nitrosoalbumin.[102] Following hemorrhage, an early “compensatory” response results in an increase in the total peripheral resistance and a redistribution of blood flow. NO is a prime candidate as a vasodilator because of its pivotal role in the control of tissue perfusion. It is known that nonselective inhibition of NOS in early hemorrhage increases tissue injury.[103] The increased NO production was suggested either during hemorrhage or immediately after resuscitation.[104-106] There remains a need, however, for more direct evidence of increased NO production during hemorrhage-induced hypotension, which can be obtained by measuring the accumulation of relatively stable NO reaction products, i.e., *S*-nitrosylated proteins in plasma and red blood cells.

3.3 DETECTION OF S-NITROSYLATION

The biotin switch method, which was developed by Jeffery and Snyder in 2001,[107] enables the detection of both *in vitro* S-nitrosylated proteins. Through a series of reactions, the NO portion of an RSNO is replaced by biotin. Biotin has high affinity for avidin, which can be used for affinity enrichment (or specific histochemical detection). This way, S-nitrosylated proteins can be indirectly enriched through streptavidin-affinity chromatography followed by candidate-specific immunoblotting.

The total concentration of plasma RSNO has been estimated to be 1 μ M, in which only 3 nM is free NO. [102] S-Nitrosoalbumin, which is derived from reaction of NO and the only free sulfhydryl on serum albumin, Cys34, accounts for more than 85% of total plasma RSNO content. Therefore, before one can selectively enrich the S-nitrosylated plasma proteins using the biotin switch assay, the depletion of serum albumin has to be done in advance to ‘amplify’ the content of other S-nitrosylated proteins.

3.4 EARLY HEMORRHAGE MODEL AND NO DONOR TREATMENT

Hemorrhage is a common scenario in clinics and battlefield. Its outcomes are virtually similar across patient populations and organ systems. Systemic inflammatory response, multiple organ dysfunction, and multiple organ failure are often the results of hemorrhage.[108] Nitric oxide (NO) plays an important role in the pathogenesis of neuronal injury after brain ischemia, and decreased levels of NO have been implicated in the pathogenesis of vasospasm after subarachnoid hemorrhage (SAH). Inhibition of NO production results in significant reduction of

local tissue damage, and improves survival after hemorrhage because NO may have numerous functions in the pathophysiology of hemorrhage. [109-113]

Direct measurement of NO-hemoglobin complexes by electron spin resonance (ESR) spectroscopy in blood samples of rats subjected to hemorrhage gave the first evidence for enhanced formation of NO, where significant increases in the ESR signal were already detectable at 2 hours after the onset of hemorrhage. A further increase was found to be sustained at 4 and 6 hours after the onset of hemorrhage.[114] However, the initial increase in NO formation due to the induction of iNOS should be followed by a progressive decrease of NO in prolonged hemorrhage (≥ 6 hours) due to the suppression of eNOS.[115] Therefore, the increased NO level is regarded as the representative signal for early hemorrhage.

NOC-7 (3-(2-hydroxy-1-methyl-2-nitroso-hydrazino)-*N*-methyl-1-propanamine) is an NO donor, one of the drago-type complexes that are intramolecular zwitterions that are stabilized with an intramolecular hydrogen bond through dispersion of the negative charge, which prevents protonation. The rate of NO release depends on the weakness of the hydrogen bond. Thus, if NOC series compounds are used, careful selection of the compound allows control of the rate of adding NO to the sample. The half-life of NOC-7 is 5 min. Since the decomposition of NOC is triggered by protonation, the NO-releasing rate becomes faster as the pH decreases. Practically, NOC can be diluted into alkaline solution, e.g., 0.1 M NaOH, and then added into the sample buffer solution. NOC-7-treated rat plasma proteins should, theoretically, be over-*S*-nitrosylated on their reactive free thiol groups as compared to plasma proteins recovered after hemorrhage. Therefore, a NOC-7-treated rat plasma sample was used as the positive *S*-Nitrosylation control for hemorrhaged rat plasma.[116, 117] In the present study, a physiological level of 100 μM NOC-7 was used to treat rat plasma samples *in vitro*, so as to investigate the early hemorrhage

response system in rat plasma proteins. This is the first attempt to investigate the *S*-nitrosylated rat plasma proteome in an *in vitro* early hemorrhage model using proteomics techniques.

3.5 IDENTIFICATION OF *S*-NITROSYLATION AND ALTERATION OF RAT PLASMA PROTEOME IN HEMORRHAGE

3.5.1 Materials and methods

Reagents and antibodies. Polyclonal (rabbit) antibody to human transferrin was from Innovex Biosciences, Richmond, CA. Anti-IgG (ab6747) and rabbit anti-ceruloplasmin polyclonal IgG (ab8813) were from Abcam, Cambridge, MA. Monoclonal mouse anti-biotin (A11242) was from Invitrogen, Carlsland, CA. Highly abundant rat serum protein depletion kit, which utilizes chicken immunoglobulin Y antibodies, was from GenWay Biotech, San Diego, CA. Human recombinant ceruloplasmin, human transferrin, NOC-7, acetone, bromophenol blue, *N*-[(biotinamido)hexyl]-3'-(2'-pyridyldithio)propionamide (Biotin-HPDP) were from Pierce Biotechnology. Dimethylsulfoxide (DMSO), dimethylformamide (DMF), ethylenediaminetetraacetic acid (EDTA), glycerol, TritonX-100, methyl methanethiosulfonate (MMTS), 3-([3-cholamidopropyl]dimethylammino)-1-propanesulfonate (CHAPS), streptavidin agarose, EDTA, ascorbate, neocuproine, sodium dodecyl sulfate (SDS) and 2-mercaptoethanol (2-ME) were purchased from Sigma-Aldrich, St. Louis, MO.

Animal treatment. Animal handling and treatments were conducted at the Walter Reed Army Institute of Research by Nikolai Gorbunov, Ph.D., in compliance with the Animal Welfare Act and other Federal statutes adhere to principles stated in the *Guide to the Care and Use of*

Laboratory Animals, National Research Council. The facilities were fully accredited by the Association for Assessment and Accreditation of Laboratory Animal Care International.

Experimental design Ten male Sprague-Dawley rats (Charles River Laboratories, Wilmington, MA) weighing 280~320 g received a standard diet and water ad libitum. They were randomly assigned to hemorrhage (H) or sham groups, ($n=5$ per group). All animals were anesthetized with ketamine (60mg/kg *i.p.*) (NLS Animal Health, Owings Mills, MD) and anesthesia was maintained by supplementary injection of ketamine as required. Blood samples were taken [118] at 1, 30, 60 and 90 min after hemorrhage (0.7 ml of blood for each timepoint was removed, and this volume was replaced with an equal volume of normal saline). The rat plasma withdrawn at the zero time point was treated in vitro with 100 μ M NOC-7 at room temperature for 10 min.

Immunoblot analysis. Alterations in the amounts of ceruloplasmin and *S*-nitrosated proteins in blood plasma were assessed using immunoblot techniques followed by protein separation in polyacrylamide gels [119]. After transferring electrophoresed proteins to polyvinylidene difluoride (PVDF) membranes using the Mini-gel wet-transfer system (Bio-Rad), the membrane was rinsed twice in PBS-T (PBS containing 0.05% Tween-20), and placed in blocking buffer (5% nonfat milk in PBS-T) shaking at room temperature for 1 h. Primary antibody was then added into fresh block buffer and shaken with the membrane for 1 h at room temperature. After blocking, the membrane was rinsed three times in PBS-T for 5 min each, wash buffer was discarded to eliminate non-specific binding. Secondary antibody was then added with fresh blocking buffer and incubated with the membrane for 30 min to 1 h at room temperature. Finally, the membrane was rinsed 3 times in PBS-T for 10 min each rinse, and developed by enhanced chemiluminescence (ECL plus, Amersham Biosciences, Piscataway,

NJ) and subsequently exposed to Kodak Biomax MR-2 photographic film (Sigma-Aldrich, St. Louis, MO). Protein bands were identified by comparison with a molecular weight marker (Bio-Rad). β -Actin was probed to monitor equal loading. Semi-quantitative assessment of immunoblots was conducted using ImageJ image processing software.

Chemiluminescence analysis of N-oxides. The NO-derived products (N-oxides) in the blood erythrocytes and plasma were analyzed with a NO analyzer NOA 280 (Sivers Instruments, Boulder, CO). The assay can detect chemiluminescence response of the reaction of ozone with NO released from adducts, catalytically producing NO_2^- and NO_3^- , the end products of NO oxidation. The labile NO compounds, i.e., NO, NO^- , and NO^+ , and NO_2^- in erythrocytes was analyzed at room temperature. NO_2^- and NO_3^- in plasma were analyzed at 25 and 90 °C, respectively, following protein elimination on 5 kDa molecular mass cutoff filters within 1 h after blood sampling. The recorded chemiluminescence signals were analyzed using NO Analysis Software (Sivers Instruments).

Depletion of rat albumin. Albumin was removed from rat plasma with columns containing IgY antibodies immobilized on beads following the manufacture's instruction. Briefly, the bottom tip of the spin column was snapped off and the column was centrifuged at 2,000 rpm to obtain dried beads. Diluted rat plasma sample (1:10 in the proprietary dilution buffer) was added onto the center of the column after sealing the bottom with the cap. Sample and beads were mixed by end-over-end shaking at room temperature for 30 min. The flow-through (the depleted fraction) was collected by centrifuging at 2,000 rpm for 30 sec. After washing column three times with 200 μl dilution buffer, 200 μl of the proprietary stripping buffer was added onto the column after sealing the bottom, and mixed well by end-over-end

shaking. The bound albumin was then removed by spinning at 2,000 rpm for 30 sec. Repetition of elution can be done to recover more bound albumin.

Biotin switch method. The biotin switch method was adapted from the original protocol developed for the detection of *S*-nitrosylated proteins by Jeffery et al. [107] The modified procedures will be described as following steps. Excess NO donors were removed using MMTS blocking: the spin column resin was inverted to form a suspension, and the resin was drained and resuspended twice in 500 μ l of HEN buffer (250 mM HEPES-NaOH, pH 7.7, containing 1 mM, EDTA 1 mM and 0.1 mM neocuproine). The column was then centrifuged at 1000 g for 2 min to remove remaining buffer. The sample solution (diluted to $< 0.8 \mu\text{g}/\mu\text{l}$ of total protein content) was then applied onto the center of the resin and centrifuged at 100 g for 4 min. Free thiol groups were then blocked by adding four volumes of blocking buffer (9 volumes HEN Buffer mixed with 1 volume of 25% w/v SDS in H₂O) and incubated at 50 °C for 20 min with frequent vortex mixing. Excess MMTS was removed by acetone precipitation at 1:4 v/v at -20 °C overnight (Please see the discussion below for details on the modification of acetone precipitation). Biotinylation of nitrosothiols was done by adding 1:3 (v/v) labeling solution (4 mM biotin-HPDP in DMF) and 1:50 (v/v) of 50 mM sodium ascorbate in H₂O into the blocked protein samples. The sample was then incubated in the dark at room temperature overnight while shaking at 500 rpm horizontally. Biotinylated proteins were detected by immunoblotting using mouse monoclonal anti-biotin antibody, and purified by acetone precipitation to remove the biotin-HPDP, treated with neutralization buffer (20 mM HEPES-NaOH, pH 7.7, containing 100 mM NaCl, 1 mM EDTA and 0.5% (v/v) Triton X-100). Fifteen μ l of packed streptavidin-agarose per mg of protein was added to purified samples and incubated for 1 h at room temperature. The resin was then washed five times with 10 volumes of neutralization buffer containing 600 mM NaCl,

and centrifuged between each wash. Finally, biotinylated protein was eluted using elution buffer (20 mM HEPES-NaOH, pH 7.7, containing 100 mM NaCl, 1 mM EDTA and 100 mM 2-thioethanol).

An aliquot of the purified biotinylated proteins was segregated by 1-D SDS-PAGE using non-denaturing sample loading buffer and analyzed by Western blot using the anti-biotin antibody. Another aliquot was examined by 1-D SDS-PAGE and SYPRO-Ruby staining and, subsequently after destaining, Coomassie blue staining. Remaining samples were segregated by 2-D gel electrophoresis using immobilized pH gradient (IPG) strips and 11 cm Criterion® gels (Bio-rad) and stained with SYPRO-Ruby. Gel bands/spots were visualized by visual and/or fluorescence image acquisition on a custom-built instrument with a high-resolution cooled {Prometrix charge-coupled device camera (CH350 model, 16-bit chip, Photometrics, Munich, Germany) and analyzed with Image J software. Gel plugs were picked with a robotic system on the imaging instrument, placed into Eppendorf tubes, washed to remove the dye, dehydrated with acetonitrile, lyophilized, and re-swollen with a solution of sequencing grade trypsin (Promega, Madison, WI) in 25 mM ammonium carbonate.

Traditional 2D Gel Electrophoresis. The lysates were treated with a ReadyPrep 2D Cleanup Kit (BioRad, Hercules, CA, USA) to remove ions, DNA, RNA, etc. Their protein contents were measured using a 2D Quant kit (Amersham Biosciences, Piscataway, NJ, USA). After overnight rehydration in buffer consisting of 6M urea, 2M thiourea, 4% CHAPS, 25mM dithiothreitol, and 0.2% ampholyte, the protein samples were loaded on a 11 IPG strip (Bio-Rad, nonlinear pH 3–10). Focusing was accomplished with 250V for 15 min, 10,000V for 3 h, and a third step of 40,000 total volt hour (Vh), and then maintained at 500V as needed. The resolved proteins were equilibrated in SDS buffer with reducing agents present and separated by SDS-

PAGE through 4–12% gradient Tris-HCl gels in a Criterion apparatus (Bio-Rad) operated at 4W per gel for 8 h. SYPRO-Ruby staining was used to detect abundant proteins. Spots were manually retrieved with spot-picking pipette tips, digested with trypsin, and submitted for protein mass fingerprinting (PMF) analysis.

Difference gel electrophoresis. The electrophilic fluorescent dyes, PrCy3-N-hydroxysuccinimide ester and MeCy5-N-hydroxysuccinimide ester (Cy3 and Cy5, respectively), were synthesized and provided by the Day lab and stored as single use aliquots in anhydrous DMF at –80 °C. Rat albumin, depleted control and hemorrhage samples were separately mixed with volumes of each dye solution to produce balanced covalent labeling of 1–5% of the available lysine side chains, without significant alteration of the protein isoelectric points. Unreacted dye was quenched with 40% aqueous methylamine, pH 8.6. Paired control and hemorrhage treated rat plasma samples were mixed together for focusing and subsequent separation by on a Protein II 2-D gel electrophoresis system (Bio-Rad). The gels were viewed in the fluorescent gel-imaging device and spots were excised with the integral gel-cutting robotic tool. Imaging was performed at two excitation wavelengths, 545~710 and 635~715nm for Cy3 and Cy5, respectively. Image manipulation and viewing was done with Image J (National Institutes of Health, Bethesda, MD, USA) and V++ Precision Digital Imaging System software (Digital Optics, Auckland, New Zealand). Two-frame, ‘flash’ movies of the overlying Cy3 and Cy5 images were viewed in a continuous loop to visually detect differences in the protein signatures between the two samples separated in the same gels. Sample-dependent differences in protein distributions were confirmed and quantified using the image analysis software package DeCyder Differential Analysis Software, version 5.0 (DeCyder® Amersham Biosciences). DeCyder analyzes images as fragments and sums them to generate a composite image with

proprietary algorithms that detected overlapping, differently colored images within the same gel to match spots and subtract background for normalization. DeCyder was used to create measurement masks, each outlining an area of the gel containing a protein spot, that was applied to each of the matching fragments in the paired fluorescent images of each gel. The masks defined areas in which the pixel values were integrated to create three-dimensional topographical maps with peaks representing each protein spot. An estimate of the local background for each spot determined the base values across the masked area. Output from the image analysis, designated as fluorescence intensity, was the sum of pixel values in the mask area minus the background. Volumes of the peaks representing the relative strengths of fluorescent signals from matched spots were compared. A threshold was set at 1.5-fold to screen for differences: only proteins with >1.5-fold difference were reported. Visual inspection confirmed the differences indicated by the DeCyder software. Dust and artifacts were detected as peaks with slope values of less than one or as clusters of sharp spikes. Images of some protein spots were also scanned and digitized to compare total pixels, as described below for immunoblots. Protein spots that differed on DiGE between the labeled lysates were harvested from the gels using a robotic gel picker integrated with the high resolution CCD camera, digested with trypsin with reduction and alkylation steps, and submitted for mass spectrometric PMF analysis.

Trypsin digestion with reduction and alkylation. One hundred μ l of a 1:1 mixture of 25 mM aqueous NH_4HCO_3 and acetonitrile was added to the gel pieces and vortexed for 10 min; repetition of this washing step was performed four times until the gel plug became transparent and sticky. Gel pieces were then dried in a SpeedVac . Thirty μ l of reducing buffer (50 mM tris(2-carboxyethyl)phosphine in 25 mM NH_4CO_3) was added to each sample and incubated at 60 °C for 10 min. After the sample was cooled to room temperature, the reducing buffer was

removed and discarded. Thirty μl of alkylation buffer (100 mM iodoacetamide, prepared just before use) was then added to the sample, and the mixture was incubated in dark at room temperature for 2 h. After removing and discarding the alkylation buffer, the sample was washed with 200 μl of destaining buffer (1:1 50 mM aq. NH_4HCO_3 -acetonitrile) and incubated at 37 °C with shaking for 15 min. Destaining buffer was removed and discarded. After two repetitions of the reduction and alkylation steps, gel pieces were shrunk by adding 50 μl of acetonitrile and incubation at room temperature for 15 min. Acetonitrile was carefully removed after the gel pieces turned pale white. Gel pieces were then air-dried for up to 10 min and stored at -80 °C (if trypsin digestion did not immediately follow). Trypsin digested was performed by first adding 20 μl of activated trypsin solution to swell the gel pieces, just covering the gel plugs, and incubation at 4°C for 15 min. The samples were then moved to 42 °C incubator and shaken gently for 4 h. When digestion was finished, samples were cooled to 4 °C and the digestion mixture was transferred to a clean Eppendorf tube. Further extraction of peptides from gel pieces was done by dehydrating the gel pieces with a gradient of TFA in acetonitrile:H₂O mixtures (typically from 40% to 100% acetonitrile with 0.2% up to 3.0% TFA). The extracts were pooled with the digestion mixture and taken to complete dryness in a SpeedVac.

Protein Identification Following trypsin digestion, the peptides derived from each protein spot were analyzed with MALDI-TOF-MS-MS in a 4700 Proteomics Analyzer with TOF/TOF Optics (Applied Biosystems, Foster City, CA, USA). Dried peptide extracts were resuspended in MALDI spotting medium (50% acetonitrile in H₂O with 0.3% TFA). Well-mixed and any debris pelleted by centrifugation. The extracts were mixed 1:1 (v/v) with CHCA matrix solution (10mg/ml CHCA in spotting medium). The mixture was then vortexed and solids pelleted by centrifugation before applying a 0.5 μl aliquot onto the MALDI target plate. The Applied

Biosystems GPS Explorer Protein Analysis Software on a remote client workstation provided automated acquisition of optimized mass spectra and the derivation of monoisotopic PMF information. Searches of the NCBI nonredundant database, based on the peptide mass results using MASCOT (Matrix Science, Boston, MA, USA) via the GPS Explorer workstation and MS-Fit (University of California, San Francisco MS Facility) via the internet identified proteins with matching PMFs. The MASCOT parameters were set to include all species (with the exception of spots from the gel region containing BSA), tolerance of one missed trypsin cleavage per protein, allowance of protein modification by methionine oxidation, peptide tolerance of 50 ppm and restriction of peptides to 700–4000 Da. The MS-Fit parameters included tolerance of one missed trypsin cleavage per protein, cysteine modification by acrylamide, oxidation of methionine, and changes at the amino termini, such as conversion of glutamine to pyro-glutamate and acetylation. Protein identifications were accepted when the observed and predicted pI's and Mr's were consistent and scores indicated nonrandom identifications at a significance level of $P < 0.05$, and were confirmed by acquisition of MS/MS data that were consistent with the predicted *b*, *y* and immonium ion series of the peptides.

3.5.2 Results

The albumin depletion enriched other plasma protein signals in 2-D gels. Due to the high-abundance proteins such as albumin and immunoglobulins, low-abundant proteins are often undetectable in proteomic analyses of plasma. Plasma proteins can be present in the range of milligrams per milliliter (e.g., albumin) to picograms per milliliter (for some interleukins). Such a dynamic range of protein levels represents an enormous problem for detection and quantitation in a single assay. The high abundance of albumin and immunoglobulin G (IgG) in serum can

significantly affect the resolution and sensitivity of many techniques. For instance, plasma proteins resolved on 2-D gel electrophoresis become crowded from 45 to 80 kDa and pI range of 4.5 to 6.0. The removal of highly abundant proteins such as albumin from plasma is necessary for the detection of low-abundant proteins by 2-D gel electrophoresis, isotope-coded affinity tag labeling, or multidimensional protein identification technology. [120] The main reason for choosing chicken IgY antibodies over mammalian IgG antibodies was to take the major advantage of the evolutionary distance between chickens and mammals, which allows for greater immunogenicity against conserved mammalian proteins such as albumin. [121] As shown in Figure 10-A and B, the amplification of plasma proteins with albumin depletion largely improved their detection number, intensity, and resolution. Using the chicken IgY antibody-based albumin depletion method, the level of intact rat transferrin after albumin depletion was kept better than that of ceruloplasmin. (Shown in Figure 10-C and D) This could be due to the closer association of ceruloplasmin with albumin as a copper carrier and a ferroxidase than transferrin as a Fe(III) pool. [122, 123] Overall, the recovery from albumin depletion for the plasma sample was about 90%. Although the transferrin antibody was found to cross-react with albumin/IgG in Western blot experiments,[124, 125] in the elutions, transferrin was still preserved after albumin depletion. (Figure 10-D)

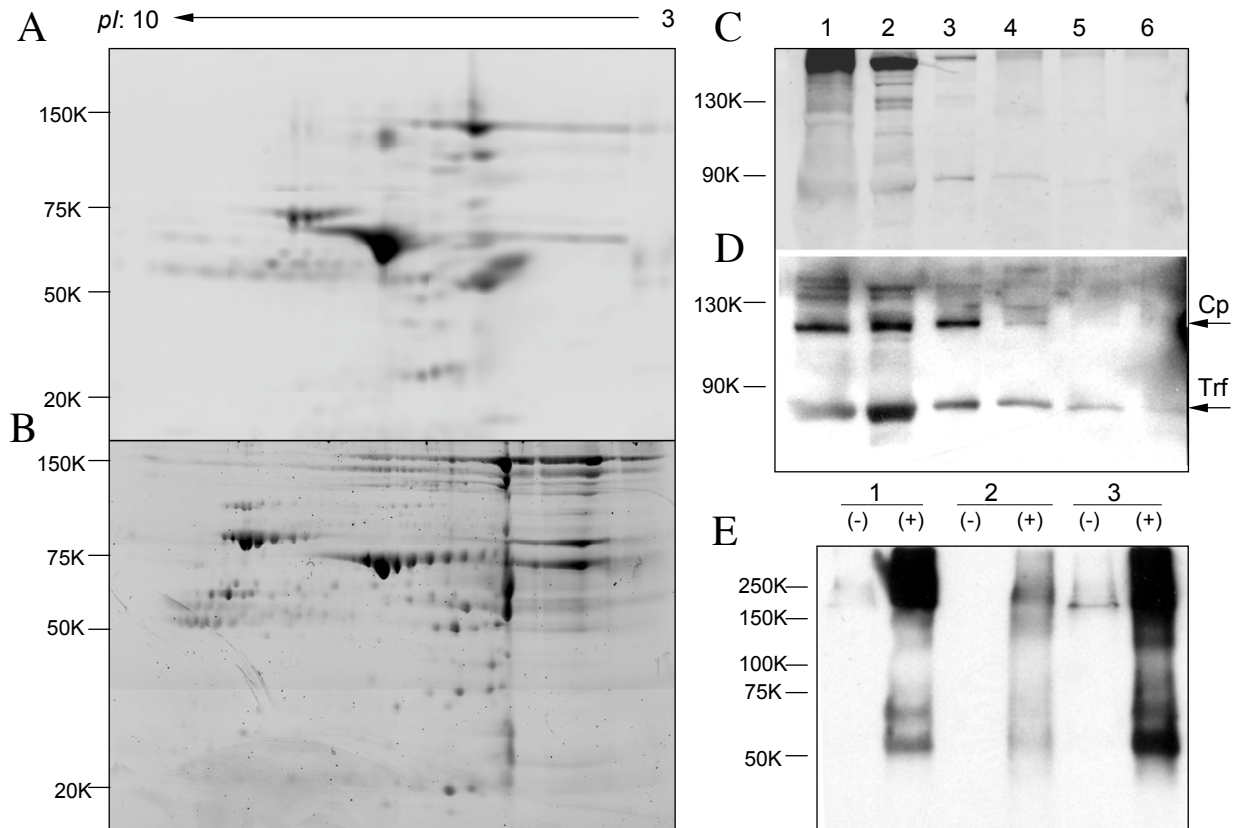


Figure 10 Quality control during the biotin switch assay with albumin depletion for rat plasma samples

Figure 10-A~D: Traditional 2-D electrophoresis analysis of sham-treated rat plasma sample: pre-albumin depletion (A), and post-albumin depletion (B). 1-D gel electrophoresis for rat plasma samples: SYPRO-Ruby image (C) and Western blot (D) analysis with anti-ceruloplasmin (Cp) and anti-transferrin (Trf) -- 1: pre-albumin depletion; 2: the first albumin fraction; 3: the second albumin fraction; 4: the first depleted elution; 5: the second depleted elution; 6: the third depleted elution. Figure 10-E: Western blot analysis using mouse monoclonal anti-biotin after biotinylation of rat plasma samples following albumin depletion -- 1: sham rat plasma with vehicle; 2: plasma from hemorrhaged rat treated with vehicle; 3: NOC7-treated rat plasma. (-): DMF control; (+) biotinylated sample. Loading in each lane were all calculated to be equal to one-fifth of the reaction starting total protein content (i.e., 10 μ g for each lane).

Biotinylation of the plasma samples followed by positive Western blot signals. Using the negative reaction control (DMF only), the biotinylated samples gave strong signals when probed with a mouse anti-biotin monoclonal antibody. The faint bands in negative control samples were non-specific binding events and/or endogenously biotinylated proteins (biotin is vitamin B7)

(Figure 10-E). The vertical streaking on the SDS-PAGE gel represented the heterogeneity of biotinylated products from the plasma proteins. When probing with anti-ceruloplasmin and anti-transferrin antibodies, there were no detectable chemiluminescent signals, which indirectly shows the potential SNO product formation for those two proteins, because proteins with PEO-biotin addition would barely have the affinity reaction with corresponding antibodies as strong as for native proteins.

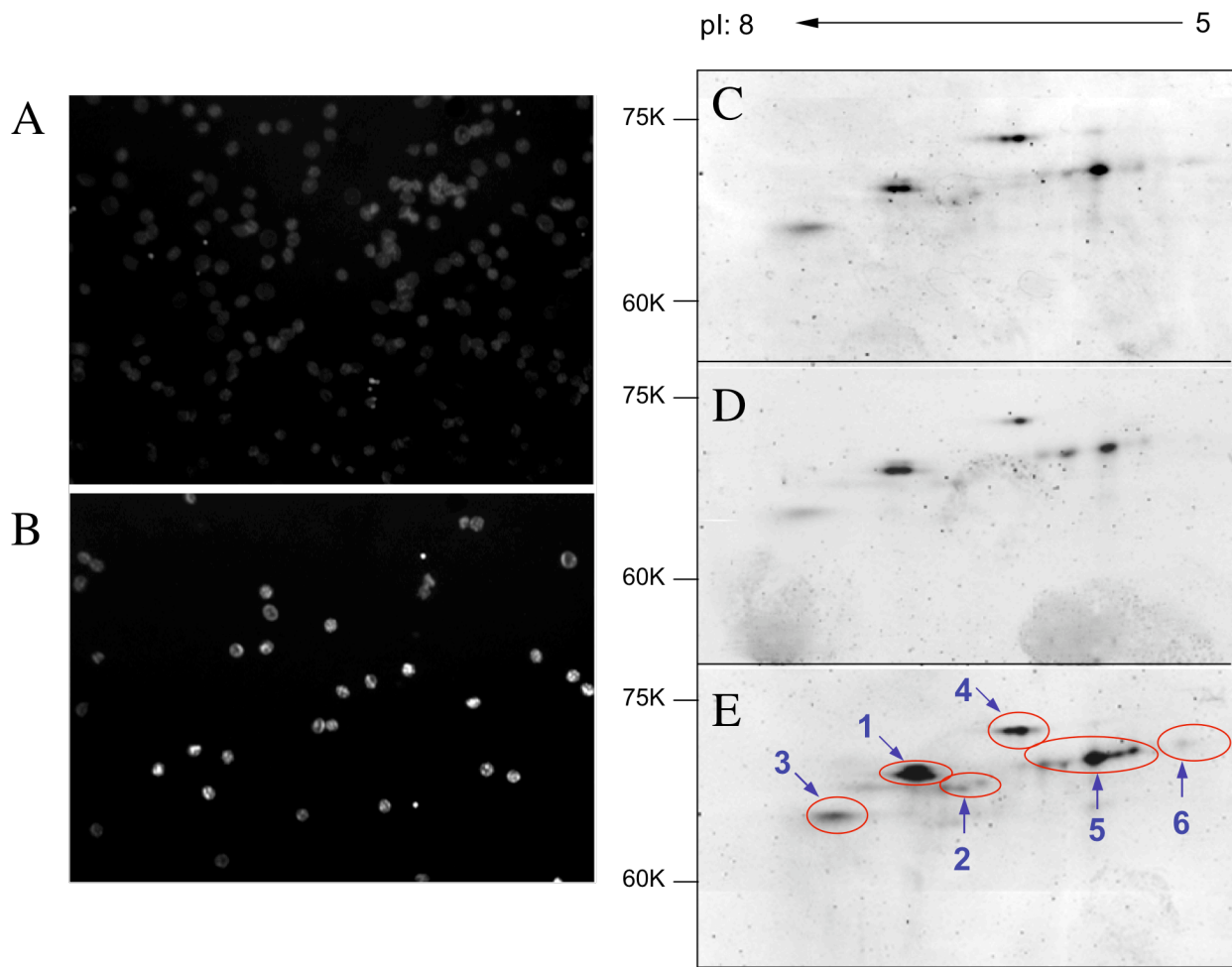


Figure 11 Fluorescence analysis of deposition of *S*-nitrosothiols in red blood cells and traditional 2-D gel stained by SYPRO-Ruby fluorescence dye.

Representative images of fluorescent adducts of *S*-nitrosothiols in RBCs obtained from sham-treated (A) and hemorrhaged (B) animals (re-formatted from ref. [118]). 2-D images were captured and analyzed according to section 3.2.1 Rat plasma samples were from: animal sham-treated with vehicle (C); Hemorrhage + Vehicle treated

rat (D); and NOC-7 treated animal (E), Each sample was loaded with 10 μ g of total protein, based on BCA assay results. The identities of the spots in (E) are: 1: prosaposin; 2: transferrin; 3: ribonuclease/angiogenin inhibitor; 4: keratin, type II; 5: keratins, (type I & type II); 6: IgG gamma 2A

NO adducts in red blood cells including S-nitrosothiols were increased by hemorrhagic shock. As detected by fluorescence image analysis (the RSNO-associated red blood cell fluorescence was 138 ± 56 AU in hemorrhaged sample vs. 28.7 ± 13.1 AU in sham-treated sample. $P\leq 0.01$, $n=150$ cells, 3 animals) (Figure 11-A, B), the data showed that the overall level of S-nitrosothiols increased in red blood cells.

Six S-nitrosylated proteins were identified from three rat plasma samples. After applying the biotin switch method, theoretically, all proteins with S-nitrosated thiol groups should be among the final reaction products. The overall yield from the biotin switch assay was often low and needed higher input than other reaction-free proteome samples. Strict quality controls were required to avoid possible false positive/negative results (Figure 10). As shown in Figure 11, S-nitrosylated plasma proteins were resolved in traditional 2-D gels after albumin depletion and applying the biotin switch assay. All three samples had the same alignment of the protein spots on the gels, which indicated the similarity of the pattern of S-nitrosylation with and without the hemorrhage treatment or NO donor treatment. The loading on each gels for the three samples, (vehicle control, hemorrhaged and NOC-7 treated) could not be equalized, because the absorption of samples on the IPG strips were not quantifiable from the protein content measurement before equilibration and absorption. From the identification results, S-nitrosylated proteins in rat plasma included: prosaposin (a.k.a. sulfated glycoprotein-1, SGP-1); transferrin (a.k.a. serotransferrin, serum siderophilin; beta-1-metal binding globulin); ribonuclease/angiogenin inhibitor; 4: keratin type II; keratins type I and type II; and IgG gamma 2A. Detailed protein sequence analysis can be found in the Appendix section.

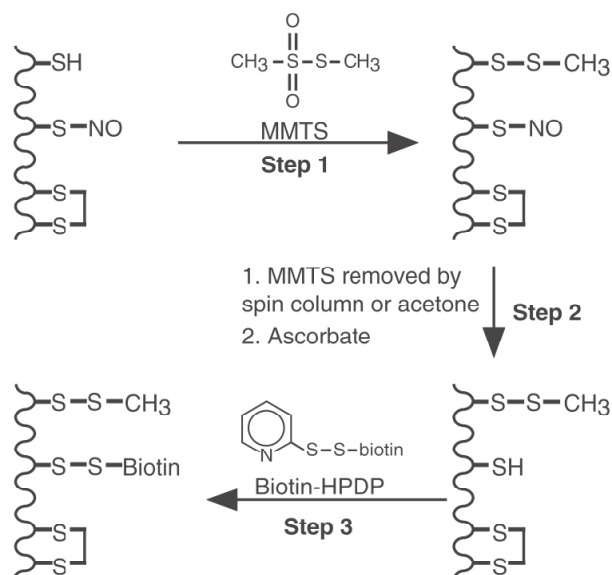


Figure 12 Schematic diagram of the biotin switch *S*-nitrosylation assay.

A theoretical protein is indicated with cysteines in the free thiol, disulfide, or nitrosothiol forms. In a preliminary step of the procedure, free thiols are made unreactive by methylthiolation with MMTS. This modification can be reversed by reduction with 2-thioethanol. Unreacted MMTS is removed in a subsequent step either by passing the protein mixture through a spin column or by acetone precipitation. In the final step, nitrosothiols are selectively reduced with ascorbate to re-form the thiol, which is then reacted with the thiol-modifying reagent biotin-HPDP. (Adapted from Ref. [107])

Many isoforms of keratin types I and II presented in all three samples, giving multiple clustered protein spots (Figure 11, spots 4 and 5) on the 2-D gels, due to their multiple cysteine residues and heterotypic properties. Type II cytokeratins are encoded on chromosome 12q and include CK1, CK2, CK3, CK4, CK5, CK6, CK7 and CK8. Their molecular weight ranges from 52 KDa (CK8) to 67 KDa (CK18). Type I cytokeratins are encoded on chromosome 17q and include CK9, CK10, CK11, CK12, CK13, CK14, CK15, CK16, CK17, CK18, CK19 and CK20. Their molecular weight ranges from 40 KDa (CK19) to 64 KDa (CK9). *In vivo*, type I and type II cytokeratins are arranged in pairs of heterotypic Type I and Type II keratin chains and co-expressed. From the molecular weight of IgG gamma 2A, which has only 326 amino acids, intensive *S*-nitrosylation on its total of 10 cysteines as well as its dimerization [126] may be the

reason for it to migrate to such a high molecular region of the gel. The relative intensity of *S*-nitrosylation, however, was weaker for IgG than it was for keratins based on intra-gel staining results. The *S*-nitrosylation intensity of prosaposin was increased in NOC-7 treated samples over that seen in control and hemorrhaged samples, because the relative intensity of *S*-nitrosylation was almost equal between keratins and prosaposin in the latter two samples, whereas after NOC-7 treatment, it was increased almost two-fold based on colorimetric reading using the Image J software.

The differential tyrosine-nitration of human transferrin in vitro. Transferrin is a blood plasma protein designed to bind and deliver iron ions. It is a glycoprotein, which binds Fe(III) ion very tightly but reversibly. Although iron bound to transferrin is less than 0.1% (4 mg) of the total body iron, it is in a dynamic sense the most important iron pool, with the highest rate of turnover (25 mg/24 h). Transferrin has a molecular weight of around 80,000 and contains 2 specific high affinity Fe(III) binding sites. The affinity of transferrin for Fe(III) is extremely high ($1 \times 10^{23} \text{ M}^{-1}$ at pH 7.4) but decreases progressively with decreasing pH below neutrality.[127-129]

Peroxynitrite (ONOO^-) is considered an endogenously formed cytotoxic factor derived from NO and the superoxide anion.[130] 3-Morpholinopyrrolidine (SIN-1) can be used as a possible peroxynitrite donor. Hydrolysis of the mesoionic ring to SIN-1 is required for spontaneous decomposition. Thus, peroxynitrite release depends on the pH of the solution. The time course of the decomposition of SIN-1 was nonlinear, and some delay occurred because of the hydrolysis.[131] SIN-1 generates nearly the same amount of nitrate (NO_3^-) and nitrite (NO_2^-) as the final products.

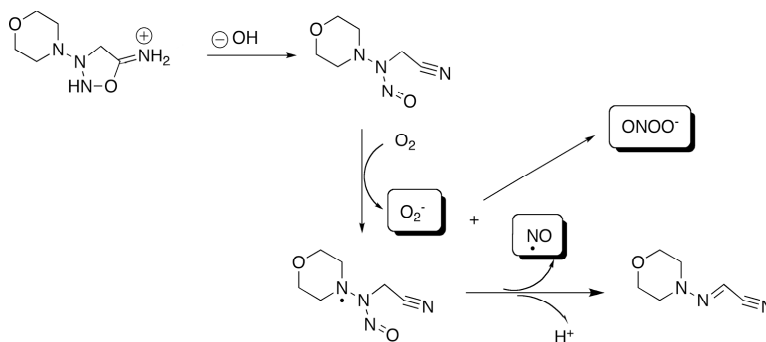


Figure 13 The decomposition of SIN-1 and generation of ONOO^- .

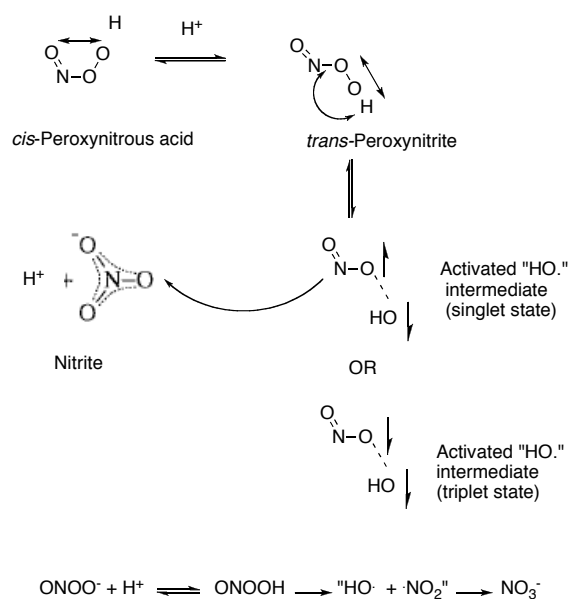


Figure 14 Schematic of the formation of nitrite from peroxyntiride.

Structures of *cis*- and *trans*-peroxyntirite and nitrate ions. The two oxygens in *cis*-peroxyntirite interact weakly, which helps stabilize peroxyntirite. However, *cis*-peroxyntirite cannot directly rearrange to peroxyntirite. *Trans*-peroxyntirite can directly isomerize to nitrate by the terminal oxygen swinging out to attack the nitrogen. Consequently the decay of peroxyntirite depends upon *cis*-peroxyntirite becoming protonated, isomerizing to *trans* peroxyntirous acid, and then rearranging to nitrate. The activated “HO•” state might be a triplet rather than singlet state. (Recreated from Ref.[132])

Tyrosine nitration is a covalent protein modification resulting from the addition of a nitro ($-\text{NO}_2$) group onto one of the two equivalent *ortho* carbons of the aromatic ring of tyrosine residues. The addition of the nitro group implies the formation of a nitrating species, with nitric

oxide providing the source of nitrogen.[133] The formation of peroxynitrite by the reaction of nitric oxide and superoxide and the subsequent reaction of peroxynitrite with CO₂ leads to the formation of an intermediate capable of nitrating tyrosine residues in proteins [130, 134].

The frequency of tyrosine occurrence in proteins is approximately 3-4 mol%, which is similar to that of phenylalanine but substantially higher than that of tryptophan (~1 mol%). Tyrosine is mildly hydrophobic, the calculated hydrophobicity value of tyrosine in a side chain is -1.47 kcal/mol. This value is considerably smaller than the value of -2.27 kcal/mol of phenylalanine and -2.13 kcal/mol of tryptophan and places tyrosine in the middle of the hydrophobicity peaking order of amino acids.[2] Transferrin has 3.78 mol% tyrosine residues (26 out of 688). Many studies indicate the involvement of nitrotyrosine formation during hemorrhage stimulation, mainly in cerebral fluids.[135-140] Investigation into the differential *in vitro* human transferrin nitration of tyrosine in response to nitric oxide stimulation has not been studied. The results of such studies can be used as a reference for samples from hemorrhaged rats to relate the reactive nitric oxide species, (e.g., peroxynitrite), with two separate but co-present chemical modifications, namely cysteine S-nitrosylation and tyrosine nitration.

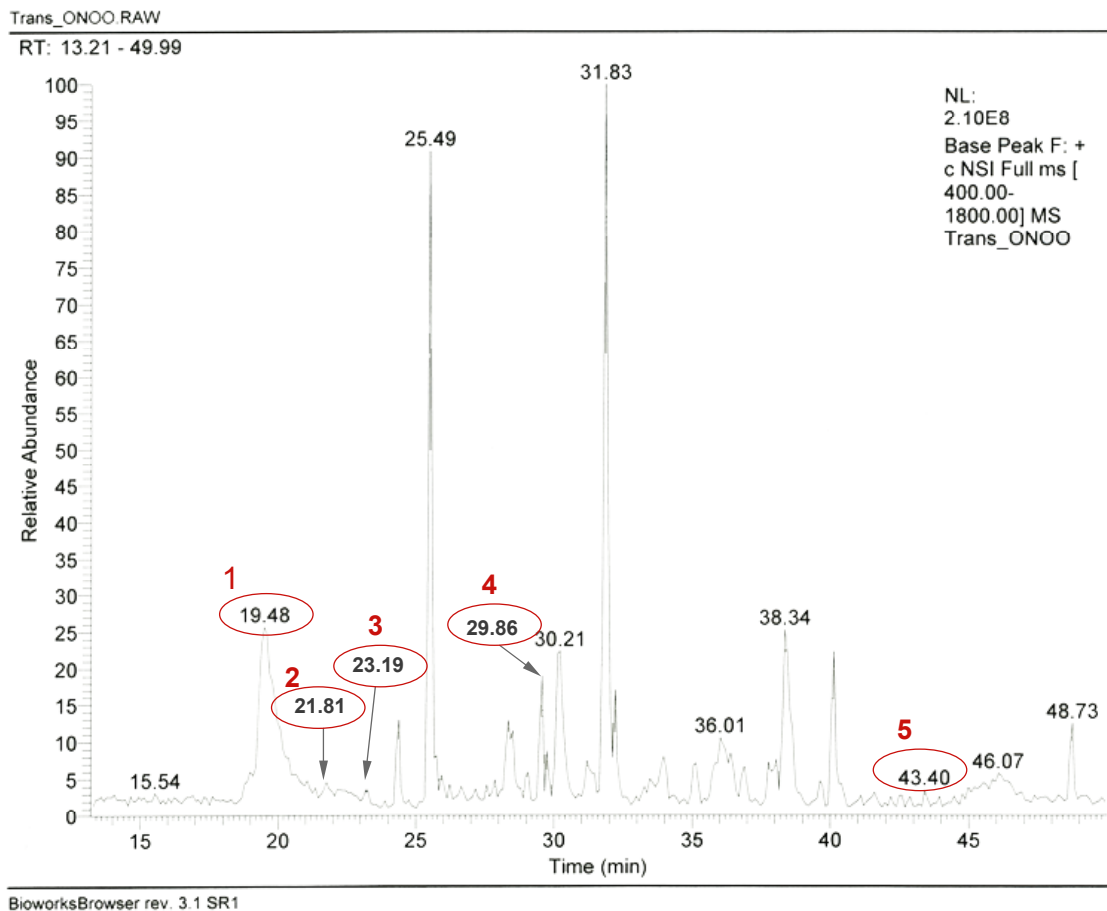


Figure 15 Base peak of full scan mode for human transferrin tryptic digest after treatment with ONOO⁻

LC-ESI-3D ion trap MS-MS spectrum for in-solution digested, ONOO⁻-treated human transferrin. The circled peaks are those that match human transferrin after forcing the SEQUEST searching to index only human transferrin as its database. The matched peptide fragments are listed in table 5.

No.	Retention time (min)	Peak No.	Sequence	MH+	z	XCorr	Ions
1	18.43	946	DSGFQM*NQLRGKK	1525.72	3	2.011	16/48
	20.74	988	KDSGFQM*NQLRGK	1397.54	3	2.713	14/22
2	21.57~22.06	1003~1012	KDSGFQM*NQLR	1340.49	3	2.210	21/40
3	23.12~23.27	1031~1034	DSGFQM*NQLR	1212.32	2	2.470	15/18
4	29.86	1154	KPVEEYANC@HLAR	1562.73	3	1.044	12/48
5	43.50	1402	M*YLGYEYVTAIR	1495.73	2	3.226	19/22

Table 3. Peptide fragments from LC-MS/MS for “TRFE_HUMAN serotransferrin precursor (transferrin)”.

Protein score=3280.2, Accession No= 136191, Post-translational modifications were indicated in the table:
*: methionine oxidization; @: cysteine reduction. Sample numbers in the table correspond to the numbers in Figure 12.

A Transferrin + SIN Measured peptides: 121 Min. Sequence coverage: 41%
Matched peptides: 19 Z Score (profound) =2.30

No.	Measured Mass	Computed Mass	Error (ppm)	Residues		Missed cut	Peptide sequence	Modification
				Start	End			
1	2383.339	2383.129	88	328	346	2	MDAKMYLGYEYVTAIRNLR	(1)+NO2-H@Y; (2) +O@M
2	2400.312	2400.261	21	311	331	3	DLLFKDSAHLKVPFRMDAK	(1)+O@M
3	2463.192	2463.221	-12	122	143	4	KDSGFQMNQLRGKKSCHTGLGR	(1)+O@M
4	3385.469	3385.669	-59	465	494	4	GKKSCHTAVGRTAGWNIPMGLLYNKINHCR	(1)+NO2-H@Y; (1) +O@M
5	3656.996	3656.788	57	652	682	4	DDTVCLAKLHDRNTYEKYLGEYVKAAGNLR	(1)+NO2-H@Y
6	3853.924	3853.773	39	531	564	3	EGYYGYTGFRCLVEKGDVAFVKHQTPQNTGGK	(3)+NO2-H@Y

B Transferrin + ONOO⁻ Measured peptides: 313 Min. Sequence coverage: 47%
Matched peptides: 53 Z Score (profound) =2.34

No.	Measured Mass	Computed Mass	Error (ppm)	Residues		Missed cut	Peptide sequence	Modification
				Start	End			
1	1210.531	1210.539	-7	122	132	0	DSGFQMNQLR	(1)+O@M
2	1338.63	1338.634	-3	122	132	1	KDSGFQMNQLR	(1)+O@M
3	1395.649	1395.656	-5	123	134	1	DSGFQMNQLRK	(1)+O@M
4	1493.714	1493.722	-5	332	343	0	MYLGYEYVTAIR	(1)+O@M
5	1523.742	1523.731	3	123	135	2	DSGFQMNQLRKK	(1)+O@M
6	1523.742	1523.731	3	122	134	2	KDSGFQMNQLRK	(1)+O@M
7	2462.159	2462.171	-5	324	343	2	VPPRMDAKMYLGYEYVTAIR	(2)+NO2-H@Y
8	2545.224	2545.226	-1	252	273	1	SMGGKEDLIWELLNQAQEHFGK	(1)+O@M
9	2788.36	2788.347	5	274	297	2	SMGGKEDLIWELLNQAQEHFGKDK	(1)+O@M
10	3282.628	3282.637	-3	133	162	3	GKKSCHTGLGRSAGWNIPGLLYCDLPEPR	(1)+NO2-H@Y
11	3557.799	3557.772	8	588	618	4	KPVEEYANCHLARAPNHAVVTRKDKEACVHK	(1)+NO2-H@Y

Table 4. MALDI-MS matching results for NO donor-treated human transferrin *in vitro*.

Human transferrin was treated *in vitro* with 3-morpholiniosydnonimine (SIN) or ONOO⁻, digested with trypsin, and the peptide fragments were analyzed using by MALDI-TOF-TOF-MS. A: peptide fragments from transferrin treated with SIN that were identified with modification. B: peptide fragments from transferrin treated with ONOO⁻ that were identified with modification. (The other, numerous non-modified matching peptide fragments are not shown in the table.)

As shown in Table 3 and Figure 15, the NO donor peroxyntirite (ONOO⁻)-treated human transferrin had several identified peptide sequences identified by LC-ESI-3D ion trap MS-MS analyses. However, chemical modifications beyond methionine oxidation and cysteine alkylation were not identifiable using the SEQUEST algorithm. This may partly due to the great reaction complexity of the free radical NO, or to the low resolution and mass accuracy of the ion trap instrument. The SEQUEST searching criteria involved: chemical modifications, species, missed tryptic cleavages and accuracy in ppm. Due to the overwhelming signal from high intensity peptides derived from keratin and serum albumin, which were contaminants during the transferring manufacturing (and perhaps sample processing), transferrin signals were “buried”

under them and the matching scores (an XCorr score of ≥ 2.0 is considered a trustable match) of majority the majority of the peptides were very low. Human transferrin that was treated with SIN-1 has even lower matching score when data from LC-MS-MS analyses were examined with Sequest algorithm.

Using high resolution MALDI-TOF-TOF-MS, several sites of tyrosine nitration were identified with high confidence (as seen in Table 4). Briefly, SIN-1 treated human transferrin has four methionine oxidation sites, 128, 328, 332 and 483, and six possible tyrosine nitration sites. One tyrosine nitration occurred among one of three tyrosines in the peptide: “³²⁸MDAKMYLGYEYVTAIRNLR³⁴⁶”. One tyrosine nitration occurred among one of the three tyrosines in the peptide “⁶⁵²DDTVCLAKLHDRNTYEKYLGEEYVKAVGNLR⁶⁸²”. Tyrosine nitration occurred on all three tyrosines in the peptide “⁵³¹EGYYGYTGFRCLVEKGDVAFVKHQTVPQNTGGK⁵⁶⁴”. One nitrotyrosine site, Y487, was found in the peptide “⁴⁶⁵GKKSCHTAVGRTAGWNIPMGLLYNKINHCR⁴⁹⁴”, since there is only one tyrosine residue in this sequence, its site of formation is clear.

ONOO⁻ treatment resulted in human transferrin nitrotyrosine formation different from its SIN-1-treated counterpart. There was one fewer possible tyrosine nitration site than in the SIN-1 treated samples. Two nitrotyrosines were found in the peptide “³²⁴VPPRMDAKMYLGYEYVT AIR³⁴³”, which has three candidate tyrosines. This peptide has overlapping amino acids with “³²⁸MDAKMYLGYEYVTAIRNLR³⁴⁶”, which had only one nitrotyrosine in SIN-1-treated sample, but two in the ONOO⁻-treated sample. Two other nitrotyrosine residues were found in ONOO⁻-treated samples, which were Y155 from peptide “¹³³GKKSCHTGLGRSAGWNIPIGLLYCDLPEPR¹⁶²” and Y603 from peptide “⁵⁸⁸KPVEEYANCHLARAPNHAVVTRKDKEACVHK⁶¹⁸”. In contrast with differential

tyrosine nitration, the methionine oxidation sites were consistent between the two samples. The difference in nitrotyrosine pattern may be due to the kinetics of the generation of free NO radical from the two NO donors, where SIN-1 is an indirect NO donor, while ONOO⁻ is a more direct yet short-lived NO donor.

Identification ceruloplasmin in NOC-7-treated rat plasma. Ceruloplasmin (caeruloplasmin, ferroxidase or iron (II): oxygen oxidoreductase) is an enzyme synthesized in the liver that can bind eight atoms of copper. Although it is often considered a copper transport protein, this is not its primary function, just as hemoglobin is not merely a carrier of iron. The main carrier for copper in the plasma of humans is albumin. Ceruloplasmin's major function is to catalyze the oxidation of ferrous iron (Fe²⁺) to ferric iron (Fe³⁺), therefore assisting in its transport in the plasma in association with transferrin, which can only carry iron in the ferric state. [15]

Ceruloplasmin is abundant its mean, unevoked concentration in adults of about 300 µg/ml.[141] It is an approximately 130 KDa, monomeric glycoprotein composed of three 42~45 KDa domains that are homologous to each other. Purified human ceruloplasmin typically contains an average of seven copper atoms belonging to three coordination classes or "types"; however, there is significant variability in the reported amounts and type classification. In this study, the rat was used as the model system, and the effects of hemorrhage as well as NO donor-treated samples of rat ceruloplasmin, which has been previously been studied in this specific setting before. Therefore, when the database searching (NCBI database in Mascot) criteria for protein limited the species to *Rattus norvegicus*, especially for truncated forms, the results came out with identities that all started with such as "hypothetical protein" as identified names. After analyzing the sequence homology between human and rat ceruloplasmin, (as shown in Figure

16) it could then be confirmed that those before “hypothetical” proteins are, in fact, rat ceruloplasmin.



Figure 16 Sequence homology between human and rat ceruloplasmin.

The representative amino acid sequences used in mass spectrometric identification (Mascot database searching) of ceruloplasmin from rat plasma. The red rectangular encloses the variances between human and rat ceruloplasmin. In the Mascot-based search, ceruloplasmin was identified as “gi|3485549|ref|XP|215541.2 Hypothetical protein XP_215541.2 [*Rattus norvegicus*] with peptide coverage=10%, Estimated Z value=1.83, *pI*=5.4, MW=120.65 KDa.

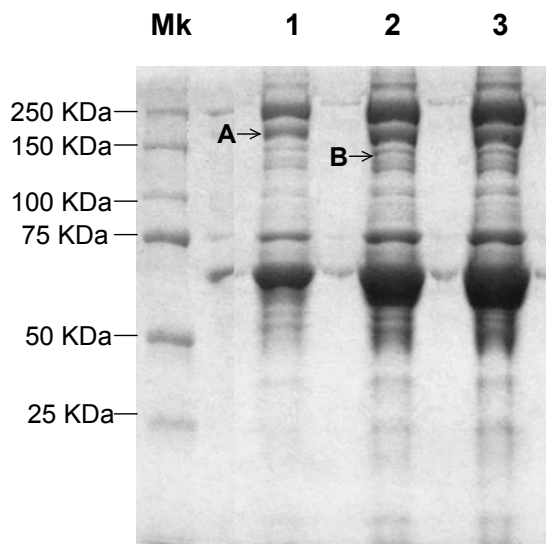


Figure 17 1-D SDS-PAGE gel (Coomassie blue staining) for *in vitro* ONOO⁻-treated rat plasma samples.

NuPAGE 3~8% Tris-Acetate gel (Invitrogen) was run at 60V for 150 min for samples: (1~3) ONOO⁻-

treated rat plasma: sample loading were 5, 10 and 20 µg, respectively. The gel was stained with Coomassie blue for 1 h and destained for 3 h at 4 °C for sharper bands (for details, please see Material and Methods).

Sample name	Matching peptide name	Matching peptide	Modifications	Observed m/z	Computed m/z	Start	End	Missed cut
Plasma band A	gi 21955142 ref NP_665722.1 pregnancy-zone protein; alpha-1-macroglobulin [Rattus norvegicus]	ALLAYAFALAGNRAKR	(1)+NO2@Y	1750.958	1750.971	1162	1177	2
		DAKDLTFYYLIKAR	(1)+NO2@Y	1761.93	1761.917	488	501	2
		SKAISYLISGYQR	(1)+NO2@Y	1530.762	1530.791	1016	1028	1
		IEHSFEVKEYVLPK	(1)+NO2@Y	1762.957	1762.901	213	226	1
		DLSSSDLTTASKIVKWISK	(2)+HPO3@STY	2238.135	2238.058	1245	1263	2
Plasma band B	gi 6970046 gb AAF34175.1 GPI-anchored ceruloplasmin [Rattus norvegicus]	DLYSGLIGPLIVCRKSYVK	(2)+HPO3@STY	2283.177	2283.113	882	900	2
		NMASRPYSIHAGHVTKSSTVTPTLPGEVR	(3)+HPO3@STY	3460.627	3460.575	820	849	2
	gi 34855491 ref XP_215541.2 hypothetical protein XP_215541 [Rattus norvegicus]	ALYSEYTDGTFTK	(1)+NO2@Y;	1540.696	1540.68	70	82	0
		TYIWQIPERSGAGTEDSPCIPWAYYSTVDR		3460.627	3460.602	850	879	1

Table 5 MASCOT searching result for rat plasma treated with NOC7

Summary table of peptides matched after comparing the theoretical digest with experimental digest and MALDI-TOF-TOF-MS fragment ion information. The peptide sequences shown are from the highest ranking matching proteins. (Detailed matching lists are provided in Appendix section at the end of this document)

In the secondary matching for identity of plasma band B, “hypothetical protein XP_215541 [Rattus norvegicus]”, the sequence ⁷⁰ALYSEYTDGTFTK⁸² with one 3-nitrotyrosine modification and *m/z* 1540.696 was identical with the sequence ⁷⁰ALYSEYTDGTFTK⁸² with no modification and *m/z* 1496.8259 (computed mass) of “Ferroxidase (EC 1.16.3.1) precursor [Rattus norvegicus], accession No=gi|92233”. The other sequence for plasma band B, ⁸⁵⁰TYIWQIPERSGATEDSPCIPWAYYSTVDR⁸⁷⁹ with no modification, is another identical sequence matched with rat ferroxidase, i.e., ceruloplasmin. These pieces of evidence confirmed that the mis-match of the identity of ceruloplasmin is due to the redundancy of entries in the database and the difference in modification level. Detailed data are compiled in the appendix.

Identification of altered rat plasma proteome after in vitro NOC-7 treatment. To understand the alteration of protein level before and after hemorrhagic shock, the rat plasma

proteome was examined using difference gel electrophoresis after depletion of rat plasma albumin in the *in vitro* NOC-7 treated rat plasma sample.

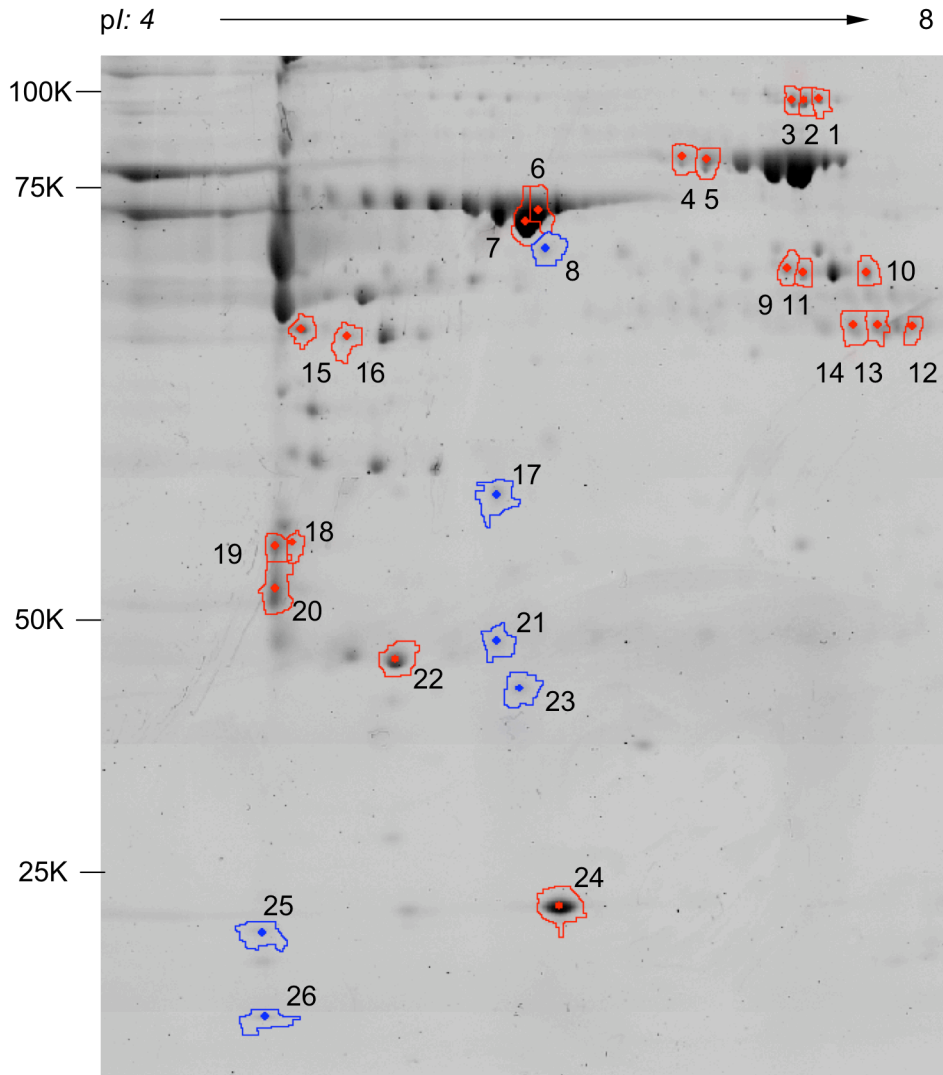


Figure 18 Representative DiGE results after DeCyder software analysis of albumin depleted rat plasma.

The fluorescence gel image of rat plasma 2-D gel electrophoresis, in which the primary image is from the control sample and the secondary image is from hemorrhaged rat. The relative ratio was reflected in the color of gel spots: red spots are those that have a decreased protein level in hemorrhage treated sample; blue spots are those that have an increased protein level. The pixel volume ratio was calculated based on the enclosed area and intensity of the gel spots with the image analysis on pixel and image depth algorithm in DeCyder. The pI range on the gel was, from left to right, 4 to 8.

No. on gel	Vol. Ratio	Protein Name	MW	Accession No.	Sum. Vol. Ratio	Function
1	-2.04	Plasminogen	90537	NP_445943.1	-2.02	A serine protease that is released into the circulation that degrades many blood plasma proteins, most notably fibrin clots. Its deficiency may lead to thrombosis.[142, 143]
2	-1.79					
3	-2.31					
4	-1.59	Transferrin	76396	NP_001013128.1	-1.58	Plays a role in iron transport and homeostasis.[144, 145]
5	-1.54					
6	-1.52	Albumin	68719	NP_599153.1	-1.69	May play a role in nitric oxide signaling; may mediate formation of S-nitrosothiols.[146-153]
7	-1.83					
8	1.52	Futuina beta	41533	NP_44580.1	1.52	Inhibits insulin receptor tyrosine kinase activity, protease inhibitory activities; developmentally regulates calcium, metabolism and osteogenesis.[154-157]
9	-1.68	Fibrinogen beta	54304	NP_064456.1	-1.92	Cleaved by thrombin; plays a role in wound healing.[158, 159]
10	-2.24					
11	-1.77	Fibrinogen alpha	86658	NP_001008724.1	-1.77	Plays a role in blood coagulation; may be involved in liver regeneration.[160-163]
12	-1.91	IgG gamma 2A	36319	AAB59660.1	-1.79	Most abundant immunoglobulin, consists as 75% of serum immunoglobulin in human.[164-166]
13	-1.76					
14	-1.75					
15	-2.60	Fibrinogen gamma chain precursor	49652	NP_036691.2	-1.96	Combines with fibrinogen alpha and beta to form the mature fibrinogen molecule; plays a role in inflammatory response.[167-171]
16	-1.56					
17	2.57	Type I keratin	40~64K	CK9~CK20	2.57	Components of intra-cytoplasmic cytoskeleton, Type I keratins co-express and form heterotypic pairs with type II keratins. [172-177]
18	-2.46	Type II keratin	52~76K	CK1~CK8	-1.96	
19	-1.60					
20	-2.19					
21	2.95	IgG kappa chain	14050	AA41413.1	2.95	Binds with IgG heavy chains, recognition of antigens.[178-187]
22	-2.09	Apolipoprotein A I	30062	NP_036870.1	-2.09	Major component of high-density lipoprotein (HDL) that is involved in intercellular cholesterol transport in astrocytes; cofactor for lecithin cholesterolacyl- transferase (LCAT).[188-191]
23	2.27	Plasma glutathione S-peroxidase precursor	22259	P04041	2.27	Protects the hemoglobin in erythrocytes from oxidative breakdown.[192-195]
24	-2.02	Transthyretin	15748	NP_036813.1	-2.02	Binds thyroxine (T4) and 3,5,3' thiiodothyronine (T3) [196, 197]
25	1.66	Apolipoprotein C III precursor	11117	NP_036633.1	1.66	Very low density lipoprotein (VLDL) that comprises a major component of the lipid transport system; increased levels induce hypertriglyceridemia. [198-201]
26	2.34	Apolipoprotein C II	8690*	AAB59380.1	2.34	Activate lipoprotein lipase, thus activate the catabolism of chylomycons and VLDL. [200, 201]

Table 6 Protein identification and relative ratios of protein levels (compared to control) for rat plasma proteome with NOC-7 treatment.

Analysis results were compiled from DeCyder relative ratio analysis and the x,y coordinates on the DiGE image for spot locations (in Figure 18). The red numbers indicate the decreased proteins in hemorrhage treated rat plasma when compared to control rat plasma; the blue numbers indicate the increased proteins. The accession numbers of Type I and Type II keratins, because of their heterotypic co-existence, are not specified. *: For Spot 26, the immature form of Apolipoprotein C II has a molecular weight of ~11KDa.

There were 16 proteins in the rat plasma proteome that were identified to show a significant change in level. Relative levels were determined by DiGE, and identities were determined by MS peptide fingerprinting (PMF) analysis. (Table 6) Out of these 16 proteins, six were present at increased levels of more than 1.5-fold in NOC-7 treated rat plasma than in control rat plasma. Four out of these six proteins had an even more significant increase of >2-fold. Type I keratin, IgG kappa chain, plasma glutathione *S*-peroxidase precursor, and apolipoprotein CII had 2.57, 2.95, 2.27 and 2.34-fold increases, respectively. Less of a difference was observed for fetuin beta and apolipoprotein C III, with 1.52- and 1.66-fold increases, respectively.

There were 10 proteins whose levels were decreased more than 1.5-fold in the NOC-7 treated rat plasma sample. Three out of these ten had significant decreases of >2-fold. They include, plasminogen, apolipoprotein A I, and transthyretin, with 2.02, 2.09, and 2.02-fold decreases, respectively. Less decrease in protein level was found for fibrinogen beta, fibrinogen alpha, fibrinogen gamma, IgG gamma 2A, type II keratin, transferrin, and albumin, with 1.92, 1.77, 1.96, 1.79, 1.96, 1.56, and 1.69-fold decreases, respectively.

3.5.3 Discussion

False negatives/positives in the biotin switch method. The biotin switch assay assumes that only an *S*-nitrosylated cysteine residues will become biotinylated. However, if not all cysteines have been successfully blocked with the methylthiolating reagent MMTS, the remaining free thiol groups on cysteines may produce a signal, giving a false positive result. SDS is included to ensure accessibility of MMTS to each thiol by promoting denaturation. Another

false positive scenario happens when an MMTS-inaccessible cysteine become accessible to biotin-HPDP during the labeling step if time- or DMSO-dependent denaturation occurs and results in the unhindered exposure of a thiol. To ensure the maximal accessibility of cysteines to MMTS, a minimum ratio of SDS to protein is essential to ensure maximal protein denaturation. Thus, protein samples that exceed a concentration of 0.8 μg per μl are more prone to be incompletely blocked by MMTS. In the biotinylation labeling reaction, a key control is the use of a DMF vehicle control, instead of biotin-HPDP. A blocked sample that has been subjected to DMF treatment rather than biotin-HPDP treatment shows two bands, which represent endogenously biotinylated proteins. To ensure that a signal is due to NOS activity and not to incomplete blocking, tissue samples that are devoid of NOS are ideal. Thus, protein samples prepared from NOS^{-/-} mice provide ideal controls. If these types of controls are unavailable, then samples prepared with NOS inhibitors, such as nitroarginine, can also be used as negative controls. In the present study, 80 μg of biotin per mg of protein substrate was used for biotinylation reactions. The reaction was carried out in the dark at 4 °C overnight, or at room temperature for 4 h, depending on the stability of the protein samples at ambient temperature. A false negative can be caused by incomplete biotinylation on S-nitrosothiols. Incomplete biotinylation could be the outcome of insufficient incubation time or oxidation of reaction material, especially via overexposure to light.

Modification of acetone precipitation in biotin-switch assay. Unlike complex protein mixtures that can be purified by classical acetone precipitation, for pre-fractionated samples, which have fewer components, the standard biotin switch procedure needs to be modified. In this study, the initial trials of using acetone to precipitate proteins during the assay provided very low recovery and a viscous precipitated pellet. Part of this may be due to the relative simplicity of the

protein samples after albumin depletion and MMTS reaction. Most of this may be due to the dramatic change of pH values of the solution under the strong basic condition of β -elimination. Therefore, the work-around was to neutralize the acetone precipitation to obtain a high recovery. Briefly, the modified precipitation procedures were as follows: After adding 10 volume of pre-chilled acetone, the solution was incubated at $-20\text{ }^{\circ}\text{C}$ overnight. The supernatant of the mixture was discarded after centrifuging at $>2,500g$ for 10 min. Ten volumes of pre-chilled 10% trichloroacetic acid in acetone was added and the mixture was vortexed thoroughly and incubated at $-20\text{ }^{\circ}\text{C}$ for 2 h. The supernatant was then removed after centrifugation at $12,000g$ for 10 min. The pellet was then resuspended into $100\text{ }\mu\text{l}$ of HENS buffer and the pH was adjusted to 7. Ten volumes of pre-chilled acetone were added to the new pellet and the mixture was incubated at $-20\text{ }^{\circ}\text{C}$ overnight. After centrifugation at $12,000g$ for 10 min, the pellets were washed once more with pre-chilled acetone. HENS buffer ($200\text{ }\mu\text{l}$) was then added to the pellet to resuspend it for the biotinylation reaction.

In present study, the overall recovery from biotin-switch assay was increased from less than 10% to at least 30% via a simple but previously unrecognized modification to the process. With three-fold improvement in reaction yield, the method's capability was enhanced for investigation of *S*-nitrosylation in biological systems, where low stoichiometry as well as dynamic turn over of *S*-nitroso groups naturally exists. Furthermore, the low-yield problem of the original biotin-switch assay was tackled by modifying a simple property – pH. This modified biotin-switch assay can now be applied to a wider spectrum with less limitation of sample size. Part of the results from this study of *S*-nitrosylated plasma proteins was published in [118].

Decreased plasminogen in NOC-7 treated rat plasma. The primary *in vivo* function of the serine protease plasmin (Pm) is to regulate vascular patency by degrading fibrin-containing

thrombi. Activation of the fibrinolytic system is dependent on the conversion of the plasma zymogen, plasminogen (Pg) to Pm by the physiological activators urokinase-type Pg activator (uPA) or tissue-type plasminogen activator (tPA).[142, 143] As a β -globulin with 2% carbohydrate and molecular weight of 90 KDa, Pg is found in healthy adult plasma or serum in a concentration of 200 mg/l (i.e., 2.2 μ M).[202] The relationship between acute hemorrhage and decreased protein level of Pg (by 2.02 fold) may due to the Pm, which is released into the circulation in the form of Pg, and activated by uPA, tPA, thrombin, fibrin and Haeman factor. Therefore, the lower the level of Pg, the less the extent of fibrinolysis, the process that dissolves fibrin and results in removal of small blood clots. Furthermore, there are a number of indirect investigations that indicate Pg plays a critical role in events involved in vascular remodeling.[203-205] In addition to its role in vascular injury and repair, as one of the components of the fibrinolytic system, Pg also has been implicated in a number of events associated with skin wound healing. Pg-deficient mice demonstrate an inability to efficiently remove necrotic tissue and heal wounds in myocardial infarction [206] and liver injury/repair. [207] There is also an indirect relationship between the level of Pg and tPA or uPA. The activation of Pg by tPA depends on the presence of fibrin, whereas the activation of Pg by uPA is not.[208, 209] uPA, not tPA, specifically mediates arterial neointima formation in mice. [210] Interestingly, the extent of SNO modification of tPA positively coorelates with its anti-platelet activity, which means that the increase in the polynitrosylated form of tPA will decrease its fibrinolytic activity shown through the Pg/Pm pathway.[211] tPA, found to have multiple S-nitrosylation sites *in vitro* after treatment with acidified nitrite (NO_2^-), is as major a S-nitrosothiol reaction target as albumin. During acute hemorrhage, the decreased Pg level could have resulted from its regulation by tPA through its decreased S-nitrosylation level in overall

elevated RSNO plasma protein, or by the promoted liver function that increased the degradation of tPA, which then prohibits the bleeding through the fibrinolysis system. [212]

Decreased fibrinogen isoform levels in NOC-7-treated rat. In this study, the levels of three major isoforms of fibrinogen were decreased -- 1.92-fold for beta, 1.77-folds for alpha, and 1.96-fold for gamma precursor. These findings agrees with previous investigations in which experiments done with swine showed that the decreased concentration of fibrinogen in hemorrhagic shock is due to the accelerated degradation of fibrinogen, not the production of it. [213, 214] It has also been suggested that a decrease in fibrinogen levels should be treated as an early indicator of human postpartum hemorrhage (PPH). In humans at the 0 hour timepoint, the risk for severe PPH is 2.63-fold higher for each 1 g/L decrease of fibrinogen. The negative predictive value of a fibrinogen concentration of >4 g/L is 79% and the positive predictive value of a concentration ≤ 2 g/L is 100%. [215]

Decreased transthyretin level in NOC7 treated rat. Transthyretin (TTR) (a.k.a. proalbumin), was found to be decreased by 2.02-fold in rat plasma after hemorrhagic shock. Although TTR has higher thyroid hormone binding activity than does albumin, its plasma concentration is much lower. TTR is a serum and cerebrospinal fluid carrier of the thyroid hormone thyroxine (T4). Since TTR binds promiscuously to many aromatic compounds, including polychlorinated biphenyls (PCBs), and generally does not bind T4 in serum, there is speculation that TTR's "true function" is to generally sweep up toxic and foreign compounds in the blood stream. The isolated monomer of TTR does not have such binding capacity, which is a function of the quaternary structure formed by its homeotetramer. [216-218] A low serum thyroxine level is associated with intraventricular hemorrhage (IVH) and death in very low birth weight infants. [219] According to an earlier findings, [220] there is no apparent change in the

rate of thyroxine disappearance, nor in its serum concentration, from the circulation after hemorrhage. Furthermore, thyroid-stimulating hormone (TSH) secretion is not significantly elevated after hemorrhage, either. It comes as no surprise that the thyroxine level is decreased by several peripheral inhibition mechanisms, rather than by simply elevating the degradation or lowering the secretion of TSH.[221, 222] Therefore, the decrease in the TTR level may be a retrospective result from reduced transportation of thyroxine in rat plasma after hemorrhage.

Differential alteration of Apolipoprotein isoforms in NOC-7 treated rat plasma. Three Apolipoprotein isoforms, AI, CII, and CIII, had different alterations in rat plasma sample after NOC-7 treatment, in which a decrease of 2.09-fold in AI, an increase of 1.66-fold in CIII, and an increase of 2.34-fold in CII was observed. Apolipoprotein AI is one of the major components of high-density lipoproteins (HDL), whereas CII and CIII both belong to the family of low-density lipoproteins (LDL). The increase in LDL indicates the adjustment of lipoprotein metabolism, which was probably triggered by activation of lipoprotein lipase (LPL) by LDL in the body's attempt to inhibit the hemorrhage.[223, 224] An experiment needs to be done wherein the level of triglycerides in rat plasma, which can serve as an end product of activated LPL pathway, is measured.[223, 224] While HDL is considered unrelated to hemorrhagic events, the incidence of thromboembolic stroke declines consistently with increasing HDL cholesterol levels ($p = 0.003$) in elderly men.[225] Extremely low HDL levels are a risk factor for ischemic strokes, in which HDL of 3 mg/dL leads to rapidly progressive stroke with a fatal outcome.[226] The posterior circulation damage caused by acute hemorrhage is then demonstrated by the decreased level in HDL, which then enhances the risk of ischemic stroke by loss of blood. Therefore, the orchestrated effect of modulating the lipoprotein levels in plasma can be explained in two aspects: on the one hand, increased LDL leads to increased LPL activity, which then helps

inhibit hemorrhage-induced damage; on the other hand, the extent of acute hemorrhage was demonstrated by the decreased HDL level, which in turn elevates the risk of ischemic shock that could be caused by acute hemorrhage.

Increase of fetuin beta in early hemorrhage. Fetuin beta protein levels increased by 1.52-fold in rat plasma after hemorrhage. Fetuin beta (a.k.a. Fetuin-B) is a newly discovered member of the fetuin family,[227] which has homology to and overlapping function with fetuin alpha (a.k.a. Fetuin-A). There is close genetic proximity between fetuin-A and fetuin-B. Unlike fetuin-A, the amount of fetuin-B protein in human serum is higher in females than in males. Functional analysis shows that fetuin-B, similar to fetuin-A, is an inhibitor of basic calcium phosphate precipitation, albeit less active.[228] Recent studies have revealed a function of fetuin-B that differs from fetuin-A's major function, which is systemic calcification. Instead, fetuin-B has been noted to show tumor suppressor activity, as its overexpression suppresses the growth of skin squamous carcinoma cell xenograft tumors in nude mice.[229] Since the research on fetuin-B is not as developed as that on fetuin-A, and they share many similarities in function, the potential role of fetuin-B in the present study may be explainable through the function of fetuin-A. One notable function for fetuin-A was found during the course of renal failure, a common sequela of hemorrhagic shock -- increased fetuin-A levels positively correlate with vascular calcification in patients with diabetes and mild to moderate renal impairment, and an inverse relationship is observed in dialysis patients.[230] Early hemorrhage-triggered organ failure, especially kidney failure, could be one of the main stimulæ for the increased level of fetuin-B. If that is the case, fetuin-B may be involved in the same pathway related to inflammatory response cascades, which includes IgG free light chain kappa. Further investigation is needed to establish any such relationship, however.

Increase of IgG kappa chain after NOC-7 treatment. The increased protein level of free IgG kappa chain was observed to be nearly 3-fold in rat plasma after hemorrhage. Although this protein was discovered in 1848 (and known as Bence-Jones protein), measurement of its free forms became possible only earlier this century.[231, 232] Nephrotoxicity is gauged by monitoring this protein in cancer patients' urine samples. It is, however, not common to detect free IgG kappa chain in plasma, not only because of the predominant presence of albumin and immunoglobulin heavy chains in plasma, but also because of its fast clearance by the kidney and fast filtration by urinary system. Normally, IgG kappa chains are synthesized in higher amounts than are lamda chains, resulting in normal serum ratio of κ/λ of 1.2~2.0.[233] In plasma, IgG kappa chain has high affinity binding to heavy chains through both disulfide bond and non-covalent interactions. Renal excretion and catabolism is the primary means for elimination of proteins with molecular masses <60 kDa, including free light chains, which are filtered through the glomerulus, reabsorbed by cells of the proximal tubules, and catabolized within those cells. The clearance of light chains is estimated to be ~6-10% of the glomerular filtration rate. [234] The selective secretion of light chain monomers in urine makes the plasma form of light chain to be preferably dimers. Hemorrhage leads to cardiovascular collapse and death in adrenal-insufficient animals. Kidney failure is, in many cases of hemorrhage, one of the first responsive symptoms in order to restore the blood flow that in response to the massive loss of erythrocytes, [235] and degenerated kidney function can also trigger the decreased secretion and catabolism of free light chain kappa, causing the increase in the plasma kappa chain level. In the present study, kidney function was not monitored in parallel to the hemorrhage. An in-depth study could be carried out using standard urinary protein electrophoresis (UPE), immunoelectrophoresis (IEP), or immunofixation electrophoresis (IFE) methods to measure the urinary level of free kappa

chain so as to test whether the increase in plasma kappa chain level is due to the decreased secretion or due to a compensation in blood flow.

Increase of plasma glutathione S-peroxidase precursor after hemorrhage. Plasma glutathione S-peroxidase precursor increased 2.27-fold in rat plasma after hemorrhage. The anti-inflammatory properties of glutathione peroxidase (GPx) was found in ophthalmic lens-induced uveitis to decrease the uveal hemorrhage in Lewis rat. [236] As a key player in free radical scavenging mechanisms, GPx can be induced by excess free radicals. This has been shown in cerebral vasospasm in a monkey model,[237] and GPx-deficient mice are known to exhibit severe hemorrhage, as compared to wild-type animals, in response to apoptosis-inducing treatment.[238] It has been found in many organ hemorrhage cases, especially brain hemorrhage,[239-243] that reactive oxygen species formation is greatly induced in naïve endothelial cells and is correlated to shock severity.[244] Being the most potent antioxidant enzyme,[245] GPx content can modulate the threshold of oxidative attacks that cells can sustain. In other words, the increased GPx level may be one of the many feedback survival responses induced during hemorrhage. Since hydrogen peroxide (H_2O_2) and reduced monomeric glutathione (GSH) are the preferred substrates for GPx, (The reaction is: $2GSH + H_2O_2 \rightarrow GSSG + 2H_2O$) the kinetics of the product - glutathione disulfide (GSSG), and substrate - the plasma H_2O_2 , can be measured in rat plasma to relate the oxidative stress level with the GPx induction. Compartmental localization of GPx can also be assessed to testify whether the increase of GPx was due to the elevated release from cytosol or mitochondria compartment of erythrocytes. In addition, an inhibitory assay using either small molecule inhibitors of GPx, reduced selenium for decreasing GPx activity, or direct inhibition by specific antibodies could be used to investigate retrospectively the importance of the changed GPx level to the severity of hemorrhage in the rat.

Decrease of transferrin, IgG gamma 2A and albumin after hemorrhage. The changes in the levels of transferrin, IgG gamma 2A and albumin after hemorrhage were found to be comparable with 1.56-fold 1.79-fold and 1.69-fold decreases, respectively.

Since at least 80% of serum albumin was depleted before the biotin switch assay was started, the *S*-nitrosylated albumin was not detectable in the traditional 2D gel electrophoresis; this was probably exacerbated by the low yield of biotin switch assay. However, the level of albumin after depletion did decrease by 1.69-fold as seen from the 2-D DiGE experiment. This is consistent with some other observations, particularly the one in which plasma albumin was found to be decreased after acute but non-traumatic hemorrhage in the rat.[246] There have been many clinical applications of albumin compensatory treatment for hemorrhagic injuries [247-252].

IgG gamma 2A and transferrin were both detected in their *S*-nitrosylated forms, and were found to be present in decreased levels after NOC-7 treatment. However, as these two assays were carried out independently, the two apparently related changes cannot be correlated. It would be ideal to do a biotin-switch assay followed by a DiGE experiment to simultaneously monitor the protein level and *S*-nitrosylation for the rat plasma proteome. The challenge of doing a biotin-switch assay coupled with a reciprocal-labeling DiGE experiment could be surmounted only if the final measurable protein concentration is within range of at least 250~500 $\mu\text{g/ml}$. In the current study, the resulting total protein concentration after albumin depletion was about 250 $\mu\text{g/ml}$ for rat plasma, and the yield after biotin switch assay was about only 20%. So the combined recovery from a 10 mg/ml plasma sample is only 50 $\mu\text{g/ml}$. Therefore, the sample size will have to be multiplied 5-10 times larger. For the rat model used in this study, 0.7 ml of blood was withdrawn, of which only 20 μl of plasma (out of total of 200 μl) was used for the biotin switch assay. It will still be feasible to use 50% or 100% of this volume for such an experimental

design. Otherwise, samples from different animals would need to be pooled, or a larger animal would need to be used as the model (to have the required larger total blood volume).

As an 80KDa glycoprotein with two specific high affinity Fe(III) binding sites, transferrin has an extremely high affinity for Fe (III) ($1 \times 10^{23} \text{ M}^{-1}$ at pH 7.4) that decreases progressively with decreasing pH below neutrality.[127-129] Clinical studies have demonstrated that after subarachnoid hemorrhage (SAH), the concentration of transferrin increases in cerebrospinal fluid (CSF). Moreover, individuals exhibiting vasospasm have a significant 3-fold increase in transferrin levels vs. those in the non-vasospasm group ($p < 0.05$). The mRNA of inducible nitric oxide synthase (iNOS) in smooth muscle cells is also induced by transferrin.[253] All of the above appear contradictory with the observation of a decreased transferrin level.

The traditional 2-D gel electrophoresis results indicated that *S*-nitrosylation occurred on both IgG gamma 2A and transferrin. (Figure 11) From the DiGE image analysis, their levels were both decreased by about 1.6-fold after hemorrhage. As observed in both the traditional 2D biotin switch assay and the DiGE gel, IgG gamma 2A migrated to a molecular weight equal to that of IgG gamma dimer. Since it is known that the expression of the immunoglobulin VH gene family is not induced by hemorrhage,[254] the decrease in dimerized IgG gamma protein may be the result of increase of macrophage intake of *S*-nitrosylated IgG after NOC-7 treatment. Again, this hypothesis cannot be examined without performing a biotin switch coupled to a DiGE experiment. Meanwhile, the same scenario for transferrin also needs further investigation in order to elaborate the relationship between its change in protein level and *S*-nitrosylation status.

Increased prosaposin S-nitrosylation level in NOC-7 treated rat plasma. As mentioned earlier, from intra-gel comparison, the level of prosaposin *S*-nitrosylation was significantly

increased by 2-fold. (Figure 11) Prosaposin is a multifunctional protein with diverse functions. Intracellularly, prosaposin is a precursor of four sphingolipid activator proteins, saposins A to D, which are required for hydrolysis of sphingolipids by several lysosomal exohydrolases. Secreted prosaposin has been implicated as a neurotrophic, myelinotrophic, and myotrophic factor as well as a spermatogenic factor. It has also been implicated in fertilization.[255-260] Alternative splicing in the prosaposin gene is conserved from fish to humans, is tissue specific, and is regulated in the brain during development and nerve regeneration-degeneration processes.[261, 262] As the origin, or template for sphingolipids, the regulation of prosaposin may be due to the demand that is sensed by sphingolipids, which are commonly believed to protect the cell surface against harmful environmental factors by forming a mechanically stable and chemically resistant outer leaflet of the plasma membrane lipid bilayer.[263-266] Recently, relatively simple sphingolipid metabolites, such as ceramide and sphingosine-1-phosphate, have been shown to be important mediators in the signaling cascades involved in apoptosis, proliferation, and stress responses.[267, 268] Therefore, the increase of the S-Nitrosylation level of prosaposin in NOC-7 treated plasma could be a reflection of the stimulation from the downstream signaling, e.g., the sphingolipid metabolites, in order to keep the stability of the plasma membrane.

The present study mapped out the parts of the rat plasma proteome that exhibited change after *in vitro* NOC-7 treatment. Although the result has not been verified (by, e.g., western blot analysis or pathway-assisted component analysis), this is the first time that an altered proteome associated with early hemorrhage was investigated with a relative quantitation method. The pioneering results and established methodology from this study will facilitate further investigation of *in vivo* plasma proteome in early hemorrhage. If combined with the modified

biotin-switch assay, the relative change of *S*-nitrosylated plasma proteins can be further analyzed *in vivo*.

4.0 SERUM RESPONSE FACTOR

4.1 THE FUNCTION OF SERUM RESPONSE FACTOR IN CARDIAC HYPERTROPHY

Heart failure is a disease that affects over 5 million Americans. Despite progress in the treatment of this disease, prognosis remains dismal, with 5-year survival rates of less than 50% [269]. Heart failure develops from a stage of cardiac hypertrophy that results from mechanical and neuroendocrine stimulation of cardiomyocyte growth. Hypertrophy is heterogeneous, since different stimuli result in different phenotypes with expression of different isoforms of cardiac proteins. For example, adrenergic stimulation leads to re-expression of fetal isoforms of cardiac genes while the hypertrophic factor cardiotrophin-1 results in a different program. Hypertrophy ultimately results in a stage of dilated cardiomyopathy with contractile failure ensues, due to cardiomyocyte elongation, cell slippage and extracellular matrix remodeling.[270-272] The molecular mechanisms underlying both of these stages, however, are poorly understood.

In isolated cardiomyocytes from neonatal rats, serum response factor (hereafter called SRF) is required for the induction of atrial natriuretic factor (ANF), c-fos, NCX1, BNP, alpha-actins, alpha-myosin heavy chain, and beta-myosin heavy chain genes.[273] However, simple over-expression of SRF is not sufficient for induction of the complete set of hypertrophic response gene. This suggests that SRF-dependent gene expression is modulated in a complex

manner not only by different cardiac stress levels, but also by protein-protein interaction and post-translational modifications of SRF.

One of the skeletal muscle-specific regulatory proteins of the MyoD family, myogenin, which belongs to the basic helix-loop-helix (bHLH) super family of transcription factors, was found increased in skeletal muscle cells that undergo terminal differentiation in culture under growth-factor-deficient medium conditions. [274] It was used in this study as a positive indicator of C2C12 (a mouse skeletal muscle cell line) cell differentiation.

4.2 THE PHOSPHORYLATION OF SRF

Transcription factors are proteins with DNA-binding domains, and activation domains through which they can activate or repress DNA transcription in response to extra-cellular stimulations. Protein phosphorylation plays a key role in regulating transcriptional activity in response to specific extracellular signals.

Phosphorylation of transcription factors by MAP kinases can produce multiple effects on gene expression. The regulatory sequence of the *c-Fos* gene contains a serum-response element (SRE), so named because it is activated by many growth factors in the serum. As a ubiquitous nuclear transcription factor, SRF is required for the formation of the vertebrate mesoderm, leading to the origin of the cardiovascular system. High levels of SRF expression are restricted to cardiac, skeletal, and smooth muscle tissues. SRF belongs to a family of DNA-binding proteins, characterized by a conserved DNA-binding/dimerization domain of 90 amino acids, termed the MADS box. SRF can be phosphorylated by at least six broadly expressed kinase families in its amino- or carboxyl-terminal domains, and the effects of SRF phosphorylation lies in variable

cellular events, including DNA binding on/off rate [275], DNA binding activity [276], transcription [275] and cell proliferation [277, 278]. SRF binding to CArG boxes is involved in the tissue-specific expression of muscle genes, such as those coding for the α -actins. [279, 280]

SRF binds to the SRE of the human *c-Fos* gene as part of a trans-activating complex involving ets domain proteins, such as SAP-1 or Elk-1, which bind to an ets motif, 5' to the CArG box, only upon protein-protein interaction with SRF.[281] As the core sequence of SRE, CArG is in the control of activation of two gene sets, muscle differentiation and growth. The question, therefore, is how SRF toggles from a pro-differentiation function to a growth-promoting function. [282]

Much evidence shows likely that the activity of SRF is regulated by its phosphorylation, as suggested for other transcription factors such as CREB [283] and c-Jun.[284, 285] Increases in SRF-DNA binding is not due to an increase in SRF protein expression, but rather the phosphorylation of SRF. [286]

There are four phosphorylation sites found on SRF, including serines within amino acids 77-85 [276, 287], while another phosphorylation site has been identified at Ser103 [288]. The combination of abolishing phosphorylation at amino acids 77-85 and 103 causes greatly reduced on/off rates of DNA binding by SRF, but the reduction of DNA binding activity is partially alleviated.[276] None of these mutations affect either the ability to interact with p62TCF or stimulation of transcription *in vitro*. [289] These findings imply possible roles for SRF phosphorylation in the regulation of *c-Fos* transcription.

The hypothesis in this study was that the alteration of extent and sites of phosphorylation of human SRF triggers the change in direct binding partners during skeletal muscle cell differentiation. This hypothesis states two aspects of targeted functional proteomics, one about

protein-protein interaction and the other about the phosphorylation of protein, which causes conformational change of itself, thus in turn a trigger for changes in association with its direct binding partners.

4.3 SELECTIVE PHOSHOPEPTIDE LABELING

To selectively analyze the three common phosphorylated residues, pSer, pThr, and pTyr, their unique chemical properties have to be considered during experimental design. The major difference between pSer/pThr and pTyr is that phosphorylated tyrosine has an aromatic ring in its side chain, which protects its phosphate group from β -elimination reaction. Some early developments of chemical alterations in facilitating the enrichment include modification of *O*-linked phosphoproteins with 1,2-ethanedithiol and a thiolate-reactive reagent containing a maleimide group and biotin tag. [290] Zhou et al. used chemicals to block the reactive amine and carboxylate groups on peptides, which allows phosphate groups to be selectively modified to facilitate the covalent attachment of the peptides to an immobilized matrix via the modified phosphate group.[291] Although isotopic labeling was not used in this approach, the blocking procedure helped the development of the phosphopeptide isotope-coded affinity tag method, i.e., PhIAT. It was first introduced in 2001. A schematic diagram of the chemical reactions in PhIAT is shown Figure 19. [44, 45] The standard multi-phosphorylated β -casein sample was analyzed vi this method, described as having fewer non-specific interactions than what is obtained with immunoaffinity or metal affinity isolation methods, allowing the detection and identification of lower abundance phosphopeptides. [45] The importance of serine phosphorylation (SRF) in the

function of serum response factor and its low stoichiometry in the nucleus led to the use of the PhIAT method in the present study to attempt identification the sites of its phosphorylation.

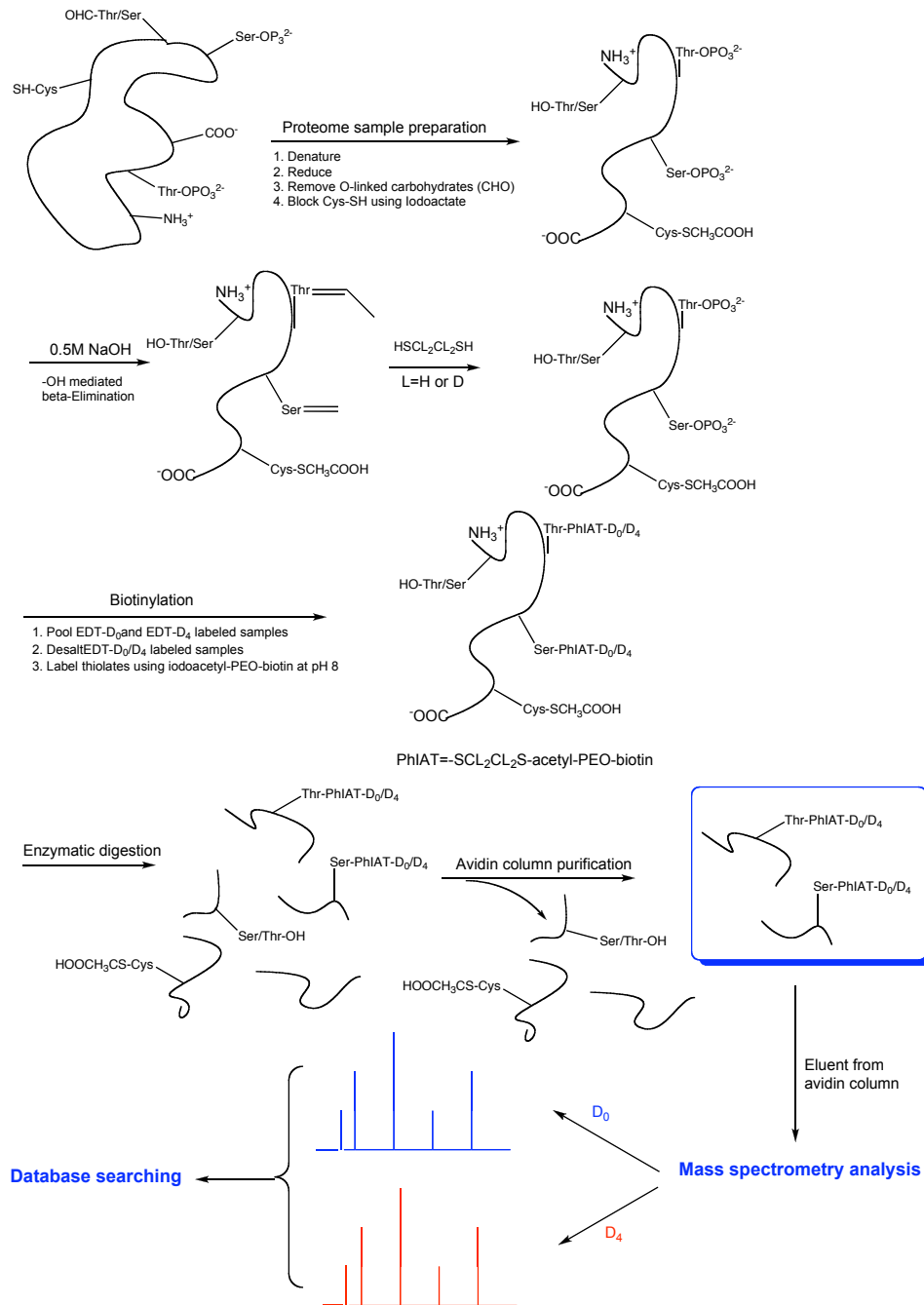


Figure 19 The reactions in the phosphopeptide isotope affinity tag (PhIAT) method

The first phase involves PhIAT labeling the phosphoseryl (Ser-OPO₃²⁻) and phosphothreonyl (Thr-OPO₃²⁻)

residues. After *O*-linked carbohydrates are removed and the cysteine amino acid residues are converted into cysteic acid via iodoacetic acid oxidation, the phosphate groups are removed via hydroxide ion-mediated β -elimination and PhIAT labeled as shown. The proteins are digested and the sample is enriched for PhIAT-labeled peptides by avidin affinity chromatography. This enriched mixture is then analyzed by mass spectrometry and the results are used for database searching to determine peptide sequence and site(s) of phosphorylation.

Unlike the overall strategy that was illustrated in Figure 12, the present study of phosphorylation sites on SRF did not incorporate isotope labeling, but did conserve the chemical reaction steps to fulfill the selectivity and enrichment advantage of this method. Trying to discover new phosphorylation site of SRF, non-isotopic labeled PhIAT method was used and several new phosphorylation sites were found.

4.4 NEW PHOSPHORYLATION SITES ON SRF

4.4.1 Materials and methods

Chemicals and reagents. The stock solution of beta-casein was made at 30 mg/ml in 0.1M NH_4HCO_3 , pH 8.2, containing 6M guanidine-HCl (GnHCl). β -Casein has a molecular weight of 25099 Da and a pI of 5.1. If starting with 1 ml of 30mg/ml stock, the original casein is 1.0 mg (40 nM). For de-phosphorylated β -casein from bovine milk, a stock solution was made at 10 mg/ml. Stocks of 1M TCEP-HCl (1mM, 6 μ M) 1M iodoacetic acid (1mM, 2 μ M), 0.1M NH_4HCO_3 , pH 8.2 (500 mM, 50 mM), 250mM EDTA, 5M NaOH, 0.5M EDTA (stock), 100mM PMSF, 2mM D -biotin in PBS, 12M GnHCl, and 0.1M iodoacetyl-PEO-biotin (MW=542.43) were prepared. Including the above, PBS, TFA, acetonitrile; ethanedithiol (EDT), carbenicillin (Carb), Luria–Bertani (LB) medium (10 g Tryptone, 10 g yeast extract, 5 g NaCl, 10 g deionized

H₂O, to 950 ml and adjust the pH to 7.0 with 5 N NaOH), IPTG (0.1M stock solution: 0.238g/10ml sterile H₂O, store at -20 °C in 1ml aliquots), DMSO and ethanol were, except as noted below, from Sigma. Desalting spin columns, D-biotin and the Immunopure monomeric avidin purification kit were from Pierce Biotechnology). A stock solution of 20 µg/ml trypsin (sequencing grade, Promega, Madison, WI) was prepared. Chemicon 10 KDa molecular cut-off membrane tubes (10 ml) were from Millipore (Billerica, MA)

Viral infection and cell culture. Culture medium supernatant from HK293 cells with SRF-pA adenovirus was obtained after infection. The adenovirus was provided by Dr. Robert Schwartz, Baylor College of Medicine, Houston, Texas. Virus was purified using CsCl₂ gradient centrifugation method. HK293 cells in DMEM containing 10% fetal bovine serum were exposed to purified virus at 1×10^9 particles/µl to give an MOI of 5. A non-transfected mouse myoblast smooth muscle cell line, C2C12, was maintained in with medium changed every 3 days so as to keep cell confluence $\leq 40\%$.

GST-SRF expression and purification from bacteria culture. *E. coli.* with pGEX-SRF plasmid was seeded into 100 ml LB medium with 0.1% Carb, and grown with shaking overnight at 37 °C. The culture medium was transferred the following day 1:10 to 100 ml LB medium with 0.1% Carb, and the culture was grown at 37 °C with shaking for 1 h. IPTG stock solution (100 µl) was added to give a final concentration of 0.1 mM was added and the culture was incubated at 37 °C for an additional 6 h. Cell pellet was collected by centrifuging at 4,000 rpm for 5 min at R.T. The resulting pellet was then resuspended in 10 ml of ice-cold PBS. 10% Triton X-100 (1 ml) was added to give a final concentration of 1%, mixed and centrifuged for 10 min at 10,000 rpm at 4 °C. The supernatant was collected as the bacterial lysate. Glutathione agarose beads (500 µl) were washed with cold PBS, and supernatant from the bacteria cell lysate was added

and mixed with the beads gently for 30 min at room temperature (the capacity of glutathione-agarose is ≥ 8 mg protein per ml of swollen beads.) After binding, beads were washed three times by adding 25 ml of ice-cold PBS, mixed and spun down for 10 sec at 500g at room temperature. The washed agarose beads were then resuspended with 1 ml of ice-cold PBS and transferred to a 1.5 ml Eppendorf tube. Fusion protein, GST-SRF, was eluted from the beads by adding 1 ml of 50 mM Tris-HCl (pH 8.0) and 5 mM reduced glutathione (Sigma-Aldrich), and was mixed gently with the beads for 2 min. The supernatant was collected by centrifuging for 10 sec at 500g. Elution was repeated three times and each fraction was analyzed by SDS-PAGE.

Thrombin cleavage for GST-SRF purified from bacterial culture. Soluble lysate from the bacteria culture was incubated with $\frac{1}{2}$ volume of 50% glutathione agarose beads at 4 °C with shaking for 30-60 min. The bead-lysate mixture was then poured into a spin column and drained. Beads were washed with 3 column volumes of resuspension buffer (PBS with 0.05% Tween-20, 2mM EDTA and 0.1% mercaptoethanol), and 1 volume of thrombin cleavage buffer (50mM Tris, pH 8.0, with 150mM NaCl, 2.5mM CaCl₂ and 0.1% mercaptoethanol). The bottom of the column was then sealed and 1 volume of thrombin cleavage buffer plus thrombin enzyme (10 μ g per mg fusion protein). Incubation was done for 60 min at 4 °C with gentle shaking. After incubation, the column was drained and soluble cleaved fusion protein was collected in the filtrate. One column volume of thrombin cleavage buffer was added to rinse out all cleaved protein. (An optional second thrombin cleavage in half the previous volume could be performed to get more recovery of the fusion protein).

PhIAT sample preparation. Corresponding aliquots of β -casein, dephospho- β -casein, SRF-pA adenovirus-infected nuclear extract from 293 cells, and BSA, all dissolved in 6M guanidine-HCl in 0.1 M NH₄HCO₃, pH 8.2. All samples were then lyophilized to complete

dryness, and kept at -20 °C for later experiments. To the dried samples, 30 molar excess of TCEP-HCl (according to total SRF) was added to reduce disulfide bonds, and the mixtures incubated with stirring at 37 °C for 60 min, followed by addition of 10 molar excess of iodoacetate according to total cysteine in each sample. Samples were then incubated with stirring at room temperature in the dark for 90 min. The β -elimination reaction solution was made fresh before use under anaerobic conditions, (i.e., the following reagents were added under N₂: water, DMSO, ethanol, acetonitrile, 250 mM EDTA and 5M NaOH)[45]. The reaction solution was mixed well under N₂ for about 10 min to ensure homogeneity. EDT was added to the mixed reaction solution under N₂ just before β -elimination. The complete β -elimination solution was added to lyophilized samples and incubated at 55 °C for 1 h under N₂. After β -elimination, the reaction was cooled to room temperature, and was neutralized with acetic acid to pH 7. The neutralized solution was then passed through a Pierce desalting spin column equilibrated with 0.1M NH₄CO₃. Aliquots (10 μ l each) of desalted samples were quantified with the BCA assay for protein content. The remainder of the samples was lyophilized for biotinylation.

Biotinylation and in-solution trypsin digestion. Lyophilized samples were resuspended into 1 ml of 0.1M NH₄HCO₃, pH 8.2. Guanidine-HCl was then added to 6M. Free cysteines were then reduced as in the PhIAT sample preparation. After reduction, 5 molar excess of iodoacetyl-PEO-biotin was added according to cysteine content in each sample, and incubation was carried with stirring at dark at room temperature for 90 min to overnight. After biotinylation, the reacted mixture was desalted using Pierce desalting spin column equilibrated with 0.1M NH₄HCO₃. Desalted samples were lyophilized down to 100 μ l. Trypsin digestion was performed with sequencing grade trypsin, using a 1:50 (w:w) trypsin to protein ratio, overnight at 37 °C. Samples were boiled for 5 min to quench the trypsin digestion. Serine protease inhibitor, or

phenylmethylsulfonyl fluoride (PMSF) was then added to the digestion solution to a final concentration of 1mM.

Avidin purification. After equilibrating the avidin column material to room temperature, 200 μ l of biotin blocking buffer (2 mM D-biotin in PBS) was added to the column to block any non-reversible biotin reactions. Biotins from the reversible binding sites were removed by adding 0.6 ml of regeneration buffer (30% acetonitrile/ 0.4% TFA). The column was then washed with 1 ml PBS and was placed in a tube. The biotinylated samples were added to the center of the disc after adjusting the volume with PBS to 400 μ l. After the entire sample passed through the disc, 250 μ l PBS was added to force the sample completely into the gel bed. The bottom of the column was capped and the column was incubated for 30 min at room temperature. The column was then placed in a new tube and 200 μ l of PBS was added to wash the column until the OD₂₈₀ reading of the fraction returned to baseline. Elution buffer (200 μ l of 30% acetonitrile/0.4% TFA) was added to elute the biotinylated peptides and at least eight 200 μ l eluent fractions were collected to ensure maximum recovery. The OD₂₈₀ was measured and the fractions of interest were reserved for further analysis.

BCA assay for protein content measurement. Human immunoglobulin G (IgG, Sigma) was used as a standard protein (0.05, 0.1, 0.2, 0.4, 1.0 μ g/ml) to make a standard curve. A working solution for BCA assay was prepared up to 6 h prior to the sample assay, and 200 μ l was added into each well of 96-well microtiter plate. Protein assay samples were diluted and added to the microtiter plate wells at 1:20 (sample:working buffer (v/v)). The reaction was then carried at 37 °C for 30 min-1 h to obtain a stable colorimetric reading. After incubation, samples were cooled to room temperature and the OD₅₆₂ was measured for standard and samples. Protein content for each sample was then calculated based on the standard curve and the dilution factor of each

sample. Sample absorbances were used only when they were within the range of the standard curve.

Traditional 2-D gel electrophoresis. The lysates were treated with a ReadyPrep 2D Cleanup Kit (BioRad, Hercules, CA, USA) to remove ions, DNA, RNA, etc. Their protein contents were measured using a 2D Quant kit (Amersham Biosciences, Piscataway, NJ, USA). After overnight rehydration in buffer consisting of 6M urea, 2M thiourea, 4% 3-[(3-chloamidopropyl)dimethylammonio]-1-propanesulfonate (CHAPS), 25mM dithiothreitol, and 0.2% ampholytes, the protein samples were loaded on a 11cm or 18 cm immobilized pH gradient (IPG) strip (Bio-Rad), nonlinear pH 3-10, or nonlinear pH 5-8. Focusing was accomplished by applying 250V for 15 min, 10,000V for 3 h, and a third step of 40 000 total Vh for 11 cm IPG strips, or 60,000 total Vh for 18 cm IPG strips, and then maintained at 500V, as needed. The resolved proteins were equilibrated in sodium dodecyl sulfate (SDS) buffer with reducing agents present and separated by SDS-PAGE using 4–12% gradient Tris-HCl gels in a Criterion apparatus (Bio-Rad) operated at 4W per gel for 8 h. SYPRO-Ruby stain (Bio-Rad) was used to detect proteins. Spots were manually retrieved with spot-picking pipette tips, digested with trypsin, and submitted for peptide mass fingerprinting (PMF) analysis.

Nuclear extraction of SRF. For adhesive cells grown in 10 cm culture plates, before cell collection, medium was aspirated and cells were washed with 2x3ml ice-cold cell washing solution (PBS containing 1mM NaF and 1mM Na₃VO₄). After aspirating the washing solution, cells were removed by gentle scraping, and were transferred to a pre-chilled 15 ml conical tube. The cell suspension was centrifuged for 5 min at 1,500 rpm in a centrifuge pre-cooled to 4 °C. The cell pellet was kept on ice and the supernatant was discarded. The cell pellet was then gently resuspended in 500 µl of hypotonic buffer (10 mM HEPES, pH 7.9, containing 0.1 mM EDTA

and 10mM KCl) per 10 cm plate by pipetting up and down several times. The suspension was then transferred to a pre-chilled Dounce homogenizer, and given 10~18 stokes. The lysate was put into a 1.5 ml microcentrifuge tube and incubated for 15 min on ice. The homogenate was centrifuged for 2 min at 6,500g in a microcentrifuge pre-cooled to 4 °C. The supernatant was kept as the cytoplasmic fraction and the pellet was kept for nuclear fraction, both on ice. The nuclear pellet was resuspended in 100 µl of freshly made complete digestion buffer (10mM HEPES, pH 7.8, containing 250mM KCl, 0.25% NP-40, 5mM EDTA, 5% glycerol, 0.05% SDS, 1mM NaF, 1mM Na₃VO₄ and 1x HALT protease inhibitor cocktail) per 10 cm plate by pipetting up and down 3-5 times. One unit of DNAase (10 units/µl) per 10 cm plate was added and incubated on ice for 10 min. One unit of benzonase (10 units/µl) per 10 cm plate was added to the suspension and the mixture was incubated on ice for 4 h with gentle vortex mixing every one hour. When a low-salt condition was desired, complete digestion buffer was replaced with modified RIPA buffer (50mM Tris, pH 8.0, containing 1% TritonX-100, 0.2% SDS, 0.5% deoxycholate, 150mM KCl, 1mM EDTA, 1mM EGTA and 1x HALT protease inhibitor) with the DNAase and benzonase the same as above. After incubation, the cell suspension was centrifuged at >10,000g for 10 min in a 4 °C ultracentrifuge. The supernatant was obtained and stored at -80 °C as the nuclear extract, and the cell pellet was discarded.

Immunoblot analysis. Proteins segregated by SDS-PAGE were transferred to polyvinylidene fluoride (PVDF) membranes using a Mini-gel wet-transfer system (Bio-Rad). Membranes were rinsed twice in PBS-T (PBS containing 0.05% Tween-20), placed in block buffer (5% nonfat milk in PBS-T) and shaken at room temperature for 1 h. Primary antibody was then added into fresh block buffer and the membrane was shaken for 1 h at room temperature. After blocking, the membrane was rinsed three times in PBS-T for 5 min each. Secondary

antibody was then added with fresh blocking buffer and the membrane was incubated for 0.5-1 h at room temperature. Finally, membrane was rinsed three times in PBS-T for 10 min each rinse, and developed according to the instructions of the enhanced chemiluminescence detection kit (ECL Plus, Amersham Biosciences, Piscataway, NJ) and exposure of Kodak Biomax MR-2 photographic film (Sigma-Aldrich, St. Louis, MO). Protein bands were identified by comparison with a molecular weight marker (Bio-Rad). β -Actin was probed to monitor equal loading.

In-gel trypsin digestion with reduction and alkylation. Gel pieces were washed four or more times in 100 μ l of 25mM NH_4HCO_3 in 50% acetonitrile with 10 min of vortex mixing until the gel turned transparent and sticky. Gel pieces were then dried in a SpeedVac. Reducing buffer (30 μ l of 50mM tris(2-carboxyethyl)phosphine in 25mM NH_4CO_3) was added to each sample and incubated at 60 °C for 10 min. After the sample was cooled to room temperature, the reducing buffer was removed and discarded. Alkylation buffer (30 μ l of 100mM iodoacetamide solution in water, prepared just before use) was then added to the sample and incubated in the dark at room temperature for 2 h. After removing and discard the alkylation buffer, the gel plug was washed using with 200 μ l of destaining buffer (50 mM NH_4HCO_3 in 50% acetonitrile) and incubated at 37 °C with shaking for 15 min. Destaining buffer was removed and discarded. After two repetitions of the reduction and alkylation steps, gel pieces were shrunk by adding 50 μ l of acetonitrile and incubation at room temperature for 15 min. Acetonitrile was carefully removed after the gel pieces turned pale white. Gel pieces were then air-dried for up to 10 minutes and stored at -80 °C for storage if trypsin digestion did not follow immediately. Trypsin digestion was performed by first adding 20 μ l of activated trypsin solution, just enough to swell the gel pieces and cover the gel plugs at 4°C with incubation for 15 min. The samples were heated at 42 °C with gentle shaking for 4 h. Samples were cooled down to 4 °C and the digestion mixture was

transferred to a clean Eppendorf tube. Further extraction of peptides was done by dehydrating the gel pieces with a gradient of acetonitrile in H₂O containing TFA (typically from 40% to 100% acetonitrile with 0.2% to 3.0% TFA). The extracts were pooled with the digestion mixture and taken to dryness in a SpeedVac.

In-solution trypsin digestion without reduction and alkylation. High-salt content samples were desalted using Chemicon[®] 10KDa molecular cut-off membranes from Millipore following the manufacturer's protocol. Trypsin (5 μM) digestion solution was made by adding Trypsin Gold[®] (Promega, Madison, WI) into 50mM ammonium bicarbonate, pH 8.0. Protein samples were mixed with trypsin digestion solution (trypsin-protein ratio of 1:100, w/w) and incubated at 37 °C for 2 h. An additional, equal amount of trypsin digestion buffer was added and the digestion was continued at 37 °C overnight. The digested sample solution was desalted using C₁₈ ZipTips(Millipore, Billerica, MA) followed the manufacturer's instructions. Briefly, H₂O containing 0.2% TFA was added to the sample solution, mixed and centrifuged to precipitate any debris. The Ziptip was pre-wet using 10 μl of 50% acetonitrile-H₂O, and then pre-equilibrated with 10 μl of H₂O containing 0.5% TFA. Peptides were bound to the ZipTip by pipetting the digestion solution through it at least 10 times, and salt contaminants were washed of the ZipTip by pipetting 0.5% TFA-H₂O through it five times. Peptides were eluted pipetting a gradient of 25%~100% aqueous acetonitrile through the ZipTip. Eluates were pooled and lyophilized to complete dryness.

Protein Identification Following avidin column elution, the peptides derived from each protein spot were analyzed with matrix assisted laser desorption ionization time of flight mass spectrometry (MALDI-TOF-MS) in a 4700 Proteomics Analyzer with TOF/TOF Optics (Applied Biosystems, Foster City, CA, USA). Dried peptide extracts were resuspended in

MALDI spotting medium (50% acetonitrile in H₂O with 0.3% TFA). Mixed well and centrifuged to pellet any debris. Extracts were mixed 1:1 v/v with CHCA matrix solution (10mg/ml CHCA in spotting medium). The mixture was then vortex mixed and 0.5 μ l of the supernatant was applied to the MALDI target plate. Analysis of data with GPS Explorer Protein Analysis Software on a remote client workstation (Applied Biosystems) provided automated acquisition of optimized mass spectra and the derivation of monoisotopic PMF information. Searches of the NCBI nonredundant database, based on the peptide mass results using MASCOT (Matrix Science, Boston, MA, USA) via the GPS Explorer work station and MS-Fit (University of California, San Francisco MS Facility) via the internet identified proteins with matching PMFs. The MASCOT parameters were set to include only mammalian proteins, tolerance of one missed trypsin cleavage per peptide, allowance of protein modification by methionine oxidation and cysteine carbamidomethylation, peptide tolerance of 50 ppm and restriction of peptides to 700–4000 Da. The MS-Fit parameters included tolerance of one missed trypsin cleavage per protein, cysteine modification by acrylamide, oxidation of methionine, and changes at the amino termini, such as conversion of glutamine to pyro-glutamate and acetylation. Peptides adduct molecular masses were calculated for complete PhIAT adducts, incomplete PhIAT adducts (i.e., combination of EDT and PhIAT adducts), and multi-phosphorylation adducts. Protein identifications were accepted when the observed and predicted monoisotopic mass and centroid mass were consistent, and scores indicated nonrandom identifications at a significance level of $P < 0.05$.

4.4.2 Results

Identification of SRF phospho-peptides by non-isotope labeled PhIAT method. In the PhIAT experiment, after trypsin digestion, EDT was used as ethylthiolation reagent following the beta-elimination of phosphoric acid from pSer/pThr groups. After biotinylation of thiolated Ser/Thr residues, avidin column elution was performed using three quality control samples (Figure 20) and monitoring of absorbance at 280 nm to select fractions with PhIAT-labeled peptides.

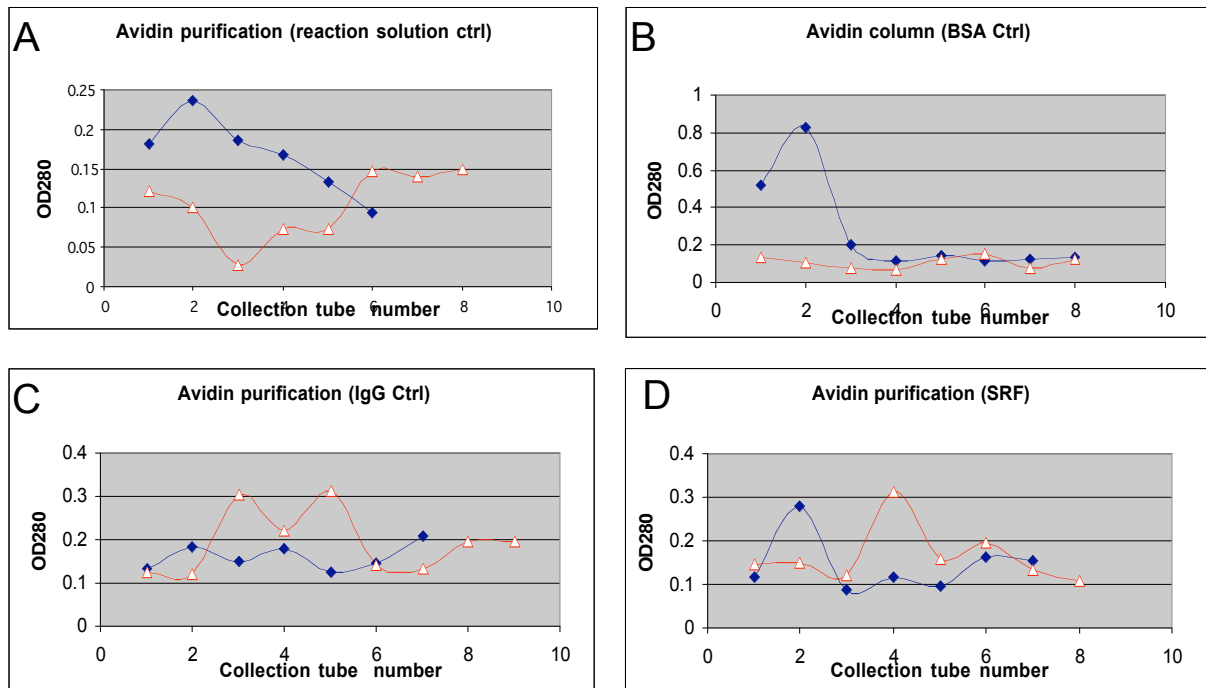


Figure 20 Avidin column OD₂₈₀ readings for elutions and washings of PhIAT-labeled peptides.

Closed circles are washing fractions using PBS; open triangles are eluted fractions using 30% acetonitrile/0.4% TFA. Samples are: (A) avidin column control; (B) BSA negative control; (C) IgG column control; (D) SRF

According to the result from avidin column elution, OD₂₈₀ values of ≥ 0.15 were selected as positive elutions for the SRF sample. Eluted fractions of SRF sample (Figure 20-D, E4, E5, and E6) were used for MALDI-TOF-TOF analysis. Fractions E5 from the BSA control sample and E8 from the reaction solution control sample were used as negative controls for mass

spectrometry analysis. E5 from IgG control sample was used to generate an IgG contamination exclusion list for mass spectrometry analysis.

A

Number of phosphorylated sites	1	2	2	3	3	3	4	4	4	4
PhIAT: X-CH ₂ CH ₂ S-acetyl-PEO-Biotin	1	1	2	1	2	3	1	2	3	4
EDT: X-CH ₂ CH ₂ SH	0	1	0	2	1	0	3	2	1	0

B

Amino acid Residue Code	Modification	C	H	S	N	O	MW	MW Without Ser/Thr
u	Thr-Phospho	24	43	3	5	7	609	490
v	Thr-EDT	6	12	2	1	2	194	75
w	Ser-Phospho	23	41	3	5	7	595	490
x	Ser-EDT	5	10	2	1	2	180	75

Table 7 Calculation table for PhIAT reaction adducts.

(A) The combinations of adducts formed on Ser/Thr residues. (B) The chemical composition table for phosphorylated and nonphosphorylated Ser/Thr with or without EDT addition. Amino acid residue codes are used in manual database matching using ProteinProspector peptide matching algorithms “MS-Product” and “MS-Comp”. “u, v, w, x” are, respectively, substitutes for the modified Ser/Thr residues listed in (B).

Considering the complexity of mass changes associated with a peptide that went through a series of chemical modifications, without using stable isotope labeling, such as deuterium, the adducts after the biotinylation and avidin elution were still a complicated pool of peptide mixture with complete and incomplete modifications. When the yield of the end product was sacrificed, the specificity toward pSer/pThr was greatly increased, especially for SRF, which has been found exclusively phosphorylated on serine residues. [276, 292-294] Any multi-phosphorylated peptide residues will have several combinations of EDT adduct and complete PhIAT adduct. (Table 7-A) With these possibilities of combination, the mass shift after the PhIAT reaction can be summarized using the formula listed in Table 7-B. A theoretical digestion list was then

generated using these two tables as the reference to match to the experimental data. Final results of the peptide identification is summarized in Table 8, in which the eluted fractions of SRF, E4~E6, was analyzed using MALDI-TOF-TOF-MS.

Position	Phospho-peptides from SRF-Pro A	PhiAT	EDT	Theoretical	SRF-E 4	SRF-E 5	SRF-E 6
165-170	KTGIMK	1	0	1167.6	1167.7626		
166-171	TGIMKK						
228-235	SDPTTDQR	1	0	1409.6	1409.7969	1409.78	1409.716
157-163	RYTTFSK	1	2	1544.6			1544.794
158-164	YTTFSK R						
537-546	NFIAVSAANR	1	0	1552.7	1552.8588		
228-235	SDPTTDQR	1	2	1561.5		1561.915	1561.85
25-37	TPTGRPGGGGTR	1	0	1660.8		1660.459	1660.358
536-546	KNFIAVSAANR	1	0	1680.8		1680.962	
537-548	NFIAVSAANRF K	1	0	1827.9	1828.1146		
621-635	DDPSQSANLLAEAKK	1	0	2077.0			2077.028
679-693	DDPSQSANLLAEAKK						
213-227	ALIQTCLNSPDSPP R	1	1	2178.0	2178.3293		

Table 8 Peptide identification chart for PhiAT labeled SRF-pA digest after avidin column elution.

Identification result for avidin elutions E4, E5, and E6 from PhiAT labeling for SRF sample, which was IgG purified nuclear extracted from SRF-pA viral infected 293 cells. Bold letters represent the potential phosphorylated sites; bold numbers indicate the mass precursors whose amino acid compositions were confirmed by MS/MS spectra.

The use of normoisotopic EDT during the PhiAT experiment provided a strategy for selective enrichment of serines and phosphorylated threonines. The following are three peptide sequences that had phosphorylated serines/threonines confirmed by MS-MS analyses. They are: “¹⁶⁵KpTGIMK¹⁷⁰”, “¹¹⁸SDPpTpTDQR²³⁵”, and “⁵³⁷NFIAVpSAANR⁵⁴⁶”. (Table 8) The only peptide eluting from all three of the elutions was “¹¹⁸SDPpTpTDQR²³⁵”, whereas the other two peptides only eluted from the first positive elution (E4). Unfortunately, all the other peptide fragments that had matching precursor ion *m/z* values matching theoretical values did not have sufficient intensities on which to perform tandem MS experiments, so their amino acid composition were not confirmable. Therefore, the conclusion from the PhiAT experiment is that,

on 293-expressed SRF-proA, Threonines 166, 121, 122, and Serine 542 were phosphorylated under *in vitro* phosphatase inhibited environment.

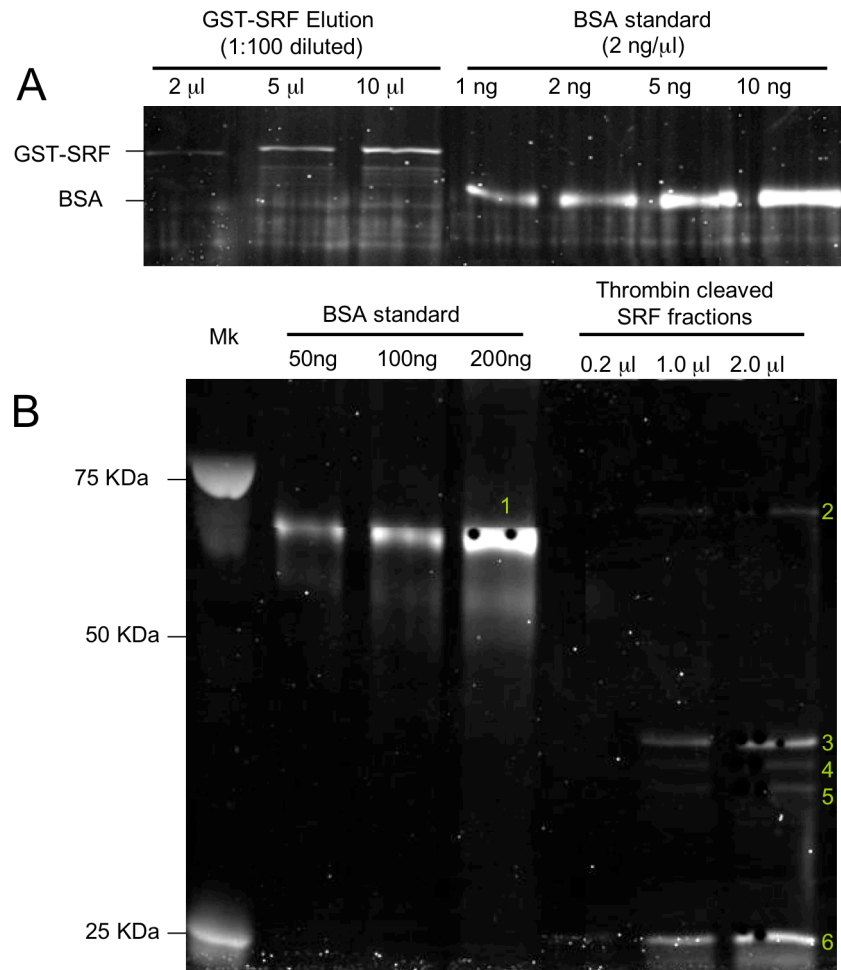


Figure 21 SYPRO-Ruby stained gel images for GST-SRF quantification and phospho-SRF identification.

(A) SYPRO-Ruby staining for the titration of GST-SRF via a BSA standard curve; (B) Image of the SYPRO ruby-stained gel after cutting of spots for MS analysis. Protein identification results: 1 - BSA; 2 - GST-SRF; 3-5 - Degradation products from GST-SRF (mostly degraded SRF; the GST tag portion of the protein remained more intact than the SRF portion); 6: IgG fragment.

Phosphorylation sites identified from thrombin-cleaved GST-SRF. Using the “two protein mixture” as the searching criteria, peptide mass fingerprinting (PMF) analysis, as shown in Table 9, supported the composition of GST-SRF. Meanwhile, taking advantage of the high resolving

power of the MALDI-TOF-MS/MS instrument used, phosphorylation sites on GST-SRF could be assigned without it being cleaved by thrombin. The potential phosphorylation sites noted, however, even though they have no presently known biological relevance, will provide valuable information for further investigation in future *in vivo* settings. There were three incompletely assigned phosphorylation sites on the peptide “¹⁵⁸YTTFSKR¹⁶⁴”, which is enclosed in the MADS box region of SRF protein. These phosphorylation sites were found on tyrosine, serine or one of the two threonines, but which of them was phosphorylated was not clear from the data obtained. In the MS/MS spectrum of this peptide fragment (precursor ion *m/z* 1142.37), there were in fact mixed b and y ions and interval peptide fragment ions from all three possible peptides, which are “YpTpTFpSKR”, “RpYpTpTFSK”, or “pYpTpTFSKR”. This result suggests that SRF has a mix of all three different phosphorylation patterns. The other phosphorylated peptide was found on the N-terminal domain of SRF, “¹⁵GpSALGGpSLNRpTPpTGRPGGGpTR³⁷”, where all five of phosphorylatable serines and threonines were found to be phosphorylated.

A [gi|4507205|ref|NP_003122.1](#) serum response factor (c-fos serum response element-binding transcription factor) [*Homo sapiens*]

Peak No.	Measured Mass(M)	Computed mass	Error (ppm)	Residues		Missed cut	Peptide sequence	Modification
				Start	End			
1	1169.569	1169.589	-17	25	37	0	TPTGRPGGGGGTR	
2	2481.886	2481.907	-8	15	37	1	GsALGGsLNRIpTGRPGGGGGtR	5PO4
3	1667.821	1667.829	-5	213	227	0	ALIQTCLNSPDSPPR	
4	1050.541	1050.556	-15	44	55	0	VPGNAGAGLGPR	
5	3551.605	3551.564	12	59	95	0	EAAAAAATTPAPTAGALYSGSEGDSESGEEEEELGAER	
6	2714.156	2714.137	7	236	260	0	mSATGFEEEDLTYQVSESDSSGETK	1Met-ox
7	1152.57	1152.584	-13	146	154	1	IKmEFIDNK	1Met-ox
8	1141.3726	1141.372	2	158	164	1	YttFsKR or RytFfsK or yttFfsK	3PO4

B [gi|4929901|pdb|1B8X|A Chain A](#), Glutathione S-Transferase Fused With The Nuclear Matrix Targeting Signal Of The Transcription Factor Aml-1

Peak No.	Measured Mass(M)	Computed mass	Error (ppm)	Residues		Missed cut	Peptide sequence	Modification
				Start	End			
1	962.498	962.522	-25	1	8	0	SPILGYWK	
2	1025.553	1025.575	-21	182	190	0	IEAIPQIDK	
3	1047.557	1047.574	-17	64	72	0	LTQSMAIIR	1Met-ox
4	1181.668	1181.676	-7	181	190	1	RIEAIPQIDK	
5	1440.755	1440.749	4	113	124	1	DFETLKVDFLSK	
6	1515.789	1515.796	-5	89	102	0	AEISMLEGAVLDIR	
7	1531.795	1531.791	3	89	102	0	AEISMLEGAVLDIR	1Met-ox
8	1618.769	1618.759	6	73	86	1	YIADKHNMGGCPK	1Met-ox
9	1681.75	1681.721	17	27	39	1	YEEHLYRDEGDK	
10	1816.948	1816.934	8	87	102	1	ERAEISMLEGAVLDIR	1Met-ox
11	2228.11	2228.103	3	45	63	0	FELGLEFPNLPYYIDGDVK	
12	2268.137	2268.13	3	18	34	1	LLLEYLEEKYEEHLYER	
13	2325.139	2325.132	3	197	217	0	YIAWPLQGQWATFGGGDHPPK	
14	2356.205	2356.198	3	44	63	1	KFELGLEFPNLPYYIDGDVK	

Table 9 The peptides identified by MALDI-TOF-MS and –MS/MS for GST-SRF.

Peptides identified by MALDI-TOF-MS and –MS/MS and database searching from the plugs picked from gel shown in Figure 21-B, sample No. 2. The results showed a mixture of two proteins: (A) SRF, [gi|4507205|ref|NP_003122.1](#) serum response factor (c-fos serum response element-binding transcription factor) [*Homo sapiens*]; (B) GST, [gi|4929901|pdb|1B8X|A chain A](#), glutathione S-transferase (fused with the nuclear matrix targeting signal of the transcription factor Aml-1). The combined Z score for two proteins mixture equals to 2.15, with a probability to be correct of 100%. Non-capitalized letters represent: m: oxidized methionine; y, t and s: phosphorylated tyrosine, threonine and serine.

4.4.3 Discussion

The generally very low stoichiometry of phosphorylated form(s) of a protein within the overall population of the protein presents a very challenging analytical problem, even if the analysis is done with over-expressed target protein. This situation becomes worse if the analytes have multiple phosphorylation sites. [295] An attempt was made to analyze the peptides from GST-SRF using the negative ion detection mode of the MALDI-TOF-MS instrument with both CHCA and trihydroxyacetophenone (THAP) as matrices. For the THAP experiments, a 1:9 w/w mixture of matrix-sample solutions was used with the THAP solution having a concentration of 20 mg/ml, in an attempt to observe the $[M-H]^-$ ions of the phosphopeptides. [296] However, the THAP-based MS spectra were not of a quality better than that observed for the positive ion CHCA-based spectra, and no selective effect was observed for multi-phosphorylated peptide ions, either. This problem may ultimately be due to the low copy of SRF in the cell, because detection of sub-femtomole levels of peptides, although sometimes achievable, truly stretches the limits of the MALDI-TOF-MS instrument. With the over-expression systems utilized, in 293 cells or bacteria, neither of which being particularly biologically relevant to the situation in smooth muscle cell, some of the phosphorylation sites were identifiable. Although more phosphorylation sites were identified from the 293 cell system than in bacterially expressed GST-SRF, there were no overlapping peptide fragments in both systems. Again, realizing that those two systems are intrinsically not representative for the biological function SRF may play during myoblast cell progression, these results can only be treated as practice sets for future *in vivo* experiments.

(Femtomole= 1×10^{-15})	MALDI-TOF-TOF limit	Cells needed	No. of 10-cm plates
For partner ID	>10 femtomole	>50 million	>25
For pSRF	>100 femtomole	>500 million	>250

Table 10 Stoichiometry of SRF for study of its direct binding partners and phosphorylation.

Calculation was based on 200 copies of SRF per cell, 50% recovery rate from TAP purification process, and 6.02×10^{23} molecules per mole. The MALDI-TOF-TOF detection limit was based on data from standard protein: phosphorylated beta-casein.

Although the approach of using stably transfected C2C12 cells or immunoprecipitation to enrich endogenous SRF from C2C12 cells was used, the amount of protein obtained was too limited to use the MS as the reading system for phosphorylation status analysis, or to find novel direct protein-protein interactions. As is shown in Table 10, in order to have confirmable tandem MS-MS information for binding partner identification, at least 25 10-cm culture plates with 2×10^6 cells per plate would be necessary. This estimate was based on experiments with the standard protein beta-casein, which was of 99.5% purity. If a more complex protein mixture or gel band were analyzed, the sample requirement would be at least 5~10 times higher than for the standard protein. It is even more difficult, to find multi-phosphorylation sites or phosphorylation patterns on SRF by MS-MS, so a further 10-fold increase in sample size will be needed for those experiments, meaning 250 10-cm plates.

In addition to the low copy number of SRF, the selectivity gained from the isotope-free PhIAT method was largely compromised by the complexity of the reactions and its low final yield. The rate-limiting steps were beta-elimination and biotinylation. In attempt to rescue the low recovery, a modified acetone precipitation procedure was employed, which resulted in an increase of 30% in terms of protein recovery for the overall PhIAT experiment. A shorter reaction route wherein the biotinylation steps are removed, or simply using beta-elimination with

cysteine methylation,[36, 37] should be carried out in the future to bypass the disappointing results obtained with the initial PhIAT approach.

4.5 TANDEM AFFINITY-TAGGED PURIFICATION

Identification of protein–protein interactions is at the core of understanding biological processes occurring in living cells. Traditionally, potential interacting proteins have been identified by genetic methods (e.g., yeast and bacteria, and later to a limited extent, mammalian two–hybrid screens) [297] with subsequent verification of the interaction by co-immunoprecipitation. The advantage of yeast two-hybrid systems for protein-protein interaction studies is the high selectivity and specificity it affords.[298-303] Two proteins are separately fused to the independent DNA-binding (BD) and transcriptional activation domains (AD) of transcription factor. The protein fused to the BD may be referred to as the bait protein and is typically a known protein that the investigator is using to identify new binding partners. The protein fused to the AD may be referred to as the prey protein and can be either a single known protein or a library of known or unknown proteins. If the two proteins interact, they reconstitute a functional transcription factor that activates expression of (a) reporter gene(s). In this way, two individual proteins may be tested for their ability to interact, and a transcriptional readout can be measured to detect this interaction. Furthermore, novel interacting partners can be found using this system by screening a single protein or domain against a library of other proteins. It is this latter feature, the ability to search for interacting proteins without any prior knowledge of the identity of such proteins, that is the most powerful application of the two-hybrid technique.

There are, however, three intrinsic problems with this system. The basic problem is that it must employ an efficient transformation platform, which in practice is a very common hindrance, in addition to the problem of having self-activating transcriptional mutants. Both plasmid efficiency and false-positives are fundamental technical limitations in such large library screenings. Another intrinsic problem is the system is based on potential protein-protein interactions that are included in the library. Many unknown interactions that involve species-specific relocalization of reaction partners are not detectable using the yeast or bacteria expression libraries. The third and the major drawback of this method is that the interactions found in this system still require direct interaction proof in biological assays. Furthermore, it is of limited utility when more complex protein aggregates, such as ribosomes, spliceosome complexes or transcription complexes, are investigated.

Small epitopic protein-assisted affinity enrichment is now widely applied in large-scale proteome studies, especially for those targets that are involved in signaling pathways. Single tags commonly used include the His₆, myc, GST, HA, Flag and Protein A tags for specific affinity-based separation of the target protein and its interaction partners. A GFP tag can be used for fluorescence-assisted co-localization studies. The tandem affinity-tag purification (TAP) method combines two sequential affinity purification steps to isolate a protein complex of interest, usually followed with subsequent mass spectrometric identification of unknown protein complex components.[304, 305] The key feature of this technology is the use of the two different affinity purification tags that are fused by genetic methods to at least one known component of the protein complex of interest. The TAP protocol can therefore yield exceptionally clean protein ensembles. The tagged protein of interest and its interacting partner are recovered without disrupting the targeted interacting proteins by using gentle washing and small molecule elution

conditions. Protease digestion is not required to recover the interacting protein partners.

Many different combinations of tandem tags have been used. In addition to those single tags mentioned above, the additions in TAP are inclusion of a calmodulin binding peptide (CBP) that is separated by a TEV (tobacco etch virus) protease cleavage site. Streptavidin-binding protein (SBP) is another new substitute that has been used with CBP to yield clean proteins. The caution that must be kept in mind when employing the tandem tag approach is that the added specificity will invariably be balanced with decreased recovery and protein yield from the multi-step separation processes. Attention must be paid in order to preserve the biological function of the target protein after tagging, as well as to preserve the cellular localization of the expressed tagged target protein in the biological setting employed.

Two of the most attractive advantages of the TAP tagging system are that it can: (1) avoid harsh purification conditions, in that it is designed to keep target proteins active under close-to-physiological conditions all along its purification procedure; and (2) provide high purity that facilitates downstream MS analyses.[306, 307] Although the TAP method is not specifically designed for enrichment of phosphopeptides, it can be adapted to greatly enhance their purification and further phosphorylation analyses.

The hurdles in phosphoprotein studies are, in large part, the transient nature of many phosphorylation events, the often-low stoichiometry of phosphorylation at a given site and/or the low copy number of any particular phosphoprotein per cell. TAP-SRF transfection was employed in an attempt to provide a unique tool to understand the molecular mechanism of direct SRF-interaction partners in mammalian cells.

4.6 STABLE TRANSFECTION OF SRF

4.6.1 Materials and methods

Chemical and reagents. The QIAquick gel extraction kit was from QIAGEN., Aprotinin, pepstatin, AEBSF, antipain, and protease inhibitor cocktail were from Pierce Biotechnology. Sca I and FBS were from Invitrogen). Phenol, chloroform, isoamyl alcohol, DMEM, PMSF, HEPES, EDTA, NaF, Na₃VO₄, KCl, NaCl, Tris-HCl, DTT and G418 were from Sigma-Aldrich.

cDNA purification and linearization. Plasmid cDNA PCG-SRF-ProA and PCG-ProA (gifts from Dr. Robert, J Schwartz, Baylor College of Medicine, Houston, TX) were purified using the classical phenol-chloroform-isoamyl alcohol method. The purified cDNAs were then linearized by incubating with endonuclease Sca I (10 U/ml) at 37°C for 2 h. After linearization, the plasmid DNAs were reconcentrated into 20 µl TE buffer using the phenol-chloroform method. C2C12 cells were plated and grown for at least 4 h to allow attachment. Lipofectamine 2000 was used as a cationic lipid carrier for cDNA transfection. Briefly, lipofectamine 2000 was pre-mixed with cDNA in serum-free medium for 20 min at room temperature before the mixture was added to the SFM-washed cells. The cells were incubated with the lipofectamine-cDNA complex mixtures at 37 °C in a 5% CO₂ atmosphere for 4-6 h. Growth medium (10% FBS in DMEM) was added and the cells were then grown for at least 10 h before serial dilution.

Cell culture and stable transfection. The mouse skeletal muscle cell line C2C12 was obtained from ATCC. Cryopreserved (at -80°C) cells were thawed quickly at 37 °C then transferred into T75 cell culture flasks containing growth medium (10% FBS in DMEM with antibiotics) and grown for 4 days at 37 °C in a 5% CO₂ atmosphere until the culture reached 50% confluency. Cells were then split into 6-cm culture dishes and 6-well culture dishes for stable

transfection. After cDNA transfection, C2C12 cells were grown for 10 h until the cultures reached 80% confluency. Cultures were then split at the different dilution factors (shown in Figure 19). G418 was added the day following culture splitting. Continuous culturing involved using four concentrations of G418 in growth medium (200, 500, 800, and 1000 $\mu\text{g/ml}$) with fresh medium changing every 3 days. After growth in the presence of 500 $\mu\text{g/ml}$ G418, cells were cloned by limiting dilution. Different cell clones were used after growth in DMEM containing 10% fetal calf serum, L-glutamine and antibiotics.

Affinity separation of nuclear SRF-pA from stably transfected C2C12 cells. IgG fast flow 6 sepharose beads were warmed from their 4 °C storage temperature to ambient temperature before use. A 50% slurry of the beads was loaded onto 0.8 x 4 cm poly-prep spin columns and was incubated with 10 ng/ml BSA for 10 min to block non-specific binding. The equilibrated IgG column was then washed with five wet bead volumes of IPP150 buffer (10 mM Tris-HCl, pH 8.0, containing 150 mM NaCl, 0.5 mM EDTA and 1 mM DTT) at least twice, then with five wet bead volumes of 0.5 M acetic acid, pH 3.4 at least twice, and finally neutralized to pH 7 by additional IPP150 washes. Nuclear extracts from C2C12 cells were added to the IgG column at a final pH of 8.0 with a protease inhibitor and a phosphatase inhibitor (1 mM NaF and 1 mM Na_3VO_4). The bead and extract mixture was then incubated with end-to-end shaking at 4°C for at least 3 h. Unbound proteins were removed by spinning the column at no more than 500g and removal of the supernatant. The beads were then washed with five wet bead volumes of IPP150 buffer at least five times to eliminate the non-specifically bound components. Recombinant TEV protease was added after washing the column with TEV cleavage buffer (10 mM Tris-HCl, pH 8.0, containing 150 mM NaCl, 0.1% NP-40, 0.5 mM EDTA, 1 mM DTT, 2 $\mu\text{g/ml}$ aprotinin, 4mM AEBSF, 0.7 $\mu\text{g/ml}$ pepstatin, 50 $\mu\text{g/ml}$ antipain and protease inhibitor cocktail). Ten units

of TEV protease (10 units/ μ l) per mg of protein substrate was then added in TEV cleavage buffer and the beads were incubated at 30 °C for 2 h. The supernatant obtained after TEV cleavage, the TEV cleaved SRF fraction, was stored at -80 °C. The beads were further washed with TEV cleavage buffer.

Immunoblotting. After transfer of electrophoretically segregated proteins using the Mini-gel wet-transfer system (Bio-Rad) to a PVDF membrane, the membrane was rinsed twice in PBS-T (PBS containing 0.05% Tween-20) and placed in blocking buffer (5% nonfat milk in PBST-T) with shaking at room temperature for 1 h. Primary antibody was then added into fresh blocking buffer and shaken with the membrane for 1 h at room temperature. After blocking, the membrane was rinsed three times in PBS-T for 5 min each. Secondary antibody was then added in fresh blocking buffer and incubated with the membrane for 0.5-1 hour at room temperature. Finally, the membrane was rinsed three times in PBS-T for 10 min each rinse, and developed according to the instructions of the enhanced chemiluminescence detection kit manufacturer (ECL Plus, Amersham Biosciences, Piscataway, NJ) with subsequent exposure to Kodak Biomax MR-2 photographic film (Sigma-Aldrich, St. Louis, MO) for visualization. Protein bands were identified by comparison to a molecular weight marker set (Bio-Rad). β -Actin was probed to monitor equal loading. Semi-quantitative assessment of immunoblots was conducted using ImageJ image processing software.

Immunofluorescence. Before fixation, cells were washed twice with cold PBS. Cells were fixed in fresh 2% PFA in PBS for 20 min at room temperature, permeabilized with 0.1% Triton X-100 in PBS for 10 min, and then washed with cold PBS. Cells were blocked for 20-30 min in PBS with 5% horse serum, then washed twice with PBS. The primary antibody was added to cells in blocking solution and cells were incubated for 1 h at room temperature. The cells were

washed three times with PBS for 5 min each, and were then incubated with fluorochrome-conjugated secondary antibody in blocking solution for 1 h at room temperature. Finally, the cells were washed three times with PBS for 5 min each before being stained and mounted in Vectashield containing DAPI. Primary antibodies included rabbit anti-SRF, FITC-anti-ProA antibody, and mouse anti-myogenin. Secondary antibodies against mouse or rabbit IgG were conjugated to Cy2, Cy3 or Cy5.

4.6.2 Results

Optimization and success of stable transfection. The first variable in determining the optimal condition for stable transfection was the concentration of the selective reagent, G418. G418 sulfate is a neomycin analog used to select neomycin-resistant cells. The recombinant SRF-pA clones were selected by using G418 because a resistance gene was previously inserted during the genomic construction of the plasmid used. Another variable was the dilution factor of the cell culture when antibiotic-containing selective culture medium was used. A densely populated culture will limit the access of G418 to the cells, and thereby the growth selection. Too diluted a cell population, on the other hand, will result in a low yield of selected clones. After the systematic optimization of these two variables, the condition found to give the best single colonies of cells was a dilution factor 1:10 or 1:20, and a G418 concentration of 500 $\mu\text{g/ml}$. At a dilution factor of 1:5, cells were dead after 11 days of culturing, regardless of the G418 concentration, mostly due to the competition for nutrition in the over-populated cultures. At a dilution factor of 1:20, with $\geq 500 \mu\text{g/ml}$ of G418, the cell confluency did not exceed 40%, and a rapid decrease in cell populations was observed at 800 and 1000 $\mu\text{g/ml}$ of G418. (Figure 22) The final success rate was 50%, with eight stably transfected clones selected out of 16 single colonies

of SRF-pA transfected C2C12 cells. All eight of these clones were grown to form eight distinct stably transfected C2C12 cell lines that showed positive SRF-PA expression at no less than the endogenous SRF expression level. (i.e., protein level ratios of SRF-pA:SRF was ≥ 1.0)

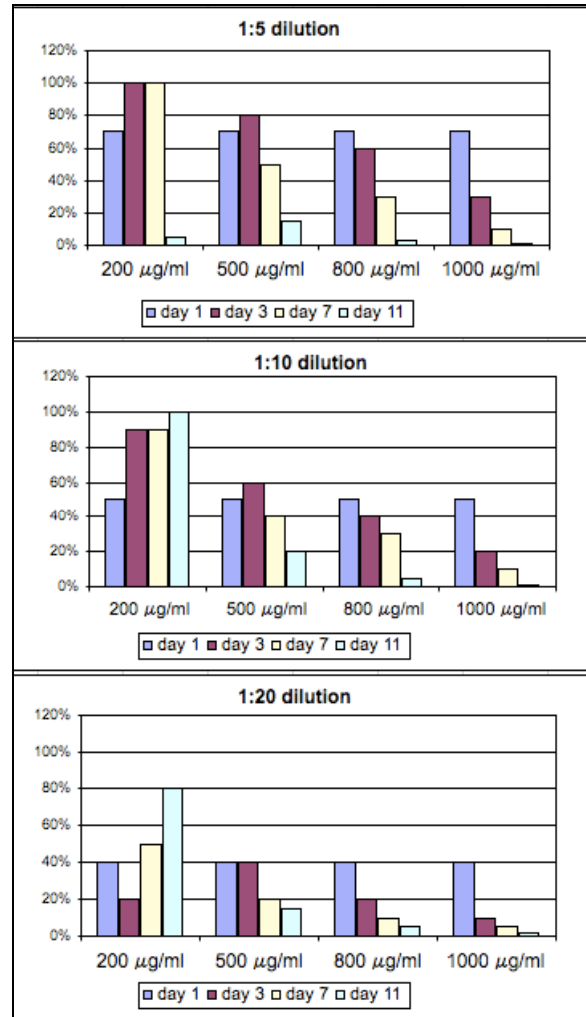


Figure 22 The optimization of G418 concentration for stable transfection of SRF-pA

The C2C12 cell confluency in response to the concentration of G418 present in growth medium per 10-cm culture plate. The y-axis is the confluency of the viable cells per plate and the x-axis is the concentration of G418. The dilutions were those employed at day 0 from the same starting concentration of 1×10^5 cells/ml. Measurements were taken at days 1, 3, 7 and 11 after the transfection of linearized SRF-pA cDNA.

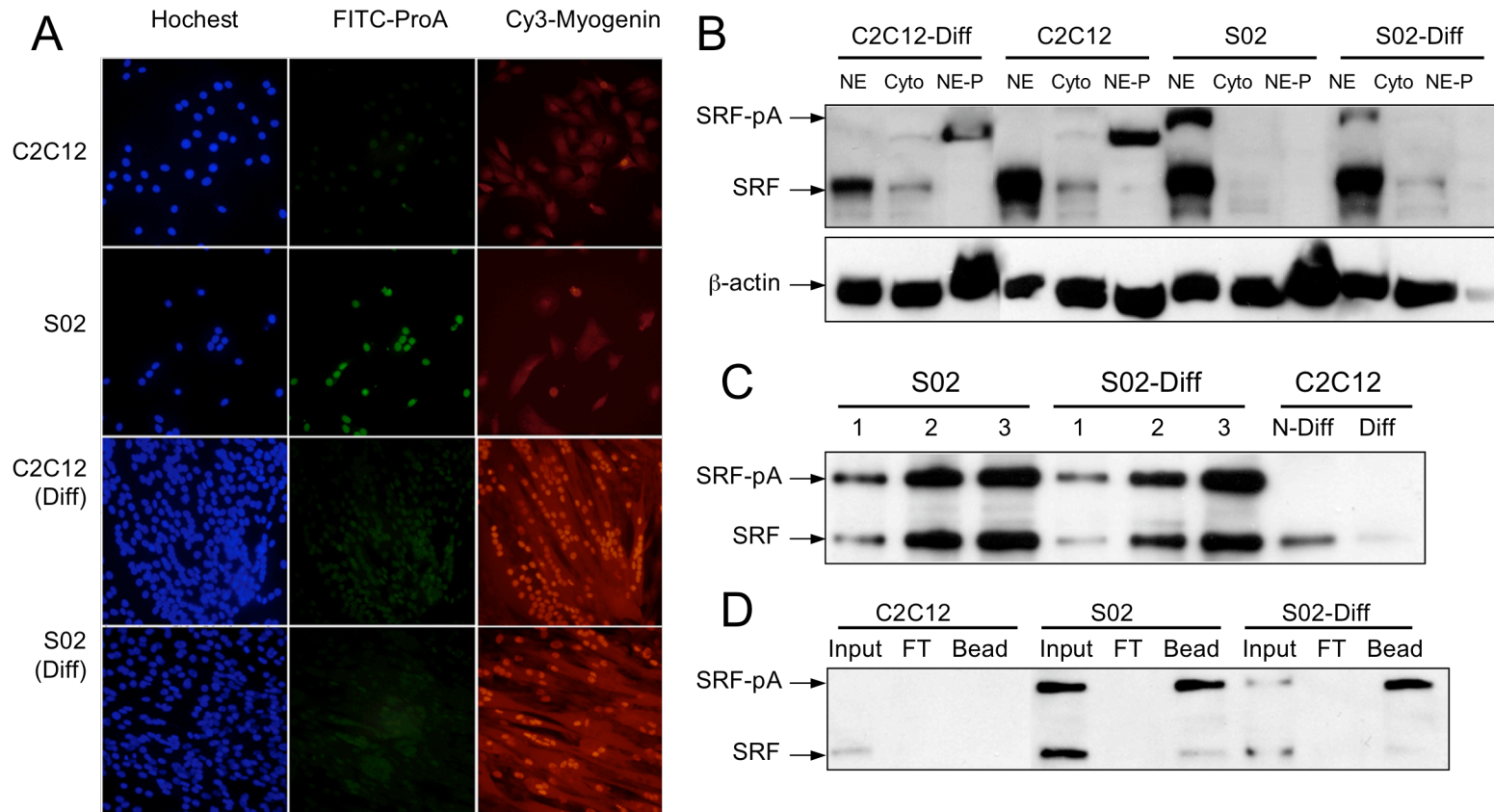


Figure 23 Retained function and cellular localization of SRF-pA, and retained differentiability of SRF-pA stably transfected C2C12 cells.

(A) Immunofluorescent staining. C2C12 cells were fixed using methanol-PBS-T, permeated with 0.05% TritonX-100-PBS-T, blocked with 5% horse serum-PBS-T for 30 min, and labeled with primary antibody containing a fluorescent Cy dye with incubation for 1 h at room temperature. The slides were then washed three times with PBS-T to remove excess primary antibodies. Hoechst was used for nuclear staining, FITC-ProA for protein A staining, and anti-myogenin for myogenin staining. S02 represents one of the SRF-pA plasmid stably transfected C2C12 cell lines. (B) Western blot results for the nuclear extract (NE), cytoplasmic extract (Cyto) and pellet after nuclear extraction (NE-P) of non- and differentiated C2C12 cell lines. β -Actin was used as the protein loading control. (C) Western blot results for expression level of SRF-pA versus endogenous SRF. Protein loading for lanes 1, 2 and 3 was, respectively, 5, 10 and 20 μ g. Loading for non-transfected C2C12 cells was 5 μ g each lane. (D) IgG-purified nuclear extract of transfected and non-transfected C2C12 cells before and after differentiation. FT: flowthrough; Bead: IgG sepharose bead loaded with 2x SDS loading buffer and boiled at 95 $^{\circ}$ C before SDS-PAGE segregation.

Nuclear localization of SRF-pA and retained differentiability of SRF-pA transfected C2C12 cells. Both the immunofluorescent assay and the western blotting results confirmed that the cellular localization of transfected SRF-pA was exclusively in the nucleus. (Figure 23-A and B) The recovery of the SRF-pA in the nuclear fraction was almost 90% of the total SRF-pA content in the cell, because there was minimal residual protein content of SRF-pA in either the cytoplasm and nuclear pellet. (Figure 23-B) The protein expression level of SRF-pA versus that of endogenous SRF was equivalent as shown from the western blotting titration experiment (Figure 23-C). Stably transfected C2C12 cells had equal differentiability as compared with non-transfected C2C12 cells. This was shown by immunohistochemistry staining for myogenin, which is a positive marker for smooth muscle cell differentiation. (Figure 23-A)

Retained affinity of SRF-pA in stable transfected C2C12 cells. As shown in Figure 23-D, the binding capacity of the protein A motif in the stably transfected C2C12 cells was intact after the plasmid was incorporated into the mouse myoblast smooth muscle cell. Furthermore, this affinity of protein A to the IgG bead was kept after the stable transfected C2C12 cells were fully differentiated.

Delayed differentiation in stably transfected C2C12 cells. After screening for the full differentiation time of stable transfected cell lines, an interesting phenomenon was noted -- the average delay for stable appearance of SRF-pA in C2C12 cells was 38 h. Of the eight selected stable clones, all of them required a long period of time to reach 100% differentiation, which was observed morphometrically by the cells adopting an elongated shape and multiple nuclei. There was no significant correlation between the delay of differentiation and the expression level of SRF-pA. (Table 11)

Cell line/ clone No.	Time to fully differentiate (\pm 2 h)	Protein expression ratio (SRF-pA:SRF)
C2C12	60	N/A
S01	90	<0.5
S02	96	1.0
S05	72	1.0
S08	120	3.0
S09	⁽¹⁾ (-)	5.0
S11	100	⁽²⁾ (-)
S12	68	3.0
S14	140	10.0

Table 11. The differentiation delay and protein expression levels of SRF-pA versus SRF.

Full (100%) differentiation was defined by the appearance of more than 90% elongated myotubes with multiple nuclei in a single myotube. Stably transfected and non-transfected C2C12 cultures were kept in differentiation medium (DMEM containing 100 μ g/ml insulin and 2% horse serum). The SRF-pA:SRF expression ratio was calculated based on the western blot image taken with a chemiluminescent counter using the level of endogenous SRF detected as the denominator. ⁽¹⁾ The S09 clone did not form multi-nuclei myotubes, but did form single nucleus-containing elongated cells. ⁽²⁾ In the S11 clone, the expression of SRF-pA was diminished after 5 passages.

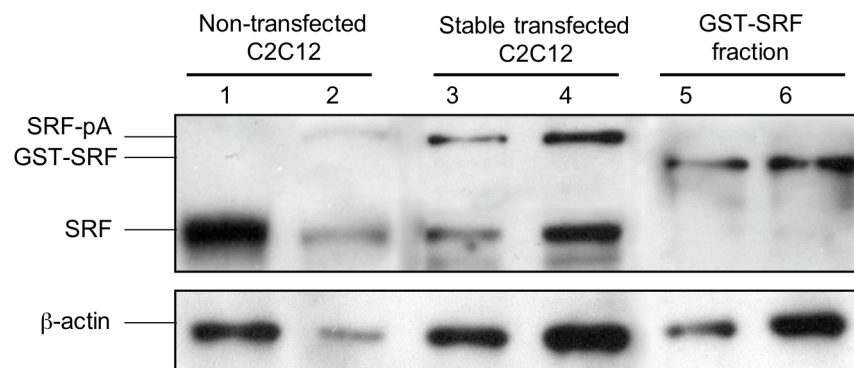


Figure 24 Level of SRF expression in different transfection systems.

Western blotting was done using rabbit anti-SRF and mouse anti- β -actin antibodies. Lane 1: Nuclear extract from non-transfected 2×10^5 C2C12 cells. Lane 2: cytosolic extract from non-transfected (2×10^5) C2C12 cells. Lanes 3 and 4: 10 μ g and 20 μ g loading of nuclear extract of SRF-pA stably transfected (2×10^5) C2C12 cells, respectively. Lanes 5 and 6: 1 μ l and 2 μ l loading of 1:1000 diluted GST-SRF fraction (1 μ g/ml), respectively.

The endogenous level of SRF. Using GST-SRF expressed in *E. coli.*, semi-quantification of endogenous SRF became possible by the western blotting method. As shown in Figure 25, the stably transfected and non-transfected C2C12 cell extracts were run with affinity purified GST-SRF in the same SDS-PAGE gel and probed with a rabbit monoclonal anti-SRF antibody. The endogenous protein level of SRF was approximately 1.5-3.0 pg per 2×10^5 cells. Therefore, there were only about 240-480 copies of SRF per cell, given the molecular weight of SRF is 67 KDa, and 6.02×10^{23} molecules per mole.

Optimized IgG-TEV purification condition for SRF-pA. The optimal condition of the TAP purification method was evaluated using several variables: (1) TEV protease incubation time; (2) TEV protease incubation temperature; and (3) the concentration of DTT in the TEV cleavage reaction. As illustrated in Figure 25, optimization was carried out in solution, where the SRF-pA adenoviral-infected 293 lysate was used as the substrate for TEV protease. At both ambient temperature and at 4 °C, the cleavage was sufficient after 1 h of incubation, with no increase in the cleaved product, SRF. Considering the stability of SRF, which is subject to other protease digestion and degradation, the reaction temperature of 4 °C was selected for optimization, rather than room temperature, for in-solution TEV cleavage.

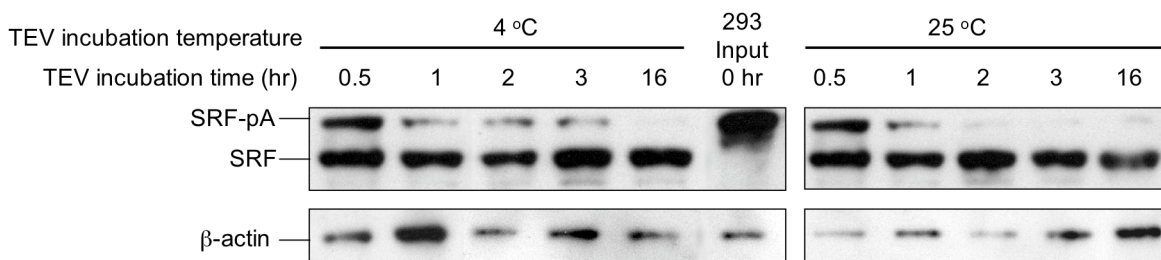


Figure 25 Optimization of temperature and time of TEV cleavage conditions.

Whole cell lysates were obtained from 293 cells infected with SRF-pA adenovirus. TEV protease was added to the cell lysate, which was diluted 1:2 with TEV cleavage buffer (provided with the TEV protease cleavage kit) to obtain a salt concentration of no more than 150 mM. An aliquot (5 μ l) of the incubated solution was sampled

at each timepoint noted, diluted 1:1 with 2x SDS reducing sampling buffer and boiled at 95 °C for 5 min before electrophoresis and western blot analysis. Rabbit anti-SRF and mouse anti-β-actin antibodies were used.

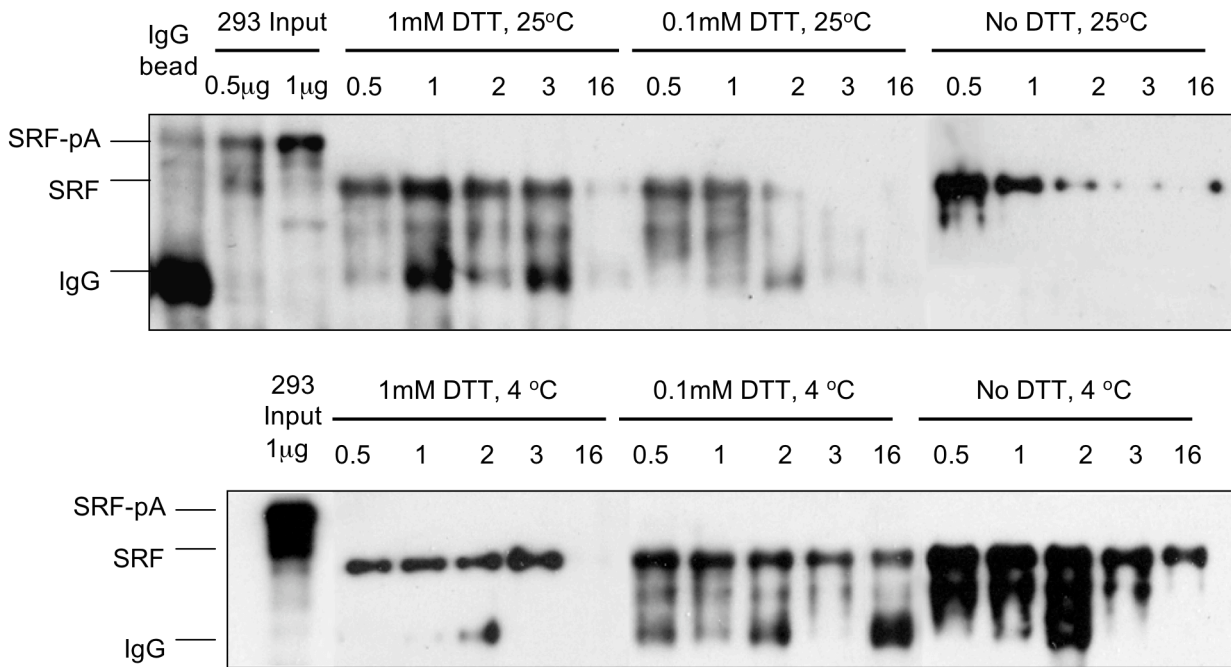


Figure 26 IgG column coupled TEV cleavage optimization for DTT concentration, incubation temperature and time.

Cell lysates were obtained from the whole cell lysate of SRF-pA adenoviral-infected 293 cells. TEV protease was added to Fast Flow 6 IgG sepharose beads, which were equilibrated with TEV cleavage buffer provided with the TEV protease cleavage kit. Fresh DTT was added in the equilibrating TEV buffer before adding the TEV protease. An aliquot (5 μl) of the incubated supernatant was sampled at each timepoint noted, diluted 1:1 with 2x SDS reducing sampling buffer and boiled at 95 °C for 5 min before electrophoresis and western blot analysis. Rabbit anti-SRF and mouse anti-β-actin antibodies were used. Numbers under each condition are TEV incubation time in hours.

Since most of the separation was carried out using IgG Sepharose beads, optimization for in-bead TEV cleavage was needed to achieve higher recovery as well as purity. DTT was added as per the manufacturer’s suggestion to help reveal the TEV protease cleavage site on the substrate. However, DTT caused greater degradation of the IgG Sepharose bead material, introducing more contaminants in the form of IgG fragments. Therefore, an experiment to optimize the DTT concentration was carried out in parallel with the temperature and incubation

time optimizations for in-bead TEV cleavage. As shown in Figure 26, two conditions gave the cleanest cleavage product. One was with no DTT and incubation at ambient temperature yielding a reaction that was complete after merely 0.5 h. However, a decrease in the cleaved product, SRF, was observed after 1 h overnight incubations, mainly due to the degradation of SRF into smaller fragments, which do not have the affinity for the anti-SRF antibodies. The other condition was with 1mM DTT at 4 °C. This gave complete reaction after 3 h with minimal loss of the SRF product. Yet, after overnight incubation, the SRF was again degraded. Even though 0.1mM DTT and an incubation temperature of 4 °C gave minimal degradation of SRF even after overnight incubation, the reaction efficiency was not as great as with 1mM DTT. Therefore, the final optimized TEV in-bead cleavage condition was 1mM DTT in TEV cleavage buffer and incubation for up to 3 h at 4 °C.

4.6.3 Discussion

Aggregation or over-expression of the target protein in mammalian cell lines when using a plasmid construct is often a problem in the study of the function of the protein *in vivo*. Overexpression can come about by an increase in the number of copies of the gene or an increase in the binding strength of the promoter region. However, this strategy does not always yield functional protein, because drastic overexpression of endogenous protein (e.g., by 10-fold) may result in several negative outcomes. Gene expression is a multi-step process that begins with transcription of DNA into messenger RNA (mRNA), followed by post-transcriptional modification of the amount of message and the timing of appearance of the functional message. After this, the mRNA is translated by the ribosome to produce a polypeptide. Further changes, including degradation, may then occur through post-translational modification. Any step of gene

expression may be modulated from the transcription step to post-translational modification of a protein. Gene regulation gives the cell control over structure and function, and is the basis for cellular differentiation, morphogenesis, and the versatility and adaptability of any organism. Once a protein is overexpressed, not only the self-response system of the cell (e.g., scavenger proteins) but also the gene regulation cascades may be changed due to the over-population of the expressed protein. In addition, over-production of a gene product *in vivo* may cause changes in cell morphology or growth capability and differentiability. Furthermore, the introduced affinity tags may also foreignize the target protein, so that the end expression product from the cell is no longer recognizable by affinity epitopes during *in vitro* protein purification.

An ideal scenario is that the introduced plasmid have an affinity tag that can keep both the protein's function and its own affinity intact after protein expression, and the endogenous protein level is negated (e.g., by siRNA) so that the biological function can be taken over by the introduced expression of the target protein. Meanwhile, the cellular localization of this protein and cell morphology has to be kept intact for it to function in the correct cellular compartment at the right time. This type of transgenic approach is a great challenge, and very technique intensive. In the present study, siRNA against SRF was not used to rule out the effect from endogenous SRF, but the stable transfection of SRF-pA gene into a mouse smooth muscle cell line, C2C12, was achieved. The successes were as follows. (1) Over-expression in terms of the exogenously introduced SRF-pA protein compared with endogenous SRF was avoided. Therefore, there was minimal protein aggregation and over-population, both of which can stimulate many other chain reactions in the cell system. (2) The expressed SRF-pA co-localized with endogenous SRF in the nucleus. This is very critical when any transcription factor is put to study. (3) The capability to form fully differentiated myotubes was preserved in C2C12 cells

after being stably transfected with SRF-pA plasmid. This success has built the foundation for further investigation, which will use this model to study the change of SRF interaction partners as well as phosphorylation patterns before and after differentiation.

The difficulty in protein-protein interaction and phosphorylation studies was not a surprise, particularly knowing now the low copy number of SRF in mouse smooth muscle cells (only around 250 copies per cell). This is the first time such information has ever been delivered in a SRF study. Because of the low copy number of SRF in each cell, and given the complication of studying protein-protein interaction using proteomics methods, which include great amounts of pre-fractionation and purification work, the end yield of this protein will be around several attomoles (1×10^{-18} mol) per 10-cm Petri dish, far less than the required femtomole (1×10^{-15} mol) level necessary for mass spectrometry analysis. (Table 10) Therefore, to cover this gap of three orders of magnitude, future studies will require the mass production of cultured cells, or to the collection of vast amounts of tissue samples by selective tissue dissection.[308-310] A future direction that might be fruitful would be to use sensitive stable isotope labeling in cell culture, with minimal purification steps prior to the mass spectrometry analysis.[311-313] A more aggressive approach would be to establish a transgenic mouse model with endogenous SRF knocked out (i.e., SRF $-/-$) and exogenously-tagged SRF knocked in (i.e., SRF-pA $+/+$), so that controllably expressed SRF-pA could be extracted from muscle-specific tissues to study cell proliferation and differentiation programming according to the different binding partner and phosphorylation patterns of SRF.

5.0 IDENTIFICATION OF PSEUDOPODIA PROTEOMES

5.1 PSEUDOPODIA PROTEOME PREPARATION

One of the characteristic features of malignant tumors is invasive and/or metastatic behavior. Diffuse astrocytomas invade widely through the surrounding central nervous system tissue. These tumors prefer to migrate through white matter tracts formed by axons, glial processes, possibly widened by tumor-induced edema and proteolysis. In contrast to normal astrocytes, tumor cells produce dynamic pseudopodial cell extensions that mediate migration with only transitory vascular and neuronal contacts. During invasion, there are many events that occur within the pseudopodial leading edge, such as signal transduction, membrane formation and turnover, cytoskeletal remodeling, adhesion, de-adhesion and energy production. The proteins involved in mediating pseudopodial extension offer potential therapeutic targets to suppress tumor cell invasion.

Proteomic investigations of migrated pseudopodia rely on obtaining sufficient lysate material for study. Traditional methods of scraping from wafer-thin filter or chemically release from chamber well surfaces in migration assays often result in low yields of recovered proteins. In this project, a new two-step method was developed to harvest migrated pseudopodia (Ps) from filters. Pseudopodia were transferred from the filters onto glass slides and were then harvested in urea lysate buffer that crystallized so that all pseudopodial material could be retrieved by

scraping. [314] Detailed proteomic analyses were then performed to discover signatures within the pseudopods that provide information about the processes occurring within these structures, as well as potential molecular targets for treating such invasive tumors.

The hypothesis examined in this study was that the alteration of protein levels in newly formed pseudopods, as compared to the whole cell lysate, gives a molecular signature of the early response of astrocytoma cells treated with migration stimulants (e.g., hepatocyte growth factor (HGF)).

5.2 IDENTIFICATION OF PSEUDOPOD PROTEOMES

5.2.1 Materials and methods

Cell culture. Cell culture work was performed in the labs of Prof. Marie Beckner, University of Pittsburgh, by Dr. Beckner and co-workers. Human U87 and LN229 astrocytoma cell lines were from American Type Culture Collection, Manassas, VA, USA and were maintained in minimal essential media (MEM) (Cellgro, Media Tech, Herndon, VA, USA) with 10% fetal bovine serum (FBS) (Invitrogen). Half volumes of media were changed the day prior to each migration assay or harvest of Ps to normalize the cells' metabolic state.

Harvesting of Pseudopodia (Ps) and Unmigrated Cells (UC). The methodology for obtaining Ps from cells has been described in detail[314]. Briefly, cell suspensions were loaded in the upper wells of four-, ten- or single-well Boyden chambers (Neuro Probe, Gaithersburg, MD, USA) that were assembled with 0.01% gelatin-coated filters containing either 1 or 3 μm pores to separate the upper and lower wells. The lower wells contained MEM fortified with 0.1-

1% FBS and hepatocyte growth factor (HGF), 2.5 ng/ml, as chemoattractants. The media in both wells contained 1 mg/ml BSA, Fraction V, unless otherwise stated. Chambers were incubated at 37° C in a 5% CO₂ tissue culture incubator for up to 6 h. At the designated times, filters were removed, immersed in methanol for 15 s, and then each was placed on a glass slide with migrated Ps on the filter's undersurface. Non-migrated cell materials were completely wiped from the top of each filter with Kimwipes or cotton swabs. Fresh Kimwipes or swabs were used to press filters firmly against the glass slides to promote adherence of migrated Ps to the glass. Unless otherwise stated, the filters were then peeled off the slides with forceps without removing Ps attached to the glass. The slides with attached Ps were stored at -80 °C. Ps were either stained for microscopy or solubilized in lysate buffer consisting of 6 M urea, 4% 3-[(3-chloamidopropyl)-dimethylammonio]-1-propanesulfonate, 2 M thiourea, 20 mM dithiothreitol, and 1.6 mM 4-(2-hydroxyethyl) piperazine-1-ethanesulfonic acid, pH 8.0. The UC, mostly whole cells, were allowed to adhere to filters in separate chambers and transferred to glass slides as described for Ps with the upper side of the filters against the glass. Due to layering, many UC cells were not in contact with the filter pores during the incubations. Protein concentrations were determined with Bradford assays (Coomassie Plus Protein Reagent, Pierce, Rockford, IL, USA).

One-Dimensional Gel Electrophoresis. Lysates of Ps and UC, equalized for total protein content (10 µg per lane) or with GAPDH, as indicated, were electrophoresed in separate lanes of 10% polyacrylamide gels under reducing conditions. Each gel was stained with Coomassie blue (Novex Colloidal Blue Stain Kit, Invitrogen) and destained with tap water. Protein standards (MagicMark and MultiMark, Invitrogen) were loaded at 8 µg per lane.

Differential gel electrophoresis (DiGE). Procedures described above were followed with the following modifications. The electrophilic fluorescent dyes, PrCy3-*N*-hydroxysuccinimide

ester and MeCy5-*N*-hydroxysuccinimide ester (Cy3 and Cy5, respectively), were synthesized in the Day lab and stored as single use aliquots in anhydrous *N,N*-dimethylformamide at $-80\text{ }^{\circ}\text{C}$. Pseudopodial and whole cell lysates were separately mixed with volumes of each dye solution to produce balanced covalent labeling of 1–5% of the available lysine side chains, without significant alteration of the protein isoelectric points (*pI*'s). Quenching was accomplished with 40% aqueous methylamine, pH 8.6. Paired pseudopodial and whole cell lysates were mixed together for focusing and subsequent separation by SDS-PAGE. The gels were repeated with reciprocally labeled pseudopodial and whole cell lysates. The gels were viewed in a fluorescent gel-imaging device built around a CCD camera (CH350 model, 16 bit chip, Photometrics, München, Germany) with an integral gel-cutting tool. Imaging was performed at two excitation wavelengths, 545-710 nm and 635-715 nm for Cy3 and Cy5, respectively. Image manipulation and viewing was done with Image J (National Institutes of Health, Bethesda, MD, USA) and V++Precision Digital Imaging System software (Digital Optics, Auckland, New Zealand). Two-frame, 'flash' movies of the overlying Cy3 and Cy5 images were viewed in a continuous loop to visually detect differences in the protein signatures between the two samples separated in the same gels. The repeat gels of reciprocally stained lysates revealed any differences due to dye uptake. Sample-dependent differences in protein distributions were confirmed and quantified using an image analysis software package, DeCyder Differential Analysis Software, version 5.0 (DeCyder® Amersham Biosciences). DeCyder analyzed images as fragments, summed to generate a composite image, with proprietary algorithms that detected overlapping, differently colored images within the same gel to match spots and subtract background for normalization. DeCyder created measurement masks, each outlining an area of the gel containing a protein spot that were applied to each of the matching fragments in the paired fluorescent images of each gel.

The masks defined areas in which the pixel values were integrated to create three-dimensional topographical maps with peaks representing each protein spot. An estimate of the local background for each spot determined the base values across the masked area. Output from the image analysis, designated as fluorescence intensity, was the sum of pixel values in the mask area minus the background. Volumes of the peaks representing the relative strengths of fluorescent signals from matched spots were compared. Although a threshold was set at 1.5-fold to screen for differences, only proteins with $Z=2.0$ -fold differences were reported. Visual inspection confirmed the differences indicated by the DeCyder software. Dust and artifacts were detected as peaks with slope values of less than one or as clusters of sharp spikes. Images of some protein spots were also scanned and digitized to compare total pixels, as described below for immunoblots. Protein spots that differed on DIGE between the labeled lysates were harvested from the gels using a robotic gel picker integrated with the high resolution CCD camera, digested with trypsin, and submitted for mass spectrometric PMF analysis.

Protein Identification. Gels were submitted to the Michigan Proteome Consortium for robotic dissection of individual Coomassie blue-stained bands that were prominent in lysates of Ps compared to UC when total protein was used for equalization. Following trypsin digestion, peptides derived from each band were analyzed with matrix assisted laser desorption ionization time of flight mass spectrometry (MALDI-TOF-MS) in 4700 and 4800 Proteomics Analyzers with TOF/TOF optics (Applied Biosystems, Foster City, CA). Internal calibration of tryptic peptide mixtures was achieved using the monoisotopic masses of trypsin autoproteolysis peaks at m/z 842.5094 and 2211.1046. Peptide mass fingerprint searches with the Mascot (<http://www.matrixscience.com>) program and the MS-Fit program (<http://prospector.ucsf.edu>) were used for protein identification utilizing the NCBI and SwissProt databases. Search

parameters included all species, all MR's and pI's, monoisotopic peptide masses, tolerance of 50 ppm m/z measurement error and up to one missed trypsin cleavage site per peptide, cysteines modified by acrylamide, partial changes of oxidation of methionine and changes at the amino termini, such as conversion of glutamine to pyro-glutamate and acetylation. Trypsin autolysis and keratin-derived peptides were listed as possible contaminants. Protein identifications were accepted when the observed and predicted pI's and MR's were consistent and scores indicated nonrandom identifications at a significance level of $p < 0.05$.

Immunoblotting Gel contents were transferred onto PVDF membranes (Invitrogen), blocked (Detector Block, Protein Detector Western Blot Kit LumiGLO System, Kirkegaard & Perry Laboratories, Gaithersburg, MD, USA), and reacted with the designated primary antibodies (anti- β -actin (1:1000), anti-HSP70 (1:1000), anti-GAPDH (1:250), anti-HGF (2 $\mu\text{g}/\text{ml}$), and anti-pMet (1:375)). Secondary antibodies, 1:1000 (Kirkegaard & Perry Laboratories) were horseradish peroxidase-labeled anti-rabbit for antibodies specific for β -actin, HSP70, GAPDH, and pMet, and anti-mouse for antibodies specific for HGF. Immunoreactive bands were visualized via horseradish peroxidase's conversion of a luminol-based solution to produce chemiluminescence, and reacted blots were scanned (Epson Perfection 2450 PHOTO transparency scanner, Epson America, Long Beach, CA, USA) to give digital images. Relative reactivities of proteins on immunoblots of Ps and UC were quantified in digitized bands of chemiluminescence with correction for background (UN-SCAN-It gel, Silk Scientific, Orem, UT, USA).

Immunohistochemistry BSA and HSA fluorescein isothiocyanate conjugates were obtained from Sigma, St. Louis, MO, USA. Other reagents were also from Sigma unless otherwise stated. To visualize localization of non-secreted albumin to Ps, 0.25 mg/ml F-BSA or

F-HAS was included in upper and lower wells of Boyden chambers during formation of Ps by cells responding to HGF and FBS. When phospholipid membranes were also visualized, suspended cells were pre-loaded with the fluorescent (red) lipophilic membrane tracer, chloromethyl derivative of 1,1'-dioctadecyl-3,3',3',3'-tetramethylindocarbocyanine I (CM-DiI), Cell Tracker (Invitrogen) at 1 µg/ml for 5 min at 37 °C and 10 min at 4 °C. In some assays, Ps and UC were stained, after removal of filters, for nuclei, actin or HGF. Nuclei were stained with Hoechst 33342 trihydrochloride trihydrate (Invitrogen), 10 µg/ml. Alexa Fluor 488 phalloidin (green) (1:200) was used to directly stain actin. HGF was indirectly stained with mouse anti-HGF (2.5 µg/ml) and Alexa Fluor 555 goat anti-mouse IgG (1:200). Ps and UC were examined using an Olympus BH2 microscope with a BHS-RFC reflected light fluorescence attachment (Olympus Corp., Lake Success, NY). Filters appropriate for fluorescent signals from the CM-DiI, fluorescein, Hoechst, and Alexa chromophores were used. Olympus MicroSuite Five Software for Imaging Applications (Soft Imaging System Corp., Lakewood, CO) was used to process and merge images of multiple emitted fluorescent signals. Yellow represented similar intensities of merged green and red fluorescent signals.

5.2.2 Results

The identification of pseudopodia proteome in comparison with un-migrated whole cells in U87 glioma cell line. After applying the differential gel electrophoresis (DiGE) to analyze the relative protein levels in the U87 glioma cell's proteome, (see Figure 27), many of the proteins found to have increased levels in pseudopodia were associated with glycolysis and tumor progression. (See Table 11) For example, annexin isoforms (AnxI & AnxII), and enolase were observed in 4.06-, 2.89- and 2.60-fold increased levels in pseudopodia over that observed in

whole cell lysates. The signals for two proteins, transketolase and mitochondrial manganese superoxide dismutase (MnSOD), were significantly decreased in pseudopodia as compared to whole cells. (See Table 12) Notably, increased BSA, an exogenous protein in the media, was observed. A previous study from the Day and Beckner labs had considered this increase to be biologically insignificant.[314] The level of combined BSA isoforms spots, shown in Figure 28, were in total 4.55-fold higher in pseudopodia than in whole cells. In the previous reports, the increased BSA was thought to have come from glass surfaces not covered by pseudopodia, or that it may have preferentially adhered to the surfaces of pseudopodia. [315, 316]

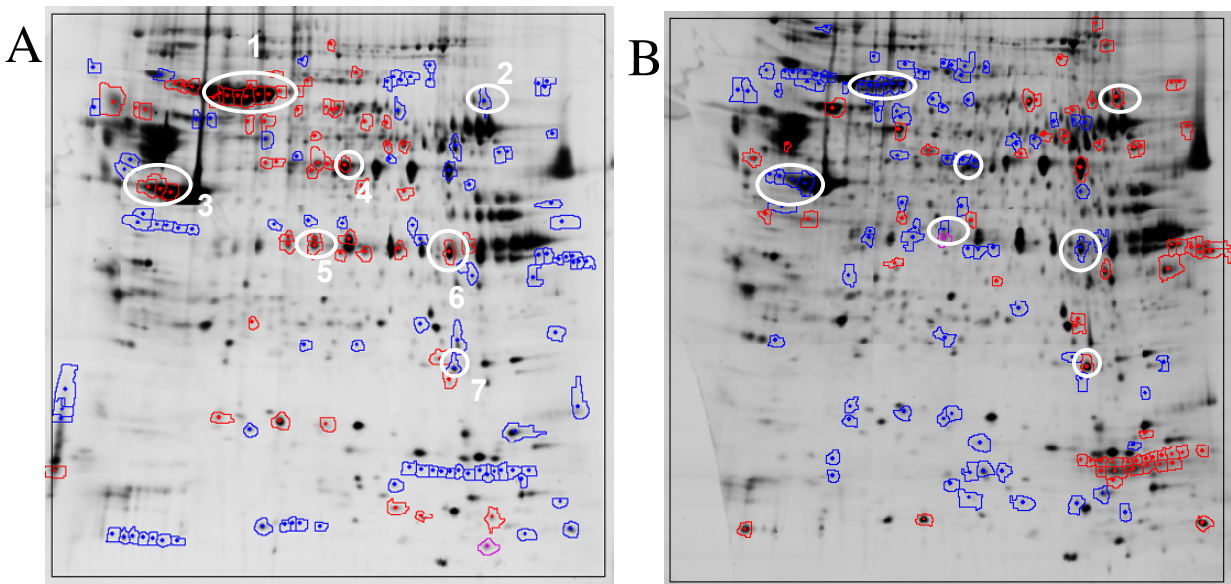


Figure 27 Representative DiGE images of paired whole cell and pseudopodia lysates

The images in figure are shown as analyzed, the inverse images of the fluorescent stains used. (A) Whole cell lysate labeled with Cy3 and pseudopodia lysate labeled with Cy5. (B) Pseudopodia lysate labeled with Cy3 and whole cell lysate labeled with Cy5. The blue-circled areas represent proteins with the relatively increased level in the Cy3-labeled sample than in the Cy5-labeled sample (i.e., in A: blue area is the increase in pseudopodia vs. whole cell). The red-circled area represents the proteins with relatively decreased levels in the Cy3-labeled sample than in the Cy5-labeled sample (i.e., in B: the red area is the decrease in whole cell vs. pseudopodia).. The pI values in the gels ranged from 3 to 10, left and right margins of the gel, respectively.

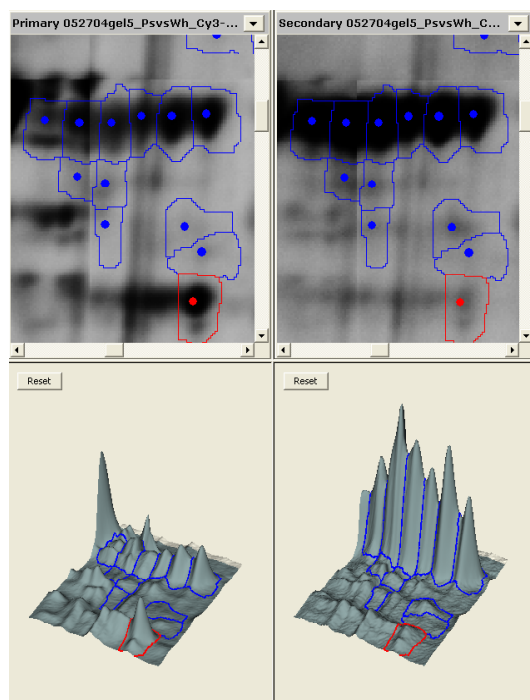


Figure 28 The topographically rendered densitometry results for BSA isoforms in the DIGE gel shown in Figure 27.

A series of six peaks represent BSA isoforms in whole cells (left) and pseudopodial (right). Their identities as determined by MALDI-TOF-MS were same with the spot 1 highlighted in Figure 27.

Protein names	Location in Figure 27	Volume ratio	Functional association
Serum albumin	1	+4.55	Growth factor
Transketolase	2	-2.00	Glycolysis
Actin	3	+3.05	Cytoskeleton
Enolase	4	+2.60	Glycolysis
Anx I	5	+4.06	Tumor progression
Anx II	6	+2.89	Proteolysis, actin bundling
MnSOD	7	-2.00	Protection from free radical damage

Table 12. Ratio of differences in protein levels between pseudopodia and whole cell lysates from U87 cells.

The reciprocal labeling of whole cell lysate and pseudopodia lysate in DiGE experiment [315] confirmed the relative ratio of protein level between two samples, as the consistency of increase/decrease of protein level was observed in two repetitions of DiGE gel analysis using DeCyder software. The parameters that were used to calculate the relative volume ratio include: section area, section volume, section peak height, and section slope and section radius. The

advantage of doing reciprocal labeling is that it greatly reduces, even eliminates, the errors that can be caused by several reasons: unequal and incomplete Cy3 and Cy5 dye labeling between the two samples could bring in error; intrinsic imaging instrumental errors could be caused by detector instability; and the fluorescent source light can fluctuate. The calculation error of the imaging software based on pixels caused by un-even background in two gels, as well as the un-even absorption of protein samples during the iso-electric focusing procedure, are also reduced to achieve comparable results in DiGE.

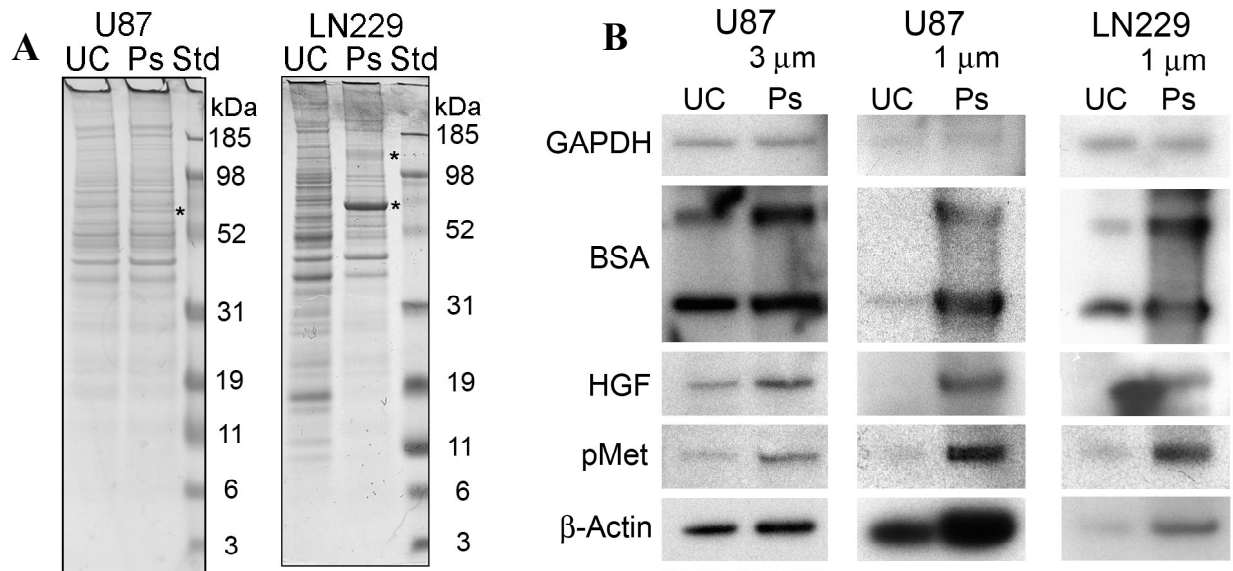


Figure 29 Identification of pseudopodia proteins compared to proteins in the unmigrated cell.

Figure 29-A: One dimensional gel electrophoresis analyses. Lysates prepared from pseudopodia (Ps) of both cell lines contained BSA that was increased compared to whole cell (UC). Bands (visible in Ps but not UC) that contained predominantly BSA, identified as tryptic peptides with mass spectrometry, are indicated with an asterisk (*). Peptides obtained from the 68 kDa band from Ps formed by LN229 cells are listed in Table 13. 10 μg protein per lane. Coomassie blue stained. Figure 29-B: Immunoblotting images of U87 and LN229 cells extracts. Specific antibodies were used to demonstrate protein distributions. Equalized loadings for whole cell with pseudopodia derived from U87 cells on filters (3 μm pores), U87 cells (1 μm pores), and LN229 cells (1 μm pores) were indicated by equal amounts of glyceraldehyde-3-phosphate dehydrogenase (GAPDH) (36 kDa) reactivity. The differences between Ps and UC were limited to a range of 1.04-fold to 1.09-fold as estimated by densitometry. Reactivities for BSA, either its monomeric (68 kDa) or dimerized (140 kDa) forms, in Ps were increased up to 15.5-fold with the greater increases occurring in Ps formed using filters with 1 μm pores. Reactivities for HGF (70 kDa), pMet (145

kDa), and β -actin (45 kDa), were increased in Ps up to 3.04, 6.37, and 3.82-fold, respectively, compared to UC. However, reactivities for L-plastin (62 kDa) and heat shock protein 70 (HSP70) (73 kDa), proteins that co-migrated with BSA and HGF, were greater in UC than Ps, 1.96 and 2.94-fold, respectively. (Reformatted and edited from ref. [316])

No.	Observed Mass	Calculated Mass	Ion score (C.I. %)	Ion score	Best sequence	Start Seq.	End Seq.	Error (ppm)
1	1479.7731	1479.8	99.993	81	LGEYGFQNALIVR	421	433	-18.2
2	1567.72	1567.74	99.838	67	DAFLGSFLYEYSR	347	359	-12.8
3	1439.7947	1439.81	97.594	56	RHPEYAVSVLLR	360	371	-10.6
4	1880.8998	1880.92	99.162	60	RPCFSALTPDETYVPK	508	523	-10.7
5	1740.8259	1740.83	99.129	60	MPCTEDYLSLILNR	469	482	-2.4
6	1639.907	1639.94	99.989	79	KVPQVSTPTLVEVSR	437	451	-20.1
7	1724.8135	1724.83	99.95	72	MPCTEDYLSLILNR	469	482	-9.6
8	1069.4985	1069.63	99.999	65	LSPEELLR	207	215	-122.9
9	1675.6543	1675.85	99.877	46	FSLVGIGGQDLNEGHR	416	431	-116.8

Table 13. MS-MS peptide summary for the 68 kDa band in lysate of Ps formed by cultured astrocytoma cells

Tryptic digestion of this band from Ps formed by LN229 cells yielded peptides 1-7 that matched “albumin [*Bos taurus*]”, Accession # 30794280. In Ps formed by U87 cells, in addition to peptides derived from BSA; peptides 8-9 matched “Lymphocyte cytosolic protein 1 (L-plastin) [*Homo sapiens*]”, Accession # = 8217500. Ion scores greater than 30 were considered to be significant for protein identification. C.I. = confidence interval.

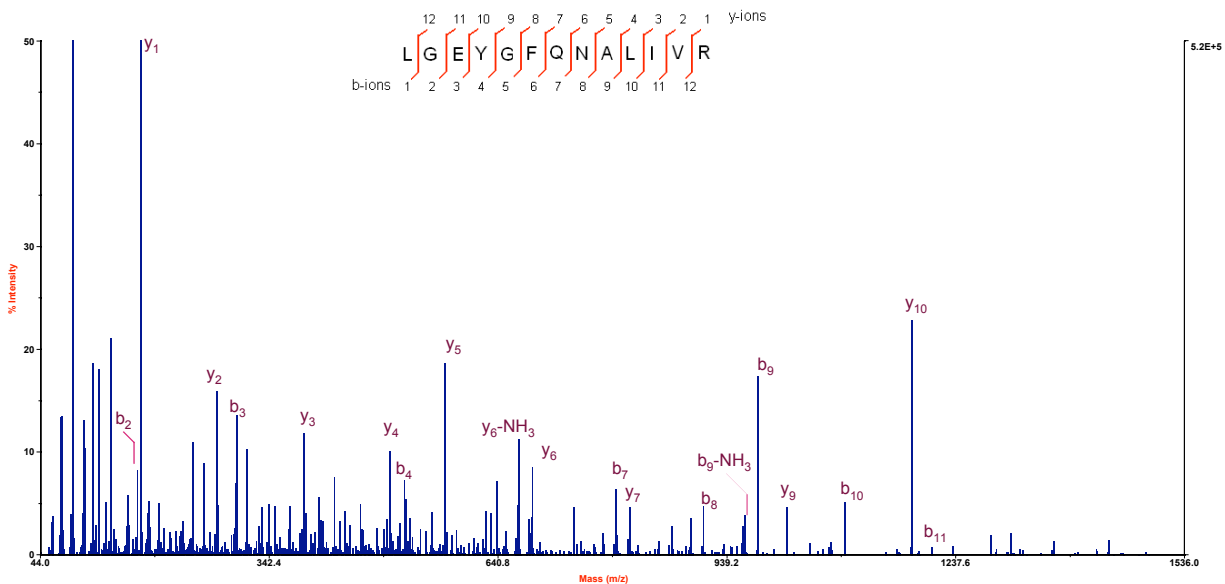


Figure 30. MALDI-TOF-TOF-MS spectra for precursor ion m/z 1479.77.

The tryptic digest was obtained from the 68 KDa band in lysate of Ps formed by U87 cells. Matched peptide sequence is: $^{421}\text{LGEYGFQNALIVR}^{433}$ (ion score=81). Confirmed fragment ions are only labeled for b or y ions; other matched peptide fragments are not shown in this spectrum. Analyzed using Data Explorer and De-Novo explorer software in the 4700 Explorer software bundle (Applied Biosystems, Inc.)

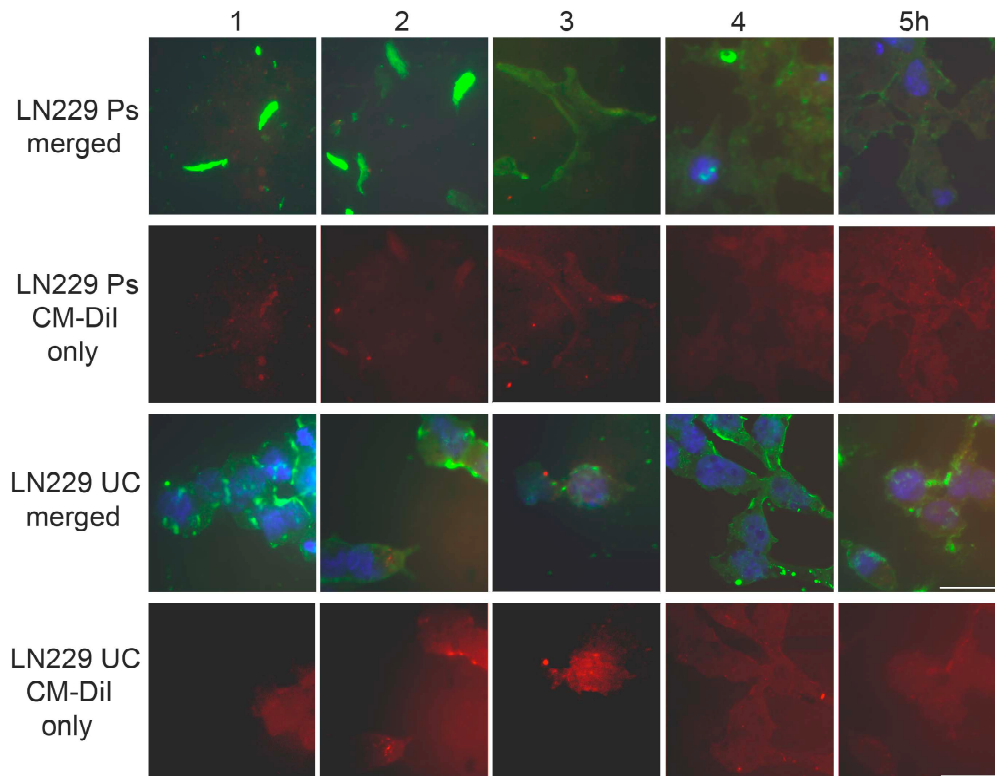


Figure 31. Adherence of F-BSA to newly-formed Ps of LN229 cells.

Cells labeled with DM-DiI (red), a membrane marker, were exposed to F-BSA (green) during 5 h time course of migration through filters with 3 m pores. Although the F-BSA signal demonstrated profiles of Ps vividly during the first 2 h, the signal was mostly dim at later time points (top row) whereas the intensity of the CM-DiI signal remained constant (second row). The newly formed Ps at 1-2 h appeared to arise from single pores, whereas Ps at 3-5 h appeared mostly syncytial (reticulopodia) with contributions from multiple pores. The UC from the top side of the filter displayed irregular signals from F-BSA (third row) rather than the evenly distributed signals on profiles of Ps formed in the first 2 h. Nuclei were stained with Hoechst (blue). The top and third rows of images represent merged signals from F-BSA, CM-DiI and Hoechst. The second and fourth rows contain only the images of CM-DiI signals. The magnification bar represents 25 μm . (Reproduced with permission from [316])

The increased intake of BSA in pseudopodia associated with glioma progression. As seen in Figure 29, *in vitro*, results from: immunoblotting, 1-D gel electrophoresis-Coomassie staining,

and MS fingerprinting (shown in Table 13) all showed that an increased level of BSA was associated with pseudopodia lysates in two glioma cell lines. The further fluorescence labeling for BSA (Figure 31) and human serum albumin (HSA) [316] confirmed that the increased level of BSA in pseudopodia was from exogenous intake rather than contamination. As a matter of fact, there have been many recent studies showing that the accumulation of serum albumin in astrocytomas *in vivo* has been largely attributed to the increased permeability of the blood-brain barrier of patients with these tumors, [317, 318] possibly aided by the well-known ability of astrocytic cells to ingest albumin. [319]

5.2.3 Discussion

The rationale of the association of albumin with glioma tumor progression. One of the characteristics of astrocytomas is the breakdown of the blood brain barrier, allowing permeation of HSA into the tumors. Albumin in the interstitial fluid of the brain flows along the common routes of tumor invasion and dispersion through white matter tracts.[320] Investigation of albumin's interactions with invasive "false feet" of astrocytoma cells - their pseudopodia (Ps), should help determine the potential for selective adherence of albumin during tissue invasion. As a marker of an early phase of cell migration, adherence of albumin to Ps can be used to further investigate the events involved in initiating tumor invasion. Albumin's differential localization to newly formed pseudopods supports a putative role for serum albumin to provide abundant fatty acids for remodeling and assembly of phospholipid membranes in cell protrusions during tumor invasion.

With high affinity for fatty acids, along with its dominant presence in the pool of bloodstream, albumin becomes an important source of lipids for tumor cells, with or without the

help from various fatty acid binding proteins in the recipient cells.[321] Although intracellular accumulation of fatty acids is cytotoxic in non-adipose tissues, rapid fatty acid utilization by membranes would permit a high rate of fatty acid uptake.[322] The availability of serum albumin via a leaky BBB and its co-dispersion with invading tumor cells along white matter tracts would provide a fatty acid substrate for rapidly forming pseudopods. Although oxidation of fatty acids could also provide energy for cell migration, it has been found that glycolysis alone can support astrocytoma and melanoma cell migration. [323, 324] According to the DiGE proteome identification results from this study, there was a significant increase in Ps of proteins of the glycolysis network, which further agrees with the role of glycolysis in glioma tumor migration. Given the fact that high levels of albumin are routinely present in brain tissue during early development, and only exogenous albumin was detected in lysates of tumor Ps in this study, fatty acids from albumin's supply would support rapid elongation of pseudopods responding to stimulation by HGF.

Therapeutic potential of albumin in invasive brain tumors. The preferential localization of albumin on pseudopodia of astrocytoma cells could play a role in novel therapies. Suppressive treatments of tumor pseudopodia could be specifically targeted by albumin's delivery of toxic fatty acids. Also, delivery of oleic acid in acidosis would support a toxic configuration of α -lactalbumin, i.e., "human alpha-lactalbumin made lethal to tumor" (HAMLET), an approach under development as an anti-cancer agent that spares normal tissues.[325-327] However, if permeability of the BBB in brain tumors is required to introduce a toxic effect on tumors, then some uncommon diseases that impair the permeability of the BBB would have to be ruled out to avoid unwanted peripheral toxicity.

The potential of DiGE and top-down functional proteomics approaches for glioma tumor

progression. Malignant rapidly-growing tumor cells typically have glycolytic rates that are up to 200 times higher than those of their normal tissues of origin. As glycolysis is a metabolic pathway by which a 6-carbon glucose (Glc) molecule is oxidized to two molecules of pyruvic acid (Pyr), it is the initial process of most carbohydrate catabolism, and it serves three principle functions: (1) the generation of high-energy molecules (ATP and NADH) as cellular energy sources as part of anaerobic respiration; (2) production of pyruvate for the citric acid cycle as part of aerobic respiration; and (3) production of a variety of six- and three-carbon intermediate compounds, which may be removed at various steps in the process for other cellular purposes. As the foundation of both aerobic and anaerobic respiration, glycolysis is the archetype of universal metabolic processes known and occurring in many types of cells in nearly all organisms, because it is, through anaerobic respiration, the main energy source in many prokaryotes and eukaryotic cells devoid of mitochondria and eukaryotic cells under low oxygen conditions (e.g. glioma cells in brain tumors) [328-330]

As the findings from the comparative DiGE proteome mapping of pseudopodia indicated, many proteins whose functions are related to glycolysis have increased level in pseudopodia. Since glycolysis can serve both as the up-stream formation and the down-stream break down of carbohydrates, glycosylation can be seen as associated with meta-molecule protein, other than glycolysis, which deals with small molecule building blocks in metabolic cycle. Changes in glycosylation of glycoproteins and glycolipids are common features of solid tumors. The covalent linkage of oligosaccharides (glycosylation) to proteins is the most common post-translational modification event and occurs in more than 50% of proteins.[331] In parallel with phosphoproteomics, there is emerging interest in studying the glycoproteomics, because of three fundamental reasons. Firstly, polysaccharide addition controls the protein 3D structure, which in

turn triggers the functionality of many enzymatic proteins;[332-336] secondly, there is close relationship between the glycosylation status of proteins and many diseases, especially cancers; [337-340] and thirdly, the fast developing proteomics technology is providing more promise in discovering the chemical details of glycosylation. For the general study of glycoproteins, some universal isotope tagging methods have been developed. Lectins, i.e., proteins that specifically recognize certain saccharide motif(s), are frequently used to enrich glycosylated proteins or peptides in the form of lectin affinity chromatography. [341-344]

Part of the results from this study was published along with additional biological assays.[314, 316] From the aspect of the application of proteomics techniques, this study showed that sub-femtomole levels of proteins in a bio-specimen could be handled to give relative comparison between control and disease stages. For a relatively simple biological sample such as a pseudopodial lysate, one dimensional gel electrophoresis coupled with the peptide fingerprinting technique using high resolution mass spectrometry can yield confirmable information about unknown proteins' identities. Reciprocal labelled two-dimensional differential gel electrophoresis was found to be another very useful tool for semi-quantitative pathology and biological research in that the fold alteration of protein level is correlated with disease states or conditions. Therefore, to aid discovery, organelle or disease state proteome mapping can be integrated into a semi-quantitative method for biomarker discovery in a routine manner.

APPENDIX A

HUMAN SRF PROTEIN AND DNA SEQUENCES.

The full-length gene contains 508 amino acids (MW = 51517 Da) or 1524 DNA bases, respectively.

```
1 ATGTTACCGACCCAAGCTGGGGCCGCGCGGCTCTGGGCCGGGGCTCGGCCCTGGGGGGC
1 M L P T Q A G A A A A L G R G S A L G G
61 AGCCTGAACCGGACCCCGACGGGGCGGCCGGGCGGCGGGCGGGACACGCGGGGCTAAC
21 S L N R T P T G R P G G G G G T R G A N
121 GGGGGCCGGGTCCCCGGAATGGCGCGGGGCTCGGGCCCCGGCCGCCTGGAGCGGGAGGCT
41 G G R V P G N G A G L G P G R L E R E A
181 GCGGCAGCGGCGGCAACCACCCCGCGCCCACCGCGGGGGCCCTCTACAGCGGCAGCGAG
61 A A A A A T T P A P T A G A L Y S G S E
241 GCGGACTCGGAGTCGGGCGAGGAGGAGGAGCTGGGCGCCGAGCGGCGCGGCCTGAAGCGG
81 G D S E S G E E E E L G A E R R G L K R
301 AGCCTGAGCGAGATGGAGATCGGTATGGTGGTGGTGGGCCCGAGGCGTGGCAGCGGCC
101 S L S E M E I G M V V G G P E A S A A A
361 ACCGGGGGCTACGGGCCGGTGAGCGGCGCGGTGAGCGGGGCCAAGCCGGGTAAGAAGACC
121 T G G Y G P V S G A V S G A K P G K K T
421 CGGGGCCGCGTGAAGATCAAGATGGAGTTCATCGACAACAAGCTGCGGCGCTACACGACC
141 R G R V K I K M E F I D N K L R R Y T T
481 TTCAGCAAGAGGAAGACGGGCATCATGAAGAAGGCCTATGAGCTGTCCACGCTGACAGGG
161 F S K R K T G I M K K A Y E L S T L T G
541 ACACAGGTGCTGTTGCTGGTGGCCAGTGAGACAGGCCATGTGTATACCTTTGCCACCCGA
181 T Q V L L L V A S E T G H V Y T F A T R
601 AAAGTGCAGCCCATGATCACCAGTGAGACCGGCAAGGCACTGATTCAGACCTGCCTCAAC
201 K L Q P M I T S E T G K A L I Q T C L N
```

661 TCGCCAGACTCTCCACCCCGTTTCAGACCCCAACAGACCAGAGAATGAGTGCCACTGGC
 221 S P D S P P R S D P T T D Q R M S A T G
 721 TTTGAAGAGACAGATCTCACCTACCAGGTGTCGGAGTCTGACAGCAGTGGGGAGACCAAG
 241 F E E T D L T Y Q V S E S D S S G E T K
 781 GACACACTGAAGCCGGCGTTCACAGTCACCAACCTGCCGGGTACAACCTCCACCATCCAA
 261 D T L K P A F T V T N L P G T T S T I Q
 841 ACAGCACCTAGCACCTCTACCACCATGCAAGTCAGCAGCGGCCCTCCTTTCCCATCACC
 281 T A P S T S T T M Q V S S G P S F P I T
 901 AACTACCTGGCACCAGTGTCTGCTAGTGTGTCAGCCCCAGTGTGTCAGCAGTGCCAATGGG
 301 N Y L A P V S A S V S P S A V S S A N G
 961 ACTGTGCTGAAGAGTACAGGCAGCGGCCCTGTCTCCTCTGGGGGCCTTATGCAGCTGCCT
 321 T V L K S T G S G P V S S G G L M Q L P
 1021 ACCAGCTTCACCCTCATGCCTGGTGGGGCAGTGGCCCAGCAGGTCCCAGTGCAGGCCATT
 341 T S F T L M P G G A V A Q Q V P V Q A I
 1081 CAAGTGCACCAGGCCCCACAGCAAGCGTCTCCCTCCCGTGACAGCAGCACAGACCTCACG
 361 Q V H Q A P Q Q A S P S R D S S T D L T
 1141 CAGACCTCCTCCAGCGGGACAGTGACGCTGCCCGCCACCATCATGACGTCATCCGTGCC
 381 Q T S S S G T V T L P A T I M T S S V P
 1201 ACAACTGTGGGTGGCCACATGATGTACCCTAGCCCGCATGCGGTGATGTATGCCCCACC
 401 T T V G G H M M Y P S P H A V M Y A P T
 1261 TCGGGCCTGGGTGATGGCAGCCTCACCGTGCTGAATGCCTTCTCCAGGCACCATCCACC
 421 S G L G D G S L T V L N A F S Q A P S T
 1321 ATGCAGGTGTCACACAGCCAGGTCCAGGAGCCAGGTGGCGTCCCCAGGTGTTCTGACA
 441 M Q V S H S Q V Q E P G G V P Q V F L T
 1381 GCATCATCTGGGACAGTGCAGATCCCTGTTTCAGCAGTTCAGCTCCACCAGATGGCTGTG
 461 A S S G T V Q I P V S A V Q L H Q M A V
 1441 ATAGGGCAGCAGGCCGGGAGCAGCAGCAACCTCACCGAGCTACAGGTGGTGAACCTGGAC
 481 I G Q Q A G S S S N L T E L Q V V N L D
 1501 ACCGCCCACAGCACCAAGAGTGAATGA
 501 T A H S T K S E *

TAP-TAG DNA SEQUENCE AND POLYLINKER

ATGGCAGGCCTTGCGCAACACGATGAAGCCGTGGACAACAAATTCAACAAA
 GAACAACAAAACGCGTTCTATGAGATCTTACATTTACCTAACTTAAACGAAGAACA

ACGAAACGCCTTCATCCAAAGTTTAAAAGATGACCCAAGCCAAAGCGCTAACCTTTT
AGCAGAAGCTAAAAAGCTAAATGATGCTCAGGCGCCGAAAGTAGACAACAAATTCA
ACAAAGAACAACAAAACGCGTTCTATGAGATCTTACATTTACCTAACTTAAACGAA
GAACAACGAAACGCCTTCATCCAAAGTTTAAAAGATGACCCAAGCCAAAGCGCTAA
CCTTTTAGCAGAAGCTAAAAAGCTAAATGATGCTCAGGCGCCGAAAGTAGACGCGA
ATTGTGATATACCTACAACCTGCTTCTGAAAATTTATATTTTCAAGGTGAACTAAAGA
GAAGATGGAAAAAGAATTTTCATAGCCGTCTCAGCAGCCAACCGCTTTAAGAAAATC
TCATCCTCCGGGGCACTTGATCCCATGGCATTGGCCAATTGTTCCGGATCC

TAP-TAG PROTEIN SEQUENCE

MAGLAQHDEAVDNKFNKEQQNAFYEILHLPNLNEEQRNAFIQSLKDDPSQSANLLAEA
KKLNDAQAPKVDNKNFNKEQQNAFYEILHLPNLNEEQRNAFIQSLKDDPSQSANLLAEAK
KLNDAQAPKVDANCDIPTTASENLYFQGELKRRW KKNFIAVSAANRFKKISSSGAL

RECOMBINANT SRF-PA PROTEIN SEQUENCE.

The full length gene contains 714 amino acids (MW = 74542 Da) Calmodulin binding site was written in red block letters, the TEV cleavage site was written in green block letters, and the arrow head points to the starting point for the TAP tag including the Protein-A tag (*Staphylococcus aureus* Protein-A sequence was written in blue block letters.)

MLPTQAGAAAALGRGSALGGSLNRTPTGRPGGGGGTRGANGGRVPGNGAGLGPGRLEREAAAAA
ATTPAPTAGALYSGSEGDSSESGEEELGAERRGLKRSLSSEMEIGMVVGGPEASAAATGGYGPVS
GAVSGAKPGKKTRGRVKIKMEFIDNKLRRYTTFSKRKTGIMKKAYELSTLTGTQVLLLLVASETG

HVYTFATRKLPQMITSETGKALIQTCCLNSPDSPPRSDPTTDQRMSATGFEETDLTYQVSESDSS
 GETKDTLKPAAFTVTNLPGTTSTIQTAPSTSTTMQVSSGSPFPITNYLAPVSASVSPSAVSSANG
 TVLKSTGSGPVSSGGLMQLPTSFTLMPGGAVAQQVPVQAIQVHQAPQQASPSRDSSTDLTQTSS
 SGTVTLPATIMTSSVPTTVGGHMMYPSPHAVMYAPTSGLGDGSLTVLNAFSQAPSTMQVSHSQV
 QEPGGVPQVFLTASSGTVQIPVSAVQLHQMAVIGQQAGSSSNLTELQVVNLDTAHSTKSEGSPG
 LQEFDIKLIDTVDLETME**KRRWKKNFIAVSAANRFKKISSGAL**DYDIPTTAS**ENLYFOG**ELKT
 AAL**AQHDEAVDNKFNKEQQNAFYEILHLPNLNEEQRNAFIQSLKDDPSQSANLLAEAKKLNDQAQ**
APKVDNKFNKEQQNAFYEILHLPNLNEEQRNAFIQSLKDDPSQSANLLAEAKKLNGAQAPKVDA
NSAGKSTGSI*

PROTEIN SEQUENCE ANALYSIS FOR FIGURE 11

Cysteines were highlighted in yellow letters, the number of cysteines was summarized in the end of each sequence.

>gi|6981424|ref|NP_037145.1| **prosaposin** [Rattus norvegicus]
 MYALALLASLLVTALTSPVQDPKI**C**SGGS**A**VV**C**RDV**K**T**A**VD**C**RA**V**K**H****C**Q**M**V**W**S**K**P**T**A**K**S**L**P**C**D**I****C**K**T**V**V**
 TEAGNLLKDNATEEEILHYLEKT**C**AW**I**H**D**S**S**L**S**A**S****C**KE**V**V**D**S**Y**L**P**V**I**L**D**M**I**K**G**E**M**S**N**P**G**E**V****C**S**A**L**N**L**C**Q**S**
 LQEYLAEQNRQLESNKIPEVDLARVVAPFMSNIPLLLYPQDRPRSQPQPKANEDV**C**Q**D****C**M**K**L**V**T**D**I**Q**T**A**
 VRTNSSFVQGLVDHV**K**E**D****C**D**R**L**G**P**G**V**S**D**I****C**K**N**Y**V**D**Q**Y**S**E**V**A**V**Q**M**M**M**H**M**Q**P**K**E**I**C**V**M**V**G**F**C**D**E**V**K**R**V**P**M**R**T**
 LVPATEAIKNILPALELTD**P**Y**E**Q**D**V**I**Q**A**Q**N**V**I**F**C**Q**V****C**Q**L**V**M**R**K**L**S**E**L**I**I**N**N**A**T**E**E**L**L**I**K**G**L**S**K**A**C**S**L**L**P**A
 PAST**K****C**Q**E**V**L**V**T**F**G**P**S**L**L**D**V**L**M**H**E**V**N**P**N**F**L****C**G**V**I**S**L**C**S**A**N**P**N**L**V**G**T**L**E**Q**P**A**A**I**V**S**A**L**P**K**E**P**A**P**P**K**Q**E**E
 P**K**Q**S**A**L**R**A**H**V**P**P**Q**K**N**G**G**F****C**E**V****C**K**K**L**V**I**Y**L**E**H**N**L**E**K**N**S**T**K**E**E**I**L**A**A**L**E**K**G**C**S**F**L**P**D**P**Y**Q**K**Q****C**D**E**F**V**A**E**Y**E**P
 L**L**L**E**I**L**V**E**V**M**D**P**S**F**V**C**S**K**I**G**V**C**P**S**A**Y**K**L**L**L**G**T**E**K****C**V**W**G**P**G**Y****W****C**Q**N**S**E**T**A**A**R****C**N**A**V**D**H**C**K**R**H**V**W**N**
 (32 cysteines)

>gi|194438|gb|AAB59660.1| **immunoglobulin gamma 2A chain** [Mus musculus]
KTTAPSVYPLAPVCGD TTGSSVTLGCLVKGYFPEPVTLTWNSGSLSSGVHTFPAVLQSDLYTLSSSVTVT
SSTWPSQSITCNVAHPASSTKVDKKIEPRGPTIKPCPPCKCPAPNLLGGPSVFIFPPKIKDVLMI SLSP I
VTCVVVDVSEDDPDVQISW FVNNVEVHTAQTQTHREDYNSTLRVVSALPIQH QDWMMSGKEFKCKVNNKDL
PAPIERTISKPKGSVRAPQVYVLPPEEEEMTKKQVTLT CMVTD FMPEDIYVEWTNNGKTELNYKNTEPVL
DSDGSYFMYSKLRVEKKNWVERNSYS CSVVHEGLHNHHTTKSFSRTPGK
(10 cysteines)

>gi|61556986|ref|NP_001013128.1| **transferrin** [Rattus norvegicus]
MRFAVGALLACAALGLCLAVPDKTVKWC AVSEHENTK CISFRDHMKT VLPADGPRLACVKKTSYQDC IKA
ISGGEADAITLDGGWVYDAGLTPNNLKPVA AE FYGSLEHPQTHYLAVAVVKKGTDFQLNQLQGKKSCHTG
LGRSAGWI IPIGLLF CNLPEPRKPLEKAVASFFSGS CVP CADPVAFPQLCQLCPGCGCSPTQ PFFGYVGA
FKCLRDGGGDVAFVKHTTIFEVLPQKADR DQYELLCLDNTRKPV DQYEDCYLARIPSHAVVARNGDGKED
LIWEILKVAQE HFGKGSKDFQLFGSPLGKDLLFKDSAFGLLRVPPRMDYRLYLGH SYVTAIRNQREGVC
PEGSIDSAPVKWCALSHQERAKCDEWSVSSNGQIECESAESTEDCIDKIVNGEADAMSLDGGHAYIAGQC
GLVPVMAENYDISSCTNPQSDVFPKGYAVAVVKASDSSINWNNLKGKKSCHTGVDRTAGWNIPMGLLFS
RINHCKFDEFFSQGCAPGYKKNSTLCDL CIGPAKCAPNNREGYNGYTGAFOCLVEKGDVAFVKHQTVLEN
TNGKNTAAWAKDLKQEDFQLLCPDGTKKPVTEFATCHLAQAPNHVVVSRKEKAARVSTVLTAQKDLFWKG
DKDCTGNFC LFRSSTKDLLFRDDTKCLTKLPEGTTYEYLGAEYLQAVGNIRK CSTSRLLEACTFHKS
(38 cysteines)

>gi|57671|emb|CAA44388.1| **ribonuclease inhibitor** [Rattus norvegicus]
MSLDIQCEQLSDARWTELLPLIQYQVVR LDDCGLTEVRC KDIRSAIQANPALTELSLRTNELGDAGVGL
VLQGLQNPTCKIQKLSLQNC SLTEAGCGVLPDVL RSLSTLRELHLNDNPLGDEGLKLLCEGLRDPQCRLE
KLQLEYCNLTATSC EPLASVLRVKPDFKELVLSNND FHEAGIHTLCQGLKDSACQLES LKLENCGITSAN
CKDLC DVVASKASLQELDLSNKLGN TGIAALCSG LLLPSCRLRTLWLWDCDVTAEGCKDL CRVLRAKQS
LKELSLAGNELKDEGAQLLCE S LLEPGCQLES LWVKTCSLTAASC PHFC SVLTKNSSLFELQ MSSNPLGD
SGVVELCKALGYPDTVLRV LVLWLGCDVTD SGCSSLATVLLANRSLRELDLSN CMGDNGLVQLLES LKQP
SCILQQLVLYDIYWTDEVEDQLRALEEERPSLRIIS

(30 cysteines)

>gi|81170667|sp|Q6IFV1|K1C14_RAT **Keratin, type I** cytoskeletal 14

(Cytokeratin-14) (CK-14) (Keratin-14) (K14) (Type I keratin Ka14)

MATCSRQFTSSSSMKGSCGIGGGSSRMSSVLAGGSCRAPSTYGGMSRFSSAGAYAVGSGYGGGFSSSSFG
GGFGGGIGGGIGGGLGGGIGGGFGGGIGGGFGGGIGSGFGGGLGDGLLVGSEKVTMQLNDRLATYLDKV
RALEEANSLEVKIRDWYQRQRPTTEIKDYSPIFYKTIEDLKSKILAATVDNANVLLQIDNARLAADDFRTK
FETEQLSRINVEDINGLRRVLDDELTLARADLEMQIESLKEELAYLKKNHEEEMASMRGQVGGDVNVEMD
AAPGVDLRILNEMRDQYKMAEKNRKAEDWFFTKTEELNREVATNSELVQSGKSEISELRRTMQLNLEI
ELQSOLSMKASLENNLEETKGRYCMQLAQIQEMIGSVEEQLAQLRCEMEQQNQYKILLDVKTRLEQEI
TYRRLLEGEDAHLSSAQFSSSSQFSSGSQSSRDVTSTNRQIRTKVMDVHDGKVVSTHEQVLRTKN

(5 cysteines)

>gi|81891677|sp|Q6IFV3|K1C15_RAT **Keratin, type I** cytoskeletal 15

(Cytokeratin-15) (CK-15) (Keratin-15) (K15) (Type I keratin Ka15)

MATTFLQTSSTFGSGSTRGGSLRVGGGSGGGSLYGGGSRSSISASSARFVSSGAGVGFGGGMSCGFGGG
FGGGFGGGFGDFGGGDGGLLSGNEKVTMQLNDRLASYLKVRALAEANTELEVKIRDWYQKQSPASPDR
DYSHYFKTMEEIRDKILAATIDNSRVILEIDNARLAADDFRLKYENELALRQVEADINGLRRVLDDELTL
ARTDLEMQIEQLNEELAYLKKNHEEEMKEFSSQLAGQVNVEMDAAPGVDLTRMLAEMREQYEAIAEKRRR
DVEAWFFSKTEELNKEVASNTEMIQTSKTEITDLRRTLQGLEIELOLSMKAGLENSLAEVECRYATQL
QQIQGLITGLETQLSELRCEMEAQNQYENMLLDIKTRLEQEI STYRNLLLEGQDAKMAAIGVREASLRGGS
SGGGSNFHISVEESVDGKVVSSRKRES

(3 cysteines)

>gi|81891678|sp|Q6IFV4|K1C13_RAT **Keratin, type I** cytoskeletal 13

(Cytokeratin-13) (CK-13) (Keratin-13) (K13) (Type I keratin Ka13)

MSCRQFSSMSYGGGFGAGSCQLGGGRNISTCSSRFVTGGSSGGYGGGMSCGFGGGAGGGYGGGFGGGFG
GSCGGGFGGGFGDFGSDGGLLSGNEKITMQLNDRLASYLEKVRALAEANADLEVKIRDWHLKQSPSTP
ERDYSAYYKTIEELRIKILEATTDDNNRIVLEIDNARLAADDFRLKYENELALRQSV EADINGLRRVLDDEL

TLAKTDLEMQIESLNEELAYLKKNHHEEMKEFSNQAVGQVNVEMDATPGIDLTRVLAEMREQYEALAEKN
RRDAEAWFQAKSAELNKEVSSNAAMIQTSKTEITELRRTLQGLEIELOSQLSMKAGLESTLAETECRYAL
OLOQIQALISSIEAQLSELRSEMECONQEYKMLLDIKTRLEQEIATYRSLLEGQDAKMTGFNTGGNSTTT
SNTSTSPSTSGRPDFRKY

(7 cysteines)

>gi|66773802|sp|Q6IG01|K2C1B_RAT **Keratin, type II** cytoskeletal 1b
(Keratin-77) (Type II keratin Kb39)

MSRQFSSQSAFSSRSRRVYSTRSSSGFGGGRQILVSVGQSRRCGGDYGGGFSSRSLYSLGGSKSIFGGLV
GRSASGFCQSRGAGGGFGGGFGGGRSFGGGGFGGGYGGGGRFGGGFGGGFGTNSFGLGGFGPSYPPGGIH
EVTVNQSLLEPLHLEVDPEIQKIKTQEREQIKTLNKNKFAFIDKVRFLQONQVLQTKWELLQOVNTSTR
TSSLEPIFEFFINQLQROVDVLTNEQLRQNSEIRSMQDIVEDYKNKYEDEINKRTNSEDFVVLKQDVDA
AFMAKSDLQSRVDVTLYGEINFLKYLFDTELSQIQTHVSDTNVILSMDNNRSLDLDSIINAVRTQYELIAQ
KSKDEAEALYQTKYQELQITAGKHGDDLKNSKMEISELNRNAQRLQAEIANIKKQIEQMHGSISDAEERG
ERALQDAKQKLQETEEALQOMKEDLARLLRDYQALLGAKLSLDVEIATYRELLEGEESRMSGALQSQVSI
WALPSNEGNDLGERLHDPQSQVPVPKLGC

(3 cysteines)

>gi|81891698|sp|Q6IG00|K2C4_RAT **Keratin, type II** cytoskeletal 4
(Cytokeratin-4) (CK-4) (Keratin-4) (K4) (Type II keratin Kb4)

MISRQSSVRGVSRGFSSGSAVAGGVKRVAFSSASMSGGAGRCSSGGFGSRSLYNLGGHKSISMSVAGSCQ
GGGYGGAGGFGVGGYGAGFGAGGFGGGFGGSFNRRGGPGFPVCPAGGIQEVNTINQSLLTPLQVEIDPEIQ
KIRTAEREQIKTLNKNKFAFIDKVRFLQONKVLETKNWLLQOQTTTTSPRNLDPPFFETYINALRKNLDT
LSNDKGRLOSELKLMQDSVEDFKTKYEEEINKRTAAENDFVVLKQDVDAAYMIKVELEAKMESLKDEINF
MRVLYEAELSQMQTHVSDTSVVLSDNRRNLDLDGIIAEVRAQYEEIARKSKAEVESWYQIKVQQLQMSA
DQHGDSLKSTKNEISELNRMIQIRIRSEIENIKKQTLQASVADAEQRGELALKDAYTKRADLETALQKAKE
DLARLMRDYQELMNVKLALDVEIATYRKLLEGEECRMSGECCKSAVVISVVGGSASIGGSGGIGLGLGSGF
GSGSCSGSGFGGGGIYGSSGKITSSATITKRSRTRQDPDGLQP

(6 cysteines)

>gi|57114290|ref|NP_001008899.1| **type II keratin Kb2** [Rattus norvegicus]

MSCQISCKSRGGGGGGGGFRGFSSGSAVVSGGSRRSTSGFSCLSRHGGGRGGSGGGGFGSQSLVGLGG
YKSISSSVAGYGGGFGGRSYGGFGGGSGFGGSGGFGGGSGFGGGRGFGGGSGFGGGSGFGGGSGFGGGSG
FGGGGFGGGRFGGGPGGFGGPGGFPGGGIHEVSVNQSLLOPLDVKVDPEIQNVKSQEREQIKTLNNKFAS
FIDTVRFLEQONQVLHTKWELLOQLDVGTRTTNLDPVFQAYIGILKKQVDRLTAERNSQDSELNNMODLV
EDFKKYEDEINKRTSAENDFVTIKKDVDS CYMDKTELQAKMEMLTQEVDLRTLTYDELSQLQONVTD
NVILSMDNNRNLDLDSIIAEVQSQYEIIAHKSKAESEELYHSKANEELQVTAVKHGDSLKEIKMEISELN
RTIQRLQGEISHVKKQCKGVQDSIADAEQRGEHAIKDARGKLTDLLEALQOGRENLARLLRDYQELMNVK
LALDVEIATYRKLLLEGEECRMMSGDFSDNVSVSVTSSTISSSVASKAGFGSGGQSSGGRGSYGGGGSTY
GSGGRSSGVRGSGSGSGGGGYSSGGGSRGGSGGGYSTGGGSRGGSSSGGGGYSSGGGSRGDSSSGGGSR
GGSGGSRGGSGGGGYSSGGGSRGGSSSGGAVSGSERGGSGSGEGCGSGVTFSFR

(7 cysteines)

>gi|57012362|ref|NP_001008809.1| **type II keratin Kb35** [Rattus norvegicus]

MSRQLTLYPGAERLGFSGCSAVISGRFSGSHASVRAGVKGAAFGSRSLFCVGGRRLLALSSGGRSGGFTL
GHGGASGGRPGGFVGTVFGSAGLGPTCPSVCPGGIPQVVVNKSLAPLNVELDPEIQKVRQEREQIKA
LNNKFASFIDKVRFLEQONQVLETKWELLOQLDQNNRRSLEPVHESYISNLQKQLEILSGDRVRLDSEL
RNMREVVEDCKKRYEVEINRRTAAENEFVVLKKDVDAAYMNKVELQAKVDSMTDDIKFFKVLFEGEIAQM
QSHISDTSVILSMDNNRQLDLDSILAEVRAQYEEIAVKSKAETENMYQCKIQELQATAGQHGDLDLTKS
EITEINRLIQRIHSEIGNMKKQCSNLETAIADAEQRGDCALKDARAKLDQLEGVLQOSKEELARMLREHQ
ELMNVKLALDMEIATYRKLLLESEESRMAGEYPPSSVSI SVSSTNAGPGGAGFSVGFGASSNYRPLALE
VKTKGSCGSELKPPAKTSASSCVSKKASROTGEVSRADGCATHSPVLFPPVPSQVRKCFLLHH

(12 cysteines)

HUMAN TRANSFERRIN AMINO ACID SEQUENCE (ALIGNED)

>gi|4557871|ref|NP_001054.1| transferrin [Homo sapiens]

Amino Acid Composition: **A61 C40 D45 E42 F28 G52 H19 I15 K58 L65 M10 N34 P32 Q17 R27 S41
T30 V48 W8 Y26**

```
1   MRLAVGALLV  CAVLGLCLAV  PDKTVRWCAV  SEHEATKCQS  FRDHMKSVIP  SDGPSVACVK
61  KASYLDCIRA  IAANEADAVT  LDAGLVYDAY  LAPNNLKPVV  AEFYGSKEDP  QTFYYAVAVV
121 KKDSGFQMNQ  LRGKKSCHTG  LGRSAGWNIP  IGLLYCDLPE  PRKPLEKAVA  NFFSGSCAPC
181 ADGTDFPQLC  QLCPGCGCST  LNQYFGYSGA  FKCLKDGAGD  VAFVKHSTIF  ENLANKADRD
241 QYELLCLDNT  RKPVDEYKDC  HLAQVPSHTV  VARSMGGKED  LIWELLNQAQ  EHFGKDKSKE
301 FQLFSSPHGK  DLLFKDSAHG  FLKVPPRMDA  KMYLGYEYVT  AIRNLREGTC  PEAPTDECKP
361 VKWCALSHHE  RLKCDWSVN  SVGKIECVSA  ETTEDCIAKI  MNGEADAMSL  DGGFVYIAGK
421 CGLVPVLAEN  YNKSDNCEDT  PEAGYFAVAV  VKKSASDLTW  DNLKGKKSCH  TAVGRTAGWN
481 IPMGLLYNKI  NHCRFDEFFS  EGCAPGSKKD  SSLCKLCMGS  GLNLCEPNNK  EGYGYTGAF
541 RCLVEKGDVA  FVKHQVTPQN  TGGKNPDPWA  KNLNEKDYEL  LCLDGTRKPV  EELYANCHLAR
601 APNHAVVTRK  DKEACVHKIL  RQQOHLFGSN  VTDCSGNFCL  FRSETKDLLF  RDDTVCLAKL
641 HDRNTYEKYL  GEEYVKAAGN  LRCSTSSLL  EACTFRRP
```

MASCOT SEARCHING RESULT FOR TOP 10 MATCHED PROTEINS AND THEIR PEPTIDE (FIGURE 17 SAMPLE A)

Spot Idx/Pos	89/D2	Instr./Spot Origin	upitlab4700/121304_4220_AE	Process Status	Analysis Succeeded
Plate [a] Name	[1] 000300004220	4700 Sample Name		Spectra	1

Rank	Protein Name	Accession No.	Protein MW	Protein PI	Protein Score	Protein C. I. %
1	ferroxidase (EC 1.16.3.1) precursor - rat	gi 92233	120587.9	5.39	68	99.556
	Peptide Information					
	Calc. Mass	Obsv. Mass	± da ± ppm	Start Seq.	End Seq.	Sequence Modification
	1136.621	1136.6128	-0.0082 -7	345	354	AGLQAFFQVR
	1205.6313	1205.6254	-0.0059 -5	850	858	TYIWQIPER
	1495.6951	1495.7428	0.0477 32	70	82	ALYSEYTDGTFTK
	1496.8259	1496.8302	0.0043 3	149	160	LFPGQQLYVLR
	1541.723	1541.7079	-0.0151 -10	714	726	GQFEDVTLYGGER
	1813.8966	1813.9005	0.0039 2	43	57	ELISVDTEQSNFYLR
	1911.0017	1910.9124	-0.0893 -47	820	836	NMATRPYSIIAHGVKTK
	2009.9093	2009.9078	-0.0015 -1	355	371	DCNKPSDDIQDRHVR
	2048.96	2048.9866	0.0266 13	727	743	TYIIAAVEVEWDYSPSR
	2155.1592	2155.1648	0.0056 3	816	834	VVFKNMATRPYSIIAHGVK
	2225.2036	2225.1357	-0.0679 -31	793	813	RAEEELGLGLIHADVGAK
	3461.6106	3461.6196	0.009 3	850	879	TYIWQIPERSGAGTEDSPCIFWAYYSTVDR
2	ceruloplasmin; Ceruloplasmin (ferroxidase) [Rattus norvegicus]	gi 6978695	120763.8	5.34	58	95.758
	Peptide Information					
	Calc. Mass	Obsv. Mass	± da ± ppm	Start Seq.	End Seq.	Sequence Modification
	1136.621	1136.6128	-0.0082 -7	345	354	AGLQAFFQVR
	1205.6313	1205.6254	-0.0059 -5	850	858	TYIWQIPER
	1495.6951	1495.7428	0.0477 32	70	82	ALYSEYTDGTFTK
	1496.8259	1496.8302	0.0043 3	149	160	LFPGQQLYVLR
	1541.723	1541.7079	-0.0151 -10	714	726	GQFEDVTLYGGER
	1813.8966	1813.9005	0.0039 2	43	57	ELISVDTEQSNFYLR
	1911.0017	1910.9124	-0.0893 -47	820	836	NMATRPYSIIAHGVKTK
	2009.9093	2009.9078	-0.0015 -1	355	371	DCNKPSDDIQDRHVR
	2048.96	2048.9866	0.0266 13	727	743	TYIIAAVEVEWDYSPSR
	2155.1592	2155.1648	0.0056 3	816	834	VVFKNMATRPYSIIAHGVK
	3461.6106	3461.6196	0.009 3	850	879	TYIWQIPERSGAGTEDSPCIFWAYYSTVDR
3	hypothetical protein XP_212966 [Rattus norvegicus]	gi 27703552	82866.9	5.2	46	21.007
	Peptide Information					
	Calc. Mass	Obsv. Mass	± da ± ppm	Start Seq.	End Seq.	Sequence Modification
	983.4614	983.4533	-0.0081 -8	338	345	DMSAKFER
	1136.5847	1136.6128	0.0281 25	296	304	GSRFWIQDK
	1312.7695	1312.7566	-0.0129 -10	612	623	SVGKPALERSLR

	1519.8478	1519.9202	0.0724	48	406	420	NVSLGNVLAVAYATK		
	2211.042	2211.092	0.05	23	1	20	MADTQYILPNDIGVSSLDGR		
	2240.0837	2240.1497	0.066	29	142	159	SLWQTCGELMFLSLEPLRL	1 Carboxymethyl (C),1 Oxidation (M)	
	2300.1267	2300.1973	0.0706	31	639	659	ALYEGYAAVTDAPPECFLTLR		
	2788.2915	2788.4116	0.1201	43	1	24	MADTQYILPNDIGVSSLDGCREAFR	1 Carboxymethyl (C),1 Oxidation (M)	
4	hypothetical protein XP_215541 [Rattus norvegicus]				g 34855491	120588.9	5.39	43	0

Peptide Information

Calc. Mass	Obsv. Mass	\pm da	\pm ppm	Start Seq.	End Seq.	Sequence	Modification
1136.621	1136.6128	-0.0082	-7	345	354	AGLQAFFQVR	
1205.6313	1205.6254	-0.0059	-5	850	858	TYWQIPER	
1495.6951	1495.7428	0.0477	32	70	82	ALYSEYTDGTFK	
1496.8259	1496.8302	0.0043	3	149	160	LFPGQQLYVLR	
1541.723	1541.7079	-0.0151	-10	714	726	GQFEDVTLYGGER	
1813.8966	1813.9005	0.0039	2	43	57	ELISVTEQSNFYLR	
2009.9093	2009.9078	-0.0015	-1	355	371	DCNKPSPODDIQDRHVR	
2048.96	2048.9866	0.0266	13	727	743	TYIIAAVEVEWDYSPSR	
3461.6106	3461.6196	0.009	3	850	879	TYWQIPERSGAGTEDSPCIPWAYYSTVDR	

5	GPI-anchored ceruloplasmin [Rattus norvegicus]				g 6970046	123670.4	5.39	43	0
---	--	--	--	--	-----------	----------	------	----	---

Peptide Information

Calc. Mass	Obsv. Mass	\pm da	\pm ppm	Start Seq.	End Seq.	Sequence	Modification
1136.621	1136.6128	-0.0082	-7	345	354	AGLQAFFQVR	
1205.6313	1205.6254	-0.0059	-5	850	858	TYWQIPER	
1495.6951	1495.7428	0.0477	32	70	82	ALYSEYTDGTFK	
1496.8259	1496.8302	0.0043	3	149	160	LFPGQQLYVLR	
1541.723	1541.7079	-0.0151	-10	714	726	GQFEDVTLYGGER	
1813.8966	1813.9005	0.0039	2	43	57	ELISVTEQSNFYLR	
2009.9093	2009.9078	-0.0015	-1	355	371	DCNKPSPODDIQDRHVR	
2048.96	2048.9866	0.0266	13	727	743	TYIIAAVEVEWDYSPSR	
3461.6106	3461.6196	0.009	3	850	879	TYWQIPERSGAGTEDSPCIPWAYYSTVDR	

6	Ab1-042 [Rattus norvegicus]				g 33086446	30831.5	10.22	38	0
---	-----------------------------	--	--	--	------------	---------	-------	----	---

Peptide Information

Calc. Mass	Obsv. Mass	\pm da	\pm ppm	Start Seq.	End Seq.	Sequence	Modification
2332.1714	2332.2583	0.0869	37	220	241	ANPPSSKNPKPTPTTPOGQNPQK	

7	dipeptidylpeptidase III [Rattus norvegicus]				g 16758578	82986.9	5.12	38	0
---	---	--	--	--	------------	---------	------	----	---

Peptide Information

Calc. Mass	Obsv. Mass	\pm da	\pm ppm	Start Seq.	End Seq.	Sequence	Modification
983.4614	983.4533	-0.0081	-8	338	345	DMSAKFER	
1136.5847	1136.6128	0.0281	25	296	304	GSRFWQDK	
1519.8478	1519.9202	0.0724	48	406	420	NVSLGNVLAVAYATK	

	2211.042	2211.092	0.05	23	1	20	MADTQYILPNDIGVSSLDCR	
	2240.0837	2240.1497	0.066	29	142	159	SLWQTCGELMFSLEPRLR	1 Carboxymethyl (C), 1 Oxidation (M)
	2300.1267	2300.1973	0.0706	31	639	659	ALYEGYAAVTDAPPECFLTLR	
	2788.2915	2788.4116	0.1201	43	1	24	MADTQYILPNDIGVSSLDCEAFR	1 Carboxymethyl (C), 1 Oxidation (M)

8 similar to RIKEN cDNA 150002O20 [Rattus norvegicus] g|34855454 68303.9 7.25 32 0

Peptide Information

Calc. Mass	Obsv. Mass	\pm da	\pm ppm	Start Seq.	End Seq.	Sequence	Modification
983.4792	983.4533	-0.0259	-26	613	621	SSALAEYSR	
1762.8811	1762.9286	0.0475	27	598	611	NWFHYAARIWDGVK	
1769.8452	1769.9084	0.0632	36	363	378	GGNQTSGIDFFITQER	
1813.9303	1813.9005	-0.0298	-16	159	173	EGQRPTQPVYQIQNR	
1923.8787	1923.9473	0.0686	36	239	255	SMVMSLLSANTPEEDQR	1 Oxidation (M)
2128.0894	2128.1086	0.0192	9	156	173	GEKEGQRPTQPVYQIQNR	
2284.1147	2284.1831	0.0684	30	490	507	QMHLMIDQLMAHSHLRYK	2 Oxidation (M)
2300.1096	2300.1973	0.0877	38	490	507	QMHLMIDQLMAHSHLRYK	3 Oxidation (M)

9 cysteine proteinase (EC 3.4.22.-) P32 - rat (fragment) g|2143675 23935.7 6.58 32 0

Peptide Information

Calc. Mass	Obsv. Mass	\pm da	\pm ppm	Start Seq.	End Seq.	Sequence	Modification
1769.827	1769.9084	0.0814	46	10	24	MDYPEMGLCIINNK	1 Oxidation (M)
2009.9518	2009.9078	-0.044	-22	60	76	NDLTREEIMELMDSVSK	
2211.1089	2211.092	-0.0169	-8	182	200	GGSWFIQSLCAMLKLYAHK	1 Carboxymethyl (C)
2846.4504	2846.4395	-0.0109	-4	82	108	RSSFVCVILSHGDEGVIFGTNGPVD LK	

10 keratin 14 [Rattus norvegicus] g|2443314 25667.9 4.67 30 0

Peptide Information

Calc. Mass	Obsv. Mass	\pm da	\pm ppm	Start Seq.	End Seq.	Sequence	Modification
1496.7638	1496.8302	0.0664	44	173	184	NHEEEMLALRVR	
1910.964	1910.9124	-0.0516	-27	38	53	VTMQNLNDRLATYLDK	1 Oxidation (M)
2239.2405	2239.1758	-0.0647	-29	95	115	SKILAAATVDNANVLLQIDNAR	
2240.1365	2240.1497	0.0132	6	154	172	ADLEMQIESLTELAYLKK	1 Oxidation (M)

MASCOT SEARCHING RESULT FOR TOP 10 MATCHED PROTEINS AND THEIR PEPTIDE (FIGURE 17 SAMPLE B)

Spot Idx/Poe	120/E16	Instr/Spot Origin	upittabi4700/121304_4220_AE	Process Status	Analysis Succeeded
Plate [#] Name	[1] 000300004220	4700 Sample Name		Spectra	1

Rank	Protein Name	Accession No.	Protein MW	Protein PI	Protein Score	Protein C. I. %
1	myosin IE; Unconventional myosin from rat 5; myosin I e [Rattus norvegicus]	gi 27465533	126747	9.14	53	85.953

Peptide Information

Calc. Mass	Obsv. Mass	± da ± ppm	Start Seq.	End Seq.	Sequence	Modification
1431.6763	1431.655	-0.0213 -15	883	895	KENWGPWSAGGSR	
1575.7808	1575.8414	0.0606 38	953	967	AAPAPPGCHRNLTR	1 Carboxymethyl (C)
1994.0017	1993.9908	-0.0109 -5	208	224	SFHFYQLIEGASPEQK	
2090.052	2089.9873	-0.0647 -31	568	585	QANDLVSTLMKCTPHYIR	
2090.9307	2090.9756	0.0449 21	934	952	NTVSSRGYSGGTNNNYPMR	1 Oxidation (M)
2370.1685	2370.2288	0.0603 25	435	453	WTPIEYFNKIVCDLIESK	1 Carboxymethyl (C)
2485.2358	2485.2441	0.0083 3	43	63	YMDDYIFTYIGSVLISVNPFFK	
2501.2307	2501.3088	0.0781 31	43	63	YMDDYIFTYIGSVLISVNPFFK	1 Oxidation (M)
2505.2241	2506.1104	-0.1137 -45	336	357	SESIHVTLNVEQACYTRDALAK	1 Carboxymethyl (C)
2743.2998	2743.2764	-0.0234 -9	423	444	AEQEYVQEGIRWTPIEYFNK	
3051.4626	3051.4756	0.013 4	735	760	NSINRNFIDYIGMEEHPELQQFVVK	1 Oxidation (M)
3281.585	3281.4265	-0.1585 -48	454	484	VNPPGMSLDDVCMTHAVGEGADQTLLQK	1 Carboxymethyl (C)

2	similar to NIPSNAP-related protein [Rattus norvegicus]	gi 34868393	72950	9.28	39	0
---	--	-------------	-------	------	----	---

Peptide Information

Calc. Mass	Obsv. Mass	± da ± ppm	Start Seq.	End Seq.	Sequence	Modification
1210.6215	1210.6726	0.0511 42	452	461	TNAFLQNFQK	
1613.8025	1613.7938	-0.0087 -5	394	408	CSAAVYLGSTMALR	1 Carboxymethyl (C)
2172.054	2172.0813	0.0273 13	89	110	HARPPKQPEEDAGPAGSGASGR	
3051.5283	3051.4756	-0.0527 -17	542	569	TPPKEGVYELATFQMKPGGFALWGDQFK	1 Oxidation (M)
3177.436	3177.5464	0.1104 35	95	127	QPEEDAGPAGSGASGRAPQGHVQESGQSCVGR	
3279.5781	3279.4978	-0.0803 -24	133	161	FSPCQCLRLALVGLSVQVCPSEFATDHR	2 Carboxymethyl (C)
3662.7068	3662.6875	-0.0193 -5	511	539	EWQEQFLISLAFMDEQEVEITYLVFWCK	1 Carboxymethyl (C), 1 Oxidation (M)

3	hypothetical protein XP_233949 [Rattus norvegicus]	gi 27716841	68787.6	9.78	36	0
---	--	-------------	---------	------	----	---

Peptide Information

Calc. Mass	Obsv. Mass	± da ± ppm	Start Seq.	End Seq.	Sequence	Modification
1210.6538	1210.6726	0.0188 16	133	142	EIEKAQLHSR	
1431.6824	1431.655	-0.0274 -19	251	262	EWPEPESVSLMK	
2090.0884	2089.9873	-0.1011 -48	286	303	TKPSPLCECLFQKQALR	
2240.1453	2240.1094	-0.0359 -16	280	298	ENYIVKTKPSFLCECLFQK	
2588.2527	2588.2432	-0.0095 -4	502	524	TQEGWRWFAQQAQPASSELPGDK	

3281.5486	3281.4265	-0.1221	-37	218	248	AIADMFPSAGGILLMLADTKSSNCNE HFSVEK	2 Oxidation (M)
3766.0378	3766.0486	0.0108	3	538	572	ALFWGAGVSIWISGPSTAPVHFTHL QKFPVKPSPR	

4 similar to RIKEN cDNA 4933405K07 [Rattus norvegicus] g|34856160 84091.2 7.51 34 0

Peptide Information

Calc. Mass	Obsv. Mass	± da ± ppm	Start Seq.	End Seq.	Sequence	Modification
2184.9834	2184.9492	-0.0342 -16	666	685	IHTGERPYVCSDCGKAMSSK	1 Oxidation (M)
2225.1343	2225.1243	-0.01 -4	50	68	CLYQEVMLEIYSHLLAVGK	1 Oxidation (M)
2284.0483	2284.1157	0.0674 30	526	545	IHTGERPYVCSDCGKAFSGK	1 Carboxymethyl (C)
2300.0586	2300.1594	0.1008 44	502	521	QKPYTCHDCGKSFYASHLK	
2506.1667	2506.1104	-0.0563 -22	237	258	VFTGQSEHDSPPQICVTTAFPR	1 Carboxymethyl (C)
3250.5005	3250.5552	0.0547 17	484	512	SLTTSPPSLQAHHEAHTKQKPYTC HDCGK	1 Carboxymethyl (C)
3400.4766	3400.5847	0.1081 32	426	455	AFTAGSASCEQQTNTLDLETHFIC HICGK	3 Carboxymethyl (C)
3887.8037	3887.8811	0.0774 20	426	460	AFTAGSASCEQQTNTLDLETHFIC HICGKSLQK	1 Carboxymethyl (C)

5 similar to MLLT6 [Rattus norvegicus] g|34873505 71496.5 9.5 34 0

Peptide Information

Calc. Mass	Obsv. Mass	± da ± ppm	Start Seq.	End Seq.	Sequence	Modification
1371.8206	1371.7705	-0.0501 -37	328	339	LQEQLSLTAKK	
1575.7682	1575.8414	0.0732 46	302	316	QGDGEAGVNVIVEMLK	1 Oxidation (M)
2211.0425	2211.1033	0.0608 27	15	37	APSPGOYKSPHVSGSGTSAGSHK	
2240.061	2240.1094	0.0484 22	620	640	ACVDLGGVVPVPGAEERDDR	1 Carboxymethyl (C)
2284.1741	2284.1157	-0.0584 -26	39	60	MPALSATLGPAAEAPETTLKEK	
2300.1689	2300.1594	-0.0095 -4	39	60	MPALSATLGPAAEAPETTLKEK	1 Oxidation (M)
2506.0457	2506.1104	0.0647 26	393	415	NCLGLDNTLSTSSSEDPHSGCPSR	2 Carboxymethyl (C)

6 similar to Ser/Arg-related nuclear matrix protein; plenty-of-prolines-101; serine/arginine repeat g|34872074 107125.3 11.72 32 0

Peptide Information

Calc. Mass	Obsv. Mass	± da ± ppm	Start Seq.	End Seq.	Sequence	Modification
1575.7972	1575.8414	0.0442 28	800	815	VSSRSVSGSPEPTAK	
2588.2832	2588.2432	-0.04 -15	283	305	GDEEILSQLDLVPMGCLVNDILK	1 Carboxymethyl (C), 1 Oxidation (M)
3652.7961	3662.6875	-0.1086 -30	272	305	ALSTDCLTGGRGDEEILSQLDLVPM GCLVNDILK	1 Carboxymethyl (C), 1 Oxidation (M)

7 similar to retinol dehydrogenase 12 (all-trans and 9-cis); retinol dehydrogenase 12 [Rattus norvegicus] g|34866247 33919.7 9.57 31 0

Peptide Information

Calc. Mass	Obsv. Mass	± da ± ppm	Start Seq.	End Seq.	Sequence	Modification
1993.9543	1993.9908	0.0365 18	107	123	LHILINNAGVMMCPYSK	1 Carboxymethyl (C), 2 Oxidation (M)
2090.0596	2089.9873	-0.0723 -35	106	123	KLHILINNAGVMMCPYSK	1 Carboxymethyl (C)
2172.1284	2172.0813	-0.0471 -22	228	244	HSFLMCLLWRLFSPFFK	

2300.2065 2300.1594 -0.0471 -20 206 227 LQGTGVTAYVVHFGCVLSEIR
 3281.5242 3281.4265 -0.0977 -30 245 274 SPVQGAQTSLHCALEEGLEPLSGK
 YFSDCK

8 similar to KIAA1096 protein [Rattus norvegicus] g|34880805 262529.1 9.28 30 0

Peptide Information

Calc. Mass	Obsv. Mass	\pm da	\pm ppm	Start Seq.	End Seq.	Sequence	Modification
1670.8352	1670.8156	-0.0196	-12	2141	2157	GLIPAGTQHGMATTGK	
2256.0737	2256.1685	0.0948	42	2183	2204	STTPTSSPFRATSTSPNSQSSK	
2370.1733	2370.2288	0.0555	23	257	277	MAYPPLHGPMPFPPLSETNK	
2485.2681	2485.2441	-0.024	-10	1490	1513	QPPPSIRLPSAQTSNGTDYVATGK	
2561.2036	2561.2876	0.0842	33	2342	2365	AQKVDSDTSKPELSDPPGTCQEK	
2588.321	2588.2432	-0.0778	-30	2158	2182	MSEMELKAFGSGIDIKPGTPPIGGR	
3887.791	3887.8811	0.0901	23	1722	1757	ESVTDYTPSSSLPNTVATNNAKME DTLVNAMESAR	

9 similar to Nck-associated protein 5 (NAP-5) [Rattus norvegicus] g|34879498 163527.1 9.16 29 0

Peptide Information

Calc. Mass	Obsv. Mass	\pm da	\pm ppm	Start Seq.	End Seq.	Sequence	Modification
1613.7476	1613.7938	0.0462	29	380	393	GKEECPTHLETSPK	1 Carboxymethyl (C)
1670.8972	1670.8156	-0.0816	-49	519	533	LVKPTQGVVAWQSNR	
2240.124	2240.1094	-0.0146	-7	55	76	SGAPALKHSGSGVVIPDHPCPR	1 Carboxymethyl (C)
2300.2166	2300.1594	-0.0572	-25	717	739	SPVLKSGSAPLVSSSPAMSEIQK	
2501.3027	2501.3088	0.0061	2	722	746	GSSAPLVSSSPAMSEIQKPKSVASR	
2588.1755	2588.2432	0.0677	26	590	613	LSQCTNAESPGTFCDOVQFESHIPK	
3281.3481	3281.4265	0.0784	24	77	106	NSCSGSELSLSTCSEYSSGSSY TWQDRK	1 Carboxymethyl (C)
3662.6353	3662.6875	0.0522	14	206	237	GIPCQNLHQTFNYDANSHEYAHEE FLSSASPR	

10 similar to ankyrin 2 Isoform 1; ankyrin-2, nonerythrocytic; ankyrin-B; ankyrin, brain; ankyrin, neu g|34859979 295891.6 4.71 29 0

Peptide Information

Calc. Mass	Obsv. Mass	\pm da	\pm ppm	Start Seq.	End Seq.	Sequence	Modification
1210.6174	1210.6726	0.0552	46	474	485	QAPGSATGKHEK	
2091.0618	2090.9756	-0.0862	-41	392	411	HSPVFSGKPEKHSPGSPSTK	
2284.0938	2284.1157	0.0219	10	263	284	GSSEESVDEDRGLAPEPLTAK	
2370.1533	2370.2288	0.0755	32	1	20	MFFIHKDOETESTETSVLK	
2743.2437	2743.2764	0.0327	12	704	729	QVIAGSGPCGSLMEGTPQISSEESY K	1 Oxidation (M)
3400.5583	3400.5847	0.0264	8	2337	2367	LDGDAAFQKELTEELGELEASSDEE AMVTTR	1 Oxidation (M)
3805.5229	3805.3616	-0.1613	-42	1457	1491	SSPEDVIMTSSSRRTDSGEASNCE GHOLDTECEGK	1 Carboxymethyl (C), 1 Oxidation (M)
3885.6953	3885.7385	0.0432	11	2181	2215	EQEASKSESSDHPPMVSEEDIIV GYSTFQDCIPK	
3888.0461	3887.8811	-0.165	-42	1492	1528	SALWPMQSDPEPLSVAPTPNAPV VTGEQVSKVIITK	

ABBREVIATION

AD	Activation domain
AEBSF	4-(2-Aminoethyl)benzenesulfonyl fluoride hydrochloride
ANF	Atrial natriuretic factor
ATP	Adenosine triphosphate
BBB	Blood brain barrier
BCA assay	Bicinchoninic acid assay
BD	Binding domain
Biotin-HPDP	<i>N</i> -[6-(Biotinamido)hexyl]-3'-(2'-pyridyldithio)propionamide
BSA	Bovine serum albumin
CBP	Calmodulin binding peptide
CHAPS	3-([3-Cholamidopropyl]dimethylammino)-1-propanesulfonate
CHCA	alpha-Cyano-4-hydroxycinnamic acid
CM-DiI	1,1'-Dioctadecyl-3,3',3',3'-tetramethylindocarbocyanine I
CREB	cAMP response element binding protein
DiGE	Differential gel electrophoresis
DMF	Dimethylformamide
DMSO	Dimethylsulfoxide
DOD	Department of Defense
DTT	Dithiothreitol
ECD	Electron capture dissociation
EDT	Ethyldithiol
EDTA	Ethylenediaminetetra acetic acid
eNOS	Epithelial nitric oxide synthase
ESI	Electrospray ionization
FBS	Fetal bovine serum
FT	Fourier transform
GPDH	Glycerol 3-phosphate dehydrogenase
GPx	Glutathione peroxidase
GSH	Reduced monomeric glutathione
GSSG	Glutathione disulphide
HAMLET	Human alpha-lactalbumin made lethal to tumor
HAS	Human serum albumin
HDL	High-density lipoproteins

HEPES	4-(2-Hydroxyethyl)-1-piperazineethanesulfonic acid
HGF	Hepatocyte growth factor
ICR	Ion cyclotron resonance
IEP	Immuno-electrophoresis
IFE	Immunofixation electrophoresis
iNOS	Inducible nitric oxide synthase
IVH	Intraventricular hemorrhage
LDL	Low-density lipoproteins
LPL	Lipoprotein lipase
MALDI	Matrix-assisted laser desorption ionization
MIT	Massachusetts Institute of Technology
MMTS	Methyl methanethiosulfonate
MnSOD	Manganese superoxide dismutase
MS	Mass Spectrometry
NAD+	Nicotinamide adenine dinucleotide
NADH	Reduced Nicotinamide adenine dinucleotide
NADPH	Reduced nicotinamide adenine dinucleotide phosphate
NCBI	National Center for Biotechnology Information
NIH	National Institutes of Health
nNOS	Neuronal nitric oxide synthase
NO	Nitric oxide
NOC7	3-(2-Hydroxy-1-methyl-2-nitroso-hydrazino)- <i>N</i> -methyl-1-propanamine
NOS	Nitric oxide synthase
PDB	Protein databank
Pg	Plasminogen
PhIAT	Phosphopeptide isotope affinity tag
Pm	Plasmin
PMF	Peptide mass spec fingerprinting
PMSF	Phenylmethylsulphonyl fluoride
PPH	Postpartum hemorrhage
PTM	Post-translational modification
PVDF	Polyvinylidene fluoride
QSAR	Quantitative structure-activity relationship
SBP	Streptavidin binding protein
SDS-PAGE	Sodium dodecyl sulfate-polyacrylamide gel electrophoresis
SIN-1	3-Morpholinopyrrolidine
SRF	Serum response factor
TAP	Tandem affinity-tag purification
TCEP	Tris-(2-carboxyethyl)phosphine
TCF	Tertiary complex factor
TEV	Tobacco etch virus
TFA	Trifluoroacetic acid
TOF	Time of flight

tPA	Tissue-type plasminogen activator
TSH	Thyroid-stimulating hormone
TTR	Transthyretin
uPA	Urokinase plasminogen activator
UPE	Urinary protein electrophoresis

BIBLIOGRAPHY

1. Alberts, B., A. Johnson, J. Lewis, M. Raff, K. Roberts, and P. Walter, *Molecular Biology of the Cell*. 6th ed, ed. S. Gibbs. 2002, New York, NY: Garland Science, a member of the Taylor & Francis Group, 29 West 35th Street, New York, NY 10001-2299.
2. Creighton, T., *Proteins: Structure and molecular properties*. 1993, New York: Freeman.
3. Anderson, N.L. and N.G. Anderson, *Proteome and proteomics: new technologies, new concepts, and new words*. *Electrophoresis*, 1998. **19**(11): p. 1853-61.
4. Humphery-Smith, I., S.J. Cordwell and W.P. Blackstock, *Proteome research: complementarity and limitations with respect to the RNA and DNA worlds*. *Electrophoresis*, 1997. **18**(8): p. 1217-42.
5. Larsen, M.R. and P. Roepstorff, *Mass spectrometric identification of proteins and characterization of their post-translational modifications in proteome analysis*. *Fresenius J Anal Chem*, 2000. **366**(6-7): p. 677-90.
6. Nyman, T.A., *The role of mass spectrometry in proteome studies*. *Biomol Eng*, 2001. **18**(5): p. 221-7.
7. Patton, W.F., *Proteome analysis. II. Protein subcellular redistribution: linking physiology to genomics via the proteome and separation technologies involved*. *J Chromatogr B Biomed Sci Appl*, 1999. **722**(1-2): p. 203-23.
8. Jensen, O.N., *Modification-specific proteomics: characterization of post-translational modifications by mass spectrometry*. *Curr Opin Chem Biol*, 2004. **8**(1): p. 33-41.
9. Dwek, M.V., H.A. Ross and A.J. Leatham, *Proteome and glycosylation mapping identifies post-translational modifications associated with aggressive breast cancer*. *Proteomics*, 2001. **1**(6): p. 756-62.

10. Ficarro, S.B., M.L. McClelland, P.T. Stukenberg, D.J. Burke, M.M. Ross, J. Shabanowitz, D.F. Hunt, and F.M. White, *Phosphoproteome analysis by mass spectrometry and its application to Saccharomyces cerevisiae*. Nat Biotechnol, 2002. **20**(3): p. 301-5.
11. Ficarro, S., O. Chertihin, V.A. Westbrook, F. White, F. Jayes, P. Kalab, J.A. Marto, J. Shabanowitz, J.C. Herr, D.F. Hunt, and P.E. Visconti, *Phosphoproteome analysis of capacitated human sperm. Evidence of tyrosine phosphorylation of a kinase-anchoring protein 3 and valosin-containing protein/p97 during capacitation*. J Biol Chem, 2003. **278**(13): p. 11579-89.
12. Ptacek, J., G. Devgan, G. Michaud, H. Zhu, X. Zhu, J. Fasolo, H. Guo, G. Jona, A. Breitkreutz, R. Sopko, R.R. McCartney, M.C. Schmidt, N. Rachidi, S.J. Lee, A.S. Mah, L. Meng, M.J. Stark, D.F. Stern, C. De Virgilio, M. Tyers, B. Andrews, M. Gerstein, B. Schweitzer, P.F. Predki, and M. Snyder, *Global analysis of protein phosphorylation in yeast*. Nature, 2005. **438**(7068): p. 679-84.
13. Venter, J.C., M.D. Adams, E.W. Myers, P.W. Li, R.J. Mural, G.G. Sutton, H.O. Smith, M. Yandell, C.A. Evans, R.A. Holt, J.D. Gocayne, P. Amanatides, R.M. Ballew, D.H. Huson, J.R. Wortman, Q. Zhang, C.D. Kodira, X.H. Zheng, L. Chen, M. Skupski, G. Subramanian, P.D. Thomas, J. Zhang, G.L. Gabor Miklos, C. Nelson, S. Broder, A.G. Clark, J. Nadeau, V.A. McKusick, N. Zinder, A.J. Levine, R.J. Roberts, M. Simon, C. Slayman, M. Hunkapiller, R. Bolanos, A. Delcher, I. Dew, D. Fasulo, M. Flanigan, L. Florea, A. Halpern, S. Hannenhalli, S. Kravitz, S. Levy, C. Mobarry, K. Reinert, K. Remington, J. Abu-Threideh, E. Beasley, K. Biddick, V. Bonazzi, R. Brandon, M. Cargill, I. Chandramouliswaran, R. Charlab, K. Chaturvedi, Z. Deng, V. Di Francesco, P. Dunn, K. Eilbeck, C. Evangelista, A.E. Gabrielian, W. Gan, W. Ge, F. Gong, Z. Gu, P. Guan, T.J. Heiman, M.E. Higgins, R.R. Ji, Z. Ke, K.A. Ketchum, Z. Lai, Y. Lei, Z. Li, J. Li, Y. Liang, X. Lin, F. Lu, G.V. Merkulov, N. Milshina, H.M. Moore, A.K. Naik, V.A. Narayan, B. Neelam, D. Nusskern, D.B. Rusch, S. Salzberg, W. Shao, B. Shue, J. Sun, Z. Wang, A. Wang, X. Wang, J. Wang, M. Wei, R. Wides, C. Xiao, C. Yan, A. Yao, J. Ye, M. Zhan, W. Zhang, H. Zhang, Q. Zhao, L. Zheng, F. Zhong, W. Zhong, S. Zhu, S. Zhao, D. Gilbert, S. Baumhueter, G. Spier, C. Carter, A. Cravchik, T. Woodage, F. Ali, H. An, A. Awe, D. Baldwin, H. Baden, M. Barnstead, I. Barrow, K. Beeson, D. Busam, A. Carver, A. Center, M.L. Cheng, L. Curry, S. Danaher, L. Davenport, R. Desilets, S.

- Dietz, K. Dodson, L. Doup, S. Ferriera, N. Garg, A. Gluecksmann, B. Hart, J. Haynes, C. Haynes, C. Heiner, S. Hladun, D. Hostin, J. Houck, T. Howland, C. Ibegwam, J. Johnson, F. Kalush, L. Kline, S. Koduru, A. Love, F. Mann, D. May, S. McCawley, T. McIntosh, I. McMullen, M. Moy, L. Moy, B. Murphy, K. Nelson, C. Pfannkoch, E. Pratts, V. Puri, H. Qureshi, M. Reardon, R. Rodriguez, Y.H. Rogers, D. Romblad, B. Ruhfel, R. Scott, C. Sitter, M. Smallwood, E. Stewart, R. Strong, E. Suh, R. Thomas, N.N. Tint, S. Tse, C. Vech, G. Wang, J. Wetter, S. Williams, M. Williams, S. Windsor, E. Winn-Deen, K. Wolfe, J. Zaveri, K. Zaveri, J.F. Abril, R. Guigo, M.J. Campbell, K.V. Sjolander, B. Karlak, A. Kejariwal, H. Mi, B. Lazareva, T. Hatton, A. Narechania, K. Diemer, A. Muruganujan, N. Guo, S. Sato, V. Bafna, S. Istrail, R. Lippert, R. Schwartz, B. Walenz, S. Yooseph, D. Allen, A. Basu, J. Baxendale, L. Blick, M. Caminha, J. Carnes-Stine, P. Caulk, Y.H. Chiang, M. Coyne, C. Dahlke, A. Mays, M. Dombroski, M. Donnelly, D. Ely, S. Esparham, C. Fosler, H. Gire, S. Glanowski, K. Glasser, A. Glodek, M. Gorokhov, K. Graham, B. Gropman, M. Harris, J. Heil, S. Henderson, J. Hoover, D. Jennings, C. Jordan, J. Jordan, J. Kasha, L. Kagan, C. Kraft, A. Levitsky, M. Lewis, X. Liu, J. Lopez, D. Ma, W. Majoros, J. McDaniel, S. Murphy, M. Newman, T. Nguyen, N. Nguyen, M. Nodell, S. Pan, J. Peck, M. Peterson, W. Rowe, R. Sanders, J. Scott, M. Simpson, T. Smith, A. Sprague, T. Stockwell, R. Turner, E. Venter, M. Wang, M. Wen, D. Wu, M. Wu, A. Xia, A. Zandieh and X. Zhu, *The sequence of the human genome*. Science, 2001. **291**(5507): p. 1304-51.
14. Kettman, J.R., C. Coleclough, J.R. Frey, and I. Lefkovits, *Clonal proteomics: one gene - family of proteins*. Proteomics, 2002. **2**(6): p. 624-31.
 15. *Advances in protein chemistry*. Metalloproteins: Structural aspects, ed. C. Anfinsen, J. Edsall, F. Richards, and D. Eisenberg. Vol. 42. 1991: Academic press, Inc.
 16. Schmidt, G. and S. Tanhauser, J Biol Chem, 1945. **161**: p. 83-89.
 17. Sharma, R.N., M. Behar-Bennelier, F.S. Rolleston, and R.K. Murray, *Electrophoretic studies on liver endoplasmic reticulum membrane polypeptides and on their phosphorylation in vivo and in vitro*. J Biol Chem, 1978. **253**(6): p. 2033-43.
 18. Obenauer, J.C., L.C. Cantley and M.B. Yaffe, *Scansite 2.0: Proteome-wide prediction of cell signaling interactions using short sequence motifs*. Nucleic Acids Res, 2003. **31**(13): p. 3635-41.

19. Iakoucheva, L.M., P. Radivojac, C.J. Brown, T.R. O'Connor, J.G. Sikes, Z. Obradovic, and A.K. Dunker, *The importance of intrinsic disorder for protein phosphorylation*. Nucleic Acids Res, 2004. **32**(3): p. 1037-49.
20. Blom, N., T. Sicheritz-Ponten, R. Gupta, S. Gammeltoft, and S. Brunak, *Prediction of post-translational glycosylation and phosphorylation of proteins from the amino acid sequence*. Proteomics, 2004. **4**(6): p. 1633-49.
21. Blom, N., S. Gammeltoft and S. Brunak, *Sequence and structure-based prediction of eukaryotic protein phosphorylation sites*. J Mol Biol, 1999. **294**(5): p. 1351-62.
22. Morton, S., R.J. Davis, A. McLaren, and P. Cohen, *A reinvestigation of the multisite phosphorylation of the transcription factor c-Jun*. Embo J, 2003. **22**(15): p. 3876-86.
23. Morton, S., R.J. Davis and P. Cohen, *Signalling pathways involved in multisite phosphorylation of the transcription factor ATF-2*. FEBS Lett, 2004. **572**(1-3): p. 177-83.
24. Cohen, P., *The regulation of protein function by multisite phosphorylation--a 25 year update*. Trends Biochem Sci, 2000. **25**(12): p. 596-601.
25. Ballif, B.A., J. Villen, S.A. Beausoleil, D. Schwartz, and S.P. Gygi, *Phosphoproteomic analysis of the developing mouse brain*. Mol Cell Proteomics, 2004. **3**(11): p. 1093-101.
26. Lim, Y.P., L.S. Diong, R. Qi, B.J. Druker, and R.J. Epstein, *Phosphoproteomic fingerprinting of epidermal growth factor signaling and anticancer drug action in human tumor cells*. Mol Cancer Ther, 2003. **2**(12): p. 1369-77.
27. Beausoleil, S.A., M. Jedrychowski, D. Schwartz, J.E. Elias, J. Villen, J. Li, M.A. Cohn, L.C. Cantley, and S.P. Gygi, *Large-scale characterization of HeLa cell nuclear phosphoproteins*. Proc Natl Acad Sci U S A, 2004. **101**(33): p. 12130-5.
28. Beranova-Giorgianni, S., Y. Zhao, D.M. Desiderio, and F. Giorgianni, *Phosphoproteomic analysis of the human pituitary*. Pituitary, 2006. **9**(2): p. 109-20.
29. Yang, F., D.L. Stenoien, E.F. Strittmatter, J. Wang, L. Ding, M.S. Lipton, M.E. Monroe, C.D. Nicora, M.A. Gristenko, K. Tang, R. Fang, J.N. Adkins, D.G. Camp, 2nd, D.J. Chen, and R.D. Smith, *Phosphoproteome profiling of human skin fibroblast cells in response to low- and high-dose irradiation*. J Proteome Res, 2006. **5**(5): p. 1252-60.
30. Nousiainen, M., H.H. Sillje, G. Sauer, E.A. Nigg, and R. Korner, *Phosphoproteome analysis of the human mitotic spindle*. Proc Natl Acad Sci U S A, 2006. **103**(14): p. 5391-6.

31. Gevaert, K., A. Staes, J. Van Damme, S. De Groot, K. Hugelier, H. Demol, L. Martens, M. Goethals, and J. Vandekerckhove, *Global phosphoproteome analysis on human HepG2 hepatocytes using reversed-phase diagonal LC*. *Proteomics*, 2005. **5**(14): p. 3589-99.
32. Nuhse, T.S., A. Stensballe, O.N. Jensen, and S.C. Peck, *Phosphoproteomics of the Arabidopsis plasma membrane and a new phosphorylation site database*. *Plant Cell*, 2004. **16**(9): p. 2394-405.
33. Loyet, K.M., J.T. Stults and D. Arnott, *Mass spectrometric contributions to the practice of phosphorylation site mapping through 2003: a literature review*. *Mol Cell Proteomics*, 2005. **4**(3): p. 235-45.
34. Byford, M.F., *Rapid and selective modification of phosphoserine residues catalysed by Ba²⁺ ions for their detection during peptide microsequencing*. *Biochem J*, 1991. **280 (Pt 1)**: p. 261-5.
35. Resing, K.A., R.S. Johnson and K.A. Walsh, *Mass spectrometric analysis of 21 phosphorylation sites in the internal repeat of rat profilaggrin, precursor of an intermediate filament associated protein*. *Biochemistry*, 1995. **34**(29): p. 9477-87.
36. Jaffe, H., Veeranna and H.C. Pant, *Characterization of serine and threonine phosphorylation sites in beta-elimination/ethanethiol addition-modified proteins by electrospray tandem mass spectrometry and database searching*. *Biochemistry*, 1998. **37**(46): p. 16211-24.
37. Jiang, X. and Y. Wang, *Beta-elimination coupled with tandem mass spectrometry for the identification of in vivo and in vitro phosphorylation sites in maize dehydrin DHN1 protein*. *Biochemistry*, 2004. **43**(49): p. 15567-76.
38. Tsuji, T., S.B. Ficarro and W. Jiang, *Essential role of phosphorylation of MCM2 by Cdc7/Dbf4 in the initiation of DNA replication in mammalian cells*. *Mol Biol Cell*, 2006. **17**(10): p. 4459-72.
39. Xie, M. and R.L. Schowen, *Secondary structure and protein deamidation*. *J Pharm Sci*, 1999. **88**(1): p. 8-13.
40. Atkinson, M.R., E.S. Kamberov, R.L. Weiss, and A.J. Ninfa, *Reversible uridylylation of the Escherichia coli PII signal transduction protein regulates its ability to stimulate the*

- dephosphorylation of the transcription factor nitrogen regulator I (NRI or NtrC)*. J Biol Chem, 1994. **269**(45): p. 28288-93.
41. Hara-Yokoyama, M., H. Sugiya and S. Furuyama, *Possible involvement of adenylylation in the modification of a 26 kDa protein in rat parotid acinar cells*. Int J Biochem, 1994. **26**(9): p. 1103-9.
 42. Rando, R.R., *Chemical biology of protein isoprenylation/methylation*. Biochim Biophys Acta, 1996. **1300**(1): p. 5-16.
 43. Saxholm, H.J., A. Pestana, L. O'Connor, C.A. Sattler, and H.C. Pitot, *Protein acetylation*. Mol Cell Biochem, 1982. **46**(3): p. 129-53.
 44. Goshe, M.B., T.P. Conrads, E.A. Panisko, N.H. Angell, T.D. Veenstra, and R.D. Smith, *Phosphoprotein isotope-coded affinity tag approach for isolating and quantitating phosphopeptides in proteome-wide analyses*. Anal Chem, 2001. **73**(11): p. 2578-86.
 45. Goshe, M.B., T.D. Veenstra, E.A. Panisko, T.P. Conrads, N.H. Angell, and R.D. Smith, *Phosphoprotein isotope-coded affinity tags: application to the enrichment and identification of low-abundance phosphoproteins*. Anal Chem, 2002. **74**(3): p. 607-16.
 46. Qian, W.J., M.B. Goshe, D.G. Camp, 2nd, L.R. Yu, K. Tang, and R.D. Smith, *Phosphoprotein isotope-coded solid-phase tag approach for enrichment and quantitative analysis of phosphopeptides from complex mixtures*. Anal Chem, 2003. **75**(20): p. 5441-50.
 47. Leitner, A. and W. Lindner, *Chemistry meets proteomics: the use of chemical tagging reactions for MS-based proteomics*. Proteomics, 2006. **6**(20): p. 5418-34.
 48. Wiese, S., K.A. Reidegeld, H.E. Meyer, and B. Warscheid, *Protein labeling by iTRAQ: A new tool for quantitative mass spectrometry in proteome research*. Proteomics, 2007. **7**(3): p. 340-50.
 49. Manning, G., D.B. Whyte, R. Martinez, T. Hunter, and S. Sudarsanam, *The protein kinase complement of the human genome*. Science, 2002. **298**(5600): p. 1912-34.
 50. Kim, J.H., J. Lee, B. Oh, K. Kimm, and I. Koh, *Prediction of phosphorylation sites using SVMs*. Bioinformatics, 2004. **20**(17): p. 3179-84.
 51. Zhou, F.F., Y. Xue, G.L. Chen, and X. Yao, *GPS: a novel group-based phosphorylation predicting and scoring method*. Biochem Biophys Res Commun, 2004. **325**(4): p. 1443-8.

52. Kreegipuu, A., N. Blom, S. Brunak, and J. Jarv, *Statistical analysis of protein kinase specificity determinants*. FEBS Lett, 1998. **430**(1-2): p. 45-50.
53. Gygi, S.P., B. Rist, S.A. Gerber, F. Turecek, M.H. Gelb, and R. Aebersold, *Quantitative analysis of complex protein mixtures using isotope-coded affinity tags*. Nat Biotechnol, 1999. **17**(10): p. 994-9.
54. Gygi, S.P. and R. Aebersold, *Absolute quantitation of 2-D protein spots*. Methods Mol Biol, 1999. **112**: p. 417-21.
55. Ong, S.E., B. Blagoev, I. Kratchmarova, D.B. Kristensen, H. Steen, A. Pandey, and M. Mann, *Stable isotope labeling by amino acids in cell culture, SILAC, as a simple and accurate approach to expression proteomics*. Mol Cell Proteomics, 2002. **1**(5): p. 376-86.
56. Ong, S.E., I. Kratchmarova and M. Mann, *Properties of ¹³C-substituted arginine in stable isotope labeling by amino acids in cell culture (SILAC)*. J Proteome Res, 2003. **2**(2): p. 173-81.
57. Ross, P.L., Y.N. Huang, J.N. Marchese, B. Williamson, K. Parker, S. Hattan, N. Khainovski, S. Pillai, S. Dey, S. Daniels, S. Purkayastha, P. Juhasz, S. Martin, M. Bartlett-Jones, F. He, A. Jacobson, and D.J. Pappin, *Multiplexed protein quantitation in Saccharomyces cerevisiae using amine-reactive isobaric tagging reagents*. Mol Cell Proteomics, 2004. **3**(12): p. 1154-69.
58. Zieske, L.R., *A perspective on the use of iTRAQ reagent technology for protein complex and profiling studies*. J Exp Bot, 2006. **57**(7): p. 1501-8.
59. Kjellstrom, S. and O.N. Jensen, *In situ liquid-liquid extraction as a sample preparation method for matrix-assisted laser desorption/ionization MS analysis of polypeptide mixtures*. Anal Chem, 2003. **75**(10): p. 2362-9.
60. Mo, W. and B.L. Karger, *Analytical aspects of mass spectrometry and proteomics*. Curr Opin Chem Biol, 2002. **6**(5): p. 666-75.
61. McLafferty, F.W., D.M. Horn, K. Breuker, Y. Ge, M.A. Lewis, B. Cerda, R.A. Zubarev, and B.K. Carpenter, *Electron capture dissociation of gaseous multiply charged ions by Fourier-transform ion cyclotron resonance*. J Am Soc Mass Spectrom, 2001. **12**(3): p. 245-9.
62. Kjeldsen, F., K.F. Haselmann, B.A. Budnik, E.S. Sorensen, and R.A. Zubarev, *Complete characterization of posttranslational modification sites in the bovine milk protein PP3 by*

- tandem mass spectrometry with electron capture dissociation as the last stage.* Anal Chem, 2003. **75**(10): p. 2355-61.
63. Sze, S.K., Y. Ge, H. Oh, and F.W. McLafferty, *Top-down mass spectrometry of a 29-kDa protein for characterization of any posttranslational modification to within one residue.* Proc Natl Acad Sci U S A, 2002. **99**(4): p. 1774-9.
64. Galaktionov, K., A.K. Lee, J. Eckstein, G. Draetta, J. Meckler, M. Loda, and D. Beach, *CDC25 phosphatases as potential human oncogenes.* Science, 1995. **269**(5230): p. 1575-7.
65. Baldin, V., C. Cans, M. Knibiehler, and B. Ducommun, *Phosphorylation of human CDC25B phosphatase by CDK1-cyclin A triggers its proteasome-dependent degradation.* J Biol Chem, 1997. **272**(52): p. 32731-4.
66. Sebastian, B., A. Kakizuka and T. Hunter, *Cdc25M2 activation of cyclin-dependent kinases by dephosphorylation of threonine-14 and tyrosine-15.* Proc Natl Acad Sci U S A, 1993. **90**(8): p. 3521-4.
67. Lammer, C., S. Wagerer, R. Saffrich, D. Mertens, W. Ansorge, and I. Hoffmann, *The cdc25B phosphatase is essential for the G2/M phase transition in human cells.* J Cell Sci, 1998. **111 (Pt 16)**: p. 2445-53.
68. Sato, Y., H. Sasaki, S. Kondo, I. Fukai, M. Kiriyama, Y. Yamakawa, and Y. Fujii, *Expression of the cdc25B mRNA correlated with that of N-myc in neuroblastoma.* Jpn J Clin Oncol, 2001. **31**(9): p. 428-31.
69. Gabrielli, B.G., C.P. De Souza, I.D. Tonks, J.M. Clark, N.K. Hayward, and K.A. Ellem, *Cytoplasmic accumulation of cdc25B phosphatase in mitosis triggers centrosomal microtubule nucleation in HeLa cells.* J Cell Sci, 1996. **109 (Pt 5)**: p. 1081-93.
70. Molinari, M., *Cell cycle checkpoints and their inactivation in human cancer.* Cell Prolif, 2000. **33**(5): p. 261-74.
71. Morgan, D.O., *Cell cycle control in normal and neoplastic cells.* Curr Opin Genet Dev, 1992. **2**(1): p. 33-7.
72. Flatt, P.M. and J.A. Pietsenpol, *Mechanisms of cell-cycle checkpoints: at the crossroads of carcinogenesis and drug discovery.* Drug Metab Rev, 2000. **32**(3-4): p. 283-305.

73. Karlsson, C., S. Katich, A. Hagting, I. Hoffmann, and J. Pines, *Cdc25B and Cdc25C differ markedly in their properties as initiators of mitosis*. J Cell Biol, 1999. **146**(3): p. 573-84.
74. Reynolds, R.A., A.W. Yem, C.L. Wolfe, M.R. Deibel, Jr., C.G. Chidester, and K.D. Watenpaugh, *Crystal structure of the catalytic subunit of Cdc25B required for G2/M phase transition of the cell cycle*. J Mol Biol, 1999. **293**(3): p. 559-68.
75. Gottlin, E.B., X. Xu, D.M. Epstein, S.P. Burke, J.W. Eckstein, D.P. Ballou, and J.E. Dixon, *Kinetic analysis of the catalytic domain of human cdc25B*. J Biol Chem, 1996. **271**(44): p. 27445-9.
76. Denu, J.M., J.A. Stuckey, M.A. Saper, and J.E. Dixon, *Form and function in protein dephosphorylation*. Cell, 1996. **87**(3): p. 361-4.
77. Lazo, J.S., K. Nemoto, K.E. Pestell, K. Cooley, E.C. Southwick, D.A. Mitchell, W. Furey, R. Gussio, D.W. Zaharevitz, B. Joo, and P. Wipf, *Identification of a potent and selective pharmacophore for Cdc25 dual specificity phosphatase inhibitors*. Mol Pharmacol, 2002. **61**(4): p. 720-8.
78. Tamura, K., E.C. Southwick, J. Kerns, K. Rosi, B.I. Carr, C. Wilcox, and J.S. Lazo, *Cdc25 inhibition and cell cycle arrest by a synthetic thioalkyl vitamin K analogue*. Cancer Res, 2000. **60**(5): p. 1317-25.
79. Schulte, C., E. Schiltz and R. Garrent, *The characterisation of a fragment of ribosomal protein S4 that is protected against trypsin digestion by 16S ribosomal RNA of Escherichia coli*. Nucleic Acids Res, 1975. **2**(6): p. 931-41.
80. Bragg, P.D. and C. Hou, *Ligand-induced conformational changes in the Escherichia coli F1 adenosine triphosphatase probed by trypsin digestion*. Biochim Biophys Acta, 1987. **894**(2): p. 127-37.
81. Mazzoni, M.R. and H.E. Hamm, *Interaction of transducin with light-activated rhodopsin protects It from proteolytic digestion by trypsin*. J Biol Chem, 1996. **271**(47): p. 30034-40.
82. Brisson, M., T. Nguyen, P. Wipf, B. Joo, B.W. Day, J.S. Skoko, E.M. Schreiber, C. Foster, P. Bansal, and J.S. Lazo, *Redox regulation of Cdc25B by cell-active quinolinediones*. Mol Pharmacol, 2005. **68**(6): p. 1810-20.

83. Buhrman, G., B. Parker, J. Sohn, J. Rudolph, and C. Mattos, *Structural mechanism of oxidative regulation of the phosphatase Cdc25B via an intramolecular disulfide bond*. *Biochemistry*, 2005. **44**(14): p. 5307-16.
84. Sohn, J. and J. Rudolph, *Catalytic and chemical competence of regulation of cdc25 phosphatase by oxidation/reduction*. *Biochemistry*, 2003. **42**(34): p. 10060-70.
85. Leite, J.F., M.R. Hajivandi, T. Diller, and R.M. Pope, *Removal of sodium and potassium adducts using a matrix additive during matrix-associated laser desorption/ionization time-of-flight mass spectrometric analysis of peptides*. *Rapid Commun Mass Spectrom*, 2004. **18**(23): p. 2953-9.
86. Campbell, S.J., N.D. Gold, R.M. Jackson, and D.R. Westhead, *Ligand binding: functional site location, similarity and docking*. *Curr Opin Struct Biol*, 2003. **13**(3): p. 389-95.
87. Gohlke, H. and G. Klebe, *Statistical potentials and scoring functions applied to protein-ligand binding*. *Curr Opin Struct Biol*, 2001. **11**(2): p. 231-5.
88. Huang, N., C. Kalyanaraman, K. Bernacki, and M.P. Jacobson, *Molecular mechanics methods for predicting protein-ligand binding*. *Phys Chem Chem Phys*, 2006. **8**(44): p. 5166-77.
89. Laurie, A.T. and R.M. Jackson, *Methods for the prediction of protein-ligand binding sites for structure-based drug design and virtual ligand screening*. *Curr Protein Pept Sci*, 2006. **7**(5): p. 395-406.
90. Olah, M.E. and G.L. Stiles, *Site-directed mutagenesis and chimeric receptors in the study of receptor-ligand binding*. *Methods Mol Biol*, 1997. **83**: p. 25-43.
91. Fukuto, J.M. and D.A. Wink, *Nitric oxide (NO): formation and biological roles in mammalian systems*. *Met Ions Biol Syst*, 1999. **36**: p. 547-95.
92. Szabo, C. and T.R. Billiar, *Novel roles of nitric oxide in hemorrhagic shock*. *Shock*, 1999. **12**(1): p. 1-9.
93. Marshall, J.M., *Roles of adenosine and nitric oxide in skeletal muscle in acute and chronic hypoxia*. *Adv Exp Med Biol*, 2001. **502**: p. 349-63.
94. Nath, A.K. and J.A. Madri, *The roles of nitric oxide in murine cardiovascular development*. *Dev Biol*, 2006. **292**(1): p. 25-33.

95. Mur, L.A., T.L. Carver and E. Prats, *NO way to live; the various roles of nitric oxide in plant-pathogen interactions*. J Exp Bot, 2006. **57**(3): p. 489-505.
96. Wink, D.A., Y. Vodovotz, J. Laval, F. Laval, M.W. Dewhirst, and J.B. Mitchell, *The multifaceted roles of nitric oxide in cancer*. Carcinogenesis, 1998. **19**(5): p. 711-21.
97. Gow, A.J., D.G. Buerk and H. Ischiropoulos, *A novel reaction mechanism for the formation of S-nitrosothiol in vivo*. J Biol Chem, 1997. **272**(5): p. 2841-5.
98. Vanin, A.F., I.V. Malenkova and V.A. Serezhenkov, *Iron catalyzes both decomposition and synthesis of S-nitrosothiols: optical and electron paramagnetic resonance studies*. Nitric Oxide, 1997. **1**(3): p. 191-203.
99. Broillet, M.C., *S-nitrosylation of proteins*. Cell Mol Life Sci, 1999. **55**(8-9): p. 1036-42.
100. Lane, P., G. Hao and S.S. Gross, *S-nitrosylation is emerging as a specific and fundamental posttranslational protein modification: head-to-head comparison with O-phosphorylation*. Sci STKE, 2001. **2001**(86): p. RE1.
101. Martinez-Ruiz, A. and S. Lamas, *S-nitrosylation: a potential new paradigm in signal transduction*. Cardiovasc Res, 2004. **62**(1): p. 43-52.
102. Stamler, J.S., D.I. Simon, J.A. Osborne, M.E. Mullins, O. Jaraki, T. Michel, D.J. Singel, and J. Loscalzo, *S-nitrosylation of proteins with nitric oxide: synthesis and characterization of biologically active compounds*. Proc Natl Acad Sci U S A, 1992. **89**(1): p. 444-8.
103. Harbrecht, B.G., B. Wu, S.C. Watkins, H.P. Marshall, Jr., A.B. Peitzman, and T.R. Billiar, *Inhibition of nitric oxide synthase during hemorrhagic shock increases hepatic injury*. Shock, 1995. **4**(5): p. 332-7.
104. Liu, L.M., J.A. Ward and M.A. Dubick, *Hemorrhage-induced vascular hyporeactivity to norepinephrine in select vasculatures of rats and the roles of nitric oxide and endothelin*. Shock, 2003. **19**(3): p. 208-14.
105. Pieber, D., G. Horina, A. Sandner-Kiesling, T.R. Pieber, and A. Heinemann, *Pressor and mesenteric arterial hyporesponsiveness to angiotensin II is an early event in haemorrhagic hypotension in anaesthetised rats*. Cardiovasc Res, 1999. **44**(1): p. 166-75.
106. Thiemermann, C., C. Szabo, J.A. Mitchell, and J.R. Vane, *Vascular hyporeactivity to vasoconstrictor agents and hemodynamic decompensation in hemorrhagic shock is mediated by nitric oxide*. Proc Natl Acad Sci U S A, 1993. **90**(1): p. 267-71.

107. Jaffery, S. and S. Snyder, *The Biotin Switch Method for the Detection of S-Nitrosylated Proteins*. Science's STKE, 2001. **86**: p. p11.
108. Baue, A.E., R. Durham and E. Faist, *Systemic inflammatory response syndrome (SIRS), multiple organ dysfunction syndrome (MODS), multiple organ failure (MOF): are we winning the battle?* Shock, 1998. **10**(2): p. 79-89.
109. Dieguez, G., N. Fernandez, M.A. Sanchez, M.A. Martinez, A.L. Garcia-Villalon, L. Monge, and B. Gomez, *Role of nitric oxide in the cerebral circulation during hypotension after hemorrhage, ganglionic blockade and diazoxide in awake goats*. Brain Res, 1999. **851**(1-2): p. 133-40.
110. Fujisawa, Y., N. Mori, K. Yube, H. Miyataka, A. Miyatake, and Y. Abe, *Role of nitric oxide in regulation of renal sympathetic nerve activity during hemorrhage in conscious rats*. Am J Physiol, 1999. **277**(1 Pt 2): p. H8-14.
111. Nishizawa, S., S. Yamamoto, T. Yokoyama, and K. Uemura, *Dysfunction of nitric oxide induces protein kinase C activation resulting in vasospasm after subarachnoid hemorrhage*. Neurol Res, 1997. **19**(5): p. 558-62.
112. Alabadi, J.A., G. Torregrosa, F.J. Miranda, J.B. Salom, J.M. Centeno, and E. Alborch, *Impairment of the modulatory role of nitric oxide on the endothelin-1-elicited contraction of cerebral arteries: a pathogenetic factor in cerebral vasospasm after subarachnoid hemorrhage?* Neurosurgery, 1997. **41**(1): p. 245-52; discussion 252-3.
113. Yamamoto, S., S. Nishizawa, T. Yokoyama, H. Ryu, and K. Uemura, *Subarachnoid hemorrhage impairs cerebral blood flow response to nitric oxide but not to cyclic GMP in large cerebral arteries*. Brain Res, 1997. **757**(1): p. 1-9.
114. Westenberger, U., S. Thanner, H.H. Ruf, K. Gersonde, G. Sutter, and O. Trentz, *Formation of free radicals and nitric oxide derivative of hemoglobin in rats during shock syndrome*. Free Radic Res Commun, 1990. **11**(1-3): p. 167-78.
115. Szabo, C. and C. Thiemeermann, *Invited opinion: role of nitric oxide in hemorrhagic, traumatic, and anaphylactic shock and thermal injury*. Shock, 1994. **2**(2): p. 145-55.
116. Sun, J., L. Xu, J.P. Eu, J.S. Stamler, and G. Meissner, *Nitric oxide, NOC-12, and S-nitrosoglutathione modulate the skeletal muscle calcium release channel/ryanodine receptor by different mechanisms. An allosteric function for O₂ in S-nitrosylation of the channel*. J Biol Chem, 2003. **278**(10): p. 8184-9.

117. Yalowich, J.C., N.V. Gorbunov, A.V. Kozlov, W. Allan, and V.E. Kagan, *Mechanisms of nitric oxide protection against tert-butyl hydroperoxide-induced cytotoxicity in iNOS-transduced human erythroleukemia cells*. *Biochemistry*, 1999. **38**(33): p. 10691-8.
118. Atkins, J.L., B.W. Day, M.T. Handrigan, Z. Zhang, M.B. Pamnani, and N.V. Gorbunov, *Brisk production of nitric oxide and associated formation of S-nitrosothiols in early hemorrhage*. *J Appl Physiol*, 2006. **100**(4): p. 1267-77.
119. Gorbunov, N.V., L.V. Asher, V. Ayyagari, and J.L. Atkins, *Inflammatory leukocytes and iron turnover in experimental hemorrhagic lung trauma*. *Exp Mol Pathol*, 2006. **80**(1): p. 11-25.
120. Steel, L.F., M.G. Trotter, P.B. Nakajima, T.S. Mattu, G. Gonye, and T. Block, *Efficient and specific removal of albumin from human serum samples*. *Mol Cell Proteomics*, 2003. **2**(4): p. 262-70.
121. Hinerfeld, D., D. Innamorati, J. Pirro, and S.W. Tam, *Serum/Plasma depletion with chicken immunoglobulin Y antibodies for proteomic analysis from multiple Mammalian species*. *J Biomol Tech*, 2004. **15**(3): p. 184-90.
122. Denko, C.W. and P. Gabriel, *Serum proteins--transferrin, ceruloplasmin, albumin, alpha 1-acid glycoprotein, alpha 1-antitrypsin--in rheumatic disorders*. *J Rheumatol*, 1979. **6**(6): p. 664-72.
123. Killander, J., *Separation of Human Heme- and Hemoglobin-Binding Plasma Proteins, Ceruloplasmin and Albumin by Gel Filtration*. *Biochim Biophys Acta*, 1964. **93**: p. 1-14.
124. Bencurova, M., W. Hemmer, M. Focke-Tejkl, I.B. Wilson, and F. Altmann, *Specificity of IgG and IgE antibodies against plant and insect glycoprotein glycans determined with artificial glycoforms of human transferrin*. *Glycobiology*, 2004. **14**(5): p. 457-66.
125. Wernet, P., B. Kickhofen, M. Westerhausen, and S.E. Svehag, *A monoclonal IgG protein with antibody-like activity for transferrin and with kappa chains of an unusual molecular size*. *Scand J Immunol*, 1974. **3**(6): p. 859-64.
126. Tankersley, D.L., M.S. Preston and J.S. Finlayson, *Immunoglobulin G dimer: an idiotype-anti-idiotype complex*. *Mol Immunol*, 1988. **25**(1): p. 41-8.
127. Adrian, G.S., D.C. Herbert, L.K. Robinson, E.K. Adrian, C.A. Walter, F.J. Weaker, F. Yang, and B.H. Bowman, *Human transferrin: expression of chimeric genes in transgenic mice*. *Curr Stud Hematol Blood Transfus*, 1991(58): p. 104-8.

128. Chow, B.K., W.D. Funk, D.K. Banfield, J.A. Lineback, A.B. Mason, R.C. Woodworth, and R.T. MacGillivray, *Structural-functional studies of human transferrin by using in vitro mutagenesis*. *Curr Stud Hematol Blood Transfus*, 1991(58): p. 132-8.
129. Hershberger, C.L., J.L. Larson, B. Arnold, P.R. Rosteck, Jr., P. Williams, B. DeHoff, P. Dunn, K.L. O'Neal, M.W. Riemen, P.A. Tice, and et al., *A cloned gene for human transferrin*. *Ann N Y Acad Sci*, 1991. **646**: p. 140-54.
130. Beckman, J.S., T.W. Beckman, J. Chen, P.A. Marshall, and B.A. Freeman, *Apparent hydroxyl radical production by peroxynitrite: implications for endothelial injury from nitric oxide and superoxide*. *Proc Natl Acad Sci U S A*, 1990. **87**(4): p. 1620-4.
131. Bohn, H. and K. Schonafinger, *Oxygen and oxidation promote the release of nitric oxide from sydnonimines*. *J Cardiovasc Pharmacol*, 1989. **14 Suppl 11**: p. S6-12.
132. Beckman, J.S., *Oxidative damage and tyrosine nitration from peroxynitrite*. *Chem Res Toxicol*, 1996. **9**(5): p. 836-44.
133. Ischiropoulos, H., *Biological tyrosine nitration: a pathophysiological function of nitric oxide and reactive oxygen species*. *Arch Biochem Biophys*, 1998. **356**(1): p. 1-11.
134. Ischiropoulos, H., L. Zhu and J.S. Beckman, *Peroxynitrite formation from macrophage-derived nitric oxide*. *Arch Biochem Biophys*, 1992. **298**(2): p. 446-51.
135. Fang, C.X., S. Wu and J. Ren, *Intracerebral hemorrhage elicits aberration in cardiomyocyte contractile function and intracellular Ca²⁺ transients*. *Stroke*, 2006. **37**(7): p. 1875-82.
136. Fruchterman, T.M., D.A. Spain, P.J. Matheson, A.W. Martin, M.A. Wilson, P.D. Harris, and R.N. Garrison, *Small intestinal production of nitric oxide is decreased following resuscitated hemorrhage*. *J Surg Res*, 1998. **80**(1): p. 102-9.
137. Lehnert, M., G.E. Arteel, O.M. Smutney, L.O. Conzelmann, Z. Zhong, R.G. Thurman, and J.J. Lemasters, *Dependence of liver injury after hemorrhage/resuscitation in mice on NADPH oxidase-derived superoxide*. *Shock*, 2003. **19**(4): p. 345-51.
138. McGirt, M.J., A. Parra, H. Sheng, Y. Higuchi, T.D. Oury, D.T. Laskowitz, R.D. Pearlstein, and D.S. Warner, *Attenuation of cerebral vasospasm after subarachnoid hemorrhage in mice overexpressing extracellular superoxide dismutase*. *Stroke*, 2002. **33**(9): p. 2317-23.

139. Sayama, T., S. Suzuki and M. Fukui, *Role of inducible nitric oxide synthase in the cerebral vasospasm after subarachnoid hemorrhage in rats*. *Neurol Res*, 1999. **21**(3): p. 293-8.
140. Shin, H.K., J.H. Lee, C.D. Kim, Y.K. Kim, J.Y. Hong, and K.W. Hong, *Prevention of impairment of cerebral blood flow autoregulation during acute stage of subarachnoid hemorrhage by gene transfer of Cu/Zn SOD-1 to cerebral vessels*. *J Cereb Blood Flow Metab*, 2003. **23**(1): p. 111-20.
141. Ryden, L., *Copper proteins and copper enzymes*, ed. R. Lontie. Vol. III. 1984: CRC Press, Boca Raton, Florida.
142. Castellino, F.J. and V.A. Ploplis, *Structure and function of the plasminogen/plasmin system*. *Thromb Haemost*, 2005. **93**(4): p. 647-54.
143. Miyashita, C., E. Wenzel and M. Heiden, *Plasminogen: a brief introduction into its biochemistry and function*. *Haemostasis*, 1988. **18 Suppl 1**: p. 7-13.
144. Gomme, P.T., K.B. McCann and J. Bertolini, *Transferrin: structure, function and potential therapeutic actions*. *Drug Discov Today*, 2005. **10**(4): p. 267-73.
145. Lok, C.N. and T.T. Loh, *Regulation of transferrin function and expression: review and update*. *Biol Signals Recept*, 1998. **7**(3): p. 157-78.
146. Kashiba-Iwatsuki, M., M. Miyamoto and M. Inoue, *Effect of nitric oxide on the ligand-binding activity of albumin*. *Arch Biochem Biophys*, 1997. **345**(2): p. 237-42.
147. Katsumi, H., M. Nishikawa, S.F. Ma, F. Yamashita, and M. Hashida, *Physicochemical, tissue distribution, and vasodilation characteristics of nitrosated serum albumin: delivery of nitric oxide in vivo*. *J Pharm Sci*, 2004. **93**(9): p. 2343-52.
148. Katsumi, H., M. Nishikawa, F. Yamashita, and M. Hashida, *Development of polyethylene glycol-conjugated poly-S-nitrosated serum albumin, a novel S-Nitrosothiol for prolonged delivery of nitric oxide in the blood circulation in vivo*. *J Pharmacol Exp Ther*, 2005. **314**(3): p. 1117-24.
149. Marley, R., R.P. Patel, N. Orié, E. Ceaser, V. Darley-USmar, and K. Moore, *Formation of nanomolar concentrations of S-nitroso-albumin in human plasma by nitric oxide*. *Free Radic Biol Med*, 2001. **31**(5): p. 688-96.

150. Meyer, D.J., H. Kramer, N. Ozer, B. Coles, and B. Ketterer, *Kinetics and equilibria of S-nitrosothiol-thiol exchange between glutathione, cysteine, penicillamines and serum albumin*. FEBS Lett, 1994. **345**(2-3): p. 177-80.
151. Ng, E.S., D. Jourdain, J.M. McCord, D. Hernandez, M. Yasui, D. Knight, and P. Kubes, *Enhanced S-nitroso-albumin formation from inhaled NO during ischemia/reperfusion*. Circ Res, 2004. **94**(4): p. 559-65.
152. Robak, J., E. Marcinkiewicz, Z. Michalska, and R.J. Gryglewski, *Nitric oxide donation and nitrite assays in the presence of thiols and albumin as determined by Griess' and Werringloer's methods*. Pol J Pharmacol, 1997. **49**(4): p. 255-62.
153. Stamler, J.S., O. Jaraki, J. Osborne, D.I. Simon, J. Keaney, J. Vita, D. Singel, C.R. Valeri, and J. Loscalzo, *Nitric oxide circulates in mammalian plasma primarily as an S-nitroso adduct of serum albumin*. Proc Natl Acad Sci U S A, 1992. **89**(16): p. 7674-7.
154. Demetriou, M., C. Binkert, B. Sukhu, H.C. Tenenbaum, and J.W. Dennis, *Fetuin/alpha2-HS glycoprotein is a transforming growth factor-beta type II receptor mimic and cytokine antagonist*. J Biol Chem, 1996. **271**(22): p. 12755-61.
155. Dziegielewska, K.M., R.T. Williams, G.W. Knott, P.D. Kitchener, S.E. Monk, A. Potter, and N.R. Saunders, *TGF-beta receptor type II and fetuin in the developing sheep neocortex*. Cell Tissue Res, 1997. **290**(3): p. 515-24.
156. Szweras, M., D. Liu, E.A. Partridge, J. Pawling, B. Sukhu, C. Clokie, W. Jahnen-Dechent, H.C. Tenenbaum, C.J. Swallow, M.D. Grynepas, and J.W. Dennis, *alpha 2-HS glycoprotein/fetuin, a transforming growth factor-beta/bone morphogenetic protein antagonist, regulates postnatal bone growth and remodeling*. J Biol Chem, 2002. **277**(22): p. 19991-7.
157. Tajirian, T., J.W. Dennis and C.J. Swallow, *Regulation of human monocyte proMMP-9 production by fetuin, an endogenous TGF-beta antagonist*. J Cell Physiol, 2000. **185**(2): p. 174-83.
158. de Maat, M.P., J.J. Kastelein, J.W. Jukema, A.H. Zwinderman, H. Jansen, B. Groenemeier, A.V. Bruschke, and C. Kluft, *-455G/A polymorphism of the beta-fibrinogen gene is associated with the progression of coronary atherosclerosis in symptomatic men: proposed role for an acute-phase reaction pattern of fibrinogen. REGRESS group*. Arterioscler Thromb Vasc Biol, 1998. **18**(2): p. 265-71.

159. Teger-Nilsson, A.C., P.T. Larsson, P. Hjerdahl, and G. Olsson, *Fibrinogen and plasminogen activator inhibitor-1 levels in hypertension and coronary heart disease. Potential effects of beta-blockade*. *Circulation*, 1991. **84**(6 Suppl): p. VI72-7.
160. Grieninger, G., *Contribution of the alpha EC domain to the structure and function of fibrinogen-420*. *Ann N Y Acad Sci*, 2001. **936**: p. 44-64.
161. Schultz, D.R. and P.I. Arnold, *Properties of four acute phase proteins: C-reactive protein, serum amyloid A protein, alpha 1-acid glycoprotein, and fibrinogen*. *Semin Arthritis Rheum*, 1990. **20**(3): p. 129-47.
162. Tsurupa, G. and L. Medved, *Fibrinogen alpha C domains contain cryptic plasminogen and tPA binding sites*. *Ann N Y Acad Sci*, 2001. **936**: p. 328-30.
163. Weisel, J.W. and L. Medved, *The structure and function of the alpha C domains of fibrinogen*. *Ann N Y Acad Sci*, 2001. **936**: p. 312-27.
164. Mimura, Y., R. Ghirlando, P. Sondermann, J. Lund, and R. Jefferis, *The molecular specificity of IgG-Fc interactions with Fc gamma receptors*. *Adv Exp Med Biol*, 2001. **495**: p. 49-53.
165. Sondermann, P. and V. Oosthuizen, *X-ray crystallographic studies of IgG-Fc gamma receptor interactions*. *Biochem Soc Trans*, 2002. **30**(4): p. 481-6.
166. Tamm, A. and R.E. Schmidt, *IgG binding sites on human Fc gamma receptors*. *Int Rev Immunol*, 1997. **16**(1-2): p. 57-85.
167. Cote, H.C., S.T. Lord and K.P. Pratt, *gamma-Chain dysfibrinogenemias: molecular structure-function relationships of naturally occurring mutations in the gamma chain of human fibrinogen*. *Blood*, 1998. **92**(7): p. 2195-212.
168. Drouet, L., F. Paolucci, N. Pasqualini, M. Laprade, L. Ripoll, E. Mazoyer, C. Bal dit Sollier, and N. Vanhove, *Plasma gamma'/gamma fibrinogen ratio, a marker of arterial thrombotic activity: a new potential cardiovascular risk factor?* *Blood Coagul Fibrinolysis*, 1999. **10 Suppl 1**: p. S35-9.
169. Farrell, D.H., *Pathophysiologic roles of the fibrinogen gamma chain*. *Curr Opin Hematol*, 2004. **11**(3): p. 151-5.
170. Mosesson, M.W., *Fibrinogen gamma chain functions*. *J Thromb Haemost*, 2003. **1**(2): p. 231-8.

171. Remijn, J.A., K.C. Lounes, K.A. Hogan, S.T. Lord, D.K. Galanakis, J.J. Sixma, and P.G. De Groot, *Mutations on fibrinogen (gamma 316-322) are associated with reduction in platelet adhesion under flow conditions*. Ann N Y Acad Sci, 2001. **936**: p. 444-8.
172. Bowden, P.E., *The human type II keratin gene cluster on chromosome 12q13.13: final count or hidden secrets?* J Invest Dermatol, 2005. **124**(3): p. xv-xvii.
173. Coulombe, P.A. and M.B. Omary, *'Hard' and 'soft' principles defining the structure, function and regulation of keratin intermediate filaments*. Curr Opin Cell Biol, 2002. **14**(1): p. 110-22.
174. Coulombe, P.A., X. Tong, S. Mazzalupo, Z. Wang, and P. Wong, *Great promises yet to be fulfilled: defining keratin intermediate filament function in vivo*. Eur J Cell Biol, 2004. **83**(11-12): p. 735-46.
175. Parry, D.A. and A.C. North, *Hard alpha-keratin intermediate filament chains: substructure of the N- and C-terminal domains and the predicted structure and function of the C-terminal domains of type I and type II chains*. J Struct Biol, 1998. **122**(1-2): p. 67-75.
176. Porter, R.M. and E.B. Lane, *Phenotypes, genotypes and their contribution to understanding keratin function*. Trends Genet, 2003. **19**(5): p. 278-85.
177. Steinert, P.M., *Structure, function, and dynamics of keratin intermediate filaments*. J Invest Dermatol, 1993. **100**(6): p. 729-34.
178. Abraham, R.S., R.J. Clark, S.C. Bryant, J.F. Lymp, T. Larson, R.A. Kyle, and J.A. Katzmann, *Correlation of serum immunoglobulin free light chain quantification with urinary Bence Jones protein in light chain myeloma*. Clin Chem, 2002. **48**(4): p. 655-7.
179. Eulitz, M. and R.P. Linke, *Primary structure of the variable part of an amyloidogenic Bence-Jones Protein (Mev.). An unusual insertion in the third hypervariable region of a human kappa-immunoglobulin light chain*. Hoppe Seylers Z Physiol Chem, 1982. **363**(11): p. 1347-58.
180. Fine, J.M., *Study of the frequency of kappa and lambda light chains in 347 sera containing a monoclonal IgG, IgA, IgD, or Bence-Jones protein*. Rev Eur Etud Clin Biol, 1970. **15**(2): p. 199-202.
181. Kurusu, A., T. Yamada, K. Yamaji, M. Nishitani, K. Tashiro, K. Maeda, S. Horikoshi, I. Shirato, H. Rinno, and Y. Tomino, *A case of primary immunoglobulin light chain*

- amyloidosis with a delayed appearance of Bence Jones protein in urine. Nephrology (Carlton), 2004. 9(3): p. 122-5.*
182. Matthews, J.B. and R. Jefferis, *The effects of chemical modification on the antigenicity of a human kappa Bence Jones protein. Immunochemistry, 1977. 14(11-12): p. 799-807.*
183. Matthews, J.B. and R. Jefferis, *Studies on intact variable regions and variable region sub-fragments isolated from a human kappa Bence-Jones protein (sub-group I). Mol Immunol, 1979. 16(6): p. 401-8.*
184. Otto, S., J. Csikasz and E. Puskas, *"Monoclonal" IgM-gammopathy with two different light-chain types of protein (Bence-Jones I and II). Acta Morphol Acad Sci Hung, 1974. 22(1): p. 83-9.*
185. Roussel, A., S. Spinelli, S. Deret, J. Navaza, P. Aucouturier, and C. Cambillau, *The structure of an entire noncovalent immunoglobulin kappa light-chain dimer (Bence-Jones protein) reveals a weak and unusual constant domains association. Eur J Biochem, 1999. 260(1): p. 192-9.*
186. Starace, V. and P. Querinjean, *The primary structure of a rat kappa Bence Jones protein: phylogenetic relationships of V- and C-region genes. J Immunol, 1975. 115(1): p. 59-62.*
187. Stevens, F.J., F.A. Westholm, N. Panagiotopoulos, M. Schiffer, R.A. Popp, and A. Solomon, *Characterization and preliminary crystallographic data on the VL-related fragment of the human kappa Bence Jones protein. J Mol Biol, 1981. 147(1): p. 185-93.*
188. Frank, P.G. and Y.L. Marcel, *Apolipoprotein A-I: structure-function relationships. J Lipid Res, 2000. 41(6): p. 853-72.*
189. Marcel, Y.L. and R.S. Kiss, *Structure-function relationships of apolipoprotein A-I: a flexible protein with dynamic lipid associations. Curr Opin Lipidol, 2003. 14(2): p. 151-7.*
190. Obici, L., G. Franceschini, L. Calabresi, S. Giorgetti, M. Stoppini, G. Merlini, and V. Bellotti, *Structure, function and amyloidogenic propensity of apolipoprotein A-I. Amyloid, 2006. 13(4): p. 191-205.*
191. Segrest, J.P., L. Li, G.M. Anantharamaiah, S.C. Harvey, K.N. Liadaki, and V. Zannis, *Structure and function of apolipoprotein A-I and high-density lipoprotein. Curr Opin Lipidol, 2000. 11(2): p. 105-15.*

192. *Selenium-containing glutathione peroxidase: its synthesis and function in arachidonate metabolism.* Nutr Rev, 1981. **39**(1): p. 21-3.
193. *Position and function of the organic selenium in glutathione peroxidase.* Nutr Rev, 1984. **42**(4): p. 168-9.
194. De Haan, J.B., P.J. Crack, N. Flentjar, R.C. Iannello, P.J. Hertzog, and I. Kola, *An imbalance in antioxidant defense affects cellular function: the pathophysiological consequences of a reduction in antioxidant defense in the glutathione peroxidase-1 (Gpx1) knockout mouse.* Redox Rep, 2003. **8**(2): p. 69-79.
195. Kohrle, J., M. Oertel and M. Gross, *Selenium supply regulates thyroid function, thyroid hormone synthesis and metabolism by altering the expression of the selenoenzymes Type I 5'-deiodinase and glutathione peroxidase.* Thyroidology, 1992. **4**(1): p. 17-21.
196. Palha, J.A., *Transthyretin as a thyroid hormone carrier: function revisited.* Clin Chem Lab Med, 2002. **40**(12): p. 1292-300.
197. Schreiber, G. and S.J. Richardson, *The evolution of gene expression, structure and function of transthyretin.* Comp Biochem Physiol B Biochem Mol Biol, 1997. **116**(2): p. 137-60.
198. Byrne, C.D. and R.M. Lawn, *Studies on the structure and function of the apolipoprotein(a) gene.* Clin Genet, 1994. **46**(1 Spec No): p. 34-41.
199. Ichinose, A., K. Suzuki, N. Takabatake, and T. Saito, *Multi-modal expression of apolipoprotein (a) gene in vivo.* J Atheroscler Thromb, 1998. **4**(3): p. 107-11.
200. Mahley, R.W., T.L. Innerarity, S.C. Rall, Jr., and K.H. Weisgraber, *Plasma lipoproteins: apolipoprotein structure and function.* J Lipid Res, 1984. **25**(12): p. 1277-94.
201. Narayanaswami, V. and R.O. Ryan, *Molecular basis of exchangeable apolipoprotein function.* Biochim Biophys Acta, 2000. **1483**(1): p. 15-36.
202. Wohl, R.C., L. Summaria and K.C. Robbins, *Physiological activation of the human fibrinolytic system. Isolation and characterization of human plasminogen variants, Chicago I and Chicago II.* J Biol Chem, 1979. **254**(18): p. 9063-9.
203. Carmeliet, P., L. Moons, V. Ploplis, E. Plow, and D. Collen, *Impaired arterial neointima formation in mice with disruption of the plasminogen gene.* J Clin Invest, 1997. **99**(2): p. 200-8.

204. Carmeliet, P., L. Moons, M. Dewerchin, N. Mackman, T. Luther, G. Breier, V. Ploplis, M. Muller, A. Nagy, E. Plow, R. Gerard, T. Edgington, W. Risau, and D. Collen, *Insights in vessel development and vascular disorders using targeted inactivation and transfer of vascular endothelial growth factor, the tissue factor receptor, and the plasminogen system*. Ann N Y Acad Sci, 1997. **811**: p. 191-206.
205. Busuttill, S.J., C. Drumm, V.A. Ploplis, and E.F. Plow, *Endoluminal arterial injury in plasminogen-deficient mice*. J Surg Res, 2000. **91**(2): p. 159-64.
206. Creemers, E., J. Cleutjens, J. Smits, S. Heymans, L. Moons, D. Collen, M. Daemen, and P. Carmeliet, *Disruption of the plasminogen gene in mice abolishes wound healing after myocardial infarction*. Am J Pathol, 2000. **156**(6): p. 1865-73.
207. Bezerra, J.A., T.H. Bugge, H. Melin-Aldana, G. Sabla, K.W. Kombrinck, D.P. Witte, and J.L. Degen, *Plasminogen deficiency leads to impaired remodeling after a toxic injury to the liver*. Proc Natl Acad Sci U S A, 1999. **96**(26): p. 15143-8.
208. Camiolo, S.M., S. Thorsen and T. Astrup, *Fibrinogenolysis and fibrinolysis with tissue plasminogen activator, urokinase, streptokinase-activated human globulin, and plasmin*. Proc Soc Exp Biol Med, 1971. **138**(1): p. 277-80.
209. Ranby, M., *Studies on the kinetics of plasminogen activation by tissue plasminogen activator*. Biochim Biophys Acta, 1982. **704**(3): p. 461-9.
210. Carmeliet, P., L. Moons, J.M. Herbert, J. Crawley, F. Lupu, R. Lijnen, and D. Collen, *Urokinase but not tissue plasminogen activator mediates arterial neointima formation in mice*. Circ Res, 1997. **81**(5): p. 829-39.
211. Simon, D.I., M.E. Mullins, L. Jia, B. Gaston, D.J. Singel, and J.S. Stamler, *Polynitrosylated proteins: characterization, bioactivity, and functional consequences*. Proc Natl Acad Sci U S A, 1996. **93**(10): p. 4736-41.
212. Smets, K., P. Vanhaesebrouck, D. Voet, P. Schelstraete, and P. Govaert, *Use of tissue type plasminogen activator in neonates: case reports and review of the literature*. Am J Perinatol, 1996. **13**(4): p. 217-22.
213. Martini, W.Z., D.L. Chinkes, J. Sondeen, and M.A. Dubick, *Effects of hemorrhage and lactated Ringer's resuscitation on coagulation and fibrinogen metabolism in swine*. Shock, 2006. **26**(4): p. 396-401.

214. Martini, W.Z., D.L. Chinkes, A.E. Pusateri, J.B. Holcomb, Y.M. Yu, X.J. Zhang, and R.R. Wolfe, *Acute changes in fibrinogen metabolism and coagulation after hemorrhage in pigs*. Am J Physiol Endocrinol Metab, 2005. **289**(5): p. E930-4.
215. Charbit, B., L. Mandelbrot, E. Samain, G. Baron, B. Haddaoui, H. Keita, O. Sibony, D. Mahieu-Caputo, M.F. Hurtaud-Roux, M.G. Huisse, M.H. Denninger, and D. de Prost, *The decrease of fibrinogen is an early predictor of the severity of postpartum hemorrhage*. J Thromb Haemost, 2007. **5**(2): p. 266-73.
216. Ciszak, E., V. Cody and J.R. Luft, *Crystal structure determination at 2.3-Å resolution of human transthyretin-3',5'-dibromo-2',4,4',6-tetrahydroxyaurone complex*. Proc Natl Acad Sci U S A, 1992. **89**(14): p. 6644-8.
217. Cody, V., *Mechanisms of molecular recognition: crystal structure analysis of human and rat transthyretin inhibitor complexes*. Clin Chem Lab Med, 2002. **40**(12): p. 1237-43.
218. Wojtczak, A., J.R. Luft and V. Cody, *Structural aspects of inotropic bipyridine binding. Crystal structure determination to 1.9 Å of the human serum transthyretin-milrinone complex*. J Biol Chem, 1993. **268**(9): p. 6202-6.
219. Paul, D.A., K.H. Leef, J.L. Stefano, and L. Bartoshesky, *Low serum thyroxine on initial newborn screening is associated with intraventricular hemorrhage and death in very low birth weight infants*. Pediatrics, 1998. **101**(5): p. 903-7.
220. Lang, S., *Thyroid function and peripheral thyroxine metabolism after hemorrhage in the rat*. Am J Physiol, 1961. **200**: p. 1335-9.
221. Hennemann, G., R.A. Vos, M. de Jong, E.P. Krenning, and R. Docter, *Decreased peripheral 3,5,3'-triiodothyronine (T3) production from thyroxine (T4): a syndrome of impaired thyroid hormone activation due to transport inhibition of T4- into T3-producing tissues*. J Clin Endocrinol Metab, 1993. **77**(5): p. 1431-5.
222. Marx, J.V., D.A. Richert and W.W. Westerfeld, *Peripheral inhibition of thyroxine by thiohydantoin derivatives from amino acids*. J Med Chem, 1970. **13**(6): p. 1179-81.
223. Bartecchi, C.E., E.R. Mastro and C.W. Swarts, *Acute hemorrhagic pancreatitis with hypertriglyceridemia*. Rocky Mt Med J, 1976. **73**(2): p. 95-8.
224. Chan, A.O., W.M. But, G.T. Lau, W.Y. Tse, and C.C. Shek, *A novel nonsense mutation in the LPL gene in a Chinese neonate with hypertriglyceridemia*. Clin Chim Acta, 2006. **368**(1-2): p. 120-4.

225. Curb, J.D., R.D. Abbott, B.L. Rodriguez, K.H. Masaki, R. Chen, J.S. Popper, H. Petrovitch, G.W. Ross, I.J. Schatz, G.C. Belleau, and K. Yano, *High density lipoprotein cholesterol and the risk of stroke in elderly men: the Honolulu heart program*. Am J Epidemiol, 2004. **160**(2): p. 150-7.
226. Zivkovic, S.A., O.L. Lopez, M. Zaretsky, and L.R. Wechsler, *Rapidly progressive stroke in a young adult with very low high-density lipoprotein cholesterol*. J Neuroimaging, 2000. **10**(4): p. 233-6.
227. Olivier, E., E. Soury, P. Ruminy, A. Husson, F. Parmentier, M. Daveau, and J.P. Salier, *Fetuin-B, a second member of the fetuin family in mammals*. Biochem J, 2000. **350 Pt 2**: p. 589-97.
228. Denecke, B., S. Graber, C. Schafer, A. Heiss, M. Woltje, and W. Jahnen-Dechent, *Tissue distribution and activity testing suggest a similar but not identical function of fetuin-B and fetuin-A*. Biochem J, 2003. **376**(Pt 1): p. 135-45.
229. Hsu, S.J., H. Nagase and A. Balmain, *Identification of Fetuin-B as a member of a cystatin-like gene family on mouse chromosome 16 with tumor suppressor activity*. Genome, 2004. **47**(5): p. 931-46.
230. Ketteler, M., *Fetuin-A and extraosseous calcification in uremia*. Curr Opin Nephrol Hypertens, 2005. **14**(4): p. 337-42.
231. Tate, J.R., P. Mollee, G. Dimeski, A.C. Carter, and D. Gill, *Analytical performance of serum free light-chain assay during monitoring of patients with monoclonal light-chain diseases*. Clin Chim Acta, 2007. **376**(1-2): p. 30-6.
232. Levinson, S.S. and D.F. Keren, *Free light chains of immunoglobulins: clinical laboratory analysis*. Clin Chem, 1994. **40**(10): p. 1869-78.
233. Keren, D.F., J.S. Warren and J.B. Lowe, *Strategy to diagnose monoclonal gammopathies in serum: high-resolution electrophoresis, immunofixation, and kappa/lambda quantification*. Clin Chem, 1988. **34**(11): p. 2196-201.
234. Peterson, P.A. and I. Berggard, *Urinary immunoglobulin components in normal, tubular, and glomerular proteinuria: quantities and characteristics of free light chains, IgG, igA, and Fc-gamma fragment*. Eur J Clin Invest, 1971. **1**(4): p. 255-64.

235. Darlington, D.N. and M.J. Tehrani, *Blood flow, vascular resistance, and blood volume after hemorrhage in conscious adrenalectomized rat*. J Appl Physiol, 1997. **83**(5): p. 1648-53.
236. Rao, N.A., J.L. Romero, A. Sevanian, M.A. Fernandez, C. Wong, P.A. Ward, and G.E. Marak, Jr., *Anti-inflammatory effect of glutathione peroxidase on experimental lens-induced uveitis*. Ophthalmic Res, 1988. **20**(4): p. 213-9.
237. Macdonald, R.L., B.K. Weir, T.D. Runzer, and M.G. Grace, *Malondialdehyde, glutathione peroxidase, and superoxide dismutase in cerebrospinal fluid during cerebral vasospasm in monkeys*. Can J Neurol Sci, 1992. **19**(3): p. 326-32.
238. Bajt, M.L., Y.S. Ho, S.L. Vonderfecht, and H. Jaeschke, *Reactive oxygen as modulator of TNF and fas receptor-mediated apoptosis in vivo: studies with glutathione peroxidase-deficient mice*. Antioxid Redox Signal, 2002. **4**(5): p. 733-40.
239. Endo, H., C. Nito, H. Kamada, F. Yu, and P.H. Chan, *Reduction in oxidative stress by superoxide dismutase overexpression attenuates acute brain injury after subarachnoid hemorrhage via activation of Akt/glycogen synthase kinase-3beta survival signaling*. J Cereb Blood Flow Metab, 2006.
240. Nakamura, T., R.F. Keep, Y. Hua, J.W. Park, T. Itano, S. Nagao, J.T. Hoff, and G.H. Xi, *Intracerebral hemorrhage induces edema and oxidative stress and alters N-methyl-D-aspartate receptor subunits expression*. Acta Neurochir Suppl, 2005. **95**: p. 421-4.
241. Hung, C.R., *Modulation of gastric hemorrhage and ulceration by oxidative stress and histamine release in Salmonella typhimurium-infected rats*. Inflammopharmacology, 2005. **13**(1-3): p. 235-48.
242. Hall, N.C., B.A. Packard, C.L. Hall, G. de Courten-Myers, and K.R. Wagner, *Protein oxidation and enzyme susceptibility in white and gray matter with in vitro oxidative stress: relevance to brain injury from intracerebral hemorrhage*. Cell Mol Biol (Noisy-le-grand), 2000. **46**(3): p. 673-83.
243. Gaetani, P., A. Pasqualin, R. Rodriguez y Baena, E. Borasio, and F. Marzatico, *Oxidative stress in the human brain after subarachnoid hemorrhage*. J Neurosurg, 1998. **89**(5): p. 748-54.

244. Laplace, C., O. Huet, E. Vicaut, C. Ract, L. Martin, D. Benhamou, and J. Duranteau, *Endothelial oxidative stress induced by serum from patients with severe trauma hemorrhage*. Intensive Care Med, 2005. **31**(9): p. 1174-80.
245. Michiels, C., M. Raes, O. Toussaint, and J. Remacle, *Importance of Se-glutathione peroxidase, catalase, and Cu/Zn-SOD for cell survival against oxidative stress*. Free Radic Biol Med, 1994. **17**(3): p. 235-48.
246. Tucker, V.L., E. Bravo, C.J. Weber, and D.H. Wisner, *Blood-to-tissue albumin transport in rats subjected to acute hemorrhage and resuscitation*. Shock, 1995. **3**(3): p. 189-95.
247. Eilig, I., M. Rachinsky, A.A. Artru, A. Alonchin, V. Kapuler, A. Tarnapolski, and Y. Shapira, *The effect of treatment with albumin, hetastarch, or hypertonic saline on neurological status and brain edema in a rat model of closed head trauma combined with uncontrolled hemorrhage and concurrent resuscitation in rats*. Anesth Analg, 2001. **92**(3): p. 669-75.
248. Huang, Z., W. Dong, Y. Yan, Q. Xiao, and Y. Man, *Effects of intravenous human albumin and furosemide on EEG recordings in patients with intracerebral hemorrhage*. Clin Neurophysiol, 2002. **113**(3): p. 454-8.
249. Matsui, T. and T. Asano, *The hemodynamic effects of prolonged albumin administration in beagle dogs exposed to experimental subarachnoid hemorrhage*. Neurosurgery, 1993. **32**(1): p. 79-83; discussion 83-4.
250. Mayer, S.A., R.A. Solomon, M.E. Fink, L. Lennihan, L. Stern, A. Beckford, C.E. Thomas, and L.M. Klebanoff, *Effect of 5% albumin solution on sodium balance and blood volume after subarachnoid hemorrhage*. Neurosurgery, 1998. **42**(4): p. 759-67; discussion 767-8.
251. Suarez, J.I., L. Shannon, O.O. Zaidat, M.F. Suri, G. Singh, G. Lynch, and W.R. Selman, *Effect of human albumin administration on clinical outcome and hospital cost in patients with subarachnoid hemorrhage*. J Neurosurg, 2004. **100**(4): p. 585-90.
252. Zhang, H., S. Voglis, C.H. Kim, and A.S. Slutsky, *Effects of albumin and Ringer's lactate on production of lung cytokines and hydrogen peroxide after resuscitated hemorrhage and endotoxemia in rats*. Crit Care Med, 2003. **31**(5): p. 1515-22.

253. Takenaka, K.V., N. Sakai, S. Murase, T. Kuroda, A. Okumura, and M. Sawada, *Elevated transferrin concentration in cerebral spinal fluid after subarachnoid hemorrhage*. *Neurol Res*, 2000. **22**(8): p. 797-801.
254. Abraham, E., L. Andrade and A.A. Freitas, *Immunoglobulin VH gene expression following hemorrhage*. *Mol Immunol*, 1990. **27**(9): p. 921-7.
255. Calcutt, N.A., J.D. Freshwater and J.S. O'Brien, *Protection of sensory function and antihyperalgesic properties of a prosaposin-derived peptide in diabetic rats*. *Anesthesiology*, 2000. **93**(5): p. 1271-8.
256. Cohen, T., W. Auerbach, L. Ravid, J. Bodennec, A. Fein, A.H. Futerman, A.L. Joyner, and M. Horowitz, *The exon 8-containing prosaposin gene splice variant is dispensable for mouse development, lysosomal function, and secretion*. *Mol Cell Biol*, 2005. **25**(6): p. 2431-40.
257. Morales, C.R. and H. Badran, *Prosaposin ablation inactivates the MAPK and Akt signaling pathways and interferes with the development of the prostate gland*. *Asian J Androl*, 2003. **5**(1): p. 57-63.
258. Morales, C.R., M. el-Alfy, Q. Zhao, and S. Igdoura, *Molecular role of sulfated glycoprotein-1 (SGP-1/prosaposin) in Sertoli cells*. *Histol Histopathol*, 1995. **10**(4): p. 1023-34.
259. Morales, C.R., Q. Zhao, S. Lefrancois, and D. Ham, *Role of prosaposin in the male reproductive system: effect of prosaposin inactivation on the testis, epididymis, prostate, and seminal vesicles*. *Arch Androl*, 2000. **44**(3): p. 173-86.
260. Sikora, J., K. Harzer and M. Elleder, *Neurolysosomal pathology in human prosaposin deficiency suggests essential neurotrophic function of prosaposin*. *Acta Neuropathol (Berl)*, 2007. **113**(2): p. 163-75.
261. Cohen, T., L. Ravid, N. Altman, L. Madar-Shapiro, A. Fein, M. Weil, and M. Horowitz, *Conservation of expression and alternative splicing in the prosaposin gene*. *Brain Res Mol Brain Res*, 2004. **129**(1-2): p. 8-19.
262. Hiraiwa, M., S. Soeda, Y. Kishimoto, and J.S. O'Brien, *Binding and transport of gangliosides by prosaposin*. *Proc Natl Acad Sci U S A*, 1992. **89**(23): p. 11254-8.
263. Argraves, K.M., L.M. Obeid and Y.A. Hannun, *Sphingolipids in vascular biology*. *Adv Exp Med Biol*, 2002. **507**: p. 439-44.

264. Birbes, H., S. El Bawab, L.M. Obeid, and Y.A. Hannun, *Mitochondria and ceramide: intertwined roles in regulation of apoptosis*. Adv Enzyme Regul, 2002. **42**: p. 113-29.
265. el Bawab, S., C. Mao, L.M. Obeid, and Y.A. Hannun, *Ceramidases in the regulation of ceramide levels and function*. Subcell Biochem, 2002. **36**: p. 187-205.
266. Maceyka, M., S.G. Payne, S. Milstien, and S. Spiegel, *Sphingosine kinase, sphingosine-1-phosphate, and apoptosis*. Biochim Biophys Acta, 2002. **1585**(2-3): p. 193-201.
267. Hannun, Y.A. and L.M. Obeid, *The Ceramide-centric universe of lipid-mediated cell regulation: stress encounters of the lipid kind*. J Biol Chem, 2002. **277**(29): p. 25847-50.
268. Spiegel, S. and S. Milstien, *Sphingosine 1-phosphate, a key cell signaling molecule*. J Biol Chem, 2002. **277**(29): p. 25851-4.
269. Ho, K.K., G.B. Moody, C.K. Peng, J.E. Mietus, M.G. Larson, D. Levy, and A.L. Goldberger, *Predicting survival in heart failure case and control subjects by use of fully automated methods for deriving nonlinear and conventional indices of heart rate dynamics*. Circulation, 1997. **96**(3): p. 842-8.
270. Komuro, I., *Molecular mechanism of cardiac hypertrophy and development*. Jpn Circ J, 2001. **65**(5): p. 353-8.
271. Komuro, I. and Y. Yazaki, *Molecular mechanism of cardiac hypertrophy and failure*. Clin Sci (Lond), 1994. **87**(2): p. 115-6.
272. Yamazaki, T., I. Komuro, I. Shiojima, and Y. Yazaki, *The molecular mechanism of cardiac hypertrophy and failure*. Ann N Y Acad Sci, 1999. **874**: p. 38-48.
273. Nelson, T.J., R. Balza, Jr., Q. Xiao, and R.P. Misra, *SRF-dependent gene expression in isolated cardiomyocytes: regulation of genes involved in cardiac hypertrophy*. J Mol Cell Cardiol, 2005. **39**(3): p. 479-89.
274. Wright, W.E., D.A. Sassoon and V.K. Lin, *Myogenin, a factor regulating myogenesis, has a domain homologous to MyoD*. Cell, 1989. **56**(4): p. 607-17.
275. Hill, C.S., J. Wynne and R. Treisman, *Serum-regulated transcription by serum response factor (SRF): a novel role for the DNA binding domain*. EMBO Journal, 1994. **13**(22): p. 5421-32.
276. Janknecht, R., R.A. Hipkind, T. Houthaeve, A. Nordheim, and H.G. Stunnenberg, *Identification of multiple SRF N-terminal phosphorylation sites affecting DNA binding properties*. Embo J, 1992. **11**(3): p. 1045-54.

277. Lockman, K., J.S. Hinson, M.D. Medlin, D. Morris, J.M. Taylor, and C.P. Mack, *Sphingosine 1-Phosphate Stimulates Smooth Muscle Cell Differentiation and Proliferation by Activating Separate Serum Response Factor Co-factors*. J Biol Chem, 2004. **279**(41): p. 42422-30.
278. Iyer, D., D. Chang, J. Marx, L. Wei, E.N. Olson, M.S. Parmacek, A. Balasubramanyam, and R.J. Schwartz, *Serum response factor MADS box serine-162 phosphorylation switches proliferation and myogenic gene programs*. Proc Natl Acad Sci U S A, 2006. **103**(12): p. 4516-21.
279. Miwa, T. and L. Kedes, *Duplicated CARG box domains have positive and mutually dependent regulatory roles in expression of the human alpha-cardiac actin gene*. Mol Cell Biol, 1987. **7**(8): p. 2803-13.
280. Mohun, T.J., M.V. Taylor, N. Garrett, and J.B. Gurdon, *The CARG promoter sequence is necessary for muscle-specific transcription of the cardiac actin gene in Xenopus embryos*. Embo J, 1989. **8**(4): p. 1153-61.
281. Treisman, R., *Ternary complex factors: growth factor regulated transcriptional activators*. Curr Opin Genet Dev, 1994. **4**(1): p. 96-101.
282. Pellegrini, L., S. Tan and T.J. Richmond, *Structure of serum response factor core bound to DNA*. Nature, 1995. **376**(6540): p. 490-8.
283. Mayr, B. and M. Montminy, *Transcriptional regulation by the phosphorylation-dependent factor CREB*. Nat Rev Mol Cell Biol, 2001. **2**(8): p. 599-609.
284. de Ruiter, N.D., R.M. Wolthuis, H. van Dam, B.M. Burgering, and J.L. Bos, *Ras-dependent regulation of c-Jun phosphorylation is mediated by the Ral guanine nucleotide exchange factor-Ral pathway*. Mol Cell Biol, 2000. **20**(22): p. 8480-8.
285. Papavassiliou, A.G., *c-Jun phosphorylation in signal transduction and gene regulation*. Anticancer Res, 1993. **13**(6A): p. 2213-20.
286. Plows, D., P. Briassouli, C. Owen, V. Zoumpourlis, M.D. Garrett, and A. Pintzas, *Ecdysone-inducible expression of oncogenic Ha-Ras in NIH 3T3 cells leads to transient nuclear localization of activated extracellular signal-regulated kinase regulated by mitogen-activated protein kinase phosphatase-1*. Biochem J, 2002. **362**(Pt 2): p. 305-15.

287. Manak, J.R. and R. Prywes, *Mutation of serum response factor phosphorylation sites and the mechanism by which its DNA-binding activity is increased by casein kinase II*. Mol Cell Biol, 1991. **11**(7): p. 3652-9.
288. Rivera, V.M., C.K. Miranti, R.P. Misra, D.D. Ginty, R.H. Chen, J. Blenis, and M.E. Greenberg, *A growth factor-induced kinase phosphorylates the serum response factor at a site that regulates its DNA-binding activity*. Mol Cell Biol, 1993. **13**(10): p. 6260-73.
289. Rech, J., I. Barlat, J.L. Veyrune, A. Vie, and J.M. Blanchard, *Nuclear import of serum response factor (SRF) requires a short amino-terminal nuclear localization sequence and is independent of the casein kinase II phosphorylation site*. Journal of Cell Science, 1994. **107**(Pt 11): p. 3029-36.
290. Oda, Y., T. Nagasu and B.T. Chait, *Enrichment analysis of phosphorylated proteins as a tool for probing the phosphoproteome*. Nat Biotechnol, 2001. **19**(4): p. 379-82.
291. Zhou, H., J.D. Watts and R. Aebersold, *A systematic approach to the analysis of protein phosphorylation*. Nat Biotechnol, 2001. **19**(4): p. 375-8.
292. Misra, R.P., V.M. Rivera, J.M. Wang, P.D. Fan, and M.E. Greenberg, *The serum response factor is extensively modified by phosphorylation following its synthesis in serum-stimulated fibroblasts*. Mol Cell Biol, 1991. **11**(9): p. 4545-54.
293. Manak, J.R. and R. Prywes, *Phosphorylation of serum response factor by casein kinase II: evidence against a role in growth factor regulation of fos expression*. Oncogene, 1993. **8**(3): p. 703-11.
294. Heidenreich, O., A. Neininger, G. Schrott, R. Zinck, M.A. Cahill, K. Engel, A. Kotlyarov, R. Kraft, S. Kostka, M. Gaestel, and A. Nordheim, *MAPKAP kinase 2 phosphorylates serum response factor in vitro and in vivo*. J Biol Chem, 1999. **274**(20): p. 14434-43.
295. Bodenmiller, B., L.N. Mueller, M. Mueller, B. Domon, and R. Aebersold, *Reproducible isolation of distinct, overlapping segments of the phosphoproteome*. Nat Methods, 2007. **4**(3): p. 231-7.
296. Papac, D.I., A. Wong and A.J. Jones, *Analysis of acidic oligosaccharides and glycopeptides by matrix-assisted laser desorption/ionization time-of-flight mass spectrometry*. Anal Chem, 1996. **68**(18): p. 3215-23.

297. Fields, S. and O. Song, *A novel genetic system to detect protein-protein interactions*. Nature, 1989. **340**(6230): p. 245-6.
298. Causier, B., *Studying the interactome with the yeast two-hybrid system and mass spectrometry*. Mass Spectrom Rev, 2004. **23**(5): p. 350-67.
299. Causier, B. and B. Davies, *Analysing protein-protein interactions with the yeast two-hybrid system*. Plant Mol Biol, 2002. **50**(6): p. 855-70.
300. Coates, P.J. and P.A. Hall, *The yeast two-hybrid system for identifying protein-protein interactions*. J Pathol, 2003. **199**(1): p. 4-7.
301. Luban, J. and S.P. Goff, *The yeast two-hybrid system for studying protein-protein interactions*. Curr Opin Biotechnol, 1995. **6**(1): p. 59-64.
302. Miller, J. and I. Stagljar, *Using the yeast two-hybrid system to identify interacting proteins*. Methods Mol Biol, 2004. **261**: p. 247-62.
303. White, M.A., *The yeast two-hybrid system: forward and reverse*. Proc Natl Acad Sci U S A, 1996. **93**(19): p. 10001-3.
304. Puig, O., F. Casparly, G. Rigaut, B. Rutz, E. Bouveret, E. Bragado-Nilsson, M. Wilm, and B. Seraphin, *The tandem affinity purification (TAP) method: a general procedure of protein complex purification*. Methods, 2001. **24**(3): p. 218-29.
305. Rigaut, G., A. Shevchenko, B. Rutz, M. Wilm, M. Mann, and B. Seraphin, *A generic protein purification method for protein complex characterization and proteome exploration*. Nat Biotechnol, 1999. **17**(10): p. 1030-2.
306. Bauer, A. and B. Kuster, *Affinity purification-mass spectrometry. Powerful tools for the characterization of protein complexes*. Eur J Biochem, 2003. **270**(4): p. 570-8.
307. Gavin, A.C., M. Bosche, R. Krause, P. Grandi, M. Marzioch, A. Bauer, J. Schultz, J.M. Rick, A.M. Michon, C.M. Cruciat, M. Remor, C. Hofert, M. Schelder, M. Brajenovic, H. Ruffner, A. Merino, K. Klein, M. Hudak, D. Dickson, T. Rudi, V. Gnau, A. Bauch, S. Bastuck, B. Huhse, C. Leutwein, M.A. Heurtier, R.R. Copley, A. Edlmann, E. Querfurth, V. Rybin, G. Drewes, M. Raida, T. Bouwmeester, P. Bork, B. Seraphin, B. Kuster, G. Neubauer, and G. Superti-Furga, *Functional organization of the yeast proteome by systematic analysis of protein complexes*. Nature, 2002. **415**(6868): p. 141-7.

308. Gozal, Y.M., D. Cheng, D.M. Duong, J.J. Lah, A.I. Levey, and J. Peng, *Merger of laser capture microdissection and mass spectrometry: a window into the amyloid plaque proteome*. *Methods Enzymol*, 2006. **412**: p. 77-93.
309. Baker, H., V. Patel, A.A. Molinolo, E.J. Shillitoe, J.F. Ensley, G.H. Yoo, A. Meneses-Garcia, J.N. Myers, A.K. El-Naggar, J.S. Gutkind, and W.S. Hancock, *Proteome-wide analysis of head and neck squamous cell carcinomas using laser-capture microdissection and tandem mass spectrometry*. *Oral Oncol*, 2005. **41**(2): p. 183-99.
310. Li, C., Y. Hong, Y.X. Tan, H. Zhou, J.H. Ai, S.J. Li, L. Zhang, Q.C. Xia, J.R. Wu, H.Y. Wang, and R. Zeng, *Accurate qualitative and quantitative proteomic analysis of clinical hepatocellular carcinoma using laser capture microdissection coupled with isotope-coded affinity tag and two-dimensional liquid chromatography mass spectrometry*. *Mol Cell Proteomics*, 2004. **3**(4): p. 399-409.
311. Mann, M., *Functional and quantitative proteomics using SILAC*. *Nat Rev Mol Cell Biol*, 2006. **7**(12): p. 952-8.
312. Ong, S.E., G. Mittler and M. Mann, *Identifying and quantifying in vivo methylation sites by heavy methyl SILAC*. *Nat Methods*, 2004. **1**(2): p. 119-26.
313. Amanchy, R., D.E. Kalume and A. Pandey, *Stable isotope labeling with amino acids in cell culture (SILAC) for studying dynamics of protein abundance and posttranslational modifications*. *Sci STKE*, 2005. **2005**(267): p. pl2.
314. Beckner, M.E., X. Chen, J. An, B.W. Day, and I.F. Pollack, *Proteomic characterization of harvested pseudopodia with differential gel electrophoresis and specific antibodies*. *Lab Invest*, 2005. **85**(3): p. 316-27.
315. Unlu, M., M.E. Morgan and J.S. Minden, *Difference gel electrophoresis: a single gel method for detecting changes in protein extracts*. *Electrophoresis*, 1997. **18**(11): p. 2071-7.
316. Beckner, M.E., Z. Zhang, N.R. Agostino, B.W. Day, and I.F. Pollack, *Albumin marks pseudopodia of astrocytoma cells responding to hepatocyte growth factor or serum*. *Lab Invest*, 2006. **86**(11): p. 1103-14.
317. Brettschneider, J., A. Claus, J. Kassubek, and H. Tumani, *Isolated blood-cerebrospinal fluid barrier dysfunction: prevalence and associated diseases*. *J Neurol*, 2005. **252**(9): p. 1067-73.

318. Cavagna, F.M., F. Maggioni, P.M. Castelli, M. Dapra, L.G. Imperatori, V. Lorusso, and B.G. Jenkins, *Gadolinium chelates with weak binding to serum proteins. A new class of high-efficiency, general purpose contrast agents for magnetic resonance imaging*. Invest Radiol, 1997. **32**(12): p. 780-96.
319. Wolff, M. and D.K. Boker, *Immunohistochemical demonstration of immunoglobulins and albumin in human brain tumors*. Clin Neuropathol, 1989. **8**(2): p. 72-8.
320. Geer, C.P. and S.A. Grossman, *Interstitial fluid flow along white matter tracts: a potentially important mechanism for the dissemination of primary brain tumors*. J Neurooncol, 1997. **32**(3): p. 193-201.
321. Glatz, J.F., J.J. Luiken, F.A. van Nieuwenhoven, and G.J. Van der Vusse, *Molecular mechanism of cellular uptake and intracellular translocation of fatty acids*. Prostaglandins Leukot Essent Fatty Acids, 1997. **57**(1): p. 3-9.
322. van der Vusse, G.J., M. van Bilsen, J.F. Glatz, D.M. Hasselbaink, and J.J. Luiken, *Critical steps in cellular fatty acid uptake and utilization*. Mol Cell Biochem, 2002. **239**(1-2): p. 9-15.
323. Beckner, M.E., G.T. Gobbel, R. Abounader, F. Burovic, N.R. Agostino, J. Laterra, and I.F. Pollack, *Glycolytic glioma cells with active glycogen synthase are sensitive to PTEN and inhibitors of PI3K and gluconeogenesis*. Lab Invest, 2005. **85**(12): p. 1457-70.
324. Beckner, M.E., M.L. Stracke, L.A. Liotta, and E. Schiffmann, *Glycolysis as primary energy source in tumor cell chemotaxis*. J Natl Cancer Inst, 1990. **82**(23): p. 1836-40.
325. Schidlow, D.V., *Something is (not) rotten in Denmark [Hamlet (not) W. Shakespeare]*. Pediatr Pulmonol, 1997. **23**(5): p. 325-6.
326. Svanborg, C., H. Agerstam, A. Aronson, R. Bjerkvig, C. Durringer, W. Fischer, L. Gustafsson, O. Hallgren, I. Leijonhuvud, S. Linse, A.K. Mossberg, H. Nilsson, J. Pettersson, and M. Svensson, *HAMLET kills tumor cells by an apoptosis-like mechanism--cellular, molecular, and therapeutic aspects*. Adv Cancer Res, 2003. **88**: p. 1-29.
327. Svensson, M., C. Durringer, O. Hallgren, A.K. Mossberg, A. Hakansson, S. Linse, and C. Svanborg, *Hamlet--a complex from human milk that induces apoptosis in tumor cells but spares healthy cells*. Adv Exp Med Biol, 2002. **503**: p. 125-32.
328. Kirsch, W.M. and J.W. Leitner, *A comparison of the anaerobic glycolysis of human brain and glioblastoma*. J Neurosurg, 1967. **27**(1): p. 45-51.

329. Meixensberger, J., B. Herting, W. Roggendorf, and H. Reichmann, *Metabolic patterns in malignant gliomas*. J Neurooncol, 1995. **24**(2): p. 153-61.
330. Terpstra, M., R. Gruetter, W.B. High, M. Mescher, L. DelaBarre, H. Merkle, and M. Garwood, *Lactate turnover in rat glioma measured by in vivo nuclear magnetic resonance spectroscopy*. Cancer Res, 1998. **58**(22): p. 5083-8.
331. Varki, A., R. Cummings, J. Esko, H. Freeze, G. Hart, and J. Marth, *Essentials of Glycobiology*. 1999: Cold Spring Harbor Laboratory. 653.
332. Hounsell, E.F., M.J. Davies and D.V. Renouf, *O-linked protein glycosylation structure and function*. Glycoconj J, 1996. **13**(1): p. 19-26.
333. Imperiali, B. and S.E. O'Connor, *Effect of N-linked glycosylation on glycopeptide and glycoprotein structure*. Curr Opin Chem Biol, 1999. **3**(6): p. 643-9.
334. Rudd, P.M. and R.A. Dwek, *Glycosylation: heterogeneity and the 3D structure of proteins*. Crit Rev Biochem Mol Biol, 1997. **32**(1): p. 1-100.
335. Seitz, O., *Glycopeptide synthesis and the effects of glycosylation on protein structure and activity*. Chembiochem, 2000. **1**(4): p. 214-46.
336. Welply, J.K., *Protein glycosylation: function and factors that regulate oligosaccharide structure*. Biotechnology, 1991. **17**: p. 59-72.
337. Dennis, J.W., M. Granovsky and C.E. Warren, *Glycoprotein glycosylation and cancer progression*. Biochim Biophys Acta, 1999. **1473**(1): p. 21-34.
338. Gerber-Lemaire, S. and L. Juillerat-Jeanneret, *Glycosylation pathways as drug targets for cancer: glycosidase inhibitors*. Mini Rev Med Chem, 2006. **6**(9): p. 1043-52.
339. Ono, M. and S. Hakomori, *Glycosylation defining cancer cell motility and invasiveness*. Glycoconj J, 2004. **20**(1): p. 71-8.
340. Orntoft, T.F. and E.M. Vestergaard, *Clinical aspects of altered glycosylation of glycoproteins in cancer*. Electrophoresis, 1999. **20**(2): p. 362-71.
341. Bunkenborg, J., B.J. Pilch, A.V. Podtelejnikov, and J.R. Wisniewski, *Screening for N-glycosylated proteins by liquid chromatography mass spectrometry*. Proteomics, 2004. **4**(2): p. 454-65.
342. Kaji, H., H. Saito, Y. Yamauchi, T. Shinkawa, M. Taoka, J. Hirabayashi, K. Kasai, N. Takahashi, and T. Isobe, *Lectin affinity capture, isotope-coded tagging and mass spectrometry to identify N-linked glycoproteins*. Nat Biotechnol, 2003. **21**(6): p. 667-72.

343. Madera, M., Y. Mechref and M.V. Novotny, *Combining lectin microcolumns with high-resolution separation techniques for enrichment of glycoproteins and glycopeptides*. *Anal Chem*, 2005. **77**(13): p. 4081-90.
344. Yang, Z., W.S. Hancock, T.R. Chew, and L. Bonilla, *A study of glycoproteins in human serum and plasma reference standards (HUPO) using multilectin affinity chromatography coupled with RPLC-MS/MS*. *Proteomics*, 2005. **5**(13): p. 3353-66.